Exploring the α$_2$-adrenergic receptors with alkyl substituted bis-guanidinium diaryl derivatives

A thesis presented to Trinity College Dublin, the University of Dublin for the degree of Master of Science

Roisin Hyland, BSc (Hons)

Under the supervision of Prof. Isabel Rozas

School of Chemistry

Trinity College Dublin

December 2021

Declaration

This work comprises of a master thesis submitted for the consideration of Trinity College Dublin.

I declare that this thesis has not been submitted as an exercise for a degree at this or any other university and it is entirely my own work.

I agree to deposit this thesis in the University's open access institutional repository or allow the Library to do so on my behalf, subject to Irish Copyright Legislation and Trinity College Library conditions of use and acknowledgement.

Roisín Hyland

…………………………………………………

Roisin Hyland
December 2021
Trinity College Dublin

Acknowledgements

Firstly, I would like to express my utmost gratitude towards my supervisor Prof. Isabel Rozas. Her supportive and enthusiastic approach to the research along with her inspirational guidance made the past year a successful and enjoyable experience. Along with her own expertise and knowledge that she had shared with me along the way, she also instilled confidence in my own ideas and work ethic within the research and laboratory environment.

The rest of the Rozas group, Adeyemi Rahman, Nikolina Stipaničev and Helene Mihigo, who's knowledge and experiences guided me through the challenges faced in the laboratory and motivated me to keep moving forward when the chemistry was proving difficult. These special friendships made the late working nights and early mornings much easier. I am also extremely grateful to Helene Mihigo for taking the time out of her own hard work and busy schedule to help me with the computational chemistry within this research document. Without her huge assistance here, I would not have had the extra time to complete all the desired research that is documented in the coming chapters.

The technical staff must be recognised for their continued assistance throughout the year including: Dr. John O'Brien and Dr Manuel Ruether for all of the NMR data, alongside Dr. Gary Hessman for the mass spectroscopy work. I wish to extend these acknowledgements to all the administration staff within the School of Chemistry for all their support over the last year. Finally, an importance acknowledgement must be made for our collaborators; Prof. Mireia Olivella from the Universitat de Vic in Spain with her work on the development of the α_2-adrenergic receptor homology models and Prof. Callado at the Department of Pharmacology at the School of Medicine in the University of Basque County UPV/EHU (Spain). Without their expertise in pharmacology this research would not have been possible.

My family have supported me by any means possible over the last year. I am forever grateful to my parents for believing in me so much so that they chose to support me financially and make this research possible. They listened to my stories or complaints of the chemistry I was working on even though they had no background in the topic themselves. Any opportunity they had to make my day easier or brighter, they took it and for that I am forever grateful. Lastly but certainly not least, I would like to thank my best friend Dan for being a source of fun and laughter for me during this last year. Our bouldering training sessions always helped to clear my head in order to face the challenges in the lab the next day. I am very lucky to have been surrounded by such wonderful people, without them this research would not have been possible.

Abstract

The burden of mental health conditions is on the rise globally. It is well documented that noradrenaline has a key role in memory, attention, stress, and regulation of emotions. The α_2-adrenergic receptors (α_2-ARs) are an attractive biological target for therapies for neurological conditions. Thus, α_2-AR antagonists would block the activation of this autoreceptor potentially operating as therapeutic antidepressant agent. In a ligand-based drug design strategy we have investigated the effects on the binding affinity and ligand-receptor functional activity when releasing the rigid 2-aminoimidazolium moiety of *lead* compound **1**, thus affecting steric and lipophilic properties. This aim will be achieved via computational studies, synthesis, and pharmacological evaluation.

Due to their relevance in depression, three inactive α_{2A}-AR receptor templates were used in the docking study: a homology model developed by Prof. Olivella, and two crystal structures recently reported, one complexed with a partial agonist and another with an antagonist. Compounds **1** (*lead*, symmetric), **15** (asymmetric), **16** (asymmetric), **18** (symmetric) and **22c** (symmetric) were used as ligands for standard rigid receptor and fit-induced docking studies. All docked compounds were orientated based on the ionic interaction with the aspartate residue D113$^{3.32}$, a known critical anchoring interaction with the α_2-AR binding sites. Agonists **15** and **18** show interactions with S200$^{5.42}$, a known residue involved in agonist activity, Moreover, the interaction between the ligand and E94$^{2.65}$ is common to the two known antagonists **16** and **22c** and this could assist in directing the ligand away from TM5, avoiding receptor activation.

A new synthesis of di-Boc-protected mono-substituted thioureas was developed utilizing Mitsunobu reaction conditions. Additionally, five new compounds were prepared, characterised using ^{1}H and ^{13}C NMR, IR, and HRMS. The α_2-AR binding affinities of these compounds were measured in human prefrontal cortex tissue using a competitive assay with the α_2-AR selective radioligand [^{3}H]RX821002. When the ligands showed α_2-AR affinity with $K_i < 100$ nM, functional [^{35}S]GTPγS assays were used to determine their activity (i.e. antagonist, agonist or inverse agonist). Encouragingly, one of the five newly synthesised compounds (**22c**) displayed a binding affinity of 95.50 nM (best of substituted bis-guanidinium ligands to date) and antagonist activity.

Considering past and present results with compounds **1**, **16**, **17** and **22c**, a derivative containing both an imidazolium moiety and an ethyl-substituted guanidinium could be a very promising high affinity antagonist.

Abbreviations

ABC – ATP-binding cassette

AC – Adenylate cyclase

ACh – Acetylcholine

ADHD – Attention deficit/hyperactivity disorder

ADME – Absorption, distribution, metabolism, excretion

AR – Adrenoceptor / Adrenergic receptor

ATP – Adenosine triphosphate

BBB – Blood brain barrier

Ca^{2+} – Calcium ion

cAMP – Cyclic adenosine monophosphate

CNS – Central nervous system

CO – Carbon monoxide

CoMFA – Comparative molecular field analysis

COMT – Catechol-O-methyl transferase

$CuCl_2$ – Copper (II) chloride

DBH – Dopamine β- hydroxylase

DCM – Dichloromethane

DEAD – Diethylazodicarboxylate

DNA – Deoxyribonucleic acid

DMF – Dimethylformamide

D_2O – Deuterium oxide

ESOL – Estimated solubility

GDP – Guanosine diphosphate

GI – Gastrointestinal

G-protein – Guanyl-nucleotide-binding protein

GPCR – G-protein-coupled receptor

G-score – Glide score

GTP – Guanosine triphosphate

HB – Hydrogen bond

HCl – hydrochloric acid

$HgCl_2$ – Mercury (II) chloride

HIA – Human intestinal absorption

HOMO – Highest unoccupied molecular orbital

HTS – High throughput screening

HPLC – High performance liquid chromatography

IC_{50} – Half maximal inhibitory concentration

IMHB – Intramolecular hydrogen bonds

K^+ – Potassium ion

K_D – Affinity of radiolabelled 'hot' ligand

K_i – Calculated dissociation constant of affinity of non-radiolabelled ligand

L-DOPA – L-3,4-dihydroxyphenylalanine

LUMO – Lowest unoccupied molecular orbital

MAO – Monoamine oxidase

MB-COMT – Membrane-bound catechol-*O*-methyl transferase

MeOD – Deuterated methanol

MDR – Multidrug resistance

MO – Molecular orbital

MR- Molecular refractivity

NA – Noradrenaline

NaH – Sodium hydride

$NaHCO_3$ – Sodium bicarbonate

NBO – Natural bonding orbital

N.D. – Not determined

NIS – *N*-iodosuccinimide

NMR – Nuclear magnetic resonance

NO – Nitric oxide

NT – Neurotransmitter

PAINS – Pan-assay interference compounds

PDB – Protein Data Bank

PFC – Prefrontal cortex

Pgp – permeability glycoprotein

PLC – Phospholipase C

PNMT – Phenylethanolamine *N*-methyltransferase

PNS – Peripheral nervous system

PPh$_3$ – triphenylphosphine

PS – Polymer supported

PSA – Polar surface area

QSAR – Quantitative structure-activity relationship

QTAIM – Quantum theory of atoms in molecules

Ro5 – Rule of five

SBDD – Structure based drug design

S-COMT – Soluble catechol-*O*-methyl transferase

SMNT – Small molecule neurotransmitter

TCT – Trichloro-1,3,5-triazine

THF – Tetrahydrofuran

TFA – Trifluoroacetic acid

TFAA – Trifluoroacetic anhydride

TPSA – Topological polar surface area

VMAT – Vesicular monoamine transporters

VS – Virtual screening

XL – Extracellular loop

W.H.O. – World Health Organisation

3D – 3-Dimensional

5-HT – Serotonin

5-HTP – 5-hydroxytryptophan

7-TM – Seven transmembrane

Contents

1. Introduction

1.1 The Nervous System

In 1906, the Nobel Prize for Physiology or Medicine was awarded to Golgi and Ramon y Cajal for arguing that nerve cells are discrete entities that communicate by means of specialised contacts called synapses.[1] However, it was not until the invention of the electron microscope in the 1950s that a visual identification of these synapses could be recorded. There are two types of nerve cells; neurons (specialised for electrical and chemical signalling over long distances) and neuroglia (supporting cells essential in developing the human brain).

Neurons are cells responsible for processing and transmitting signals within the human brain. They comprise of a cell body with dendrites, an axon usually covered by myelin and the terminals of the axon (Fig. 1.1).[2] Neurons can be classified as:

1. Local circuit neurons or interneurons, which have typically relatively short axons
2. Afferent neurons, which carry information to the central nervous system.
3. Efferent neurons, which carry information away from the central nervous system.

Signals travel by electrical current starting on the dendrites and travelling along the axon to the terminals where, typically, they are transformed into a chemical signal (Fig. 1.1).[3] The number of signals that a neuron receives depends on the complexity of its dendritic arbor,[1] (*i.e.* the larger number of dendrites results in the cell body being innervated by a larger number of other neurons).

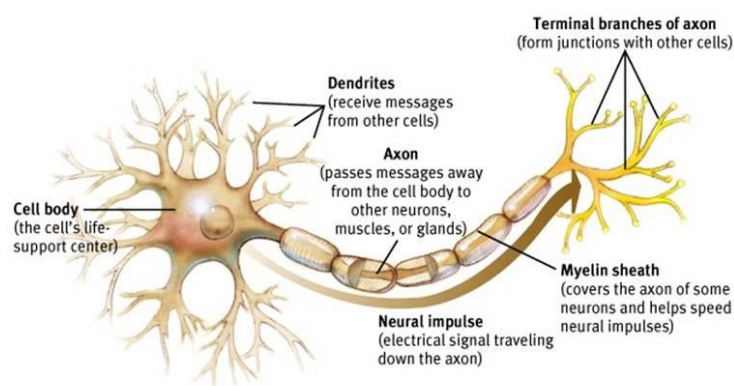***Figure 1.1*** *Labelled diagram representing the structure of a neuron* [2]

Typically, neurons lie adjacent to one another with no physical continuity; the extracellular space between each terminal is known as the synaptic cleft, thus the presynaptic and postsynaptic neurons communicate chemically via the secretion of molecules known as neurotransmitters.[1] As each impulse reaches the terminal of the presynaptic neuron, one or

more neurotransmitters, are released transporting the corresponding message across the synapse to the postsynaptic neurons to influence biological activity around the body.

Chemical synapses are the most common, releasing chemical messengers by means of communication, however electrical synapses also exist.

1.1.1 The Central Nervous System (CNS)

The nervous system can be differentiated based on general function and anatomical distinction.

General function categorises the nervous system based on the sensory system (processes information from the environment, including visual and auditory senses), the motor system (responds to such information by generating movement or behaviour) and the associational systems (mediate the most complex brain functions).[1]

This can then be further characterised into two main anatomical distinctions; the central nervous system (CNS) and the peripheral nervous system (PNS) (Figure 1.2). [4] The CNS includes the brain and the spinal cord, whereas the PNS includes sensory neurons linked to receptors at the body surface or deeper within the brain, motor axons connecting the brain and the spinal cord to skeletal muscles, and cells and axons that innervate smooth muscles, cardiac muscles and glands.[1]
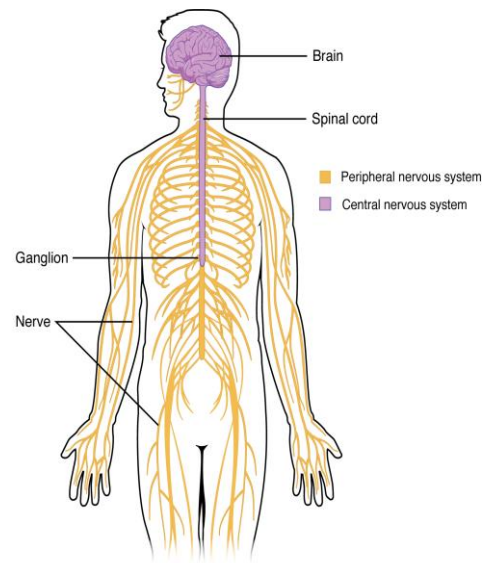
Figure 1.2 *Schematic diagram displaying a visualisation of the central nervous system and the peripheral nervous system* [4]

1.2 Synaptic Transmission

The most common type of synapse within the nervous system is the chemical synapse which functions through the release of neurotransmitters from synaptic vesicles. These neurotransmitters produce a secondary current flow by activating a specific receptor on the postsynaptic neuron, leading to a biological response.

As described by Dale Purves George *et. al* in the 2004 edition of Neuroscience, the stages in the signal transmission at the chemical synapses can be illustrated as follows:[1]

"1. Firstly, an action potential arrives at the terminals of the presynaptic neuron.

2

2. This change in membrane potential results in the opening of voltage-gated calcium ion (Ca^{2+}) channels.

3. The abrupt concentration gradient of the Ca^{2+} across the presynaptic membrane causes a rapid influx of the Ca^{2+} into the terminal.

4. The sudden increase in Ca^{2+} causes the synaptic vesicles to move to the axon terminals and fuse to the membrane releasing their content to the synaptic cleft. This process is known as exocytosis.

5. The freed neurotransmitters diffuse across the synaptic cleft, binding to specific receptors in the postsynaptic membrane, changing the ability of the ions to flow in to (or out of) the cells.

6. The resulting neurotransmitter-induced current alters the conductance and the membrane potential of the postsynaptic neuron and increases or decreases the probability that the postsynaptic neuron will produce a new action potential."

Whether the postsynaptic action of a particular neurotransmitter is excitatory or inhibitory is determined by the nature of the neurotransmitter, the ionic permeability of the ion channel and the concentration of the permeant ions inside and outside of the cell.[1]

Due to the rapid and dynamic nature of the events during synaptic transmission, the production and transport of the secretory vesicles from the cell body, to transport the necessary neurotransmitters, is far too slow. The time between the Ca^{2+} influx and exocytosis in the nerve terminal is very short (from μs to ms).[5] Thus, the synaptic vesicles are fused with the plasma membrane to be rapidly recycled via a clathrin-mediated process of endocytosis.[5]

1.2.1 Neurotransmitters

According to Kolb and Whishaw, the four experimental criteria used to characterise neurotransmitters are:

"1. The chemical must be synthesised in the neuron or otherwise be present in it.

2. When the neuron is active, the chemical must be released to produce a response.

3. The same response must be obtained when the chemical is experimentally placed on the target cell.

4. A mechanism must exist for deactivating the chemical when the reaction is complete." [3]

Using these criteria, researchers have been able to categorise the thousands of chemicals in the brain and isolate the neurotransmitters.

The neurotransmitters identified to date can be divided into three main categories: small-molecule neurotransmitters (SMNTs), neuropeptides and transmitter gases. SMNTs are mostly synthesised and packaged in the axon terminals and act relatively quickly at the synapses. This category mostly includes amines and amino acids. The classical SMNTs include acetylcholine (ACh) and monoaminergic NTs such as noradrenaline and dopamine.

Neuropeptides are multifunctional chains of amino acids that act as neurotransmitters. The process of transmitting information is relatively slow in comparison to that of the small-molecule neurotransmitters as they are mostly produced on the cell's ribosomes, packaged by Golgi bodies and transported on the microtubule highway to the axon terminal.[3] These include opioids and enkephalins.

Transmitter gases are the water-soluble gases such as nitric oxide (NO) and carbon monoxide (CO) and they are synthesised only when needed. Each gas diffuses from the site where it was made (*i.e.* the dendrites), easily crossing the cell membrane and immediately becoming active.[3]

1.2.2 Catecholamines

Catecholamines are organic compounds consisting of a catechol moiety and an alkylamine side chain. They function in the human body as neurotransmitters and hormones as SMNTs. Examples of these catecholamines include dopamine, serotonin, adrenaline and noradrenaline. The pathway of the biosynthesis of these catecholamines was hypothesised by Hermann Blaschko in 1939 and confirmed in the 1950's by Sydney Udenfriend using isotope experiments.[6] Tyrosine hydroxylase was the last enzyme to be identified by Toshiharu Nagatsu, that participates in this biosynthesis (Fig.1.3).[7,8]
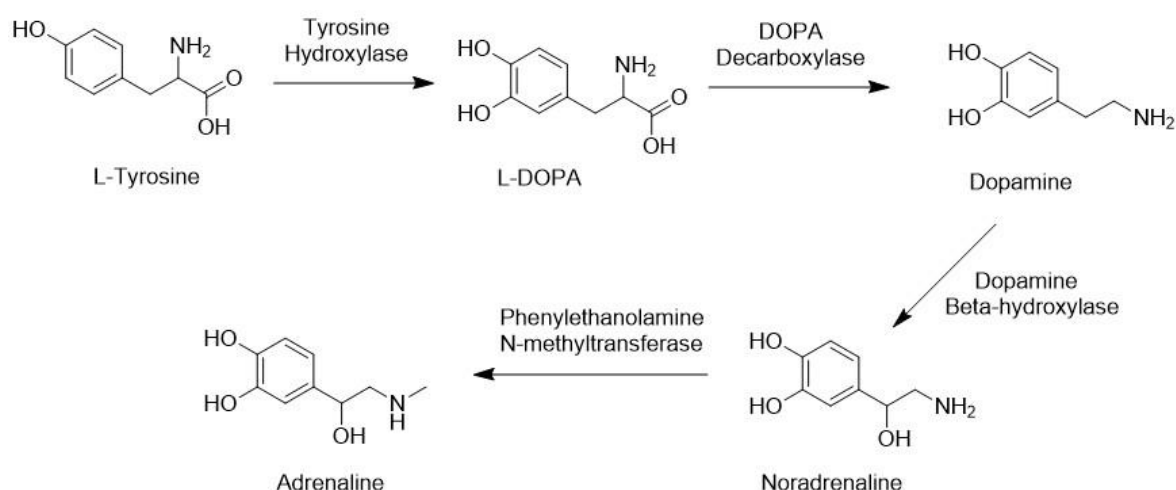

Figure 1.3 Reaction scheme for the biosynthesis of catecholamines

Tyrosine hydroxylase is the rate-limiting enzyme participating in the biosynthesis of the catecholamines found in neurons and endocrine cells. It uses molecular oxygen and

tyrosine as its substrate to synthesise L-3,4-dihydroxyphenylalanine (L-DOPA), in the cell's cytoplasm.[5] Whilst remaining in the cytoplasm, L-DOPA gets decarboxylated by the DOPA decarboxylase to form dopamine. This enzyme is also efficiently used to convert 5-hydroxytryptophan (5-HTP) to serotonin (5-HT).

From here, the dopamine neurotransmitter is taken up into the synaptic vesicle by proteins known as vesicular monoamine transporters (VMAT). VMAT's ability to transport neurotransmitters is highly dependent on the energy available and the Na^+ gradient of the neuronal membrane.[5] Within the vesicles, dopamine β-hydroxylase (DBH) catalyses the synthesis of noradrenaline. As a result of an appropriate stimulus (Ca^{2+} influx), the vesicles transport to the end of the axon, fuse with the membrane and release noradrenaline into the synaptic cleft.[9] This released noradrenaline activates the various adrenoceptors in the presynaptic ($α_2$-AR and $β_2$-AR) and postsynaptic ($α_1$-AR, $β_1$-AR and $β_2$-AR) membranes causing the appropriate post-synaptic reactions. Such reactions include protein kinase activation, protein phosphorylation or metabolism by catechol-O-methyl transferase (COMT).
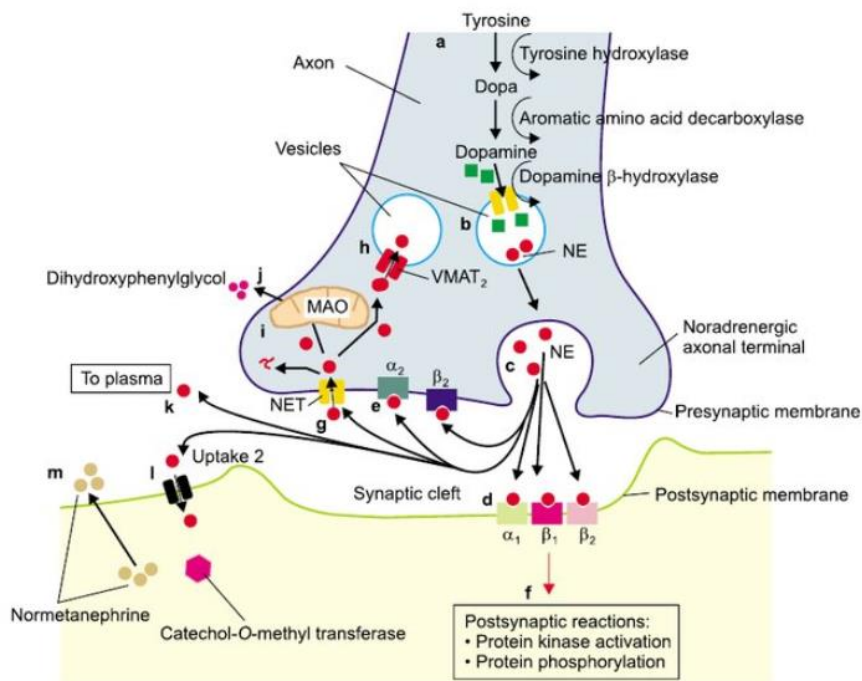
Figure 1.4 *Diagram of a noradrenergic axonal terminal showing the release and reuptake of noradrenaline (NA)* [9]

Adrenaline is one of the major hormones of the sympathetic nervous system.[10] It is classified as a hormone in comparison to noradrenaline, which is a neurotransmitter, because it is primarily produced in the adrenal glands and functions peripherally.[11] When produced in the synaptic vesicles, adrenaline is transported back into the chromaffin granules for storage.[5] Phenylethanolamine *N*-methyltransferase (PNMT) is the enzyme used by the body to catalyse the biosynthesis of adrenaline from noradrenaline. It is found primarily in the

adrenal medullary cells but also in neurons within the CNS that use adrenaline. Adrenaline is best known for the evolutionary survival instinct, the "fight-or-flight" response which is initiated in the brain when the eyes or ears register a threat. The sympathetic nervous system is then activated by the hypothalamus, resulting in a cascading effect through the body and finally the release of adrenaline into the bloodstream from the adrenal glands.[12]

There are several possible fates of catecholamines in the CNS after they have been released back into the synapse from the postsynaptic cleft. The first possible fate is the catecholamine reuptake into the presynaptic neuron by means of the noradrenaline transporter and once in the neuron cytoplasm they can be stored in the vesicles again, where they are transported by the VMAT2.

The second is the metabolism of the neurotransmitters carried out by the monoamine oxidase (MAO) and COMT enzymes (*Fig.* 1.5). MAO is a flavin-containing enzyme located on the outer membrane of the mitochondria.[5] It functions to oxidatively deaminate catecholamines to their corresponding aldehydes and removing neurotransmitters such as noradrenaline and serotonin from the brain.[5] MAO exists as an A- and B-subtype, where the A-subtype preferentially metabolised noradrenaline and serotonin and the B-subtype metabolises tyramine and benzylamine. COMT functions similarly to MAO by producing the carboxylic acid through methylation and oxidation of the catecholamine, respectively.[5] It is a ubiquitous enzyme observed in microorganisms, plants and animals.[13] COMT exists as soluble (S-COMT) isoforms, which predominantly exists in the peripheral tissues, and membrane-bound (MB-COMT) isoforms, which is predominantly expressed in the mammalian CNS.[14] The final product of both MOA and COMT metabolism of catecholamines, is a carboxylic acid which can be excreted in urine.
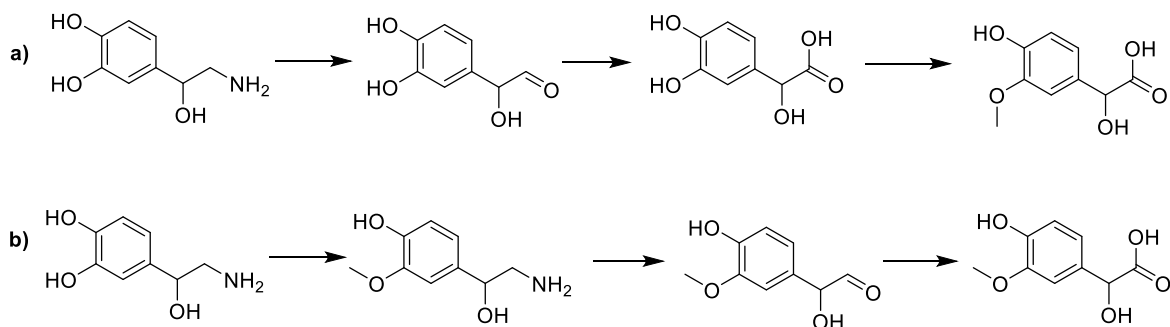

Figure 1.5 *(a) MAO metabolism and (b) COMT metabolism of noradrenaline*

The third possible fate of noradrenaline, when released from the synapse, is to interact with the different post-synaptic and pre-synaptic noradrenergic receptors to transmit the corresponding signal.

1.3 Adrenergic Receptors

In general, neurotransmitters' receptors can be divided into two main categories; ionotropic receptors for direct effect and metabotropic receptors for indirect effect.

Ionotropic receptors allow the movement of charged atoms across the cell membrane when the membrane's charge fluctuates. These receptors are ion channel receptors that contain a binding site for the neurotransmitter and a pore for the ions to travel through.[3]

The metabotropic receptors, such as the adrenergic receptors, consist of a single protein that spans the cell membrane with the neurotransmitter binding site.[3] These receptors are all associated to a guanyl-nucleotide-binding protein (G-protein) hence being called G-protein coupled receptors (GPCRs). The comparative slowness of metabotropic receptor action reflects the fact that the signal is transmitted by multiple proteins sequentially to produce the final physiological response.[1]

1.3.1 G-Proteins and G-Protein Coupled Receptors

GPCRs have a high pharmacological importance as 30% of all commercial drugs act by binding to these receptors.[15] The receptor is embedded within the cell membrane in such a way that the peptide chain in the alpha-helix secondary structure winds back and forth seven times connected by loops. Thus, GPCRs are described as seven transmembrane (7-TM) domains, where each of these 7-TM helical sections are hydrophobic and are numbered I – VII starting from the N-terminal (Fig. 1.6).[16,17] Additionally, the loops that connect the TM domains are labelled according to whether they are outside or inside the cell; thus, extracellular loops are called exo(1-3) and the intracellular loops are labelled endo(1-3).
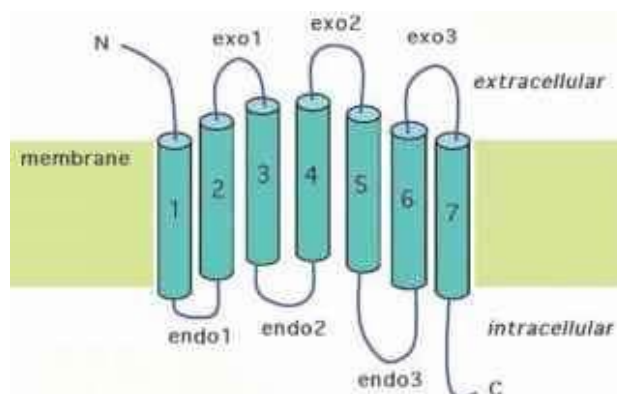

Figure 1.6 *General structure of GPCRs including the 7-TM numbering I-VII, starting from the N-terminal. The extracellular loops are labelled exo(1-3) and the intracellular loops labelled endo(1-3)* [16,17]

In general, the binding site for the neurotransmitter tends to be on the extracellular side of the receptor whereas the G-protein binding site is on the intracellular side and involves the C-terminal chain and part of the variable intracellular loop (labelled endo3 in Figure 1.6).[15] The binding site for the neurotransmitters can vary for each type of GPCR. For example, the aminergic binding site associated with small molecule ligand binding tends to be deep within a binding pocket between the TM helices but the binding site for the larger peptide ligands would be closer to the surface as they require far more space and cannot enter deeply into the 7TM bundle.[18]

As mentioned, G-proteins are membrane-bound proteins constructed of three subunits (α, β, γ). The α-subunit has a binding pocket that binds to the guanyl-nucleotides and guanosine diphosphate (GDP) when in its resting state.[15]

The general activation of the GPCR and their signal transduction are as follows (Fig. 1.7):[19]

   i) The neurotransmitter, or agonist, binds to the receptor. The induced fit causes the receptor to change shape revealing the binding site for the G-protein on the inner surface.
   ii) The trimeric G-protein, containing GDP, binds to the receptor triggering a further shift in the proteins structure.
   iii) This causes an exchange of GDP for guanosine triphosphate (GTP) at the α-subunit.
   iv) The final conformational change of the G-protein weakens the links between the subunits and releasing an α-monomer containing GTP and a βγ-dimer.

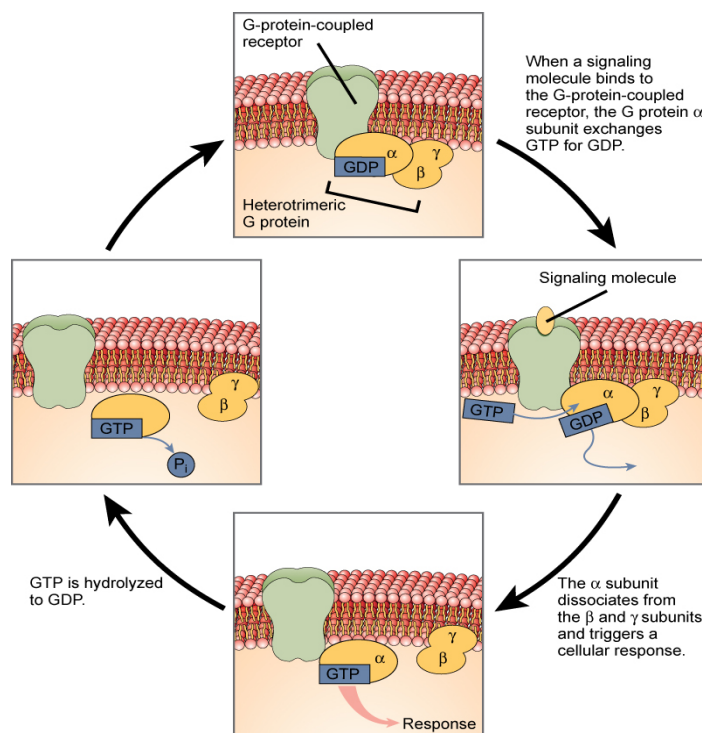***Figure 1.7*** *Visual representation of the signal transduction of a GPCR* [19]

There are three main subtypes of the G-protein; G_i/G_o, G_s, G_q/G_{11} with four possible α-subunits. The α_s-subunit stimulate adenylate cyclase (AC) whereas the α_i-subunit inhibits AC and activates potassium (K^+) channels. The α_o-subunit activates the receptors that inhibit neural Ca^{2+} channels and the α_q-subunit activates phospholipase C (PLC).[15]

The many different receptor-protein variations can lead to different biological responses. For example, adrenaline acts on the $G_{i/o}$ linked α_2-adrenoceptor (α_2-AR) leading to a contraction of smooth muscle.

1.3.2 α_2-Adrenoceptors

Adrenergic receptors, also known as adrenoceptors (AR), are described as GPCR 7-TM proteins, existing as α- and β-subtypes. They function as biological targets for the endogenous catecholamine agonist, adrenaline and noradrenaline, resulting in a variety of controlled biological responses.

In 1905, the existence of such "receptive substances" that bind drugs or transmitters onto the cells initiating a chemical response was first published in the *Journal of Physiology* by John Newport Langley.[20] Soon after, Paul Ehrlich proposed that these receptors were selective leading to the inspiration for his famous *side-chain theory*.[21] It was John Jacob Abel, in 1897, who successfully isolated adrenaline, leading to W. B. Cannon's *fight or flight theory* in the early 1900's.[22] Here he identified two chemical transmitters, sympathin E (which was excitatory in function) and sympathin I (which was inhibitory). However, it was not until 1948 that Raymond Ahlquist identified two distinct *adrenotropic* receptors (α and β), now known as adrenergic receptors, describing the actions of adrenaline and the idea was established that a single sympathetic mediator produced excitatory and inhibitory responses in each receptor.[23]

The β-ARs have now been categorised into three subtypes (β_1-, β_2- and β_3-AR). With the β_2-AR being one of the most extensively studied ARs, it was the first to have its X-ray crystal structure solved aiding with further research of the various subtypes of α- and β-ARs such as by means of computational studies.[23,24] However, the β_2-AR shares only 50% homology with the α_2-AR. Thus, the more recent advancements in 2019 made by Lu Qu *et al.*[25] and Chen *et al.*[26] via the resolution of the crystal structure of the α_{2A}-AR and α_{2C}-AR subtype proved auspicious for this area of research.

The β-ARs are central to the overall regulation of cardiac function with β-AR stimulation being a primary control point for modulation of heart rate and myocardial contractility.[23] However, the β_3-AR subtype is unique as it is primarily associated with metabolic regulations. In a healthy heart, the β-AR downregulation appears to be specific to the β_1-

subtype, the extent of which correlates with the severity of the heart condition. Furthermore, a correlation between aging and lower levels of the β_1-AR subtype has been observed.[23]

In 1974, it was proposed that the α-AR should be subdivided into different subtypes: the α_1-ARs, which tend to be postsynaptic receptors found on vascular smooth muscle; and α_2-ARs which are predominantly associated with the presynaptic receptors and widely distributed across the CNS.[27] Each of these receptors further differentiated in 3 subtypes; α_{1A}, α_{1B}, α_{1D}, and α_{2A}, α_{2B}, α_{2C}. The α_{1C}-AR was removed as it demonstrated gross similarities to the α_{1A} and thus, was recategorized as the α_{1A} or $\alpha_{1A/C}$. The α_1-AR couples with the $G_{q/11}$ proteins but the information on the exact role of each subtype is mostly limited to the receptors expressed in the vascular smooth muscles.[28]

The α_2-AR is linked to the G_i-protein which α_i-subunit inhibits the activation of adenylate cyclase; thus, preventing the formation of cAMP (which is required to open the ion channels through which Ca^{2+} can enter the neuron). As aforementioned, the influx of Ca^{2+} activates calmodulin inducing the exocytosis of the noradrenaline-containing synaptic vesicles thus releasing noradrenaline into the synaptic cleft.[3] Therefore, the prevention of cAMP formation results in the activation of a negative feedback stopping the release of noradrenaline from the presynaptic neuron. For this reason, the overexpression of the α_2-ARs and the selective increase in the high affinity conformation of the α_2-ARs in the human brain has been linked as a causative factor of depression and other neurological conditions.[29]

To date, the individual pharmacological roles of these α_{2A}-, α_{2B}-, α_{2C}-subtypes is still unknown due to the lack of highly subtype-selective ligands.[29] As aforementioned, until December 2019, only the β-adrenergic receptor existed in a crystal structure, thus the development of subtype-selective compounds has proven challenging. With the localisation of the α_2-AR being on the presynaptic neuron, it is the distribution of each of these subtypes within the body that has been used to further distinguish between them. The α_{2A}-subtype is predominantly distributed across the locus coeruleus, but was also found in the brain stem, cerebral cortex, septum, hypothalamus, hippocampus and amygdala.[30] The α_{2B}-subtype has been identified solely in the thalamus as it is mostly localised in the smooth muscle, whereas the α_{2C}-subtype, similar to the α_{2A}, was distributed predominantly across the basal ganglia, olfactory tubercle, hippocampus, and cerebral cortex.[30] This distribution profile indicates that when carrying out the pharmacological studies related to the treatment of brain disorders such as major depressive disorder and schizophrenia, the main focus should be on the α_{2A}- and the α_{2C}-subtypes.

1.4 Pharmacological Evaluation of Ligands of α$_2$-AR

In vitro pharmacological studies are a vitally important phase of the drug discovery process and are used to experimentally assess the *affinity* and *activity* of a ligand to the α$_2$-ARs.

The *affinity* of a drug for a receptor is a measure of how strongly that drug binds to the receptor. In the Rozas group, the compound's binding affinity for the receptor (K_i) is measured using a radioligand competition binding assay in the human brain PFC tissue in collaboration with the group of Prof. Callado (Department of Pharmacology, University of the Basque Country UPV/EHU, Centro de Investigacion Biomedica en Red de Salud, Mental, CIBERSAM, Spain). This is done using the standard α$_2$-AR radioligand, [^{3}H]RX821002, of known affinity and testing it against varying concentrations of the sample compound.[31] The displacement of the standard ligand can be measured using a scintillation counter after the incubation period.

The ligand activity describes whether the compound is either an agonist or an antagonist. An agonist is a ligand that binds to a receptor and produces a physiological response. They exist as a full agonist (which reaches the maximal response capability of the system), partial agonist (does not reach the maximal response capability of the system and may act as an antagonist when competing for a receptor in the presence of a full agonist) or an inverse agonist.[32] Some receptor systems display constitutive activity, thus are active in the absence of agonist. An inverse agonist would inhibit this constitutive activity and, as such, is said to display negative efficacy (Fig. 1.8).[32] An antagonist stops/block the effects of an agonist and can be competitive or non-competitive. The competitive antagonists compete against the agonists for the receptor binding sites and their binding is mutually exclusive; however, the non-competitive antagonist can prevent the action of an agonist without influencing its binding.
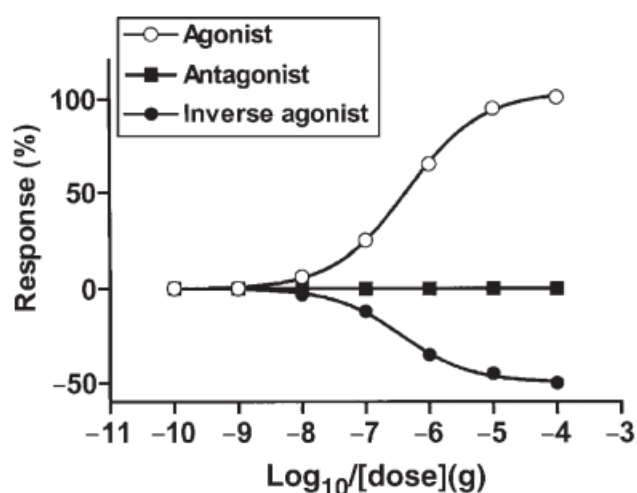

Figure 1.8 *Dose-response curve illustrating the characteristics on an agonist, antagonist and an inverse agonist* [32]

The compound's *activity* as either an agonist or an antagonist in the particular case of the α_2-AR ligands can be determined using a functional binding assay, also referred to as a GTP exchange assay. Direct evaluation of the degree of G-protein activation upon ligand binding can be made by determining guanine nucleotide exchange using radiolabelled analogue of (GTP-γ-[^{35}S]) to observe agonist, antagonist or inverse agonist activity. Here, the phosphodiester bond that links the γ-phosphate to the rest of the nucleotide cannot be hydrolysed to reform GDP, and hence prevents the GTP binding protein from being inactivated, allowing for facile scintillation counting of the radiolabelled analogue. In the case of Callado's group these assays are performed in human PFC tissue.[33]

1.5 Previous Work within the Rozas Group

The Rozas group have been synthesising ligands to target the α_2-AR for over 20 years. These ligands contain the common feature of an aryl guanidinium or 2-aminoimidazolium with varying functionalisation of electron withdrawing or electron donating groups on the aromatic ring. Initially, the work focused on bis-2-aminoimidazolium and bis-guanidinium di-aryl derivatives and these compounds resulted in the discovery of lead compound **1** which shares the same di-aryl core as the previously existing anti-depressants, mirtazapine and mianserin (Figure 1.9).[34] Through pharmacological studies carried out by the Callado group this compound was determined to be a poor α_1-AR antagonist but a potent α_2-AR agonist.[33]

Mianserin
Antagonist, Ki = 4.786 nM

Mirtazapine
Antagonist, Ki = 19.95 nM

Lead Compound **1**
Agonist, Ki = 1.585 nM

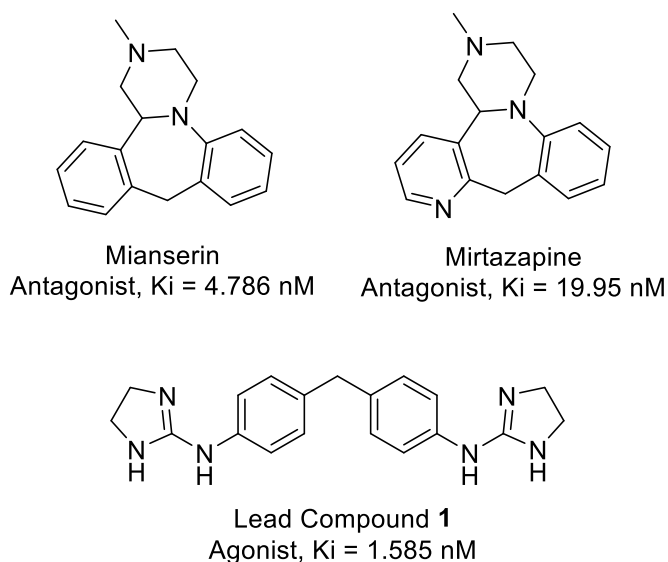**Figure 1.9** *Structure, binding affinity and functional activity of Mianserin[35], Mirtazapine[35] and Lead Compound 1 containing the diaryl moiety*

Based on these positive results, several mono- or bis-cationic molecules were synthesised in their hydrochloride salt form for ease of the pharmacological studies. Two main families of compounds were designed; Family A which contained the diaryl bis-cationic structure and Family B consisted of mono-cationic systems with mono-aromatic cores.
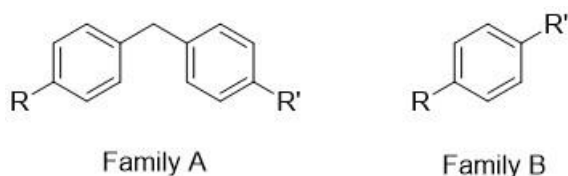
Family A   Family B

Figure 1.10 *General structures for Family A (diaryl bis-cationic) and Family B (mono-cationic with mono-aromatic core)*

Research in Family A resulted in no increase in binding affinity of compound **1**, however, compound **2** (Figure 1.10) was identified as the first di-aromatic molecule of the broad spectrum of molecules that resulted in antagonist activity in human PFC in vitro experiments as well as in vivo experiments in rat by micro-dialysis experiments.[36]
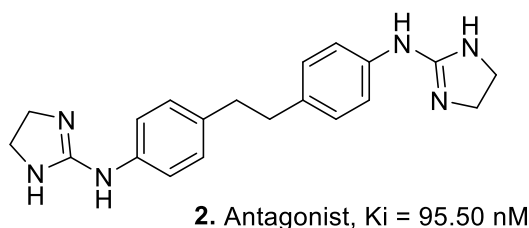

2. Antagonist, Ki = 95.50 nM

Figure 1.11 *Compound **2**, the first twin molecule developed within the Rozas group acting as an antagonist*

Family B research resulted in the preparation and identification of several antagonists with phenyl, pyridyl or thiophenyl cores (Figure 1.11).[37]
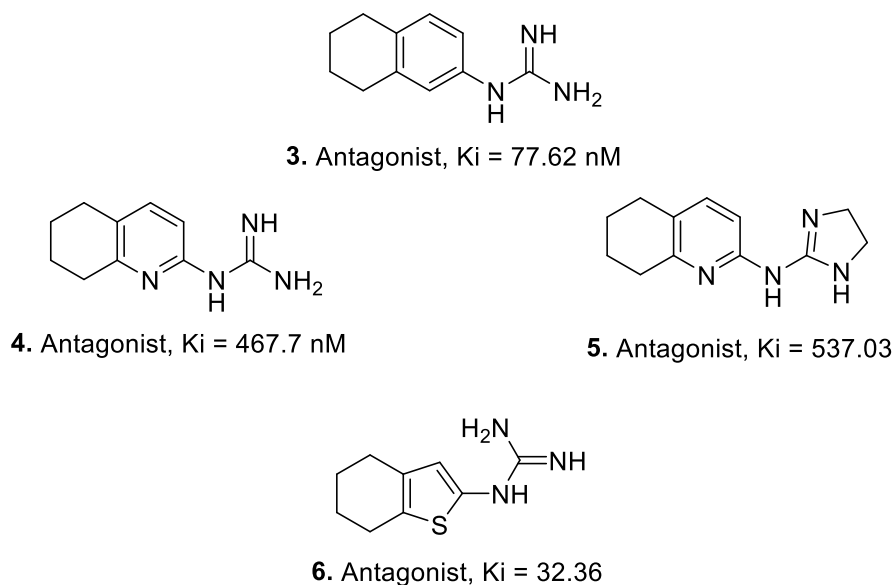

3. Antagonist, Ki = 77.62 nM

4. Antagonist, Ki = 467.7 nM

5. Antagonist, Ki = 537.03

6. Antagonist, Ki = 32.36

Figure 1.12 *Family B mono-aryl guanidinium compounds*

Through computational chemistry, a 3D pharmacophore was developed within the group, incorporating a wide range of antagonist ligands of the α_2-AR and used to design the next generation of compounds. This study demonstrated the importance of an R^2-substitution at the cationic moiety in the form of *N,N'*-disubstituted arylguanidines and 4-substituted-2-

arylimino imidazolines.[29] Thus, a new Family B' focused on the *hit-to-lead* optimization of the previously synthesised compounds. This was done by monitoring the effects of varying the cationic moiety from a 2-aminoimidazoline to a mono- (**8**) or di-substituted (**9**) guanidinium moiety through which the pharmacological studies demonstrated α_2-AR effects. Similarly, the effect of a biosteric change of the aryl core structure (**10** and **11**) was studied through functional assays and microdialysis (Figure 1.12).[38] Thus, introduction of the 2-aminoimidazoline group in the 2-position of the pyridine ring (**10**) resulted in a dramatic drop in binding affinity and accordingly did not advance to the functional assay analysis. On the contrary, when the imidazoline substituent was introduced in the position 3 of the pyridine ring while keeping both substituents *para* to each other (**11**), an increment of binding affinity was observed.
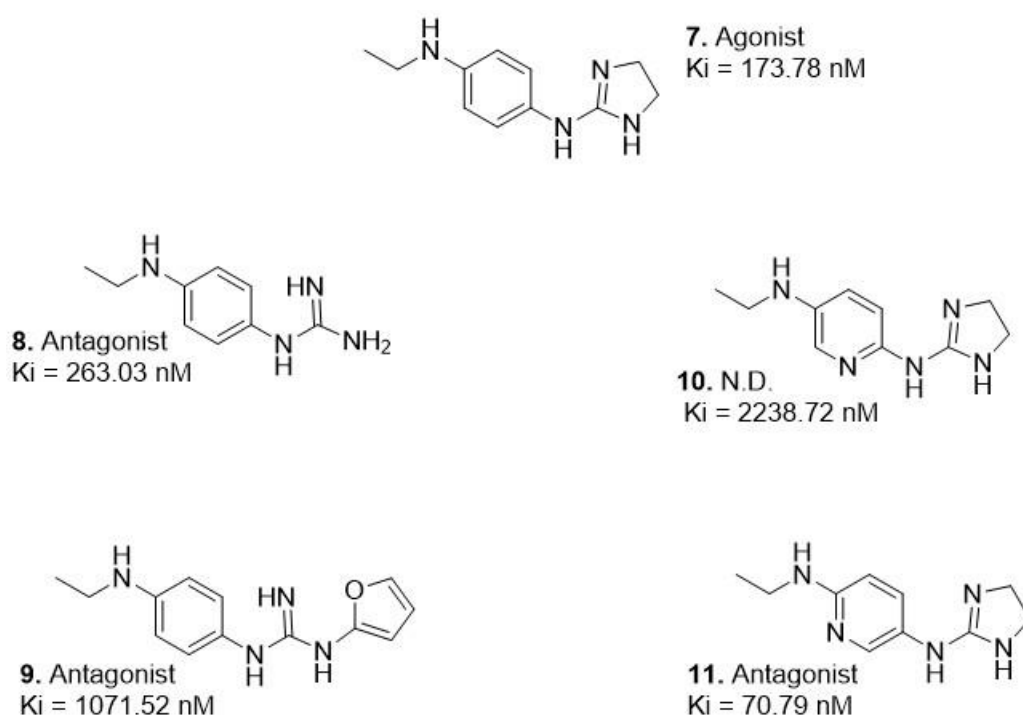

Figure 1.13 *Hit-to-lead optimization through cationic moiety modification and biosteric changes to the aryl core structure of Family B'*

Furthermore, they observed dramatic changes in ligand α_2-AR activity caused by the minimal differences in structural isomers (see an example in Figure 1.13); thus, the minute change of the *N*-ethyl functional group to an *N*-dimethyl group resulted in a change from agonist to antagonist activity and a more enhanced binding affinity.[39,40]
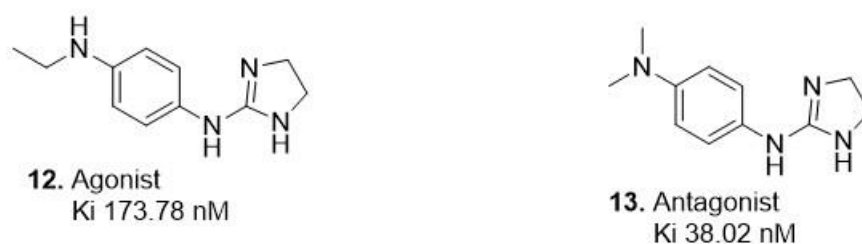

Figure 1.14 *Structural isomers demonstrating the change in ligand activity based on minute changes to the ligand structure, a phenomenon commonly encountered by medicinal chemists*

14

As previously mentioned, Family A consisted of the diaryl *bis*-cationic systems and the best example of this family is the *lead* compound **1**, which is an agonist with a high Ki value (1.585 nM). Thus, following the proposed pharmacophore that involves introducing a second substituent in the guanidinium moiety, a new family A' was developed. Functionalisation assays and microdialysis studies drove to the identification of compound **16** as the antagonist with the most promising binding affinity to date.[39]

1. Agonist, Ki = 1.585 nM

14. Partial agonist, Ki = 1.698 nM

15. Partial agonist, Ki = 13.183 nM

16. Antagonist, Ki =0.794 nM

17. n.d., Ki = 354.81 nM
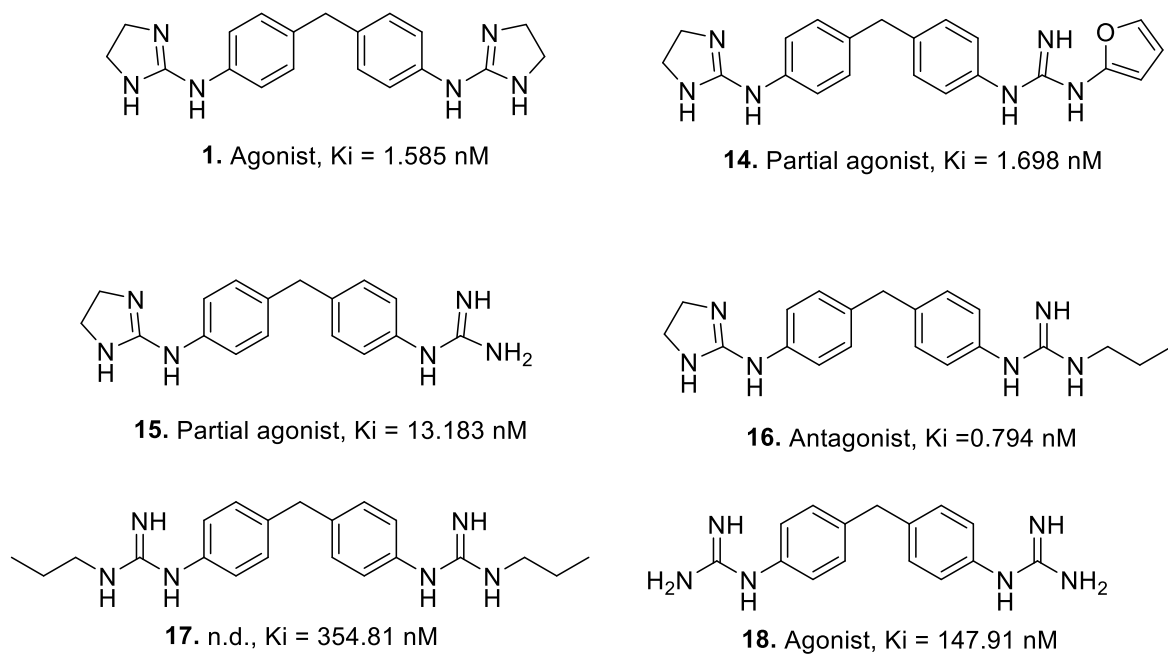
18. Agonist, Ki = 147.91 nM

Figure 1.15 *Family A' demonstrating the high affinity of di-aryl bis-cationic core structure. The functional activity for compound **17** was not determined (n.d.) because the binding affinity was too weak*

2. Objectives

The Rozas group have employed ligand-based drug design to synthesise ligands targeting the α_2-AR for over 20 years. The α_2-AR agonists and antagonists have been proven to be extremely promising in the pharmaceutical industry due to their cascading effect on noradrenergic neurotransmitters. The α_2-AR agonists have found use as anaesthetics (e.g. clonidine), treatments of attention-deficit/hyperactivity disorder (ADHD) and anti-hypertensive agents.[41] Depression is one of the leading causes of illness worldwide and has been closely linked to low concentrations of monoaminergic neurotransmitters in the brain such as noradrenaline. Activation of presynaptic α_2-AR by the endogenous noradrenaline results in a decrease in the release of monoaminergic neurotransmitters. Therefore, the administration of α_2-AR antagonists leads to increased concentrations of brain monoamines and constitutes a viable strategy for the treatment for depression.[42] As a result, the synthesis of an α_2-AR antagonists to block this overexpression of the receptor allowing for the gradual increase of noradrenaline in the synapse is very valuable.

The ligands synthesised within the Rozas group have contained a common feature of guanidinium or 2-aminoimidazolium which are attached to a mono- or di-aryl core structure with varying functionalization of electron withdrawing or electron donating groups. It is regularly observed within the development of GPCR-targeting ligands that a drastic change in functional activity (converting agonists to antagonists, or *vice versa*) stems from really minute changes to the ligands structure. Therefore, the main aim of this research was to investigate the effects on the α_2-AR binding affinity and functional activity when releasing the rigid 2-aminoimidazolium moiety of the *lead* compound (**1**) into *N*-alkyl substituted guanidinium groups, thus affecting steric and lipophilic properties (Figure 2.2). This aim will be achieved via the following objectives: synthesis, computational studies and pharmacological evaluation.

2.1 Synthetic Chemistry

As aforementioned the proposed compounds were chosen based on the current *lead* compound **1**, using a ligand-based drug design strategy. Compound **1** is a diaryl symmetric bis-2-aminoimidazoline with a Ki of 1.585 nM, the highest binding affinity within the Rozas group to date, and it shows agonist functional activity (see Figure 2.2). The imidazoline moiety is a rigid cyclic structure which causes some steric clash when docked into the binding site of the α_2-AR. Through the course of this research, the effects of releasing this cyclic moiety into mono- and di-substituted guanidines probing the binding site of models of the α_2-ARs will be investigated (Figure 2.1).
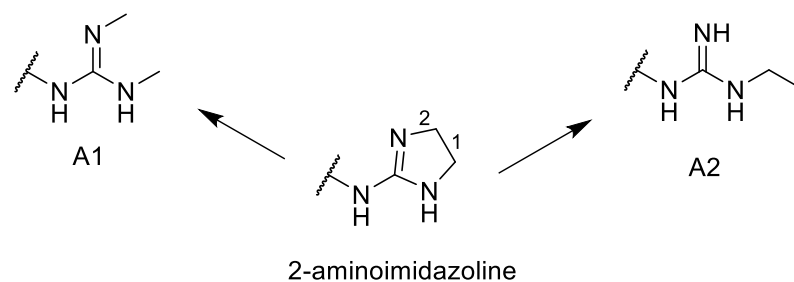
2-aminoimidazoline

Figure 2.1 *Schematic representation of the opening of the imidazoline moiety at location 1 and 2 forming A1 (N,N'-dimethyl-guanidine) and A2 (N-ethyl-guanidine), respectively*

The use of conveniently functionalized thioureas throughout the synthesis originally outlined by the Rozas group[43] will be utilised to synthesise the symmetric bis-guanidine unsubstituted derivatives (R^1 and R^2 = H), mono-substituted and di-substituted derivatives (where, R^1 and R^2 = methyl or ethyl substituents).

Therefore, the following compounds have been proposed based on *lead* compound **1** (Figure 2.2).

Figure 2.2 *The rationale behind the proposed compounds to be prepared and tested against the α_{2A}-AR in vitro. Where, R^1 – R^4 = H / Me / Et*

2.2 Computational Studies

The proposed compounds were theoretically studied to gain an understanding of their conformational and electronic features, and to predict how they would behave in the pharmacological tests with α_2-AR. The introduction of this computational analysis of the desired compounds saves both time and money throughout the drug discovery process and has become known as computer-aided drug discovery.

Freeware tools such as Marvin (ChemAxon) and SwissADME were used to calculate the theoretical values of different physicochemical parameters of these compounds that can have an effect on their drug likeliness. Thus, parameters such as log-P, $pK_{a(H)}$, aqueous solubility or hydrogen bonding descriptors (HB donors and HB acceptors), among others, were calculated.

Moreover, considering that the crystal structures of α_{2A}-AR and α_{2C}-AR were recently reported,[25,26] molecular docking was used to investigate the possible interactions between the proposed compounds and the α_2-AR binding sites. The molecules were prepared using the Maestro software and docked using Glide. The molecules were docked into three different α_2-AR models: α_{2A}-AR-MO (a homology model developed by Prof. Mireia Olivella from the Universitat de Vic in Spain, before any α_2-AR crystal structures were published), α_{2A}-AR-Y (crystal structure of the α_{2A}-AR in complex with a partial agonist), α_{2A}-AR-X (crystal structures of the α_{2A}-AR in complex with an antagonist). The chosen orientations of the docked compounds were based on the ionic interaction with the aspartate residue D113$^{3.32}$ as this has been reported to be a critical interaction with the α_2-AR binding sites.

2.3 Pharmacological Studies

In collaboration with Prof. Callado at the Department of Pharmacology at the School of Medicine in the University of Basque County UPV/EHU (Spain), in vitro pharmacological studies will be carried out of the successfully synthesised compounds to determine their affinity for the α_2-AR (K_i values) and their functional activity on the receptor (agonist or antagonist) in human brain prefrontal cortex (PFC) tissue. These *in vitro* studies can only be carried out if the compounds synthesised are above 95% pure, thus a HPLC analysis will be carried out before sending the compounds to Prof. Callado.

3 Results and Discussion
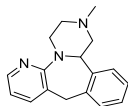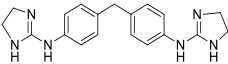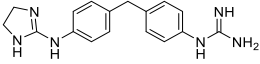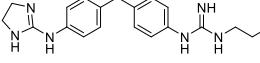
3.1 Physicochemical properties
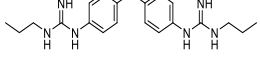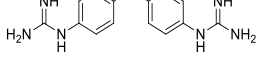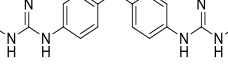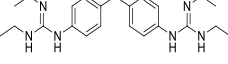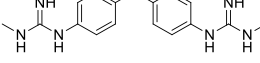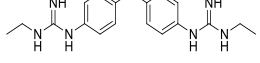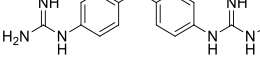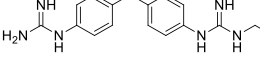
The comprehensive characterisation of physicochemical properties is a critical step in the development of drugs and the theoretical evaluation of these properties and their impact on absorption, distribution, metabolism and excretion (ADME) steps is a suitable approach to assess the drug likeliness of compounds before preparing them.

Physicochemical properties can be calculated to eliminate compounds that are likely to exhibit particular physical or toxicological hazards.[44] These theoretical parameters, which are highly accessible and relatively simple, can allow for a thorough investigation of properties that can lead to a decrease in the failure rate of a compound in the drug discovery process. The pioneering research of using physicochemical properties to determine the high probability of a drug being orally available, is attributed to Christopher A. Lipinski and his development of the "*Rule of five* (Ro5)" general guidelines for oral drug-likeability.[45] Further than those parameters used in the Ro5, there are different fundamental physicochemical properties that can be chosen based on the purpose and fate of the drug. The most common properties include logP, $pK_{a(H)}$, aqueous solubility, Polar Surface Area (PSA), number of rotatable bonds and hydrogen bonding descriptors (HB donors and HB acceptors).

In the present research, a number of physicochemical properties have been calculated for a series of derivatives of the *lead* compound **1** (Tables 3.1, 3.2, 3.3). These derivatives include previously synthesised compounds within the Rozas group (**1**, **15** − **18**), newly synthesised compounds (**19** − **22**, **25**, **28**), and those for theoretically considered for future synthesis and evaluation (**23**, **24**, **26**, **27**, **29** − **32**). This was done using freeware tools such as SwissADME [46] and ChemAxon's Marvin,[47] which rely on both physics-based methods and statistical empirical models such as quantitative structure-activity relationship (QSAR) analysis.
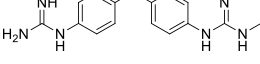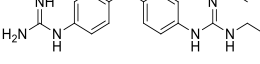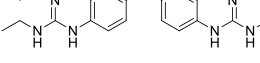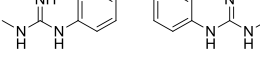
As aforementioned, the *Lipinski Ro5* is a general guideline for the oral drug-likeness of a desired compound. These rules include: the molecular weight of the compound can be no more than 500 Da, no more than 5 hydrogen bond donors and no more than 10 hydrogen bond acceptors must be present in the molecule and the logP must be less than 5. Further expansions on this Ro5 include the Veber rule[48] which states that the topological PSA must be below 140 $Å^2$ and the number of rotatable bonds must be less than or equal to 10. Each of these parameters will be discussed individually in this section; however, the explanation of the theory behind the computational methods used in the determination of the relevant parameters is beyond the scope of this study and thus will not be explained in detail, rather the appropriate reference will be provided.

Table 3.1 *Calculated physicochemical parameters for all target compounds and mirtazapine (M) calculated using SwissADME*

Code	Compound	MW (g/mol)	#HBA	#HBD	Consensus LogP	#Rotatable bonds
M		265.3	2	0	2.27	0
1*		334.4	2	4	1.97	6
15*		308.4	2	5	1.67	6
16*		350.5	2	5	2.76	9
17*		366.5	2	6	3.55	12
18*		282.3	2	6	1.39	6
19		338.4	2	4	2.71	8
20		394.6	2	4	4.00	12
21		310.4	2	6	2.13	8
22		338.4	2	6	2.79	10
23		296.4	2	6	1.81	7
24		310.4	2	6	2.08	8
25		310.4	2	5	2.04	7
26		338.4	2	5	2.70	9
27		366.5	2	4	3.24	10
28		324.4	2	5	2.40	8

29		352.5	2	5	3.04	10
30		324.4	2	6	2.42	9
31		338.4	2	5	2.74	9
32		366.5	2	5	3.36	11

*Compounds previously synthesised within the Rozas Group

3.1.1 HBD, HBA and Rotational Bonds

Each compound described in Table 3.1 demonstrated a molecular weight of less than 500 Da (calculated using OpenBabel[9], version 2.3.0)[46] which is the first of Lipinski's rules that were obeyed. Additionally, the number of HBD and HBA for all compounds studied is also within the limits established in the Ro5 and the number of rotatable bonds is only larger than 10 for compounds **17**, **20** and **32**. To better visualised the fulfilment of the different drug-likeness rules, the hydrogen bond descriptors (HBA – all N and O atoms, HBD – all N-H and O-H groups), molecular weight and number of rotational bonds are displayed in Figure 3.1. From this graph is evident that most of the compounds studied have a good profile in terms of drug-like properties.
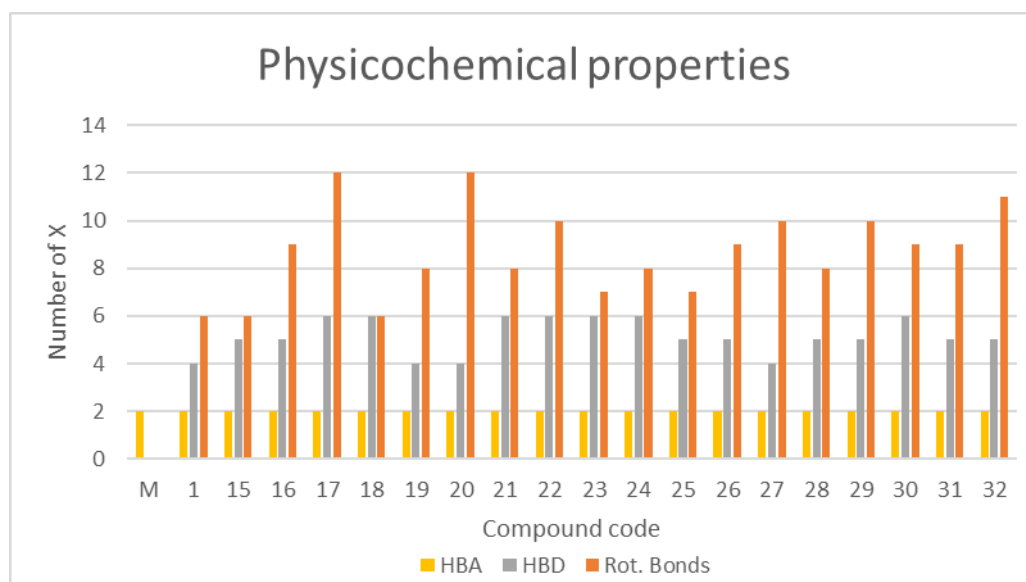

Figure 3.1 *Graphical display of the number of X for each compound, where X is HBA, HBD or RotB*

3.1.2 Lipophilicity (LogP)

Lipophilicity is the affinity of a drug for a lipid medium and can be measured as the partition coefficient (P) that estimates the distribution of a drug between *n*-octanol (the organic phase) and an aqueous phase. This parameter is usually expressed as the LogP and SwissADME applied five different methods of calculating LogP;[46]

1. XLOGP3, an atomistic method including corrective factors and knowledge-based library
2. WLOGP, SwissADME's own implementation of a purely atomistic method based on the fragmental system of Wildman and Crippen
3. MLOGP, an archetype of topological method relying on a linear relationship with 13 molecular descriptors.[49,50]
4. SILICOS-IT, a hybrid method relying on 27 fragments and 7 topological descriptors
5. iLOGP, SwissADME's in-house physics-based method relying on free energies of solvation in n-octanol and water calculated by the Generalized-Born and solvent accessible surface area (GB/SA) model.

As seen in Table 3.1, the consensus LogP has been used for comparison of the compounds studied as it is representative of the mean LogP value of all five calculated results obtained by SwissADME. In accordance with the *Ro5,* each compound listed demonstrated a LogP value less than 5, thus indicating the possibility of the drug becoming a successful orally administered drug. Compounds **18**, **15** and **23** had the lowest Log P values of 1.39, 1.67 and 1.68, respectively and compounds **20**, **16** and **32** had the highest log P values of 4.00, 3.55 and 3.36, respectively. The addition of alkyl functional groups on the guanidinium derivatives increases the lipophilicity of the compound as seen by compound **18** (*bis*-unsubstituted guanidinium derivative, 1.39), compound **19** (*bis*-dimethyl guanidinium, 2.71) and compound **20** (*bis*-diethyl guanidinium, 4.00). Figure 3.2 displays the SwissADME consensus LogP values for all synthesised compounds and the commercially available mirtazapine (M). Due to the binding sites of receptors being hydrophobic in nature, the compounds typically succumb to the hydrophobic effect,[51] i.e. when the hydrophobic molecules prefer to minimise the amount of exposure to the surface area of the surrounding water molecules and thus self-orientate to adopt the appropriate conformation within a hydrophobic environment.
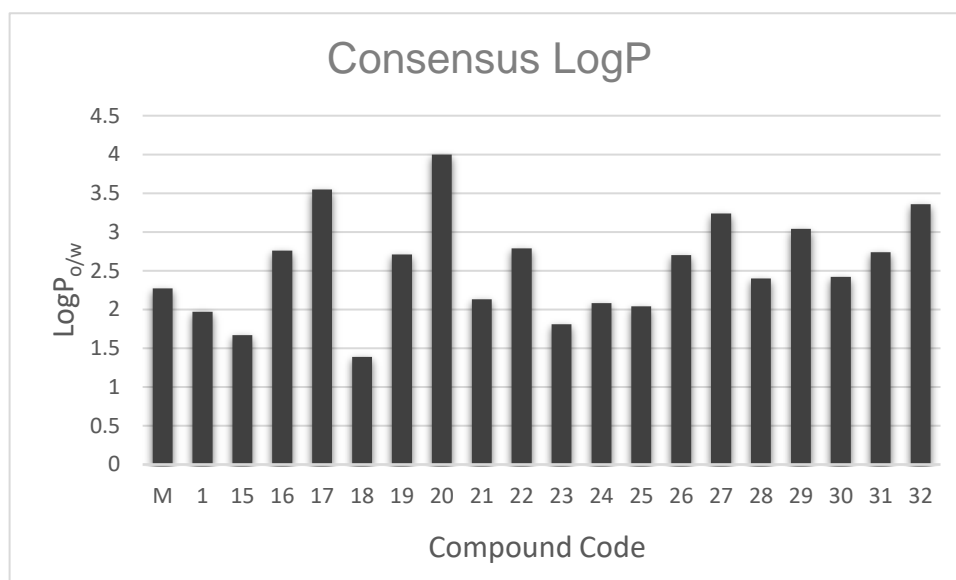
Figure 3.2 *Comparison of all the SwissADME calculated LogP for all the synthesised compounds and mirtazapine (M)*

3.1.3 PAINS and Molar Refractivity

In Table 3.2 other parameters of interest for the druggability of the compounds studied are gathered. For example, the number of pan-assay interference compounds (PAINS) is shown. PAINS are chemical compounds functionalities that are often associated to compounds that give false positive results in high-throughput screens.[52] Figure 3.3 displays sample structures obtained from Capuzzi *et al*. containing multiple high PAINS alerting functional groups. None of the compounds studied contains any of these PAINS.
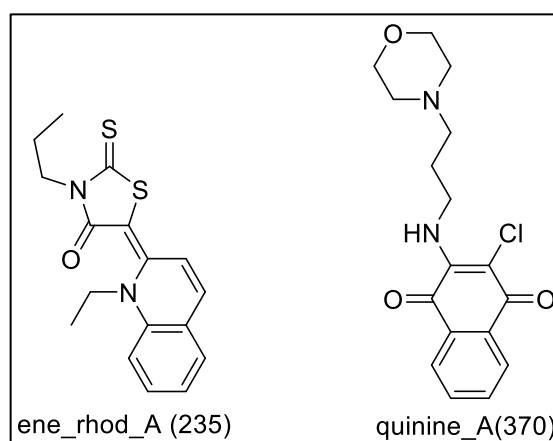
Figure 3.3 *Sample compounds with multiple PAINS alerts taken from Capuzzi et al.* [52]

Another interesting parameter related to drug likeliness is the molar refractivity (MR) which relates the molecular weight, refraction index and density of a compound; the molar refractivity represents not only the real volume of the molecule, but also the dispersive forces that act in the drug-receptor interaction.[53] The optimum MR values to increase the

23

drug-likeness of the compound lies between 40-130.[54] As seen from Table 3.2, each of the synthesised compound's calculated MR values lie within the desired criteria.

Table 3.2. *Calculated physicochemical parameters for all target compounds and mirtazapine (M) calculated using SwissADME (cont.)*

	PAINS alerts	Fraction Csp^3	MR	CYP1A2 inh	CYP2C19 inh	CYP2C9 Inh	CYP2D6 inh	CYP3A4 Inh
M	0	0.35	87.99	X	X	X	√	√
1	0	0.26	116.96	√	X	X	√	X
15	0	0.18	102.03	√	X	X	X	X
16	0	0.30	116.55	X	X	X	X	√
17	0	0.33	116.13	X	√	X	X	X
18	0	0.07	87.10	X	X	X	X	X
19	0	0.26	104.75	X	X	X	X	X
20	0	0.39	123.98	X	√	X	X	√
21	0	0.18	96.91	X	X	X	X	X
22	0	0.26	106.52	X	X	X	X	X
23	0	0.12	92.00	X	X	X	X	X
24	0	0.18	96.81	X	X	X	X	X
25	0	0.18	95.93	X	X	X	X	X
26	0	0.26	105.54	X	X	X	X	X
27	0	0.33	114.36	X	√	X	X	√
28	0	0.22	100.83	X	X	X	X	X
29	0	0.30	110.44	X	√	X	X	X
30	0	0.22	95.82	X	X	X	X	X
31	0	0.26	105.63	X	X	X	X	X
32	0	0.33	115.25	X	√	X	X	√

3.1.4 Fraction Csp^3 and the Cytochromes P450 superfamily

The level of saturation could also have an impact in druggability; thus, the optimal ratio of sp^3 hybridized carbons over the total carbon count of the molecule (Fraction Csp^3) should be at least 0.25.[46] As seen from the calculated values displayed in Table 3.2, compounds **18**, **15**, **23**, **24**, **25**, **28** and **30** fall short of the recommended criteria outlined by SwissADME.

A different aspect on the drug-likeness of a potential drug relays in their metabolic stability. The cytochromes P450 superfamily is responsible to the metabolism of the drug compounds and their elimination from the body. Inhibition of these isoenzymes is certainly one major cause of pharmacokinetics-related drug-drug interactions leading to toxic or other unwanted adverse effects due to the lower clearance and accumulation of the drug or its metabolites.[46,55] Thus, ideally, potential drugs should not be able to inhibit any CYP-type enzyme belonging to the cytochrome P450 superfamily. SwissADME gives an estimate of the potential of inhibition for a series of CYP enzymes and in most of the compounds studied the results show that they will not be able to inhibit these enzymes. Exceptions are compounds **1**, **15**, **17**, **16**, **20**, **27**, **29** and **32** which inhibit one or two of these enzymes.

3.1.5 PSA, BBB permeability and HIA

As mentioned before the Polar Surface Area (PSA) is a very useful parameter to assess drug-likeness of potential drugs since it is related to the ability of compounds to establish HBs which are one of the most usual interactions between drug and target. This parameter is calculated using the fragmental technique known as the topological polar surface area (TPSA),[46,56] primarily considering oxygen and nitrogen as polar atoms and their corresponding hydrogens. TPSA provides results which are practically identical with the 3D PSA (the correlation coefficient between 3D PSA and fragment-based TPSA for 34 810 molecules from the World Drug Index is 0.99).[56] It is a simple measure of the hydrogen-bonding capacity of a molecule through the sum of the fractional contributions to the surface area of all nitrogen and oxygen atoms.[57] Molecules with a PSA less than 140 $Å^2$ tend to have a good permeating ability through cell membranes.[58] According to the results obtained from the SwissADME calculations all the compounds studied are within this limit.

However, for the particular case of molecules to penetrate the blood brain barrier (BBB), a PSA less than 90 $Å^2$ is needed, preferentially between 60-70 $Å^2$.[58] As seen in Table 3.3, mirtazapine has an extremely low TPSA (19.37 $Å^2$) which aids in the crossing of the drug through the cellular membrane of the glial cells in the BBB. Compounds **19**, **20** and **27** demonstrated low enough TPSA values (72.84 $Å^2$ each) to be considered probable candidates for crossing the BBB and target the receptors in the CNS. However, through previous experimental research within the Rozas group it is known that the related bis-guanidines or bis-2-aminoimidazolines can reach the brain.[33]

SwissADME also evaluates the ability of compounds to undergo GI absorption by estimating their potential for human intestinal absorption (HIA). Calculated HIA probability for all compounds studied is shown in Table 3.3 indicating that all compounds have a high probability to be absorbed in the intestine.

Table 3.3. *Calculated physicochemical parameters for all target compounds and mirtazapine (M) calculated using SwissADME and (*) Marvin. [S= soluble, MS= moderately soluble]*

Code	TPSA (Å²)	HIA	BBB perm.	Pgp substr.	pK$_{aH}$*	Ali Solubility Class**	#Heavy atoms
M	19.37	High	√	X	5.36/6.67	S	20
1	72.84	High	X	√	8.36/7.76	S	25
15	98.32	High	X	√	8.00/8.97	S	23
16	84.33	High	X	√	8.03/9.24	MS	26
17	95.82	High	X	√	9.52/8.91	MS	27
18	123.80	High	X	X	9.21/8.61	S	21
19	72.84	High	√	√	9.17/8.57	S	25
20	72.84	High	√	√	9.24/8.64	MS	29
21	95.82	High	X	√	9.42/8.82	S	23
22	95.82	High	X	√	9.46/8.85	MS	25
23	109.81	High	X	√	8.70/9.33	S	22
24	109.81	High	X	√	8.71/9.35	S	23
25	98.32	High	X	√	9.19/8.59	S	23
26	98.32	High	X	√	8.62/9.23	MS	25
27	72.84	High	√	√	9.21/8.60	MS	27
28	84.33	High	X	√	9.32/8.68	S	24
29	84.33	High	X	√	9.34/8.72	MS	26
30	95.82	High	X	√	8.84/9.44	MS	24
31	84.33	High	X	√	9.34/8.69	MS	25
32	84.33	High	X	√	9.36/8.73	MS	27

**[S = soluble, MS = moderately soluble]

3.1.6 BOILED-Egg plot and the permeability glycoprotein (Pgp)

The BOILED-Egg plot (Figure 3.4) presents a correlation between calculated WLogP and calculated TPSA and is an intuitive simultaneous prediction of two key ADME parameters, brain access as BBB permeates or as passive gastrointestinal (GI) absorption.[46] The compounds that are positioned within the white area are likely to undergo GI absorption and

those positioned within the yellow area are likely to be brain permeant. Both compartments are not mutually exclusive, and the outside grey region stands for molecules with properties implying predicted low absorption and limited brain penetration.[46] In addition, SwissADME enables the estimation for a chemical to be a substrate of the permeability glycoprotein (Pgp), which is the most important ATP-binding cassette transporter responsible for an active efflux through biological membranes, e.g. from the GI wall to the lumen or exiting the brain (Table 3.3). ATP-binding cassette (ABC) transporters are a superfamily of membrane proteins that convert the energy gained from ATP hydrolysis into trans-bilayer movement of substrates either into the cytoplasm (import) or out of the cytoplasm (export) and are expressed ubiquitously in all kingdoms of life.[59] Pgp was the first of the ABC transporter family to be discovered in the 1970s as a prototypic transporter involved in multidrug resistance (MDR) of cancer cells.[60] Pgp remains a crucial factor in the drug development process as the expression of this efflux transporter in the GI tract and at the BBB limits oral absorption and CNS entry of many drugs.[60] The graphical classification model provides also a visual representation of whether the compounds are a substrate of these Pgp (Pgp+, blue or Pgp-, red).[46] According to the SwissADME calculations, all of the submitted compounds except compound **1** would efflux back into the bloodstream from the brain by the Pgp. However, from previous research carried out in the Rozas group, it is known that similar bis-guanidine and bis-2-aminoimidazoline derivatives can reach the site of action within the brain. This could be due to the protonation of both guanidinium moieties within the blood (pH 7.4) forming a di-cationic species rather than the neutral form required by the SwissADME programme for the calculations. Another causative factor relating to the transportation of the guanidine-containing derivatives through the BBB could be due to the presence of a carrier transporter as proposed in a webinar given in April 2020 by Douglas Kell. Kell *et al.,* hypothesised that the typical passive diffusion of the lipid bilayer is, in fact, a myth and that the "uptake is mainly determined by biology, not physical chemistry".[61]
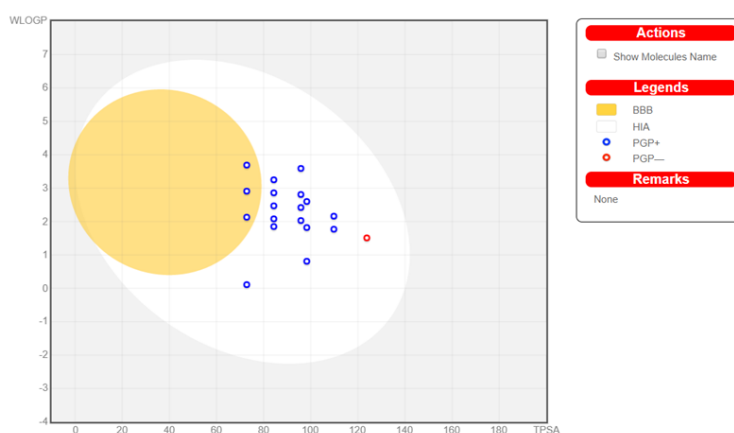

Figure 3.4 *BOILED-Egg plot representing the correlation between WLogP and TPSA. The compounds in the white section are HIA active and those in the yellow area are passive BBB permeates. However, this plot also gives an indication as to whether the compounds are PGP+ (blue) or PGP- (red)*

3.1.7 pK$_{Ah}$ and Water Solubility

To assess the basicity of the compounds studied, the ChemAxon's programme, Marvin, was used to calculate the pK$_{aH}$ values of the guanidinium moieties of the compounds studied. According to the calculated results displayed in Table 3.3, there appears to be a trend in increasing basicity from compounds **21** (pK$_{aH}$ 9.42/8.82), **22** (pK$_{aH}$ 9.46/8.85) and **17** (pK$_{aH}$ 9.52/8.91) as the length of the alkyl chain in the guanidinium increases. This could be due to the increased inductive effect applied as the length of the alkyl chain increases and there is a greater electron donation present, however the differences are miniscule. A similar increase in pK$_{aH}$ is seen from compound **19** (pK$_{aH}$ 9.17/8.57) to compound **20** (pK$_{aH}$ 9.24/8.64). An outlier in this trend is the unsubstituted *bis*-guanidinium compound **15** (pK$_{aH}$ 9.21/8.61) which has a greater pK$_{aH}$ value than the dimethyl-guanidinium derivative **19** (maybe due to the increased steric hindrance for the protonation) and is equally as basic as compound **20**.

The water solubility of a proposed compound is a fundamental factor in drug design and development. A poorly water-soluble drug tends to require a much higher dosing regimen than those which are water soluble when taken as orally administered drugs.[62] The three methods to predict water solubility implemented in the SwissADME programme include: 1) Estimated Solubility (ESOL) model, which was derived from a set of 2874 measured solubilities using linear regression against nine molecular properties,[63] 2) Ali Solubility which is adapted from Ali *et al.*,[64] based on the general solubility equation, replacing melting point with TPSA, and 3) SILICOS-IT which is named after the company that developed it.[46] As seen in Table 3.3, the method chosen for this set of compounds was the one developed by Ali *et al.,* because had demonstrated a strong linear correlation between predicted and experimental values (R^2 = 0.81);[46] in our case, each of the proposed compounds displayed moderate to high solubility properties.

3.1.8 Conclusion

In summary, the physicochemical properties of the compounds proposed for this study were calculated with the help of computational tools. All compounds described met the necessary parameters of drug-likeness (i.e. MW, HBD, HBA, rotational bonds, logP), with the exception of compounds **17**, **20** and **32** with the number of rotational bonds marginally above the desired 10 bonds. Thus, it is suggested that the rest of the compounds may become successful orally administered drugs.

Other parameters of interest for druggability such as PAINS, MR, and metabolic stability of the various compounds were also computed. Thus, none of the compounds studied contains any PAINS, and all compounds calculated MR values lie within the desired criteria.

Regarding cytochrome P450 metabolic related enzymes, the majority of the compounds studied do not inhibit these enzymes, with the exception of compounds **1**, **15**, **17**, **16**, **20**, **27**, **29** and **32** which inhibit one or two of these enzymes.

Moreover, according to the results obtained from the SwissADME calculations all the compounds studied are within the PSA limit for permeating ability to cross de cell membrane. However, for the particular case of molecules to penetrate the blood brain barrier (BBB), compounds **19**, **20** and **27** demonstrated TPSA values too low to be considered probable candidates for crossing the BBB and target the receptors in the CNS (even though there is previous experimental evidence showing that related bis-guanidines or bis-2-aminoimidazolines can reach the brain). Regarding calculated water solubility, each of the proposed compounds displayed moderate to high solubility properties (Table 3.3).

Thus, from the results obtained it can be concluded that the compounds investigated fulfil most of the drug-like properties.

3.2 Synthesis

Over the last 20 years the Rozas group have developed a wide range of *lead* compounds targeting the α_2-AR within the central nervous system to mediate excitatory functions of neurotransmitters. These compounds include mono- and bis-guanidinium or 2-aminoimidazolinium aromatic systems with different affinities towards the various α_2-AR subtypes, primarily the α_{2A}-AR and the α_{2C}-AR which are the subtypes mostly expressed in human prefrontal cortex. Various pharmacological evaluations were carried out to measure the functional activity and binding affinity of the relevant *hit* compounds. Studies within Rozas group carried out by O'Donovan *et al*,[29] and Rodriguez *et al*,[36] showed that the size and lipophilicity of the cation had an impact on the binding affinity of the synthesised compound toward the α_2-AR receptors (Table 3.4).
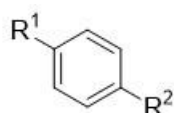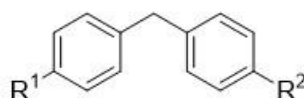
Compound 33 (a - d)   Diaryl backnone for compounds 1, 15, 18

Table 3.4 Binding affinity (displayed in K_i) and functional activity of a range of both mono- and bis-cationic derivatives, previously synthesised and evaluated within the Rozas group

Compound ID	R¹	R²	K_i (nM)	Functional Activity
33a	-NHEt		263.03	N.D.
33b	-NMe₂		87.096	Antagonist
33c	-NHEt		177.83	Agonist
33d	-NMe2		38.019	Antagonist
18			416.87	Agonist
15			13.183	Partial agonist
1			1.585	Agonist

As seen from the results previously obtained within the Rozas group for the mono-aryl guanidine and 2-aminoimidazoline derivatives (compounds **33a/b** and **33c/d** in Table 3.4, respectively), the change in regioisomers from the -NMe₂ to the -NHEt moiety had a large negative impact on the binding affinity toward α₂-AR. This indicated that the increase in steric hindrance caused by the growth in chain length of the ethyl substituent and the decreased lipophilicity of the secondary amine moiety, are crucial factors to be considered when designing future compounds. Furthermore, the improved K_i values observed in previous research when the guanidinium cation was replaced by the 2-aminoimidazolinium cation indicates that the ethylene bridge provides additional contacts for binding to the receptors active site, along with necessary increased lipophilicity while maintaining a

compact structure. Therefore, the objectives of this chapter are to discuss new di-aryl *bis*-cationic compounds with varying alkyl substitutions (*i.e.* mono- and di-ethyl or methyl) on the guanidinium moiety to probe the receptors' binding site and investigate steric and lipophilicity effects on α_{2A}-AR affinity and activity compared to the conformationally restricted 2-aminoimidazoline derivatives previously reported.

Guanidine derivatives have been extensively utilized in the field of medicinal chemistry due to their ability to form a wide variety of interactions within the body, ranging from ionic and H-bonding contacts to π-stacking. In addition, aromatic guanidines have been applied to a diverse range of therapeutic and biological applications. Examples include prevention of hyperglycaemia in diabetes type 2,[65] inhibition of human platelet Na^+/H^+ exchange,[66] anti-obesity and eating disorder regulation,[67] and radiotracers for imaging of Parkinson's disease.[68] The guanidine functional group's high basicity, $pK_{aH} = 13.6$,[69] means that protonation will occur at physiological pH and thus, this functional group has the unique ability to exist as neutral (guanidine), cationic (guanidinium), and anionic (guanidinate) entities, even though in the human body the cationic form will be the prevalent one.[70]

Finally, the Rozas group has focused on the use of guanidine derivatives as α_2-AR ligands for the treatment of CNS disorders such as depression and schizophrenia through regulation of noradrenaline,[29,31,33,71] and as DNA minor groove binders.[72,73] Guanidines in their neutral form are commonly used as strong bases in organic synthesis and the specific H-bonding pattern of its conjugate acid (guanidinium cation) has led to the increased use of guanidine derivatives as catalysts.[70] The increased stability of the guanidinium ion stems from the resonance through conjugation of the nitrogen lone pairs (Figure 3.5) where there is an abundance of H^+ ions available for hydrogen bonding interactions and facilitating its ionic interactions with negatively charged biological systems.
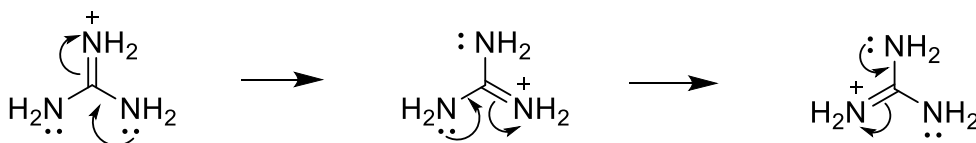

Figure 3.5 *Resonance stabilisation of the guanidinium cation*

The crystal structure of guanidine was finally resolved 148 years after its first synthesis, showing two Y-shaped symmetry-independent molecules in a unit cell, interconnected by a H-bonding network.[74] Furthermore, investigation into the conformational control induced by these intramolecular hydrogen bonds (IMHB) within 2-pyridoguanidine systems have been investigated within the Rozas group,[75] along with the presence of crucial π-cationic interactions due to the aromaticity present within the structure.[76]

3.2.1 Literature methods for the preparation of guanidine derivatives

The vast applicability of guanidines within biological and pharmaceutical sectors as well as building blocks for supramolecular chemistry, synthetic receptors, sensors and catalysis,[77] has increased the demand for multiple synthetic routes towards guanidine derivatives. The most common approach includes the use of thioureas and isothioureas as guanidylating agents reacting with primary, and some secondary, amines. The majority of molecules described in this family of compounds were synthesised – or partially synthesised – via the Kim and Qian method.[78] As described in Section *3.2.2.2*, this method required the coordination of mercury (II) chloride ($HgCl_2$) to the sulfur-containing thiourea, in the presence of triethylamine, to initiate the reaction with primary amines. This method was particularly useful for substrates with weak nucleophilic amino groups.

The use of toxic mercury chloride is undesirable within a chemical reaction, especially when the compound is destined for biological or pharmaceutical purposes. Copper (II) chloride ($CuCl_2$) was also suggested as a possible thiophilic reagent by Kim *et. al,* and thus was later investigated by B. Kelly and I. Rozas.[79] Kelly *et. al.* determined that $CuCl_2$ was equally as satisfactory at producing high yields of the desired guanidine-containing compounds as its predecessor (Scheme 3.1). However, this thiophilic reagent was inconsistent in the activation of various substituted thioureas; this could be due to the fact that Hg^{2+} salts are more thiophilic than Cu^{2+} salts as they have lower LUMO, allowing for antibonding interactions toward sulfur's high energy HOMO.[39] Furthermore, the removal of any excess $HgCl_2$ or the HgS biproduct has been very successful when filtered through a bed of celite, washed and purified via flash column chromatography. Therefore, $HgCl_2$ is still used within the Rozas' group for research purposes, and commonly across other research laboratories.

Scheme 3.1 *Generic reaction scheme for the synthesis of guanidines using CuCl2*
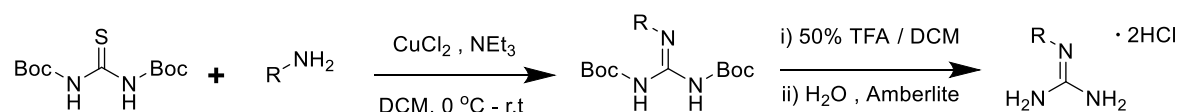
More recently (July 2019), the Kim and Qian method was again modified to replace the toxic $HgCl_2$ with the commercially available oxidant, iodine (Scheme 3.2). This I_2-mediated approach produced the desired guanidine-containing derivatives with a 52-98% yield.[80] The lower yields were generally observed for sterically or electronically deactivated amines, due to the unstable nature of the reactive intermediates.[80] This method was not suitable for any secondary amines that were explored.

*Scheme 3.2 I₂ - mediated guanidylation mechanism for primary amines*
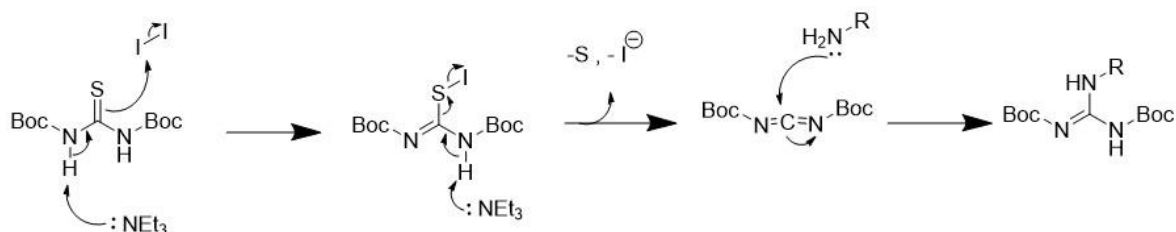
Furthermore, Mukaiyama's reagent has been frequently used as a promoter of the unreactive and sterically hindered aryl amines and the guanidylation of resin-bound amines (Scheme 3.3).[81] Yong *et al.* began their research into the development of a new thiophilic reagent due to the fact that the mercury sulphide biproduct made the Kim and Qian method inapplicable for solid-phase guanidylation. Unfortunately, Mukaiyama's reagent tends to be restricted to mono-substituted guanidylation as bis-Boc-protected thiourea is needed to obtained high yields. Moreover, Mukaiyama's reagent tends to be insoluble in many standard organic solvents resulting in the difficulty of removing any undesired side-products that may have generated.[82]

Scheme 3.3 Reaction scheme illustrating the treatment of bis-Boc-thiourea with Mukaiyama's reagent in the presence of benzylamine with a 91% yield.

Ohara *et. al.*, in 2009, published findings of the positive results obtained for the guanidylation of amines using *N*-iodosuccinimide (NIS) as a replacement promoter for the toxic mercury (II) chloride and Mukaiyama's reagent.[82] This form of reaction allowed for the guanidylation of primary and secondary amines via the use of various thioureas and di-Boc-*S*-methylisothiourea, respectively. According to Ohara *et. al.*, NIS is a source of electrophilic iodine allowing for the stereoselective and regioselective reactions on various functional groups (Scheme 3.4).[82] Furthermore, the proposed mechanism is similar to that of $HgCl_2$ as NIS should react as a Lewis acid and coordinate to the thiourea or *S*-methylisothiourea to initiate the reaction. The addition of the strong base, NEt_3, would lead to the carbodiimide intermediate and thus upon interaction with the chosen amine, the desired guanidine would be obtained.

Scheme 3.4 *Reaction scheme of the NIS-promoted guanidylation of A) primary and B) secondary amines*
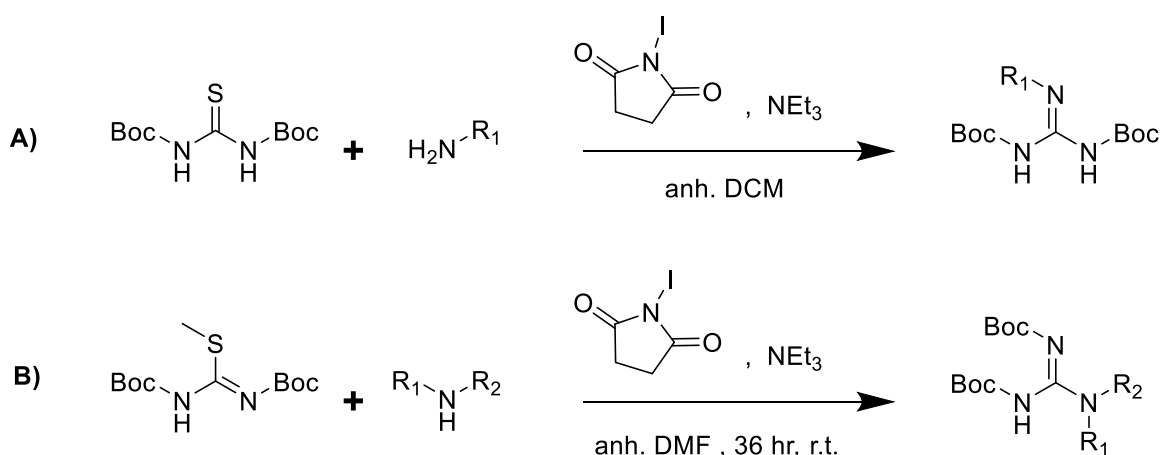
In 2002, Guisado *et. al.* published a new polymer-supported method of guanidylation that avoided the use of the previously non-commercially available promoters that often required a multi-step synthesis. These guanidylating agents include pyrazole carboxamidine and its derivatives,[83] *S*-alkyl thioureas,[84] and *N*-triflyl guanidine.[85,86] Furthermore, these previous methods often required a large excess of the starting amine to reach completion of the reaction if an efficient cleavage, in terms of purity, was required.[87]

This new approach outlined by Guisado *et. al.* combined the benefits of traditional solution phase chemistry with the application of polymeric reagents leading to the desired compounds in high throughput manner, without additional purification steps.[87] Polymer-supported (PS) carbodiimide was chosen as its commercially available as well as the *N,N'*-bis-(*tert*-butoxycarbonyl)thiourea starting material which is readily synthesised in a one-pot procedure with multi-gram yields. For this reaction a base was not necessary, unlike the previous guanidylation methods described and could be carried out in DCM or DMF to achieve high yielding results. PS-trisamine was added to remove the small amounts of bis-(*tert*-butoxycarbonyl)carbodiimide side-product (Scheme 3.5).[87]

Scheme 3.5 *Reaction scheme for the guanidylation of a secondary amine from di-Boc-thiourea in the presence of i) PS-carbodiimide and ii) PS-trisamine for purification*
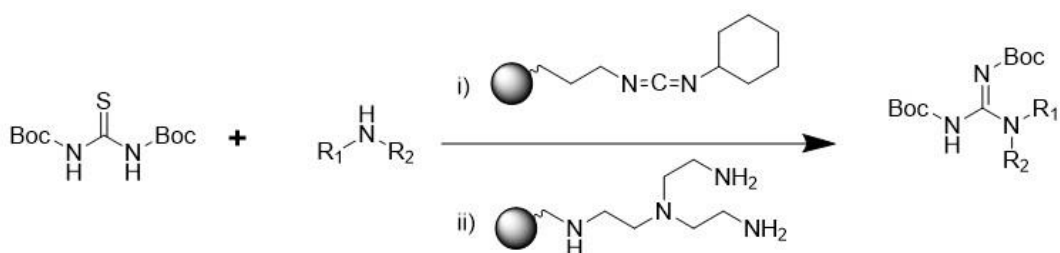
Ultrasound energy has been used commonly throughout chemical synthesis as it assists in the reactions activation via a process known as acoustic cavitation. This process involves the expansion and contraction of small bubbles of gaseous substances which inevitably reach an unstable size and collapse.[88] As these bubbles are small and rapidly collapse, they have been responsible for an enhancement in solubility, diffusivity, penetration and mass transportation of species in certain reactions.[77] Pattarawarapan *et. al.*, investigated the use of ultrasound energy for the guanidylation of a variety of amines, using the inexpensive and easy-to-handle trichloro-1,3,5-triazine (TCT) as the dehydrosulfurization agent, in minimal amounts of solvent (Scheme 3.6). The yields obtained from the reactions were positively increased when the reactions were carried out under sonochemical conditions. Furthermore, it was observed that reducing the ratio of TCT to thiourea to 0.4:1 had little-to no effect on the yields obtained. Primary amines (*e.g.* benzyl- and alkylamines) and the sterically hindered diisopropylamine reacted quickly and in high yield, suggesting that ultrasound energy could be used to overcome steric effects. The reactivity of the carbodiimide is the rate determining factor of these reactions.[77]

Scheme 3.6 *Reaction cycle illustrating the guanidylation process using TCT under sonochemical conditions. n = 1 is the first stage of the cycle. n = 2 is the second stage. n = 3 is the final cycle.*
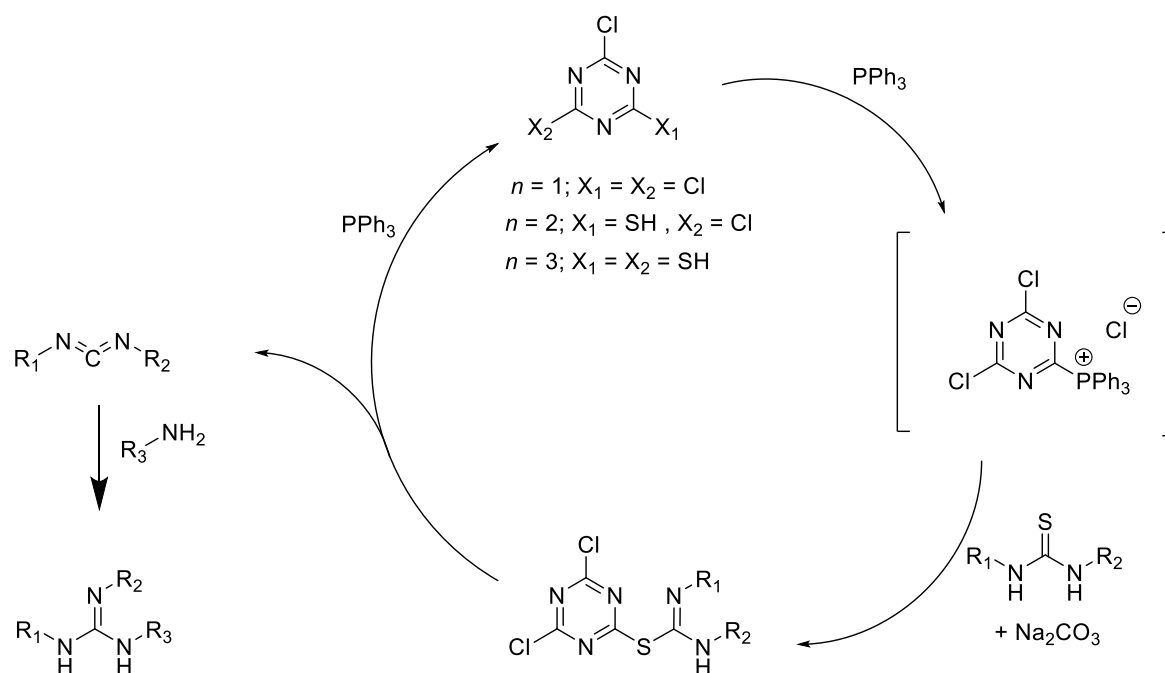
3.2.2 Preparation of the target *bis*-cationic diaryl derivatives

The Rozas group have designed and synthesised a large number of bis-guanidinium/2-aminoimidazolinium derivatives of varying linkers (NH, O, CH_2, CO, SO_2); however, pharmacological testing indicated that none of the tested compounds displayed an α_2-AR

binding affinity stronger than that of the *lead* compound **1**. Thus, the search for an α_2-AR antagonist with a K_i smaller than 1.585 nM continues.

Aiming to identify key structural features involved in the design of the desired antagonist activity, computational studies were carried out in Rozas group. Comparative molecular field analysis (CoMFA) was the 3D QSAR method chosen as it is "based on the assumption that drug–receptor interactions are noncovalent and that changes in biological activity correlate with the changes in the steric and/or electrostatic fields of the drug molecules".[15] Thus, a 3D pharmacophore was identified and hydrophobic extensions at the cationic moiety were determined to theoretically favour antagonist activity.[39] Furthermore, the design of the compounds discussed in this section arose from the addition of the hydrophobic substituents on the guanidinium moiety paired with the di-aryl backbones as they generally afforded higher binding affinities.[39]

The method most commonly utilised within the Rozas group for the guanidylation of alkyl or aryl amines is the Kim and Qian method,[78] which, in our case, involves the reaction of the relevant mono- or di-substituted *N,N'*-bis-(*tert*-butoxycarbonyl)thiourea with 4,4'-methylenedianiline.

3.2.2.1 Preparation of Boc-protected thioureas

Boc-protection of the thiourea is crucial for the mentioned Kim and Qian guanidylation method as it increases the electrophilicity of the carbon aiding the reaction with the poorly nucleophilic aryl-amines. According to these authors, the reaction goes via the initial formation of a highly electrophilic and short-lived bis-Boc carbodiimide intermediate.[78] Furthermore, the addition of Boc groups make the resulting polar products easier to handle and purify via flash column chromatography.

In this project, Boc-protection of the chosen thiourea was a straight-forward, anhydrous reaction in which NaH (60% immersion in oil) activated the relevant thiourea, which was then reacted with di-*tert*-butyl-dicarbonate (Scheme 3.7). The NaH needed to be quenched with NaHCO$_3$ saturated solution before the work-up could commence. However, the commercially available *N,N'*-bis-(*tert*-butoxycarbonyl)-*S*-methylisothiourea could be used instead of the unsubstituted *N,N'*-bis-(*tert*-butoxycarbonyl)thiourea, as a cost-effective and efficient alternative.

Scheme 3.7 *Reaction scheme for the Boc-protection of the thiourea starting materials (compounds 35a, 19a, 20a)*

35a, R = H, 42.6%
**19a, R = Me, 54.7%**
20a, R = Et, 74.6%
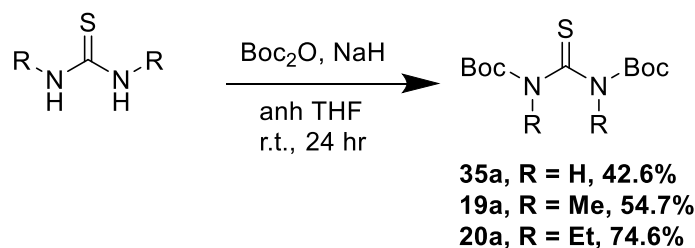
This Boc-protection method was also used to prepare the corresponding *N,N'*-substituted Boc-protected guanidines. However, when the Boc-protection was attempted using the *N,N'*-diethylthiourea there was a single water impurity signal at 1.55 ppm with an integration of 13 H with respect to the 18 H integration of the Boc-signal at 1.51 ppm. With extensive drying on the rotary evaporator and high vacuum over several hours, the water signal reduced but not completely removed. Thus, this thiourea starting material was assumed to be a highly hygroscopic compound. After exhausting time and resources attempting to remove the water impurity, it was decided to carry out the guanidylation reaction to see if there was a major impact on the guanidylation; however, only negative results were obtained (see Section 3.2.2.2).

Considering that this method of Boc-protecting the starting thiourea was unreliable for the *N,N'*-diethylthiourea and the *N*-alkylthioureas as it resulted in multiple side-products and impurities that were very difficult to separate via the usual column chromatography, alternative approaches were investigated.

A different approach was used to prepare Boc-protected *N*-methyl- and *N*-ethyl-thioureas (Scheme 3.8). Thus, Yin et al. had previously reported the preparation of *N*-Boc-*N'*-substituted thioureas by treatment of *N,N'*-di-Boc-substituted thiourea with NaH and trifluoroacetic anhydride (TFAA) in the presence of an amine.[89] They proposed that the anion formed by deprotonation of the di-Boc protected thiourea is *N*-acylated to produce the *N*-Boc-*N*-trifluoroacetyl derivative, which undergoes nucleophilic attack by the amine during the second step (Scheme 3.8).[39]

Scheme 3.8 *Mechanism proposed by Yin et al. for the preparation of mono-substituted N.N'-di-Boc protected thioureas*
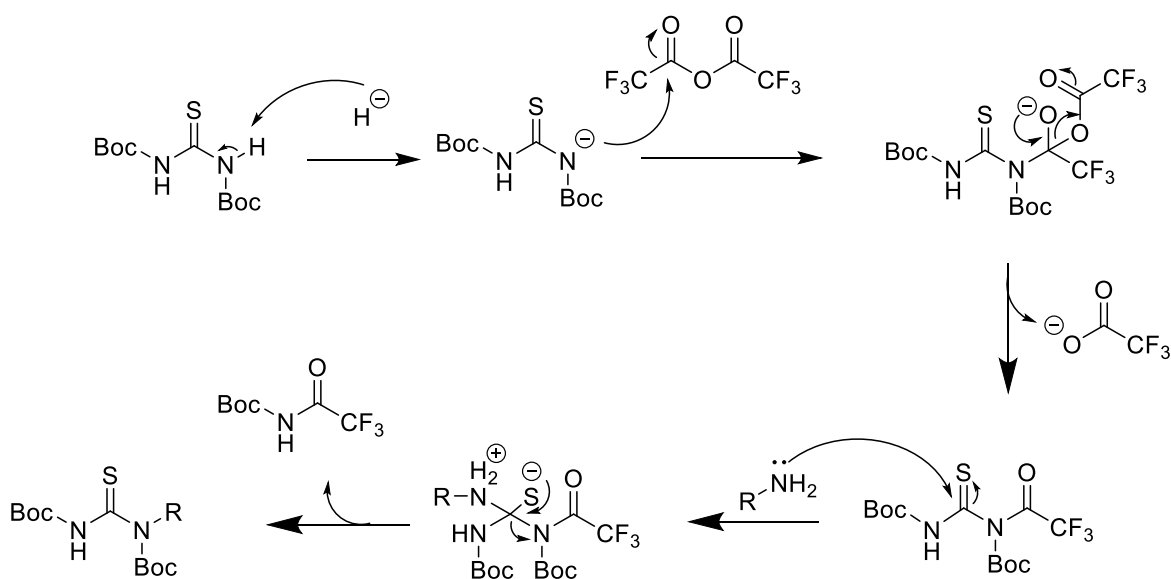
Even though this reaction had been previously used by Rozas group to yield the di-Boc protected *N*-substituted thioureas, in our case, only the mono-Boc protected *N*-methyl thiourea (**24a**) was obtained in moderate yields (~38%) (Scheme 3.9).

Scheme 3.9 *Synthesis of the N-(tert-butoxycarbonyl)-N'-methylthiourea starting material.*

24a, R = Me, 37.6%
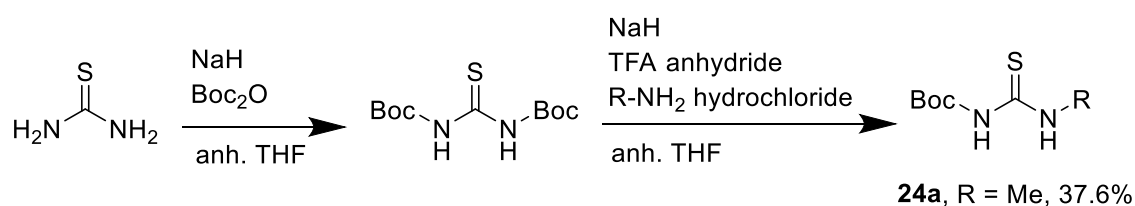
Although the introduction of the alkyl substituent was successful, the mono-Boc-protection was not satisfactory enough to fulfil the requirements of the guanidylation process and the following reaction was unsuccessful. From here, research was carried out to identify a method of synthesising a mono-substituted thiourea that maintained the electrophilicity of a di-Boc-thiourea.

Research uncovered that the Mitsunobu reaction was commonly used for synthesising substituted thioureas from primary and secondary alcohols.[90,91] If successful, this method would provide a mono-substituted pseudothiourea that would also be bis-Boc-protected, thus providing the basis for an easier desulfurization during guanidylation. Moreover, the use of the pseudothiourea leaves only one amine available for alkylation, thus reducing the risk of unwanted side-products forming and purification would be simplified (Scheme 3.10).

Scheme 3.10 Mitsunobu reaction scheme synthesising alkyl substituted thioureas from alcohol, DEAD and PPh₃. Where, R-OH is anhydrous methanol or anhydrous ethanol

21a, R = Me, 80.8%
22a, R = Et, 94.8%
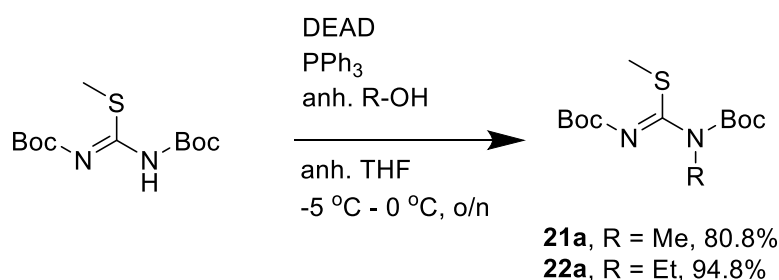
The Mitsunobu reactions are the most widely used stoichiometric phosphorus mediated S_N2 reactions of alcohols with pro-nucleophiles such as carboxylic acids, sulphonamides, imides and thioureas.[92] The reaction has been influential in medicinal chemistry and organic synthesis laboratories due to its broad scope, stereospecificity and mild reaction conditions.[93] In 2015, Camp *et. al.* published research on the solvent effects on the Mitsunobu reaction and it was determined that yields, particularly for sterically hindered alcohols, were often higher in non-polar solvents due to the slower rate of the side reactions making them less competitive. Typically, the rate constant for the formation of ethylbenzoate was 100 times greater when carried out in THF over acetonitrile.[94] This reaction was used for the preparation of *N*-substituted Boc-protected pseudothioureas **21a** and **22a**. The reaction consisted of a one-pot procedure, reacting the appropriate alcohol with pseudothiourea in the presence of diethylazodicarboxylate (DEAD) and triphenylphosphine (PPh₃).

The mechanistic details of the reaction, particularly the intermediate stages, are still subject of debate, but an estimation can be seen in Scheme 3.11.[93] The activation of the alcohol is achieved by the reaction with the Morrison-Brunn-Huisgen zwitterion intermediate (**A**) which is formed *in situ* via the reaction of PPh₃ and DEAD.[92] A zwitterion is a chemical compound that results in both positive and negative charges.

Scheme 3.11 *Suggested mechanism for the Mitsunobu reaction*
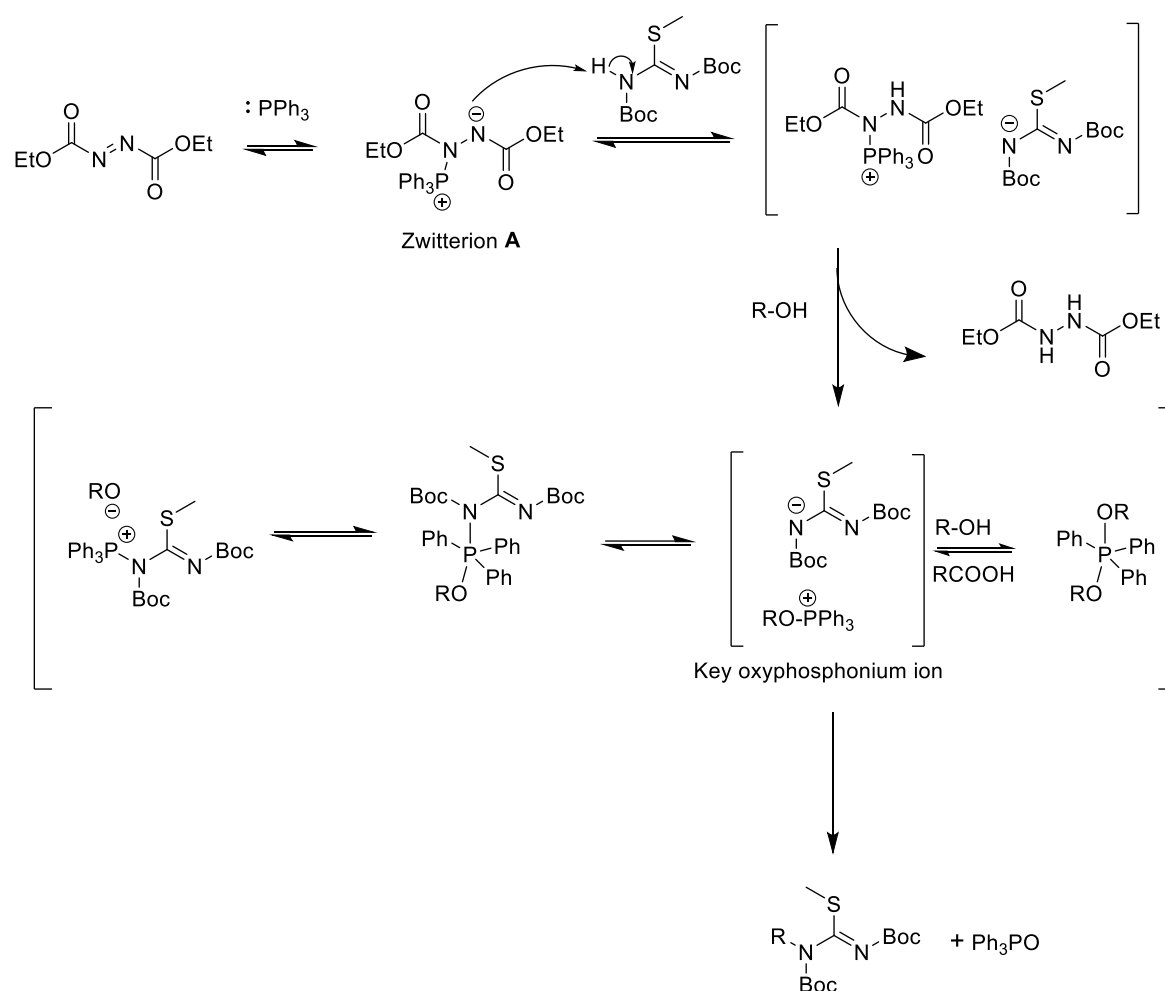
However, the by-products formed in the reaction and the high energy nature of the azodicarboxylate reagent used in the reaction, limits its use and thus Mitsunobu couplings are often deserted when designing the final synthesis of an upscaled industrial-use synthesis.[92] Since its discovery in 1967, the reaction has been used mostly in its original form; however, in more recent years attempts have been made to improve the catalysis of the reaction making it more suitable for industrial use. For example, in 2006 Toy *et al.* were the first to introduce the premise of azodicarboxylate recycling.[92,95,96] The idea was not developed until 2013 when Taniguchi published an alternative oxidation system for an *in situ* approach to azodicarboxylate recycling.[97,98] However, neither approach addressed the phosphine oxide waste produced throughout the synthesis. Aldrich *et. al.* combined the O'Brien phosphine recycling method, developed from the catalytic Wittig reaction, with the Taniguchi azodicarboxylate recycling method creating a "full catalytic system".[99,100] However, there were issues with the scope and reproducibility of Aldrich's "fully catalytic" approach.

In our case, the phosphine oxide by-product was only partially soluble in hexane; thus a recrystallisation from hexane was carried out before the column purification of the mixture

since otherwise the by-product would precipitate disturbing the chromatographic silica due to the high ratio of hexane/ethyl acetate (9:1, respectively) needed to separate the alkyl-substituted pseudothiourea from excess DEAD. Alternatively, the use of diisopropylazodicarboxylate (DIAD) does not require such a polar system as it streaks from the baseline of the TLC; thus, the column can be carried out in a 1:1 ratio of hexane / ethyl acetate and the phosphine oxide by-product remains in solution.

An investigation into the use of this reaction to synthesise a disubstituted thiourea was carried out as an alternative to prepare the *N,N'*-diethyl pseudothiourea, however, after the first substitution there appears to be a change in electrophilicity of the thiourea and the second substitution never occurs, even with an increase in stoichiometric equivalents of base and alcohol. To conclude, the Mitsunobo reaction resulted in the successful synthesis of both the methyl- (**21a**) and ethyl- (**22a**) *N*-substituted Boc-protected pseudothioureas.

3.2.2.2 Guanidylation reactions

The Kim and Qian reaction is initiated via the activation of the corresponding thiourea by HgCl$_2$, followed by the presence of triethylamine to assist in the deprotonation of the amines on the 4,4'-methylenedianiline backbone to generate the bis-Boc-protected product.

Scheme 3.12 *Kim and Qian method for guanidylation mechanism*
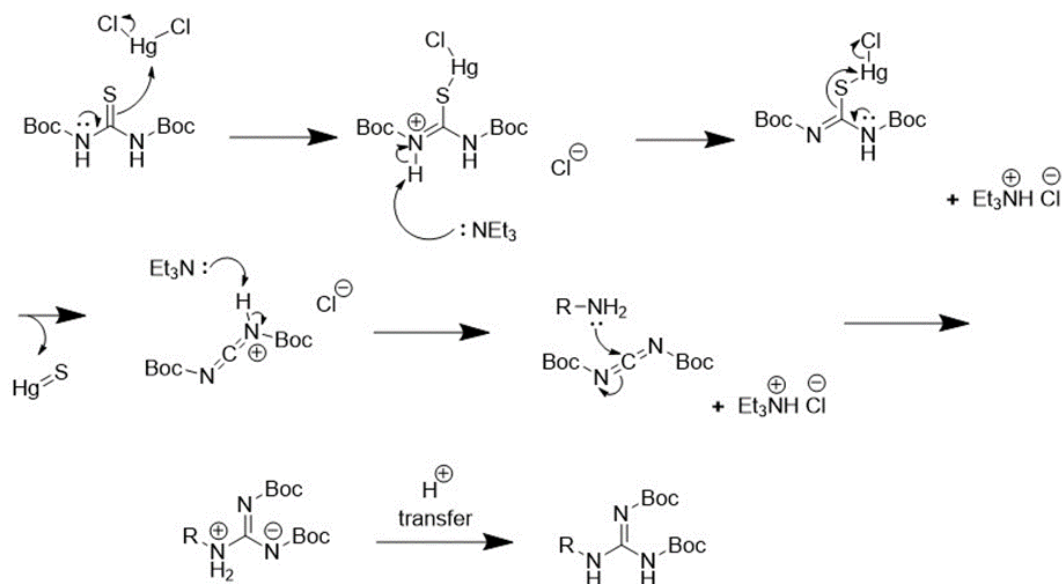

Although the use of toxic mercury chloride in the synthesis of compounds destined for medicinal purposes is proven undesirable, the efficacy of the reaction cannot be denied. In 2013, B. Kelly and I. Rozas published an alternative route for the guanylation of unreactive aryl-amine-containing compounds using CuCl$_2$ as the thiophilic salt with yields equally as

satisfactory as that of $HgCl_2$.[39] However, $CuCl_2$ was not consistent in producing acceptable yields, unlike $HgCl_2$, therefore $HgCl_2$ is still used in the Rozas laboratory today. This could be due to the fact that Hg^{2+} salts are more thiophilic than Cu^{2+} salts as they have lower LUMO, allowing for antibonding interactions toward sulfur's high energy HOMO.[101] Furthermore, the removal of any excess $HgCl_2$ or the HgS biproduct has been very successful when filtered through a bed of celite, washed and purified via flash column chromatography. Following this approach, the corresponding Boc-protected bis-guanidine diaryl derivatives have been synthesised as shown in Scheme 3.13.

Scheme 3.13 Kim and Qian guanidylation reaction scheme and table of results for the synthesised compounds
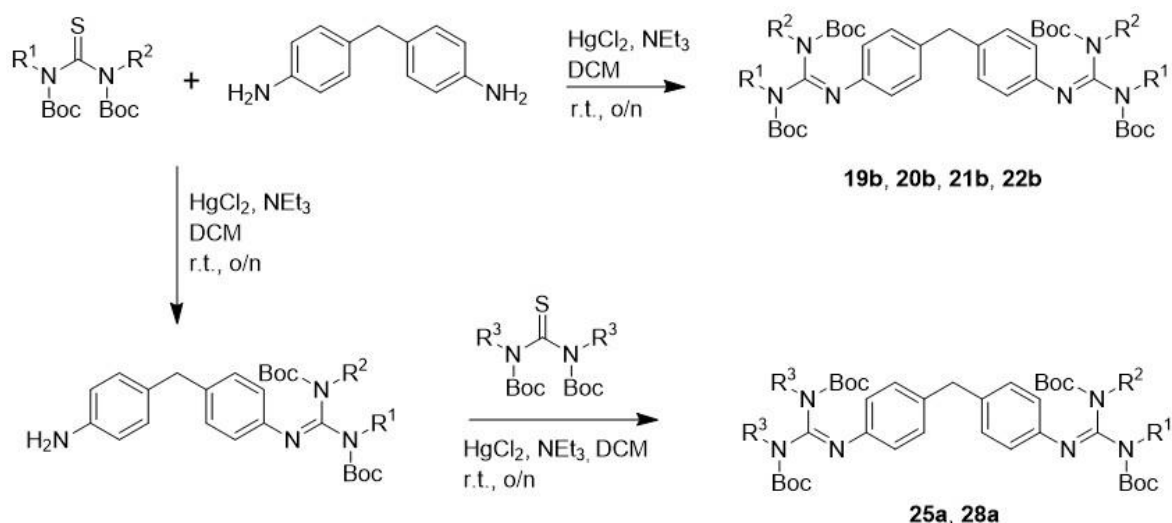
Compound	R¹	R²	R³	Yield (%)
19b	CH_3	CH_3	-	56.65
20b	CH_2CH_3	CH_2CH_3	-	25.2
21b	CH_3	H	-	47.9
22b	CH_2CH_3	H	-	42.4
25a	H	H	CH_3	71.6
28a	CH_3	H	CH_3	67.4

The guanidylation forming **20b** resulted in three spots being seen on the TLC (Rf: 0.51, 0.57, 0.64), likely due to a variation in the mono- and bis-Boc-protected thiourea and the mono- and bis-guanidylated products. Due to the Rf difference being less than 0.1, they were too difficult to separate by column chromatography. From here, the preparative TLC method was employed with the hopes of separating the three side products. The separation

remained extremely difficult and only minimal yields could be obtained from this technique. Due to the minimal amounts of product left after multiple attempts at purification, the product was next deprotected (see Section 3.2.2.3). If more time were available, more research would be invested into finding a means of isolating the product from the various by-products in the Boc-intermediate stage.

When researching methods for the synthesis of the symmetric mono-substituted bis-guanidine diaryl analogues, four possible methods were attempted. The first was based on the 2014 publication of Ríos Martínez *et al.* (Scheme 3.14),[101] which investigated the synthesis of this type of structures in a three-step procedure: (i) preparation of the diaryl ethyloxycarbonyl protected bis-thioureas, (ii) formation of the ethyloxycarbonyl protected bis-guanidinium groups and (iii) elimination of the protecting groups. Following this synthetic approach, the 4,4'-methylenedianiline starting material that makes up the diaryl core of the final product was dissolved in dry DCM and cooled below 0 ℃ before slowly adding an excess of ethoxycarbonyl isothiocyanate to yield compound **36a**. In the original research, the NHCO and NHCONH linkers within the diaryl core were investigated instead of our methylene bridge. These linkers are stronger activating agents than the CH$_2$ linker and therefore the reaction in our case never reached completion. A gravity column was carried out, but the product was only partially soluble in hexane and thus precipitated on the column in any ratio of hexane/ethyl acetate less than 1:1. Recrystallisation from hexane was attempted but the mono- and bis-substituted diamine systems had very similar solubilities and thus, separation was unsuccessful. Due to the lack of sufficient time to spend resolving this issue and investigating potential alternatives for the column chromatography solvent system, the next method for synthesising mono-substituted guanidines was explored.

Scheme 3.14 *Reaction scheme for the first attempted synthesis of the mono-substituted bis-guanidine. Where R-NH$_2$ is either methylamine (2 M solution in THF) or ethylamine hydrochloride*
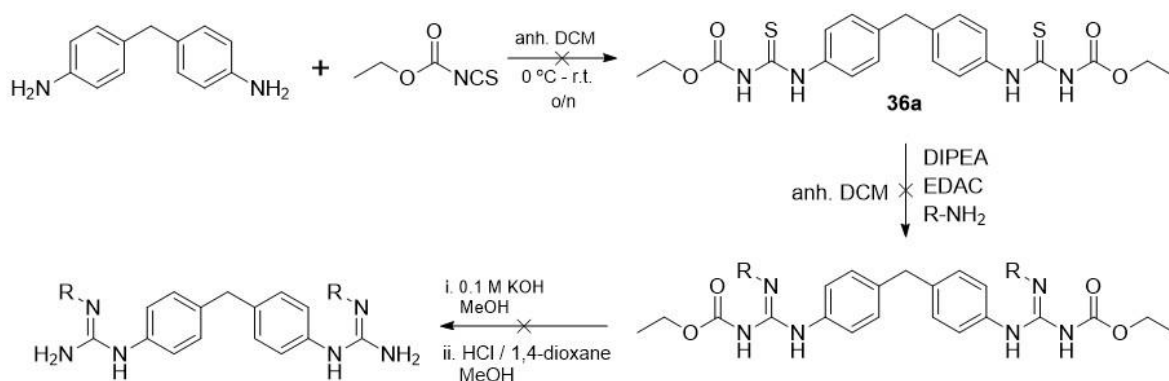
The second approach involved the reaction of 4,4'-methylenedianiline with 1,1'-thiocarbonyl bis-imidazole at room temperature in DCM overnight to obtain the corresponding isothiocynate (Scheme 3.15).[102] Again, due to the poor activation of the weakly electron

donating CH$_2$ linker, the reaction did not go to completion. The product was purified via recrystallisation from hexane followed by gravity column chromatography (1:1 hexane/EtOAc), yielding compound **37a** (97%). Compound **37a** was reacted with *tert*-butyl-carbamate in the presence of NaH (60% immersion in oil) in dry THF. The subsequent reaction, however, was far less successful yielding only 16.2% of compound **37b** as a pale-yellow solid which could be due to the combination of the poor reactivity of the CH$_2$ linker and the poor nucleophilicity of the carbamate caused by the surrounding bulky *tert*-butyl functional group. Due to the insufficient amount of product obtained, the first two steps needed to be repeated but this process was cut short during the purification of the first reaction due to the college closure because the Covid-19 outbreak. Upon returning to the laboratory the reaction was repeated; however, the purification used previously no longer yielded the desired product, thus the third approach was attempted.

Scheme 3.15 *The second approach towards the synthesis of mono-substituted bis-guanidines. Where R-NH$_2$ is either methylamine hydrochloride or ethylamine hydrochloride*
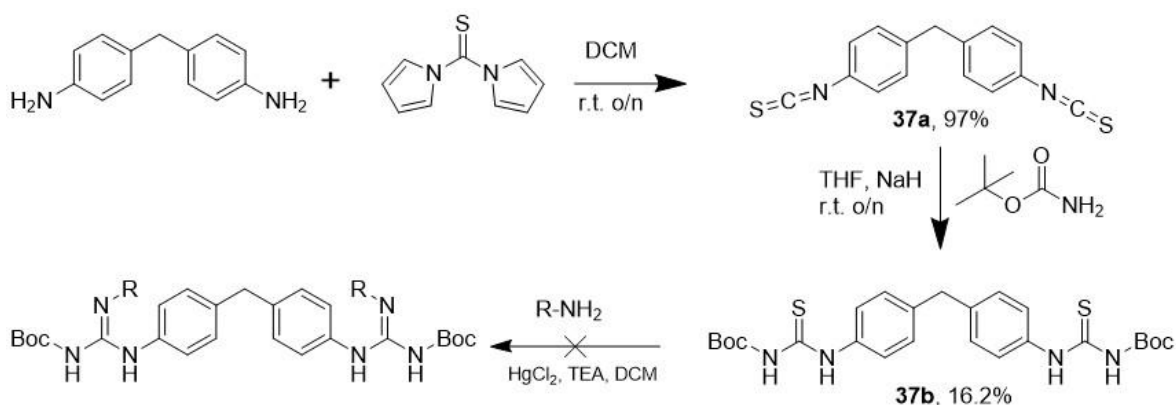
The third approach used the Kim and Qian guanidylation method, using *N*-(tert-butoxycarbonyl)-*N'*-methylthiourea as the guanidylating agent (Scheme 3.16). However, in the case of the preparation of compound **38b** and despite the successful synthesis of the starting *N*-(tert-butoxycarbonyl)-*N'*-methylthiourea (**38a**), the lack of a second Boc-protecting group reduced the electrophilicity of the thiourea thus the reaction never progressed through the guanidylation stage.

Scheme 3.16 *Reaction Schemes for the third approach to the synthesis of mono-substituted bis-guanidines demonstrating the unsuccessful guanidylation using the Kim and Quan method.*
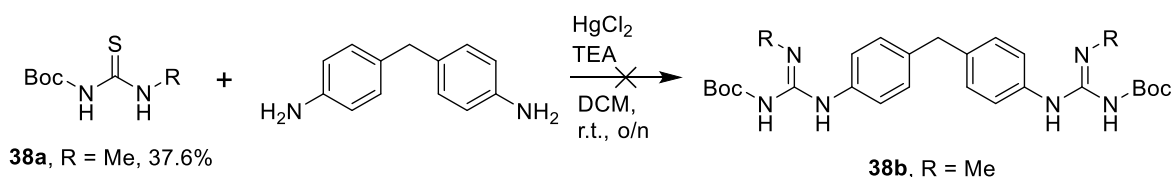
Whilst analysing the synthesis of compound **38a**, it was clear that the thiourea must be bis-Boc-protected. Furthermore, the use of the commercially available *N,N'*-bis-(*tert*-butoxycarbonyl)-S-methylisothiourea (pseudothiourea) improved the efficacy of some reactions. This may be attributed to the methylation of the sulfur encouraging a more efficient desulfurization by mercury chl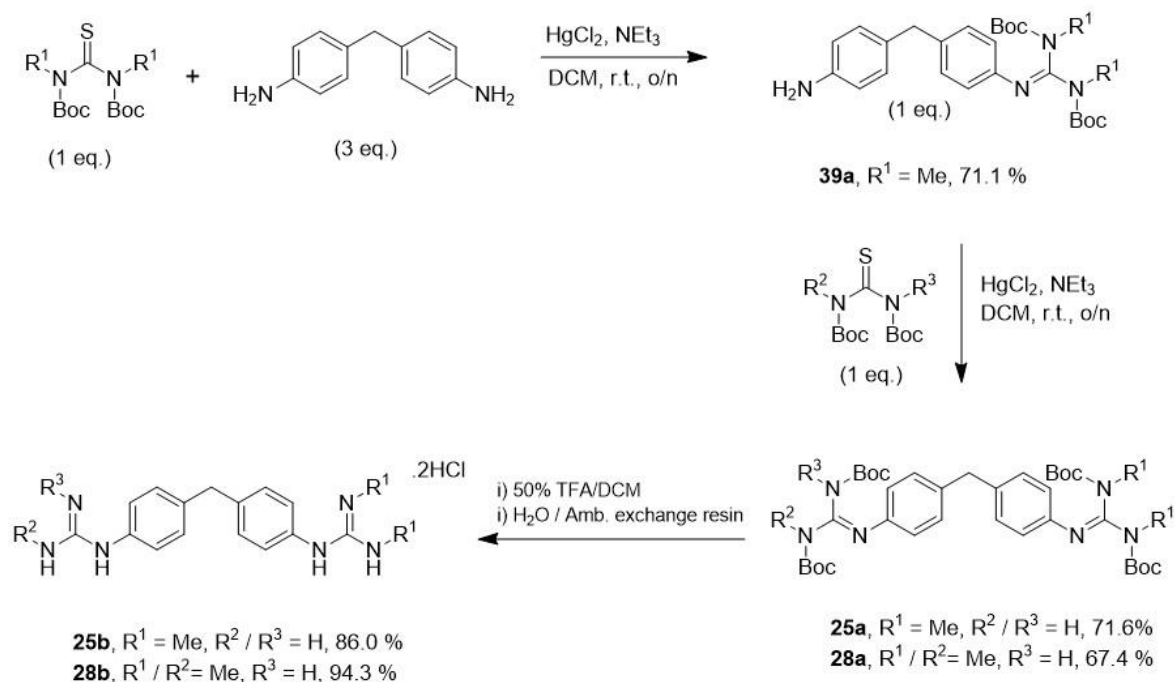oride (HgCl$_2$) forming a HgS by-product (Scheme 3.17). It was therefore concluded that the Mitsunobu reaction, described in Section 3.2.2.1 above, was the ideal approach to synthesise the mono-substituted thiourea prior to the Kim and Qian method for guanidylation.

Scheme 3.17 *Desulfurization of S-methylthiourea using HgCl$_2$, followed by guanidylation of an amine*
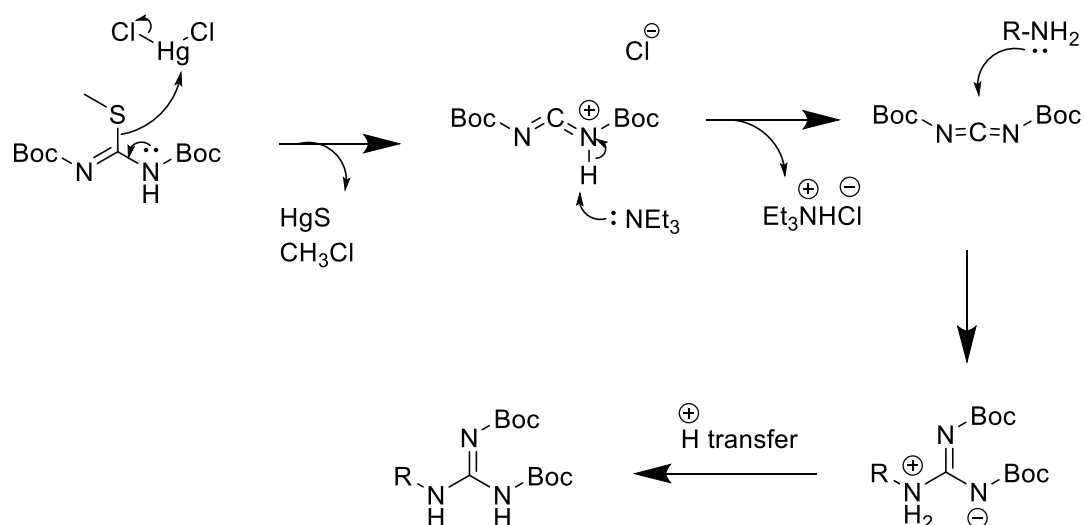
The asymmetric *bis*-guanidine compounds (**25a** and **28a**) were synthesised using a two-part guanidylation with the Kim and Qian method (Scheme 3.18). First, the mono-guanidylation reaction conditions were set up using 1 equivalent of the *N,N'*-bis-Boc-dimethylthiourea and 3 equivalents of the 4,4'-methylenedianiline, in the presence of HgCl$_2$ (3 eq.) and NEt$_3$ (6 eq.) in DCM. After purification by column chromatography yielding compound **39a** (71.1%), the second guanidylation was carried out. Thus, 1 equivalent of compound **39a** was reacted with 1.5 equivalents of the relevant thiourea in the presence of HgCl$_2$ (3 eq.) and NEt$_3$ (increase from 6 to 8 equivalents for the sterically hindered thiourea), yielding compounds **25a** (71.6%) and **28a** (64.7%). The final deprotection step shown in Scheme 3.18 is discussed in the next section.

Scheme 3.18 *Asymmetrical synthesis of compounds* **25b** *and* **28b** *where R¹ – R³ are Me or H. The diamine starting material was used in excess to assure mono-guanidylation*

39a, R¹ = Me, 71.1 %

25b, R¹ = Me, R² / R³ = H, 86.0 %
28b, R¹ / R²= Me, R³ = H, 94.3 %

25a, R¹ = Me, R² / R³ = H, 71.6%
28a, R¹ / R²= Me, R³ = H, 67.4 %

3.2.2.3 Preparation of the final salts

There are multiple recorded methods for Boc-deprotection to afford the desired salts. In this project, we initially used 1.25M solutions of HCl in methanol as it only required a 4 hour stirring period at 35 °C to obtain the corresponding hydrochloride salt; however, the stronger acid caused the decomposition of the highly sensitive guanidine moiety. Other molarities could be attempted in the future along with the possibility of using HCl/dioxane as an alternative solvent.

The method that gave the most consistent results with the highest yields (>85%) was the use of trifluoroacetic acid (TFA). Thus, a 50% solution of TFA in DCM was used in excess and stirred for overnight, at room temperature to yield the guanidine trifluoroacetate salts. However, these salts are often insoluble in water. Thus, for the purpose of the pharmacological evaluations, an ion exchange was carried out by stirring the desired trifluoroacetate in excess deionised H_2O and activated Amberlite® IRA-400 resin – a polystyrene bead – in its chloride form. After 24-48 hrs of light stirring (not to damage the resin) and filtration, the guanidine hydrochloride salts were obtained. Complete ion interchange was checked using ^{19}F NMR spectroscopy where the absence of any peaks in this spectrum confirms full conversion of TFA salt to the corresponding HCl salts.

In the particular case of compound **20b**, when TFA was added to the product, the solution turned a shade of pink. This could have been an indication that some of the *N,N'*-bis-(*tert-*

butoxycarbonyl)diethylthiourea starting material was still present, the colour being the result of a n-π* interaction between the TFA and the thiourea. Both ^{1}H and a ^{13}C NMR spectra showed that a mixture was still present. After a final reverse phase column, the product was separated into the 4-bis-[(*N,N'*-diethyl)guanidino]diphenylmethane dihydrochloride (**20c**) and 4-amino-4'-[(*N,N'*-diethyl)guanidino]diphenylmethane hydrochloride (**20d**).

Scheme 3.19 *Generic reaction scheme for the i) Boc-deprotection and ii) ion exchange to yield the desired hydrochloride salt, where R^1, R^2 = H, Me, Et, and table of results*
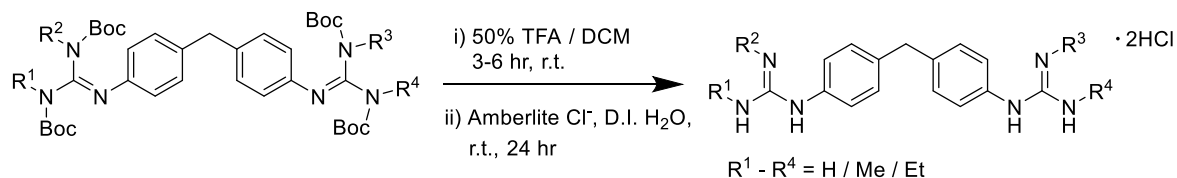
Compound	R^1	R^2	R^3	R^4	Yield (%)
19c	CH$_3$	CH$_3$	CH$_3$	CH$_3$	98.2
20c	CH$_2$CH$_3$	CH$_2$CH$_3$	CH$_2$CH$_3$	CH$_2$CH$_3$	9.7
21c	CH$_3$	H	H	CH$_3$	67.5
22c	CH$_2$CH$_3$	H	H	CH$_2$CH$_3$	83.9
25b	H	H	CH$_3$	CH$_3$	86.0
28b	CH$_3$	H	CH$_3$	CH$_3$	94.3

Compounds **19b**, **21b**, **22b** and **28b** were all prepared in sufficient quantities and to the required purity specification to allow in vitro testing to be performed. These results are discussed in Section 3.4.

3.3 Computational Chemistry – Docking Studies

The α_2-ARs mediate a wide range of physiological functions making them highly attractive biological targets for drug discovery. Until December 2019, there was an absence of any α_2-AR subtype crystal structure, which had proven to be a major hindrance in the drug design and development process. To date, the Rozas group utilized homology models of the two most relevant α_{2A}-AR subtypes in their active and inactive forms developed by Rozas' collaborator Prof. Mireia Olivella. Elucidation of the different physiological functions attributed to a given α_2-AR subtype remains challenging, largely due to the lack of subtype-selective ligands. However, due to the distribution of each of the subtypes across the CNS and PNS, the α_{2A}- and the α_{2C}-AR are most relevant due to their localisation within the human brain. Since the α_{2A}-AR is the most dominant, this has been the focus of the molecular docking studies here presented and discussed.

In December 2019, the following three crystal structures of the α_2-AR subtypes were resolved and have been recently deposited in the Protein Data Bank (PDB):

α_{2A}-AR- 6KUY- The crystal structure of the human inactive α_{2A}-AR in complex with a partial agonist, (*S*)-4-fluoro-2-(1*H*-imidazol-5-yl)-1-isopropylindoline (E39).[25] The preparation and adrenergic activity of this ligand was described in a patent in 1996.[103]
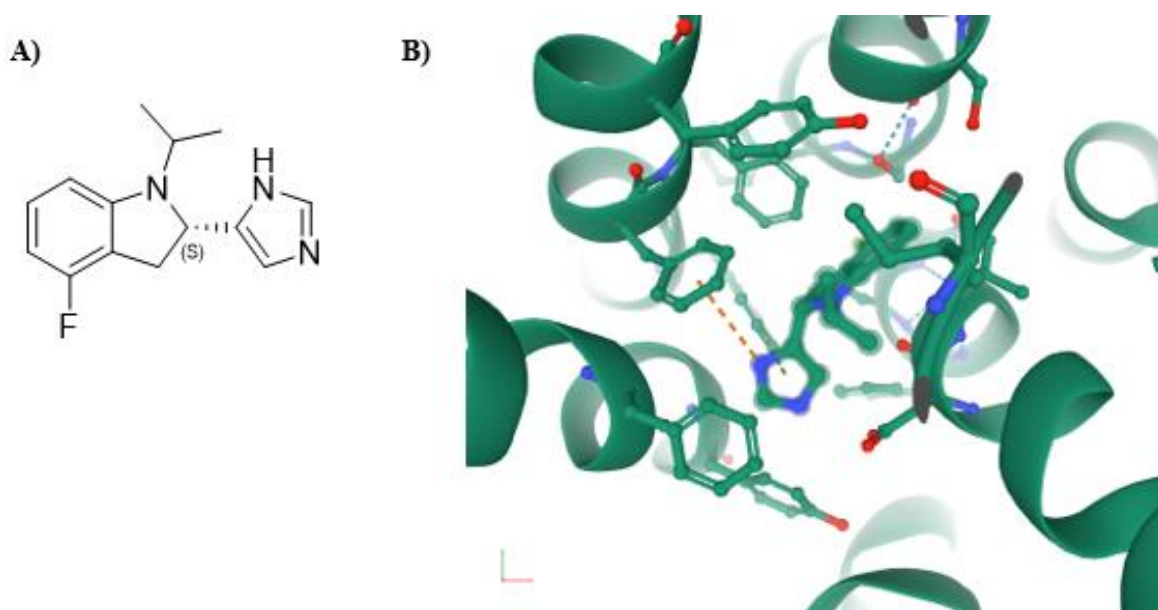
Figure 3.6 *A) structure of partial agonist, (S)-4-fluoro-2-(1H-imidazol-5-yl)-1-isopropylindoline (E39).*

B) Co-crystallised resolved structure of the E39 partial agonist in complex with the α_{2A}-AR (6KUY) in its inactive form displaying π-π interactions between Phe340 and the imidazoline ring

α_{2A}-AR- 6KUX- Crystal structure of the inactive α_{2A}-AR – from the Spodoptera frugiperda in complex with an antagonist (E33). Research carried out by Uhlen *et al.* (1998) produced

the [3H]RS79948-197 binding to rat α_{2A}-, α_{2B}- and α_{2C}-adrenoceptors with K_d values of 0.42, 0.18 and 0.19 nM, respectively.[104]
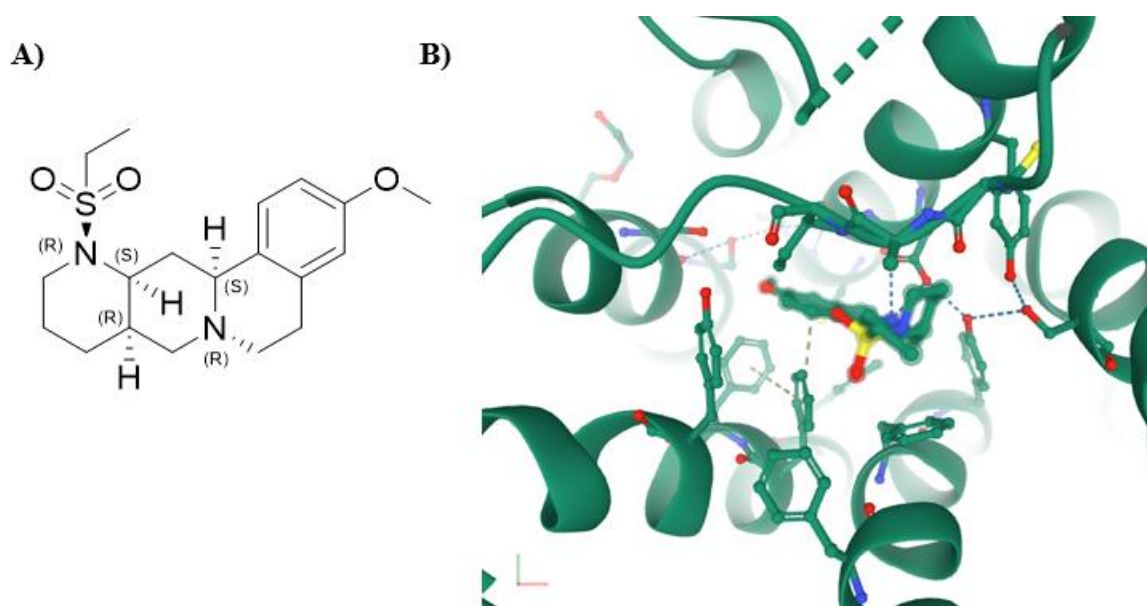

Figure 3.7 *A) structure of antagonist ligand, E3F. B) Co-crystallised resolved structure of E3F ligand in complex with the α_{2A}-AR (6KUX) in its inactive form displaying hydrogen bonding interactions between Phe340 and the phenol ring. Further bifurcated hydrogen bonds between the Asp94 and the tertiary amine in fused rings are present*

α_{2C}-AR-6KUW- The crystal structure of human α_{2C}-AR G-protein coupled receptor in complex with antagonist (E33) in its inactive form.[26,104]

The research-based pharmaceutical and medicinal chemistry industry have increasingly employed a wealth of molecular modelling methods within a variety of drug discovery programmes to study complex biological and chemical systems.[105] Molecular modelling encompasses all theoretical and computational methods used to model or mimic the behaviour of molecules (Figure 3.8). Molecular docking is a specific computational technique used to explore ligand conformations within the binding sites of macromolecular targets and predicts the preferred binding orientation. This method plays an important role in structure-based drug design (SBDD) as it provides insights into the molecules binding behaviour as well as to elucidate fundamental biochemical processes. SBDD refers to the systematic use of structural data which are usually obtained using a biophysical technique (e.g. X-ray crystallography) or derived from computational homology modelling.[105] Computational homology modelling refers to the technique used to prepare a model of a protein 3D structure from its amino acid sequence based on its similarity to a protein of known 3D structure.[106] The α_{2A}-AR-MO model is an example of a homology model, that was developed before the α_{2A}-AR crystal structures were published in December 2019.
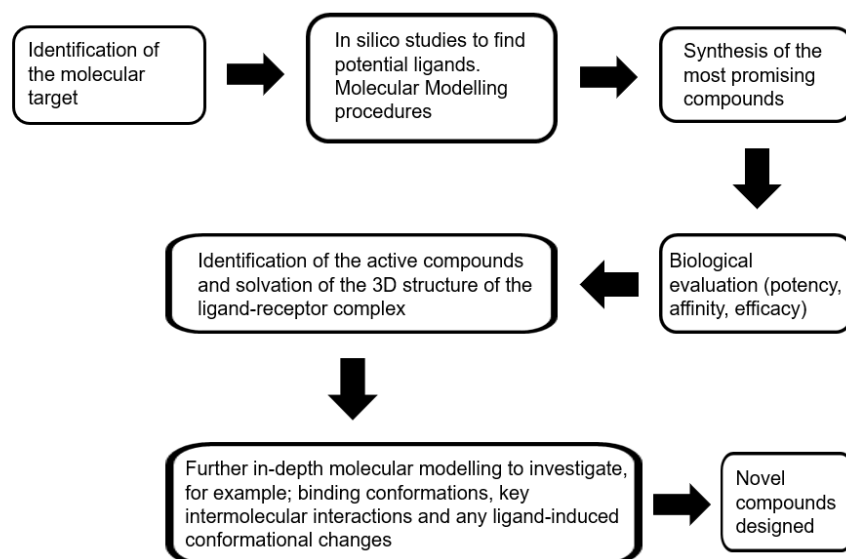
Figure 3.8 *Structure-based drug design process* [106]

The availability of 3D macromolecular structures enables a diligent inspection of the binding site topology, including the presence of clefts, cavities and sub-pockets.[105] Moreover, the electrostatic properties and potential binding interactions can also be carefully examined. The process of identifying a target and synthesising an active compound with suitable characteristics (e.g. minimal toxicity, high bioavailability and a cost-effective synthesis) and developing it to be introduced to the market is a time-consuming, extremely complex and risky endeavour.[107] Within academia, the high throughput screening (HTS) used to screen potential *hit* compounds and identify new *lead* compounds can be an extremely costly and time-consuming process. The introduction of molecular docking as a virtual screening (VS) system can be used instead of or as well as HTS to identify the new *lead* compounds in an efficient manner. To date, over 173,000 structures of potential targets have been registered on the RCSB Protein Data Base (PDB) and are available to academia and industry alike.[108] Molecular docking was first introduced to the industry in the 1970s to assist with drug discovery tasks; however, more recent applications include the prediction of adverse side effects, pharmacology, drug repurposing and target fishing and profiling.[109]

As previously mentioned, docking methods fit a ligand into a binding site by combining and optimizing variables such as steric, hydrophobic and electrostatic interactions.[107] These ligands are then "scored" based on their potential as likely ligands for that receptor. Scoring functions are categorised in three main groups:

(i) *Force-field-based scoring functions* estimate the binding energy by summing the contributions of bonded (stretching and bending) and non-bonded (electrostatic and van der

Waals) terms in a general master function.[105] It applies molecular mechanics methods to calculate energy associated with each term of the force-field, sometimes using parameters/values calculated using quantum mechanics.[110] Therefore, it is normal that inaccuracies appear when estimating entropic contributions or in the treatment of long-range effects involved in binding.[111]

(ii) *Empirical scoring function* refers to scoring functions where each of the terms describes one type of physical event involved in the formation of the ligand-receptor complex, *i.e.* hydrogen bonding, ionic and apolar interactions, desolvation or entropic effects.[105,112] Due to the simplicity of the employed energy terms, empirical functions are faster than the force-field-based methods and often preferred, even though they are less accurate. This research employed the empirical function GlideScore (G-Score), now referred to as binding affinity on autodock vina software, as the measure of ranking the docked compounds. However, the main disadvantage to empirical functions is that they depend heavily on the accuracy of the data used in the parameterization process.[111]

(iii) *Knowledge-based scoring function* uses pairwise energy potential values, extracted from known ligand-receptor complexes, to obtain a general scoring function. It is based on the inverse Boltzmann statistic principle where these potentials are constructed by observing the frequency with which two different atoms are found within a given distance in a structural data set.[105,113] These different types of interactions observed in the dataset are classified and weighted according to their frequency of occurrence. The final score is given as a sum of these individual interactions.[32,105]

In collaboration with Helene Mihigo, a PhD student within the Rozas group, the molecules seen in Section 3.3.1 were optimised using the Maestro software, the structures of the α_{2A}-AR complexed with a partial agonist (6KUY) or with an antagonist (6KUX) were retrieved from the RCSB PDB to be used for docking studies, and docking of the ligands into the mentioned targets was performed using Glide. The chosen orientations of the docked compounds were based on the ionic interaction with the aspartate residue D113$^{3.32}$ as this has been reported to be a critical interaction with the α_2-AR binding sites.

Due to time constraints and their relevance in disease, only the three inactive α_{2A}-AR receptor templates were chosen for the present docking study: the model developed by Prof. Olivella (α_{2A}-AR-MO), and the two crystal structures recently reported α_{2A}-AR-Y (complexed with a partial agonist) and α_{2A}-AR-X (complexed with an antagonist). Thus, the appropriate standard docking experiments were performed using compounds **1** (*lead*, symmetric), **15** (asymmetric), **16** (asymmetric), **18** (symmetric) and **22c** (symmetric) as ligands. Considering that the standard docking studies assume a rigid receptor system, a fit-induced study was chosen for a selected set of compounds because this is not the case

for most receptors. It is common for a receptor to alter its orientation and binding site to better 'fit' the ligand. For this reason, false negatives can be achieved in the standard docking studies as the ligand may not bind well to the rigid system but is known to be active *in vitro*. Thus, based on the pharmacological results obtained (see Section 3.4), fit-induced docking studies were also performed with compounds **1**, **22c** and **16**. These specific docking studies were carried out to investigate the possible differences and similarities of the interactions established between a known agonist (**1**) or antagonists (**16** and **22c**) with the receptor.
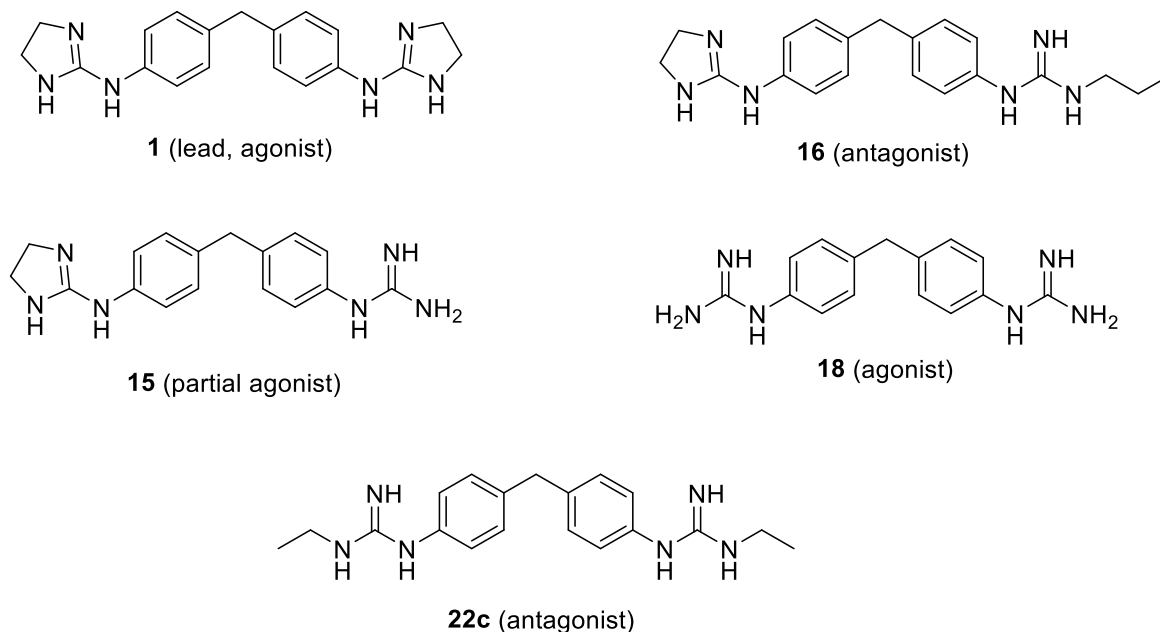

Figure 3.9 *Structure of Compounds **1, 15, 16, 18** and **22c** to be docked in the various α_{2A}-AR receptor templates*

3.3.1 Docking Results

As previously stated, compound **1** is the *lead* compound previously developed within the Rozas group and is used as a reference model for the remaining docking studies. As aforementioned, the binding affinity (kcal/mol), previously known as G-score, is an empirical scoring function that approximates the ligand binding free energy.[114] The calculated binding affinity values for the previously synthesised compounds **1, 15** and **18** and the newly synthesised compound **22c** are presented in Table 3.7, where a more negative value indicates a more favourable binding.

Table 3.5 *Autodock binding affinity values for compounds 1, 15, 18 and 22c when docked with the various receptor models*

Compound Number (Functional Activity)	Receptor Model	Binding Affinity (kcal/mol)
1 (Agonist)	α_{2A}-AR-MO	-3.57
	α_{2A}-AR-Y	-5.93
	α_{2A}-AR-X	-3.97
18 (Agonist)	α_{2A}-AR-MO	-5.26
	α_{2A}-AR-Y	-5.72
	α_{2A}-AR-X	-4.16
15 (Partial agonist)	α_{2A}-AR-MO	-5.09
	α_{2A}-AR-Y	-4.87
	α_{2A}-AR-X	-4.61
22c (Antagonist)	α_{2A}-AR-MO	-7.11
	α_{2A}-AR-Y	-3.74
	α_{2A}-AR-X	-2.58

For ease of purpose, the interacting residue's name and the position that it occupies in the whole primary sequence of the protein receptor, alongside the Ballesteros–Weinstein nomenclature will be used as a special indexing system. The Ballesteros–Weinstein nomenclature is one of the most commonly adapted systems when discussing amino acids in GPCRs. The letter indicates which amino acid is being identified and the first digit refers to which of the seven transmembrane helices the amino acid belongs to. Finally, the number after the decimal point refers to the residue's position with respect to the most conserved residue in that helix, which has been arbitrarily assigned the number 50.[25]
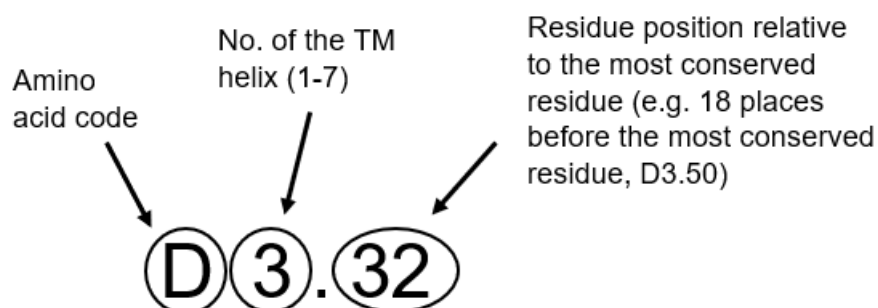

Figure 3.10 *Example of Asp113 residue using the Ballesteros–Weinstein nomenclature*

Past research into these receptor models, by means of site directed mutagenesis and homology modelling studies, identified aspartate 113 (D3.32, from now on D113$^{3.32}$) as one of the most pertinent residues in aminergic binding sites. This is due to the formation of a strong salt bridge between the anionic carboxylate of the aspartate and the cationic moieties of some known ligands (e.g. idazoxan or clonidine) at physiological pH, acting as an anchor within the binding site. Thus, D113$^{3.32}$ is the conserved residue involved in all aminergic and opioid receptors.[25] Due to its vitality, any poses in the docking sequences that did not display a salt bridge formation with D113$^{3.32}$ were not taken into consideration.

Furthermore, it has been reported that the movement of the TM6 is the "hallmark" of GPCR activation and that partial agonists lack the necessary hydrophilic tails that can form bonds with the polar residues at the extracellular end of TM5 and TM6 to trigger this activation.[115] It can therefore be suggested that when aiming for antagonist activity, the molecular docking would aim to avoid these key interactions with TM5 and TM6.

The previously synthesised compounds **15** and **18**, prepared and tested within the Rozas group, displayed similar interactions with the three targets used in the standard docking studies. Thus, hydrogen bonding with S200$^{5.42}$ was observed, which would correlate with their [^{35}S]GTPγS binding functional assay results as α$_2$-AR agonists. Moreover, these agonists displayed further similarities with an additional salt bridge and H-bonding interaction with the D192^{XL2} and E189$^{XL2.51}$ residues, which lie on the extracellular loop 2 (XL2) directly linked to the TM5 (Figure 3.11).[116]
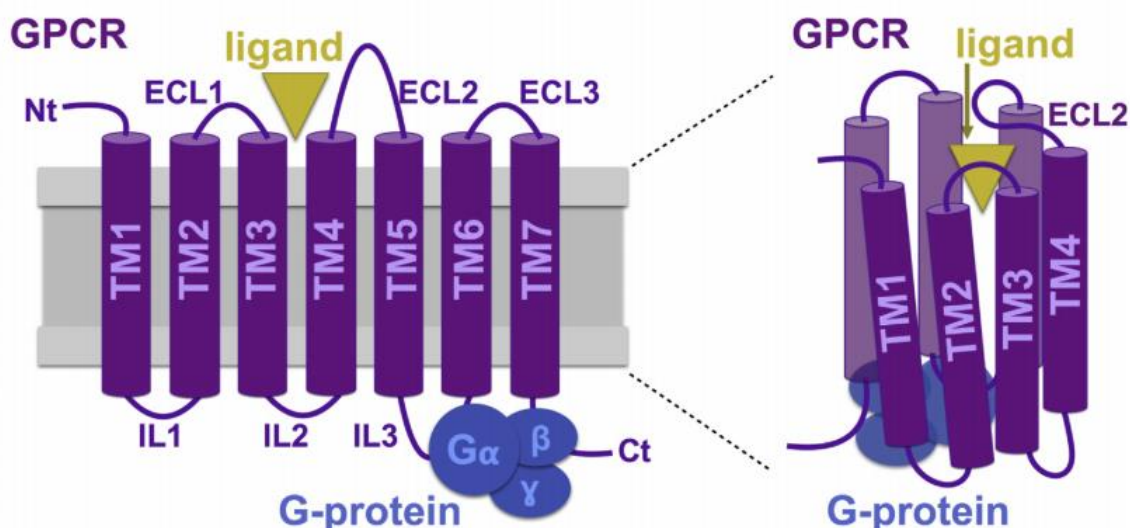

Figure 3.11 *Schematic of the basic GPCR structure; where TM 1-7 are the 7-transmembranes, ECL 1-3 and IL 1-3 are the extracellular and intracellular loops respectively* [116]

The docking of *lead* compound **1** did not result in the expected interaction with S200[5.42] in any of the receptor models, but it did display the same interactions with the residues on XL2, thus potentially indicating a correlation between these interactions and the agonist behaviour of compounds **1**, **15**, **18**, as they could be used to direct the ligands towards TM5.
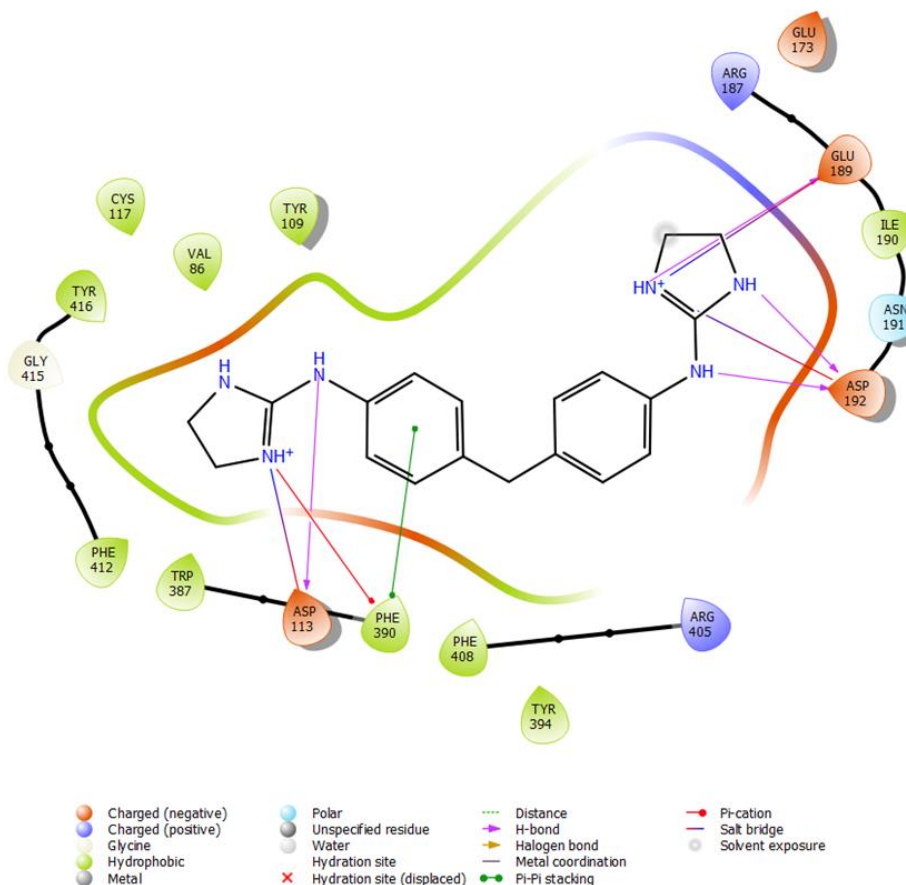

Figure 3.12 *Molecular docking pose for compound **1** and the α$_{2A}$-AR-X target indicating the most important interactions*

Unique to the α$_{2A}$-AR-Y receptor model of compound **18** is the introduction of H-bonding interactions at the isoleucine I190[XL2.52] on the XL2 (Figure 3.14).[114] The Schrödinger software utilised throughout this study automatically characterised the HB interactions displayed in Figure 3.14 *etc.* Figure 3.20 and 3.21 display the HB distance in angstrom (Å). Thompson *et al.*[117] and Laurila *et al.*[118] reported that the residues at XL2.50, XL2.51 and XL2.52 may act as a lid covering the binding cavity and may interact with certain ligands to influence the binding mode of the receptor. The residues at position XL2.52, *e.g.* the I190[XL2.52] residue of the α$_{2A}$-AR, is directed downwards into the receptor and may result in subtype specific binding.[114] Moreover, Ostopovici-Halip *et al.* stated that the negatively charged carboxyl side chain of D192[XL2] could be used in designing ligands with substituents of opposite charge that can interact with these residue side chains.[119] Furthermore, Jayaraman *et al.* reported the importance of E189[XL2.51] in subtype selectivity as it influences

the space available for ligand binding.[114] This data reports the possible importance of the XL2 in ligand selectivity in aminergic and other small molecule binding GPCRs.[114]
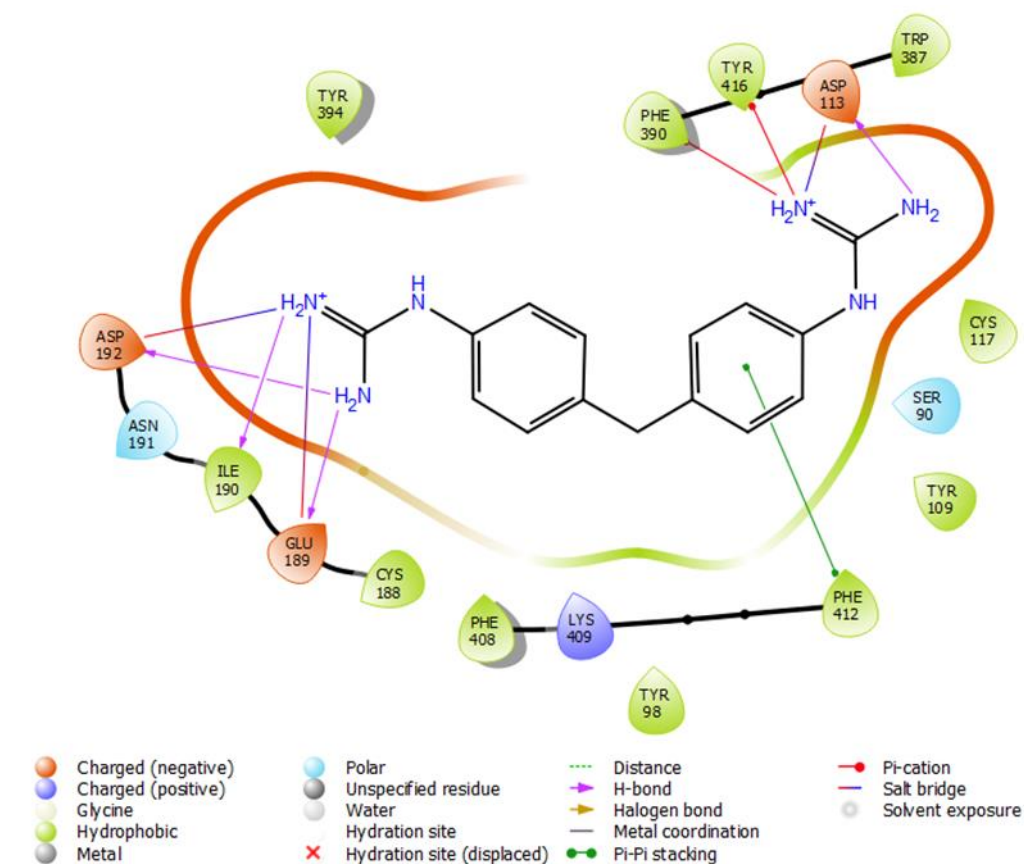

Figure 3.13 *The best pose obtained in the docking of compound **18** and the α_{2A}-AR-Y target indicating the most important interactions*

Moreover, phenylalanine 412 (F7.39) has been identified as a potentially essential residue in α_{2A}-AR agonist activity, acting as a "switching lid" of which the smaller ligands with less saturated ring systems induce closure of the "lid" to form an aromatic cage. Due to F412[7.39] being one of the three non-conserved residues within the α_{2A}-AR, this phenomenon is considered unique to the α-ARs.[25] Despite the computational docking of the antagonist **22c** into the α_{2A}-AR model showing a displacement of the π-π stacking interaction between F412[7.39] and the ligand, contradicting this reported data. Other aromatic residues F390[6.51], F391[6.52], F408[7.39], Y196[5.48], [120] Y416[7.43] [121] and W413[7.40] [115], which vary in their position depending on the ligand and receptor model used, alongside F412[7.39] form the necessary π-π stacking and π-cation interactions with the di-aryl backbone of the ligand **22c**. All this supports the good binding affinity shown by this compound into the α_{2A}-AR (see Table 3.7).

Compound **15** had been previously synthesised in the Rozas group and determined to be a partial agonist via *in vitro* studies. Due to the asymmetry within the structure, two orientations were available in each of the receptor models. However, depending on the

presence of the necessary anchoring salt bridge with $D113^{3.32}$, only one valid orientation was considered. In the particular case of the α_{2A}-AR-Y target both *up* and *down* orientations demonstrated significant binding as seen in Figure 3.15 below. The *up* orientation refers to when the anchoring salt bridge is formed between $D113^{3.32}$ and the imidazoline moiety, whereas the *down* orientation refers to when the salt bridge is formed between the guanidine moiety and the $D113^{3.32}$ residue. This reinforces the theory that the conformational restraint provided by the imidazoline moiety results in a stronger binding interaction to drive the ligand within the receptors binding pocket for a better anchoring system than that of the free guanidine. In all three receptor models (α_2-AR-MO, α_2-AR-Y and α_2-AR-X) the imidazoline forms the successful anchoring interaction; however the α_2-AR-X orientation resulted in a worse binding affinity which may be due to the drastic increase in solvent exposure across the ligand (Appendix 21).
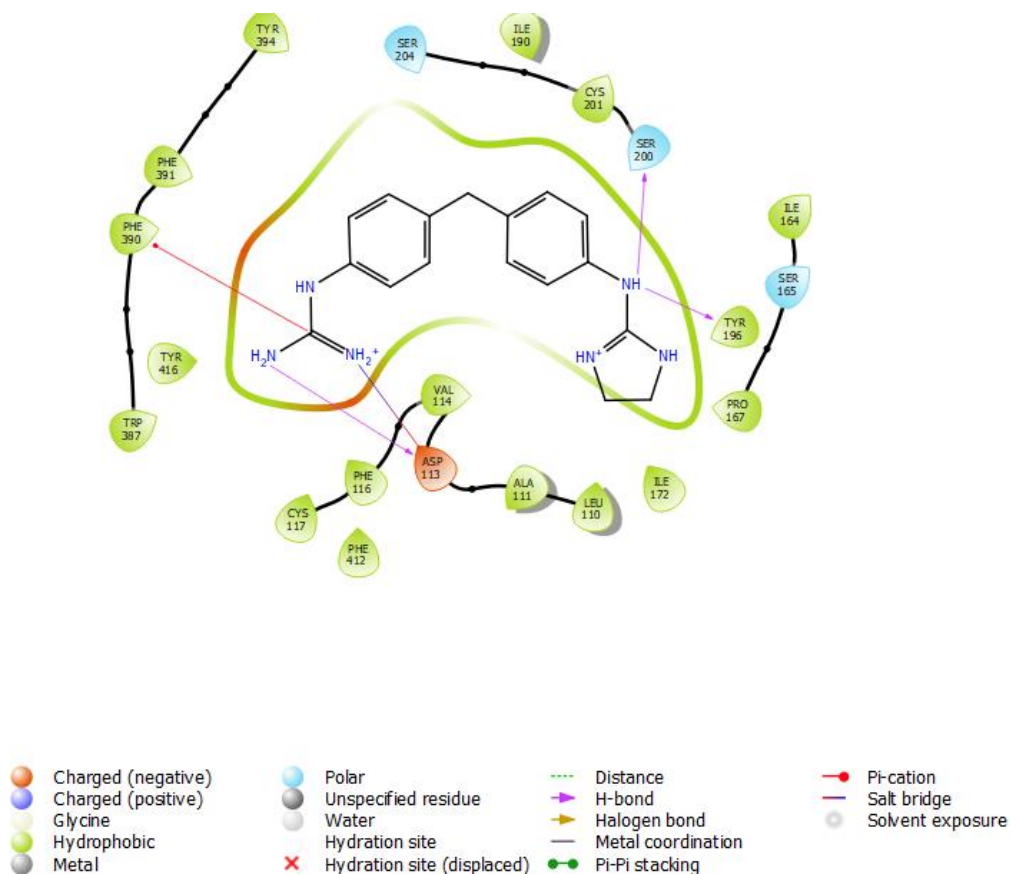
A)
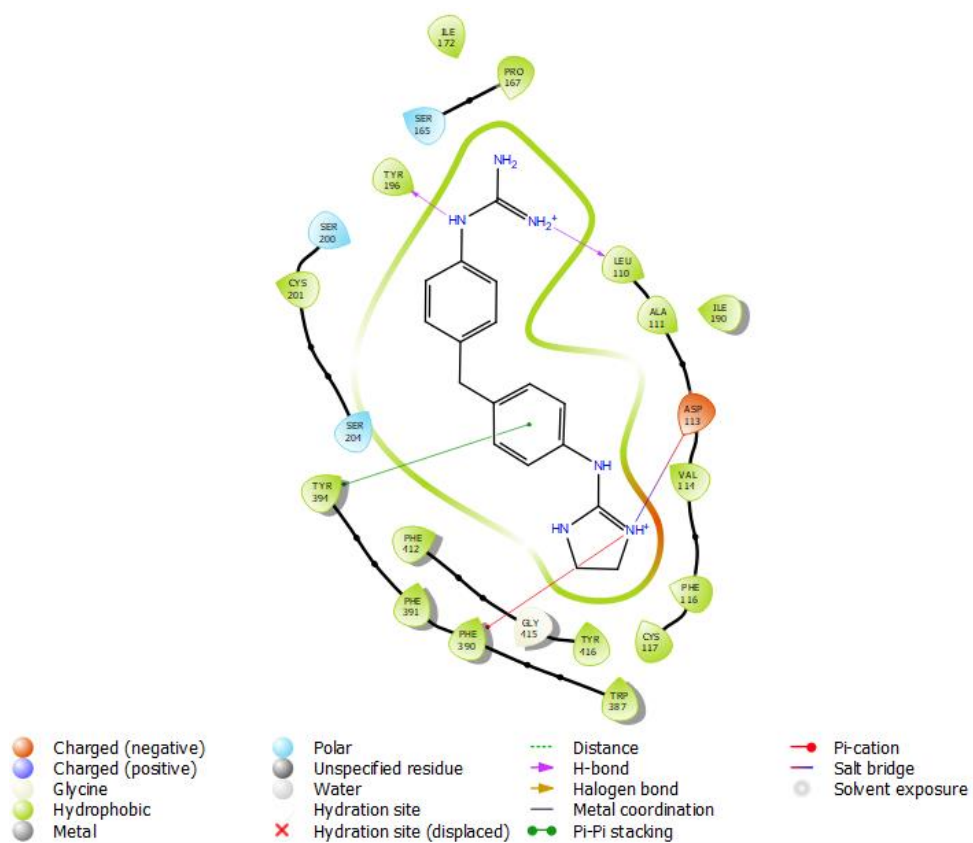
B)

Figure 3.14 A) Computational representation of the interactions between the "up" conformation of compound **15** and the α$_{2A}$-AR-Y receptor model. B) Visual representation of the interactions between the "down" conformation of compound **15** and the α$_{2A}$-AR-Y receptor model

58

As explained at the beginning of the section, induced-fit docking was carried out with the *lead* compound **1**, previously synthesised compound **16** and the newly tested compound **22c**. These particular ligands were chosen based on their structures, K_i values obtained from the *in vitro* studies and their functional activity. Compound **1** was the *lead* compound to date with a good binding affinity (K_i = 1.585 nM) but demonstrated agonist activity; compound **16** (asymmetric 2-aminoimidazoline/substituted guanidinium) was chosen due to its antagonist activity and excellent K_i value (0.794 nM); finally, bis-[(*N*-ehtyl)guanidinium] **22c** (antagonist with an average K_i = 95.5 nM) was selected for comparison. Due to time constraints, only the α_{2A}-AR-X receptor model was investigated as it is in complex with an antagonist and closely related to the desired activity of the receptor.

These studies were performed using the software Maestro (Schrödinger Inc.) and the α_{2A}-AR-X receptor model retrieved from the RCSB PDB to be used as targets. Only poses where ligands which interact with D113$^{3.32}$ were considered. The binding affinity values calculated for each compound were larger (more negative) than those obtained in the standard docking as expected due to the induced-fit being more closely related to the actual binding to the receptor since the ligand can better orient itself within the adapting binding pocket over the rigid receptor models (Table 3.8).

Table 3.6 *Autodock binding affinity of compounds **1**, **16**, **22c**, comparing the rigid receptor models with the induced-fit models of α_{2A}-AR-X*

Compound ID	Receptor model	Rigid Receptor Binding affinity (kcal/mol)	Fit-induced Receptor Binding affinity (kcal/mol)
1	α_{2A}-AR-X	-3.97	-7.44
16	α_{2A}-AR-X	n.d.	-8.16
22c	α_{2A}-AR-X	-2.58	-7.63

As previously discussed, *lead* compound **1** is a known agonist (Figure 3.17), and interestingly, when docked to α_2-AR-X it did not display any binding interactions with the residues on TM5 or TM6 (e.g. S200$^{5.42}$) which are known to activate the receptor. Alongside the necessary anchoring salt bridge, a further salt bridge and H-bond with D192^{XL2} and E189$^{XL2.51}$ were observed. As mentioned before, the XL2 is bound to TM5 and these interactions may assist in the resulting agonist activity when **1** is bound to the receptor. Further π-π stacking and π-cation interactions between the diaryl backbone of the ligand and the F390$^{6.51}$ residue assist in increasing the binding affinity of the ligand.
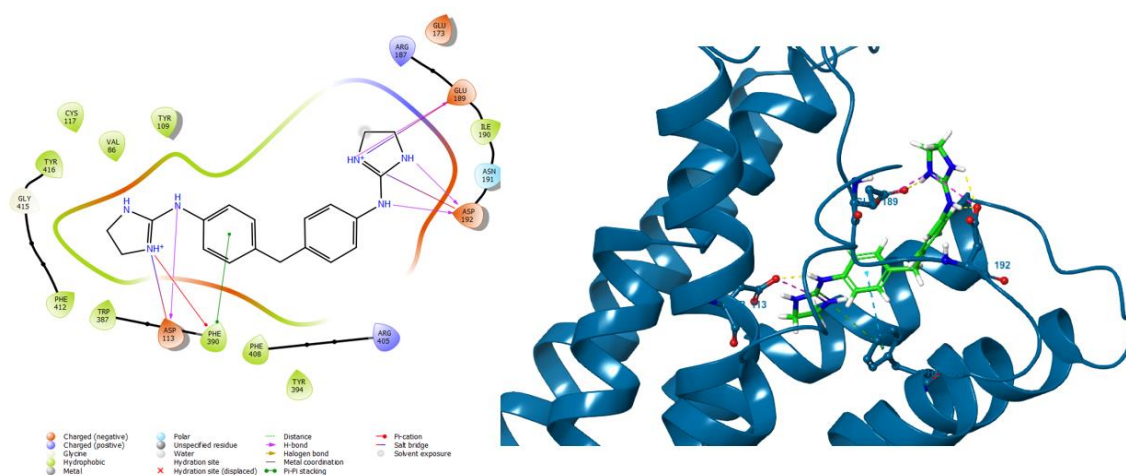
59

Figure 3.15 *Induced-fit docking study of lead compound* *1*

Compound **16** is a known antagonist previously synthesised within the Rozas group, but no computational studies had been carried out on it to date. The autodock binding affinity obtained (-8.16 kcal/mol) correlates with the high binding affinity (K_i = 0.794 nM) of the compound *in vitro*. As seen from Figure 3.17, this ligand-receptor complex also displays an additional salt bridge and H-bond interaction with E94$^{2.65}$.
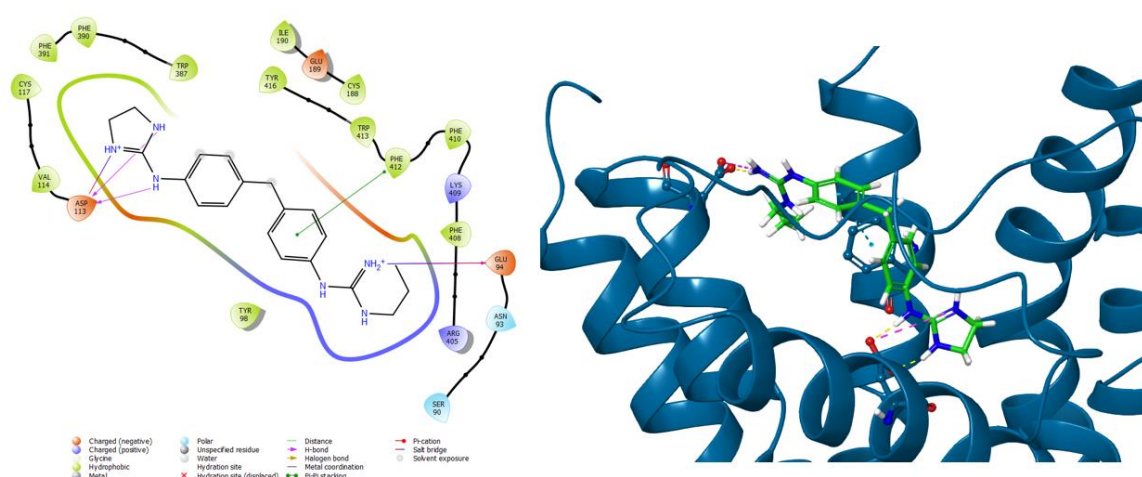

Figure 3.16 *Induced-fit docking study of compound* *16*

Surgand et al. (2006) suggested that E94$^{2.65}$, amongst other residues on TM1 and TM2 in the monoamine receptors, face antagonist ligands in the binding site, expanding this cavity and directing the ligand away from TM5 to avoid receptor activation.[118,122] For this reason, it was expected that the new compound **22c** would display this same salt bridge and H-bonding interaction with E94$^{2.65}$. This hypothesis held through when docked in the rigid receptor model α$_{2A}$-AR-X but failed when docked to the induced fit model, since the ligand formed a salt bridge with the E189$^{XL2.51}$ residue instead. However, an induced-fit docking study was also carried out using the α$_{2A}$-AR-X structure (crystallized in complex with an

antagonist) as a template, looking only for poses in which the ligand interacts with E94[2.65] and D113[3.32]. This particular pose was awarded an autodock binding affinity of -7.63 kcal/mol which was better than that of the previous orientation.
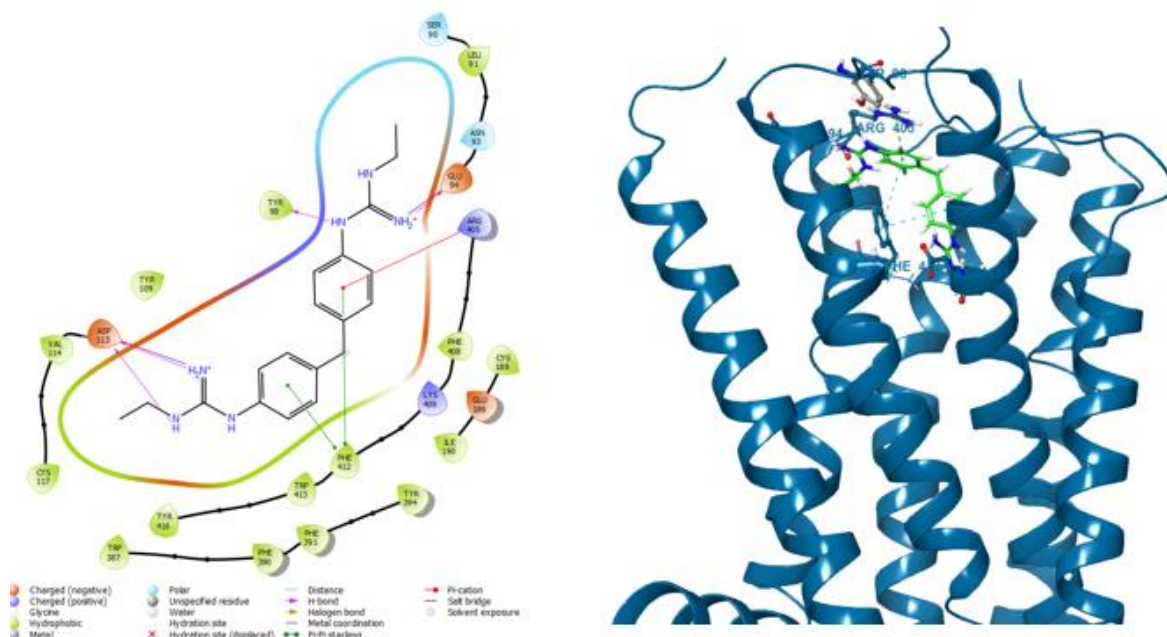

Figure 3.17 *Induced-fit docking of compound **22c** in the α_{2A}-AR-X in complex with an antagonist where only orientations with D113[3.32] and E94[2.65] were considered*

The characterisation of the different hydrogen bonds (HBs) established within the complex, distance and angles, have been carried out. By definition, the distance between the hydrogen and the acceptor atoms when a HB is formed has to be smaller than the sum of their corresponding van der Waals radii.[123] The angles of the complex must be greater than 90º to be considered a HB, those nearing 180º are indicative of strong HBs.[123] For compounds **1** (Figure 3.18) and **22c** (Figure 3.20) the distance between the hydrogen and the acceptor atom has also been used as an indication of HB strength. Distances between 1.2 – 1.5 Å would correspond to very strong HB, 1.5–2.2 Å would be found in strong HB, and 2.0 – 3.0 Å would correspond to weak HB. As seen from Figures 3.18 and 3.20, most of the HB interaction are between 1.69 Å and 2.56 Å, indicating a range from weak-strong interactions.[123]

Two of the main methods used for characterising hydrogen bonds are the Quantum Theory of Atoms in Molecules (QTAIM) proposed by Prof. Richard Bader[124] and the analysis of the natural bond orbitals (NBO) developed by Weinhold[125]. AIM theory defines chemical bonding and structure of a chemical system based on the properties of electron density in a particular point known as the bond critical point, corresponding to the saddle point in the electron density surface between the atoms.[123] This theory was applied to HBs in 1987 by

Bader *et. al.*[126] The NBO analysis is used to evaluate intermolecular interactions such as HBs.[123] This analysis transfers the delocalized molecular orbitals (MO) to the localized MO and is usually used to characterise the donation from the lone pair to the antibonding orbital, obtaining the second order energy; thus, the strength of the donation represents the strength of the interaction. Had time allowed, a more in-depth computational study of the various hydrogen bonds would have been carried out.
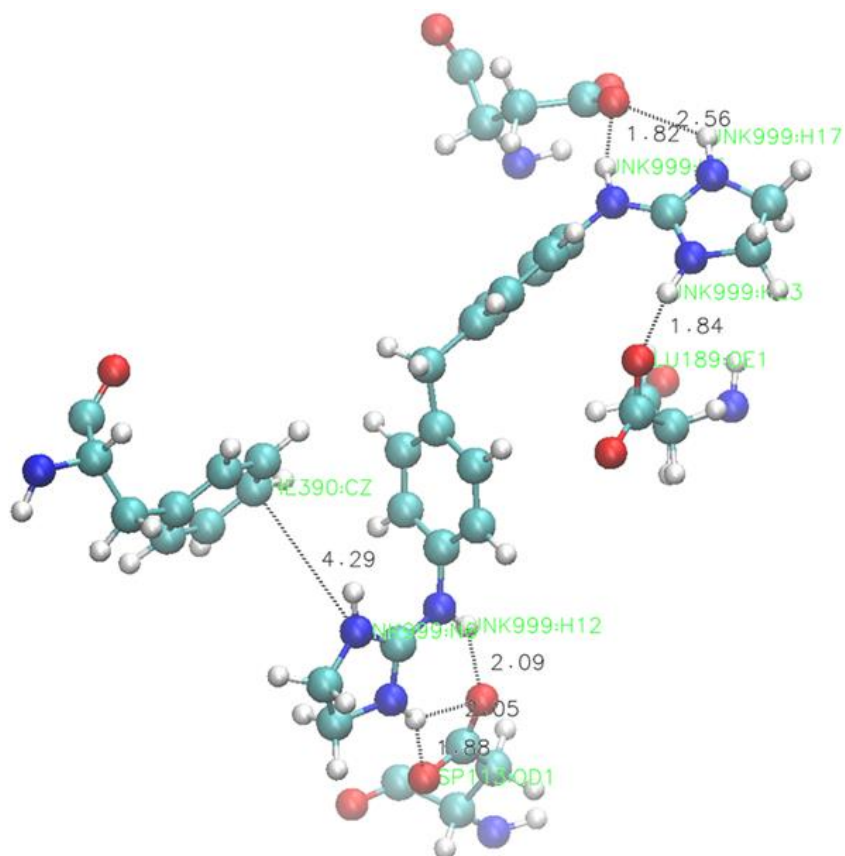

Figure 3.18 Induced-fit docking study of lead compound *1* displaying the HB bond length (Å). The shorter the bond length, the stronger the interaction
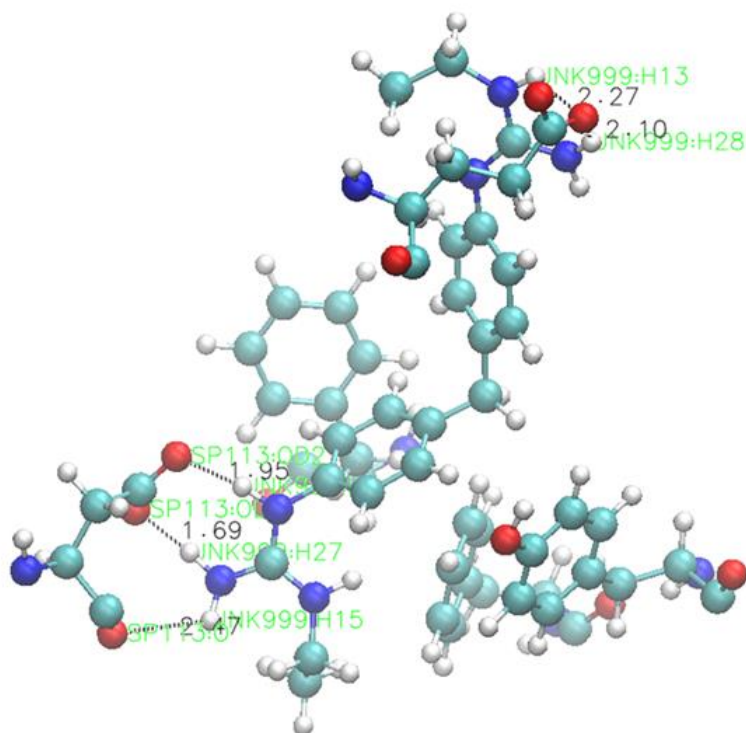
Figure 3.19 *Induced-fit docking study of lead compound **22c** displaying the HB bond length (Å). The shorter the bond length, the stronger the interaction*

When all three compounds (**1**, **16**, **22c**) were fit-induced docked into the α$_{2A}$-AR-Y structure (crystallised in complex with a partial agonist, see Appendix 22 - 24) binding interactions with S200$^{5.42}$, which is one of the most frequently reported residues on TM5 involved in receptor activation, were observed. Thus, it is queried that even though compounds **16** and **22c** are known antagonists via *in vitro* studies, the receptor may be locked into a specific conformation when in complex with a partial agonist which results in these specific interactions. For this reason, a third induced-fit docking was carried out on the homology model of Prof. Mireia Olivella (α$_{2A}$-AR-MO) as it was prepared without considering any ligand and may result in a clearer characterisation of the potential interaction between the synthesised ligands and the protein residues. Unfortunately, docking to this model did not show any obvious differences between the interactions of the agonist (**1**) and the antagonists (**16** and **22c**) and the active or inactive receptors. The main interactions present were H-bonding with S90$^{2.45}$ and N93$^{3.33}$, along with several π-π or π-cation interactions with residues on the XL1 and XL2, e.g. W99^{XL1}, W413$^{7.40}$, K409^{XL1}. None of the orientations displayed interactions with the known agonist stimulation residues on TM5 (S200$^{5.42}$).

In summary, these docking studies seem to indicate potential for the compounds proposed and synthesised and open the door to future improvements.

3.4 Pharmacological Results and Structure-Activity Discussion

In vitro pharmacological assays were used firstly to evaluate whether the potential ligands of the α_2-AR synthesised during this study bind with an acceptable affinity ($K_i < 100$ nM) to the receptor and, secondly to confirm the desired antagonist activity via functional activity assays. All these assays were performed at Prof. Callado's laboratory (University of the Basque Country, School of Medicine, Leioa, Spain) and they were carried out using human brain tissue which gives a very realistic indication of the suitability of the compounds tested to act in such a complex environment.

3.4.1 Binding Affinity Evaluation

The binding affinities of the tested compounds were measured in human prefrontal cortex (PFC) tissue using a radioligand competitive binding assay with the α_2-AR selective radioligand [^{3}H]RX821002 (2-methoxyidazoxan; see Figure 3.5) at 2 nM concentrations.

This landmark method that ultimately enabled equivalent interpretations of the affinity for both antagonists and agonists was developed by Paton and Rang in 1965 and corrected by Cheng and Prusoff in 1973, in animal tissues.[127] The Cheng-Prusoff correction allowed for the binding affinity of a non-radiolabelled ligand to be calculated.[127] These studies utilize standard radiolabelled 'hot' ligands of known affinity (K_D) at a given concentration to calculate the affinity of a competing ligand over a range of concentrations. A graph of the percentage of the bound radioligand vs the negative logarithm of the unknown ligand concentration is plotted and used to determine the IC_{50} (which is the concentration of the unknown ligand when half of the radioligand is displaced). The IC_{50} itself is not a direct measure of the binding affinity as it is dependent on the concentration of the membrane used; however, it can be directly related to the dissociation constant of affinity (K_i) using the Cheng-Prusoff equation (Figure 3.5).[128]

A)

2-methoxyidazoxan
Ki = 1.349 nM

B) $K_i = \dfrac{IC_{50}}{1 + \dfrac{[L_R]}{K_D}}$
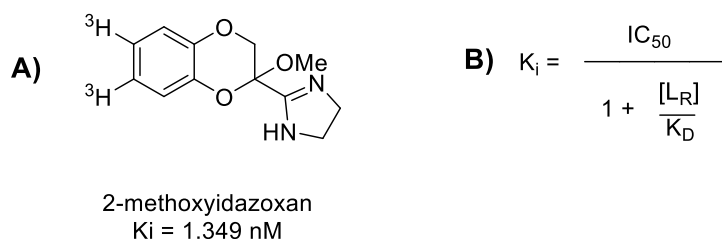
Figure 3.20 A) *The structure of the α_2-AR selective radioligand [^{3}H]RX821002 with a K_i of 1.349 nM.* **B)** *Cheng-Prusoff equation where K_i is the binding affinity of the non-radiolabelled ligand, K_D is the binding affinity of the known radioligand, the IC_{50} is determined from the previously obtained plot and represents the concentration of the unknown ligand when half of the radioligand is displaced, $[L_R]$ is the concentration of the radioligand*

In the present study these competitive α₂-AR binding assays were carried out in human brain prefrontal cortex tissue in in vitro assays developed by Rozas' collaborator Prof. Callado. The results obtained express as K_i nM values can be seen in Table 3.5.
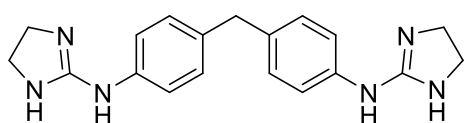
Lead Compound 1
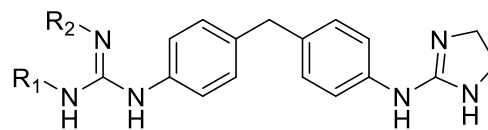
Family A

Family B

Table 3.7 *The α₂-AR binding affinities of both the previously synthesised compounds (**1,15-18**) and the newly synthesised (**19c, 21c, 22c, 25b, 28b**) measured as K_i (nM)*

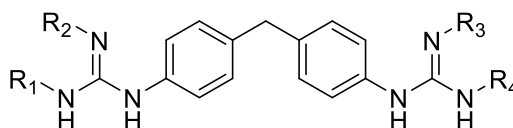| Compound	Family	R_1	R_2	R_3	R_4	K_i (nM)
RX821002	-	-				1.349
Idazoxan	-	-				10.47
1	-	imidazoline		imidazoline		1.585
15	A	H	H	imidazoline		12.30
16	A	$(CH_2)_2CH_3$	H	imidazoline		0.794
17	B	$(CH_2)_2CH_3$	H	H	$(CH_2)_2CH_3$	355
18	B	H	H	H	H	147.9
19c	B	CH_3	CH_3	CH_3	CH_3	17783
21c	B	CH_3	H	H	CH_3	263
22c	B	CH_2CH_3	H	CH_2CH_3	H	95.50
25b	B	H	H	CH_3	CH_3	6456
28b	B	CH_3	H	CH_3	CH_3	8511

The above data can be categorised into three groups to analyse the various effects on the α₂-AR binding affinity of the ligands caused by the variations in the guanidinium functional groups. In Group 1 the effect of the conformational restraint caused by the methylene bridge at the imidazoline moiety of compound **1** is investigated. This derivative is a *lead* compound within the Rozas group as it displays an excellent α₂-AR binding affinity (K_i = 1.585 nM) and

is an agonist as shown by the functional [35S]GTPγS binding experiments, which will be discussed in the following section (Section 3.3.2). When compared to compound **16**, which instead of an imidazoline on one end of the structure, has a propyl-substituted guanidine, the binding affinity was greatly improved (K_i = 0.794 nM). This seems to indicate that increased conformational freedom at one of the cationic moieties is favoured within the binding site of the $α_2$-AR receptor, since the propyl group is free to orient itself inside the binding site in a preferred manner. Considering the computational studies to be discussed in Section 3.4, it can be seen that in the best-pose of docked compound **16** within the $α_{2A}$-AR (see Figure 3.17, Section 3.4.1) the propyl group loops back towards the guanidine due to the increased steric hindrance of the lengthy sidechain. However, when the imidazoline ring was substituted by propyl-substituted guanidines at both ends of the diaryl core the $α_2$-AR binding affinity decreased drastically (K_i = 355 nM), indicating that the methylene bridge of at least one of the imidazoline moieties forces a desired orientation of the whole molecule to drive the initial binding interactions deep within the binding site.

In Group 2 the increased length of the substituents (i.e. aliphatic from compounds **18** (H atom), **21c** (CH_3-), **22c** (CH_3CH_2-), **17** ($CH_3CH_2CH_2$-) is analysed. Only the symmetrical compound **22c** (K_i = 95.50 nM) with two ethyl-substituted guanidines was shown to have an $α_2$-AR binding affinity good enough to be considered for the functional [35S]GTPγS binding assays. This result appears to be an outlier in the trend and could be related to the similarities of the ethyl-substituted guanidine to the imidazoline's five-membered ring (similar number of C atoms attached to the guanidine-like system). Compound **18** (unsubstituted bis-guanidinium derivative) showed the next best $α_2$-AR binding affinity (K_i = 147.91 nM), followed by the methyl-substituted guanidine **21c** (K_i = 263.03 nM) and the propyl-substituted guanidine **17** (K_i = 345.81 nM) symmetric derivatives. From this trend in $α_2$-AR binding affinity it could be predicted that an increase in the chain length of the alkyl substituents would result in more steric hindrance within the receptor's binding site. Moreover, when considering the results concluded from the analysis of Group 1 and Group 2, modifications to compound **22c** could result in a further increase to its $α_2$-AR binding affinity if an asymmetrical compound could be synthesised with an imidazoline moiety and the ethyl-substituted guanidine as seen in Figure 3.6.
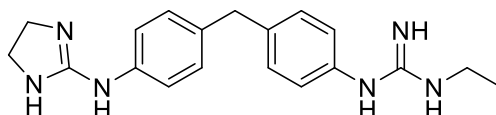

Figure 3.21 *A future compound to be investigated based on the results from group 1 and group 2*

Finally, in Group 3 the comparison between the closed imidazoline ring and open alkyl substituted guanidines at breaking points (A) and (B) as shown in Figure 3.7 is discussed.

As expected from the outcomes of Group 1 analysis, there was a decrease in the α_2-AR binding affinity by opening the methylene bridge of the imidazoline ring at both ends of the molecule. There was a drastic increase in the binding for compound **19c** (K_i = 17782 nM) which correlates with the increased steric bulk caused by the dimethyl-substituted guanidine. Furthermore, in the computational studies presented in Section 3.4, it can be seen that both the ethyl- and propyl-substituted guanidines' preferred orientation exhibits the alkyl chain curling back towards the guanidine; however, this conformation is not possible in the case of the dimethyl-substituted guanidine system. The remaining tested compounds, **25b** (K_i = 6456 nM) and **28b** (K_i = 8511 nM), were both asymmetrical molecules containing the dimethyl-guanidine in one side and both of them gave very low α_2-AR binding affinities further indicating the disfavouring of guanidine arrangement. Even the slight increase in the K_i values of compound **1** to compound **22c** additionally suggests the benefit of further investigating the asymmetric compound proposed in Figure 3.6 above.
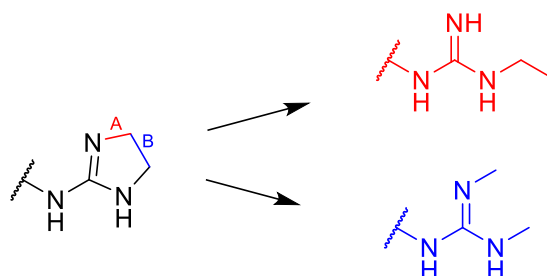

Figure 3.22 *Schematic representation of the ring opening possibilities. Incision at the A) position resulted in the mono-ethyl substituted guanidinium and the B) position resulted in the dimethyl substituted guanidine*

3.4.2 Functional Activity Assays

Functional [^{35}S]GTPγS binding experiments are used to determine whether the tested ligands are antagonists, agonists or inverse agonists toward the α_2-ARs. These assays directly measure the guanine nucleotide exchange of G proteins, an early event after GPCR activation, which is not subjected to amplification or regulation by other cellular processes.[129] A non-hydrolysable radiolabelled analogue of GTP ([^{35}S]GTPγS) is used to facilitate measurement of GPCR activation after the addition of a known agonist by measuring the amount of radiolabelled [^{35}S]GTPγS is bound to the cell membrane after washing away the unbound [^{35}S]GTPγS. This particular GTP is labelled on the γ-phosphate with ^{35}S, thus hydrolysable GTP cannot be used as it would convert to GDP too quickly, removing this radiolabelled γ-phosphate and then escaping detection.

GPCRs exhibit constitutive activity which refers to the ability of a GPCR to undergo agonist-independent isomerization from an inactive/resting (R) state where the GPCR is uncoupled

from the G-proteins, to an active (R*) state.[130] The first evidence for this constitutive activity of GPCRs was obtained for the δ opioid receptor (Koski *et. al*, 1982)[131] and β$_2$-adrenoceptor (Cerione *et. al*, 1984)[132]. The full agonist stabilizes the active R* state of GPCRs. The conformational change in GPCRs associated with the R to R* isomerization enables the dissociation of GDP from the G-proteins; thus, resulting in the GDP to [^{35}S]GTPγS exchange which can be monitored during the functional assay. In the case of full inverse agonists, they maximally stabilize the R state and reduce basal GDP/[^{35}S]GTPγS exchange.[130] Finally, inverse agonists block and decrease the activity of an agonist which, prior to the development of highly sensitive model systems and GPCR mutants, were often mistaken for antagonists. Antagonists do not alter the activity of the GPCR, rather they block both the inhibitory effects of an inverse agonist and the excitatory effects of the agonist.

Compounds which displayed an affinity less than 1 µM (Ki < 100 nM) were subjected to *in vitro* [35S]GTPγS binding experiments in human prefrontal cortex tissue to determine their nature as agonists or antagonists in the laboratory of Prof. Callado, and the results obtained are displayed in Table 3.6.

Table 3.8 *Results for the [^{35}S]GTPγS exchange functional assay in PFC human tissue. See Table 3.5 for the general structures of families A and B.*

Compound	Family	R$_1$	R$_2$	R$_3$	R$_4$	[^{35}S]GTPγS Binding Activity
RX821002	-	-				Antagonist
Idazoxan	-	-				Antagonist
1	-	imidazoline		Imidazoline		Agonist
15	A	H	H	Imidazoline		Agonist
16	A	(CH$_2$)$_2$CH$_3$	H	Imidazoline		Antagonist
18	B	H	H	H	H	Agonist
22c	B	CH$_2$CH$_3$	H	CH$_2$CH$_3$	H	Antagonist

As seen in Table 3.5 (Section 3.3.1), most of the newly synthesised compounds did not show the level of α$_2$-AR binding necessary to carry out the *in vitro* [^{35}S]GTPγS functional assay. Compounds **19c**, **21c**, **25b**, **28b**, had binding affinities (K$_i$) >100 nM largely due to the unfavoured methyl groups present in the guanidine systems. Only the symmetrical *bis*-guanidinium compound **22c** demonstrated a strong enough binding to the α$_2$-AR to be tested in the functional assay. Satisfactorily, this compound showed to act as an α$_2$-AR antagonist, not modifying the basal [^{35}S]GTPγS binding to the receptor, which was desired

as it would result in blocking the activity of an agonist at the receptor and could be used as a potential antidepressant. In Section 3.4, the computational studies performed with compounds **16** and **22c** suggest that the alkyl chain preferred to orient itself towards the guanidine in a pseudo-cyclic formation. These compounds were both α_2-AR antagonists contrary to the lead compound **1** which was an agonist; this may suggest that the conformational freedom of the guanidinium substituents in these two compounds may be identified as preferred antagonist features in comparison to the rigid imidazoline moieties of the agonist. We have previously seen how such minute changes in ligand structure can cause a drastic change in the ligand's functional activity at the α_2-AR receptor. The new compound **22c** had a high α_2-AR binding compared to the other *bis*-guanidines studied; thus, it is expected that the addition of an imidazoline ring at one end could result in a new *hit* compound (Figure 3.6, Section 3.3.1) in further studies and following the trend of compounds **16** and **22c**, it could also result in the target antagonist activity.

4. Conclusions and Future Work

The aim of this research was to investigate the effects on the binding affinity and ligand-receptor functional activity when opening the rigid 2-aminoimidazolium moiety of the *lead* compound **1** thus affecting steric and lipophilic properties. This was done by exploring the potential drug-likeness of the compounds prepared by calculating a number of pharmacokinetic and physicochemical parameters, synthesising five new compounds followed by an *in vitro* pharmacological evaluation of the binding affinity and functional activity of the compounds prepared and finally studying the binding interactions between various ligands and the α_{2A}-AR via molecular docking.

4.1 Physicochemical parameters

Using different software such as SwissADME and Chemaxon, relevant parameters (e.g. Ro5 parameters, rotatable bonds, TPSA, metabolic stability towards cytochrome P415 enzymes, solubility, ability to cross GI or BBB membranes) were calculated for all the compounds proposed indicating their suitability as potential drugs.

4.2 Synthesis

Through the course of this study, five new compounds were synthesised (**19c**, **21c**, **22c**, **25b**, **28b**). It was determined that the Kim and Qian method for guanidylation was the most effective in the synthesis of these compounds. As described in Section *3.2.2.2*, this method required the coordination of mercury (II) chloride (HgCl$_2$) to the sulfur of a suitable thiourea, in the presence of triethylamine, to initiate the reaction with primary amines. For the unsubstituted guanidinium derivatives (**25b** and **40a**) there was no need to synthesise any starting materials as the commercially available *N,N'*-bis-(*tert*-butoxycarbonyl)-*S*-methylisothiourea was a cost-effective and efficient alternative. For the rest of the compounds prepared, the di-Boc-protected *N,N'*-dimethylthiourea (**19a**, 54.69%) and *N,N'*-diethylthiourea (**20a**, 74.63%) had to be prepared. Thus, the Boc-protection is a straight-forward, anhydrous reaction in which NaH (60% immersion in oil) activated the relevant thiourea, which was then reacted with di-*tert*-butyl-dicarbonate. However, this method of preparing the Boc-protected thiourea was unsuccessful for the methyl- and ethyl-substituted thioureas (**21a** and **22a**), and thus, alternative approaches were attempted to prepare the mono-substituted bis-guanidylated products (Section 3.2.2.1). Finally, a new method for the preparation of mono-substituted di-Boc protected thioureas within the Rozas group was established using the Mitsunobu reaction conditions. This method provided a mono-

70

substituted pseudothiourea that was also bis-Boc-protected, thus providing the basis for an easier desulfurization during guanidylation. Moreover, the use of the pseudothiourea leaves only one amine available for alkylation, thus reducing the risk of unwanted side-products forming and purification is simplified. This method was used to synthesise **21a** and **22a** with good yields (80.8% and 94.8%, respectively).

Boc-deprotection was carried out using a 50% solution of TFA in DCM, in excess and stirred overnight, at room temperature to yield the guanidine trifluoroacetate salts. However, since these salts are insoluble in water what is a requisite for the pharmacological evaluations, an ion exchange was carried out using activated Amberlite® IRA-400 resin in its chloride form. Accordingly, the guanidine hydrochloride salts of compounds **19c**, **21c**, **22c**, **25b**, **28b** were obtained in good yield (>85%).

Scheme 4.1 *General reaction scheme illustrating the successful synthesis of the five final compounds*
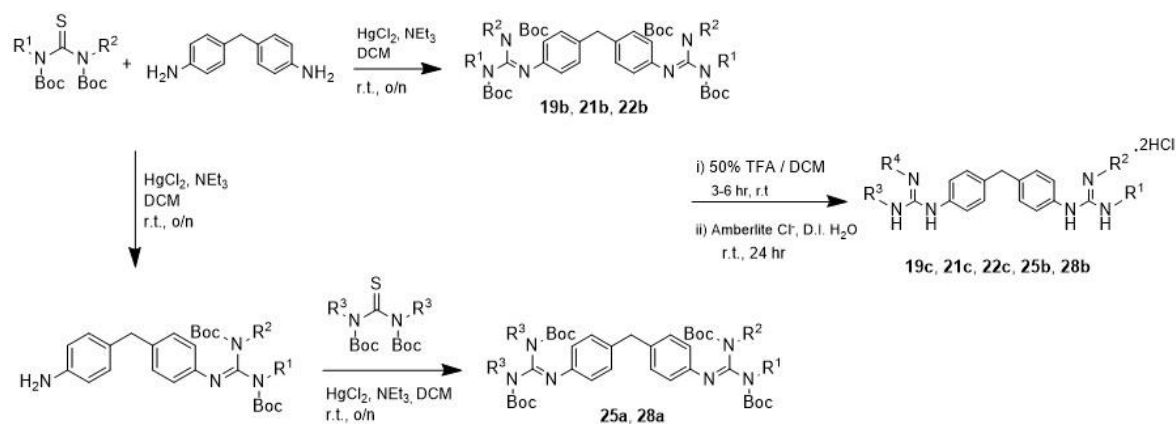
4.3 Computational Studies

The docking studies were carried out using the software Maestro (Schrödinger Inc.). The molecules were docked into three different α_2-AR models: α_{2A}-AR-MO (an homology model developed by Prof. Mireia Olivella from the Universitat de Vic in Spain, before any α_2-AR crystal structures were published), α_{2A}-AR-Y (6KUY: crystal structure of the α_{2A}-AR in complex with a partial agonist), α_{2A}-AR-X (6KUX: crystal structures of the α_{2A}-AR in complex with an antagonist). The crystal structures of the α_{2A}-AR were retrieved from the RCSB PDB to be used for docking studies. Standard and induced-fit docking studies were carried out and the chosen orientations of the docked compounds were based on the ionic interaction with the aspartate residue D113[3.32] as this has been reported to be a critical anchoring interaction with the α_2-AR binding sites. Both rigid receptor models and induced-fit docking were carried out on compounds **1**, **16** and **22c**. As expected, the autodock binding affinity

related to those compounds were increased drastically based in the receptor's ability to orient itself to better fit the ligand docked.

The previously synthesised agonists, **15** and **18**, displayed H-bonding with S200[5.42], a known residue involved in agonist activity. Additional salt bridge and H-bonding interaction with the D192[XL2] and E189[XL2.51] residues were also common between compounds **1**, **15**, **18**. The XL2, which is directly linked to TM5, could be participating in directing the ligand towards TM5 to initiate the receptor activation. Moreover, the salt bridge interaction between the ligand and the E94[2.65] residue is a common denominator amongst the two known antagonists, **16** and **22c** since these interactions could assist in directing the ligand away from TM5, thus avoiding receptor activation.

4.4 Pharmacological Studies

In collaboration with Prof. Callado at the Department of Pharmacology at the School of Medicine in the University of Basque County UPV/EHU (Spain), in vitro pharmacological studies were carried out of the successfully synthesised compounds to determine their affinity for the α_2-AR (K_i values) and their functional activity on the receptor (agonist or antagonist) in human brain prefrontal cortex (PFC) tissue. These *in vitro* studies could only be carried out if the compounds to be tested are above 95% pure, thus the purity of all compounds prepared was proved to be within this threshold by HPLC analysis before sending the compounds to Prof. Callado's laboratory.

The binding affinities of the tested compounds were measured in human PFC tissue using a radioligand competitive binding assay with the α_2-AR selective radioligand [^{3}H]RX821002 (2-methoxyidazoxan) at 2 nM concentrations. Only one of the five newly synthesised compounds showed a strong enough binding affinity to be tested for its functional activity in the [^{35}S]GTP-γ-S exchange assay (**22c**, 95.50 nM). The corresponding SARs were deduced comparing different aspects of the compounds. First, comparison of the conformational freedom provided by the opening of the imidazolinium moiety to form the previously synthesised compound **16** was considered. The release of the conformational restraint on one end forming an asymmetrical product greatly improved the binding affinity from 1.585 nM (**1**) to 0.79 nM (**16**); however, by releasing both imidazolium moieties the binding affinity was negatively impacted resulting in a K_i of 355 nM (**17**). Therefore, it was concluded that maintaining one imidazolium moiety within the compound would assist in driving the initial binding, due to the conformational restraint potentially forming a strengthened anchoring system with the D113[3.32] residue. Secondly, the increased carbon chain length appeared to be inversely proportional to the binding affinities for the symmetric compounds **18** (unsubstituted guanidines, 147.9 nM), **21c** (methyl substituted, 263.03 nM), **17** (propyl substituted, 355 nM). From this trend in the data it would be predicted that the increase in

alkyl chain length would result in more steric hindrance within the receptor's binding site. Compound **22c** (ethyl substituted, 95.50 nM) was an outlier as it had a very promising binding affinity, which was unexpected for the symmetrical mono-substituted bis-guanidiniums. As seen in the computational studies, this substituent appeared to fold back towards the guanidinium, potentially occupying the desired space within the receptor and forming weak van der Waals contacts with the residues within the binding site. On the other hand, the binding affinities of the compounds decreased dramatically when the dimethyl substituted guanidinium derivatives were tested, with the symmetrical di-substituted molecule resulting in the highest K_i value (17782.79). This is indicative of the disfavoured conformation formed by the methyl substituents.

Only compound **22c** had a binding affinity within the threshold necessary to test functional activity. As confirmed with the computational results, this compound was an antagonist which was the desired result for potential antidepressant activity. As aforementioned this compound achieved the lowest K_i value for binding affinity of all the alkyl substituted bis-guanidiniums (95.50 nM).

4.5 Future work

From the comparative study between the previously synthesised compounds **1**, **16**, **17** and the newly synthesised **22c** it was determined that a further investigation into a compound containing both an imidazolium moiety and an ethyl-substituted guanidinium could potentially demonstrate a very promising binding affinity along with potential antagonist activity. Moreover, a more detailed computational study would be carried out on the characterization of the HBs of each of the compounds.
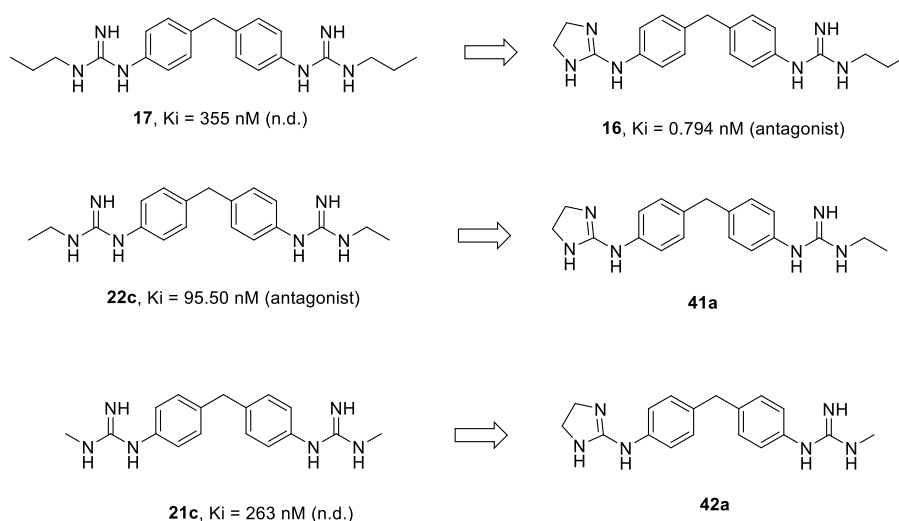

17, Ki = 355 nM (n.d.)

16, Ki = 0.794 nM (antagonist)

22c, Ki = 95.50 nM (antagonist)

41a

21c, Ki = 263 nM (n.d.)

42a

Figure 4.1 *Compounds **41a** and **42a** theoretically fit the profile of some good binding compounds to the α2A-AR with antagonist activity*

5. Experimental

5.1 General Materials and Methods

All solvents used in this project were analytical (HPLC) grade. All chemicals and reagents used were supplied by Merck (Sigma Aldrich), Fischer or VWR and were used as received. All glassware was pre-dried in an oven before use with anhydrous solvents. Anhydrous THF was obtained from the PureSolv MD-4EN Solvent Purification System (SPS) using molecular sieves. All glassware was washed with water and acetone before use. Silica gel 40 – 63 µm (Merck, 230-400 mesh) was used for gravity column chromatography. All compounds were subject to this purification unless stated otherwise. The analytical thin layer chromatography (TLC) was carried out with silica gel 60 (fluorescence indicator F254; Merck) or aluminium oxide 60 (F_{254}, neutral; Merck) TLC plates and visualised under UV radiation (Spectroline, model ENF-204C/FE).

The proton, carbon and fluorine NMR spectra were carried out at room temperature using a Brucker 400 MHz UltraShield™. The spectra were recorded at 400 MHz and 600 MHz for ^{1}H NMR and 100 MHz for ^{13}C NMR. TMS was used as the internal standard reference (^{1}H, δ = 0.00 ppm) with the remaining chemical shifts appearing downfield from the reference. All Boc-protected samples were dissolved in deuterated chloroform ($CDCl_3$) and the final salts were performed in deuterated water (D_2O), unless stated otherwise. A rapid exchange occurs between the protons of the NH_2 substituents on the final hydrochloride salts and the deuterium within the D_2O NMR solvent, thus these proton signals do not appear on the attached spectra (See Appendices). The NMR data was processed using the Bruker TOPSPIN and MestReNova software.

FTIR spectra was obtained using a Perkin Elmer spectrum 100 FT-IR spectrometer and fitted with a Universal Attenuated Total Reflectance (ATR) sampling accessory and the ATR method was used throughout the project.

The melting point was determined using a Stuart Scientific Melting Point SMP1 apparatus.

Electrospray Ionisation (ESI) mass spectra were obtained in positive and negative modes, as required, using a Micromass time of flight (TOF) mass spectrometer with a WATERS 2690 HPLC autosampler using methanol or chloroform as the carrier solvent.

Reverse phase HPLC was used to determine that the purity of the final hydrochloride salts was above the minimum requirement of 95.0 %. This was done using a Varian ProStar system equipped with a Varian Prostar 335 diode array detector and a manual injector (20 µL), scanning wavelengths from 200 to 950 nm. For purity assessment, UV detection was performed at 245 nm and peak purity was confirmed using a purity channel. The stationary

phase consisted of an ACE 5 C18-AR column (150 mm × 4.6 mm), and the mobile phase used the following gradient system, eluting at 1 mL/min: aqueous formate buffer (30 mM, pH 3.0) for 10 min, linear ramp to 85% methanol buffered with the same system over 25 min, hold at 85% buffered methanol for 10 min.
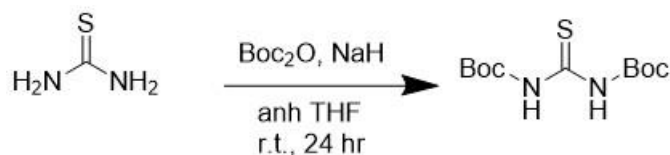
5.2 Computational Details

The computational docking studies were carried out using the software maestro (Schrödinger Inc.).[133] The ligands were generated via the LigPrep function with default ionizer and tautomerizer and the protein preparation was carried out using the Protein Preparation Wizard (PrepWizard) in Maestro.[134]

Structures for the induced-fit docking were prepared using the Maestro[133] software package and aligned using the Protein Structure Alignment module in Prime.[135]

The structures of the α_{2A}-AR complexed with a partial agonist (6KUY) or with an antagonist (6KUX) were retrieved from the RCSB PDB to be used for docking studies. Induced docking was carried out, and only ligands which interact with ASP113 were considered.

5.3 General Chemical Procedures

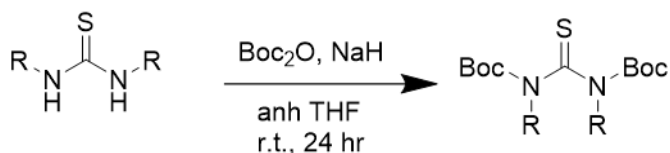**Method A:** *Boc-protection of unsubstituted thiourea*[43]

To a solution of commercially available, unsubstituted thiourea (1.0 eq.) in dry THF, sodium hydride 60 % immersion in oil (4.5 eq.) was added carefully at 0 ºC with stirring. The reaction was slowly brought to room temperature and allowed to stir for 45 minutes. The reaction was then cooled back down to 0 ºC and di-tert-butyl-dicarbonate (2.2 eq., 57.794 µmol) was added. The reaction was brought back to room temperature and allowed to stir overnight.

Upon completion, the reaction was quenched slowly using $NaHCO_3$ saturated solution (10 cm^3) and the solvent was reduced. The solid obtained was re-dissolved in DCM and washed with water (3x 20 cm^3). The combined organic layers were dried over $MgSO_4$, filtered and concentrated in vacuum.

The product was then recrystallised from hot combination solvents, hexane and ethyl acetate, to obtain the purified product.

Method B: *Boc-protection of N,N'-disubstituted thiourea*[43]


To a solution of commercially available *N,N'*-disubstituted-thiourea (1.0 eq.) in dry THF, sodium hydride 60 % immersion in oil (4.5 eq.) was added carefully at 0 °C with stirring. The reaction was slowly brought to room temperature and allowed to stir for 45 minutes. The reaction was then cooled back down to 0 °C and di-*tert*-butyl-dicarbonate (2.2 eq.) was added. The reaction was brought back to room temperature and allowed to stir overnight.

Upon completion, the reaction was quenched slowly using NaHCO3 saturated solution (25 cm^3) and added to deionised water (150 cm^3) and extracted with ethyl acetate. The combined organic phases were then washed with brine. The extracted organic phase was dried over MgSO$_4$, filtered and concentrated in vacuum.

The purified product was obtained by gravity column chromatography using the appropriate ratio of hexane and ethyl acetate.

Method C: *Synthesis of mono Boc-protected N-substituted thiourea* [136]
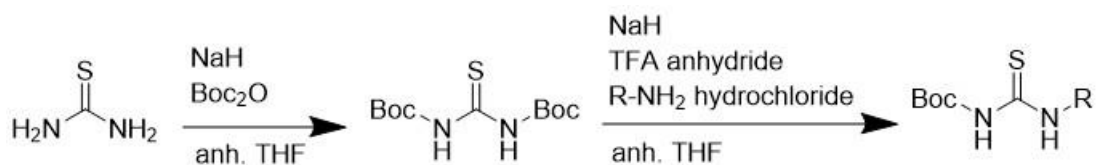

Unsubstituted thiourea (1.0 eq.) was dissolved in dry THF (110 cm^3) under argon gas and brought to 0 °C before adding the NaH 60% immersion in oil (4.5 eq.). The solution was stirred in the ice-bath for 5 minutes to allow the reagents to fully dissolve. Once complete the reaction was stirred at room temperature for 45 minutes before being cooled to 0 °C once more. Di-*tert*-butyl-dicarbonate (2.5 eq.) was added. After 30 minutes stirring at 0 °C, the ice bath was removed, and the reaction was allowed to stir overnight at room temperature.

After monitoring the formation of the *N,N'*-bis-Boc-thiourea by TLC, the reaction was cooled back to 0 °C and NaH 60% immersion in oil (1.7 eq.) was added carefully. After 1 hour, TFA anhydride (1.54 eq.) was added. After a further 1 hour of stirring at 0 °C, methylamine hydrochloride (1.54 eq.) was added and allowed to fully immerse in solution before the removal of the ice-bath. The reaction was gradually brought back to room temperature and allowed to stir overnight.

Upon completion, the reaction was cooled to 0 °C and quenched with deionised water (40 cm^3), dropwise. The product was extracted using ethyl acetate (4 x 50 cm^3) and the combined organic layers were washed with brine (4 x 50 cm^3). The organic phase was dried over MgSO$_4$, filtered and concentrated under vacuum. Purification of the product by column chromatography using a hexane and ethyl acetate gradient mixture was carried out to afford the final product.

Method D: *General procedure for the bis-Boc-protected N-substituted pseudothiourea*[91]
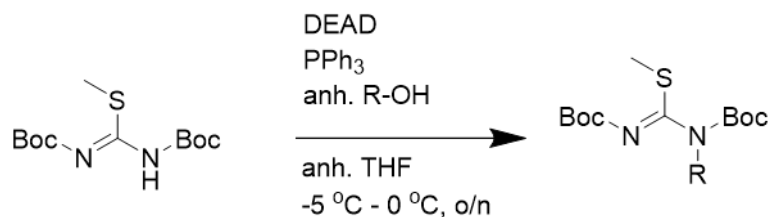
A solution of 1,3-Bis(*tert*-butoxycarbonyl)-2-methyl-2-pseudothiourea (1 eq.), anhydrous alcohol (1.5 eq.), and triphenylphosphine (1.5 eq.) in dry THF (15 cm^3) under argon gas was cooled to -5 °C. Diethyl azodicarboxylate (3 eq.) was added dropwise at a rate such that the reaction mixture was completely colourless before the addition of the next drop. The reaction was then gradually brought to room temperature and stirred overnight. The reaction was monitored by TLC. Once complete, methanol (10 cm^3) was added to the solution and then the solvent was reduced. The product was purified by flash chromatography a hexane and ethyl acetate gradient mixture, yielding the final compound.

**Method E:** *General procedure for the synthesis of Boc-protected mono-guanidine derivative*[43]
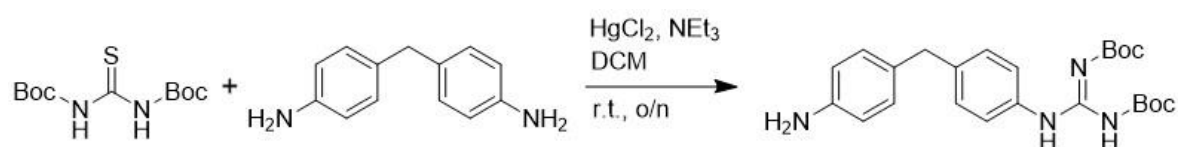
4,4'-Methylenedianiline (3.0 eq.) was dissolved in DCM, cooling the mixture below 0 °C, and reacted with *N,N'*-di(*tert*-butoxycarbonyl)thiourea (1.0 eq.). The mixture was treated with HgCl$_2$ (1.5 eq.) and NEt$_3$ (6 eq.) and stirred for 15 minutes at 0 °C. The reaction was gradually brought back to room temperature while stirring and monitored by TLC analysis until complete.

The reaction was filtered through Celite and rinsed with DCM to remove any of the mercury by-product (mercury chloride and mercury sulfide mixture). The filtrate was extracted using

DCM (3 x 20 cm^3) and then washed with deionised water (3 x 20 cm^3). The combined organic layers were dried over magnesium sulphate (MgSO$_4$), filtered and concentrated using the rotary evaporator to obtain the crude product. The product was then purified by gravity column chromatography using the appropriate ratio of hexane and ethyl acetate.

Method F: *Synthesis of Boc-protected N,N'-disubstituted mono-guanidine derivative*[43,78]
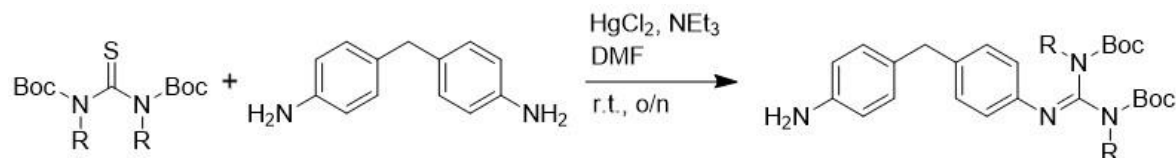
4,4'-Methylenedianiline (3.0 eq.) was dissolved in DMF and cooled below 0 ºC. The respective Boc-protected *N,N'*-disubstituted thiourea (1 eq.,) was added to the mixture and then treated with HgCl$_2$ (1.5 eq.) and sodium bicarbonate (6 eq.). The reaction mixture was stirred for 15 minutes at 0 ºC and then gradually brought back to room temperature and stirred overnight.

The reaction was monitored by TLC and once complete it was filtered through a bed of Celite and rinsed with DCM to remove any of the mercury by-product. The filtrate was washed with brine (2 x 20 cm^3) and extracted using DCM (3 x 20 cm^3) and deionised water (3 x 20 cm^3). The combined organic layers were dried over magnesium sulphate (MgSO$_4$), filtered and concentrated using the rotary evaporator to obtain the crude product. The product was then purified by gravity column chromatography using the appropriate ratio of hexane and ethyl acetate.

Method G: *General procedure for the synthesis of Boc-protected disubstituted bis-guanidine derivatives*[43,78]
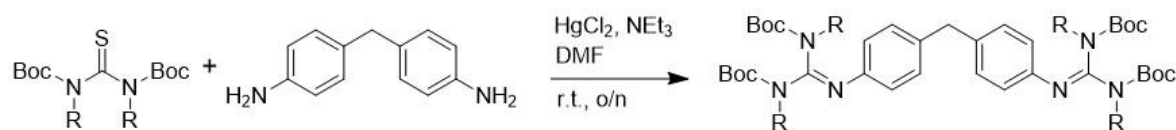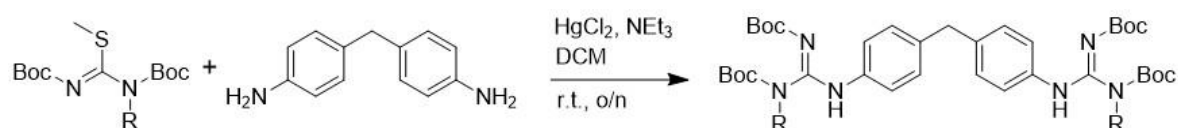

4,4'-Methylenedianiline (1.0 eq.) was dissolved in DMF at 0 ºC and reacted with *N,N'*-di(*tert*-butoxycarbonyl)disubstituted thiourea (2.5 eq.). The mixture was treated with HgCl$_2$ (1.5 eq.) and an excess of sodium bicarbonate (6 eq.) and stirred for 15 minutes at 0 ºC. The reaction was gradually brought back to room temperature and stirred overnight. The reaction was monitored by TLC analysis.

Upon completion the mixture was filtered through a bed of Celite and rinsed with DCM to remove any of the mercury by-product. The filtrate was washed with brine (2 x 20 cm^3) and

extracted using DCM and deionised water (3 x 20 cm³). The combined organic layers were dried over magnesium sulphate (MgSO₄), filtered and concentrated using the rotary evaporator to obtain the crude product.

The product was then purified by gravity column chromatography using the appropriate ratio of hexane and ethyl acetate.

Method H: *General procedure for the synthesis of Boc-protected mono-substituted bis-guanidine derivatives* [43,78]


4,4'-Methylenedianiline (1.0 eq.) was dissolved in DCM below 0 °C and reacted with the respective *N,N'*-di(*tert*-butoxycarbonyl)monosubstituted thiourea (2.5 eq.). The mixture was treated with HgCl₂ (1.5 eq.) and an excess of triethylamine (6 eq.). The reaction was gradually brought back to room temperature and stirred overnight. The reaction was monitored by TLC analysis.

Upon completion the mixture was filtered through a bed of Celite and rinsed with DCM to remove any of the mercury by-product. The filtrate was washed with brine (2 x 20 cm³) and extracted using DCM and deionised water (3 x 20 cm³). The combined organic layers were dried over magnesium sulphate (MgSO₄), filtered and concentrated using the rotary evaporator to obtain the crude product.

The product was then purified by gravity column chromatography using the appropriate ratio of hexane and ethyl acetate.

Method I: *Synthesis of the hydrochloride salts – TFA method* [102]
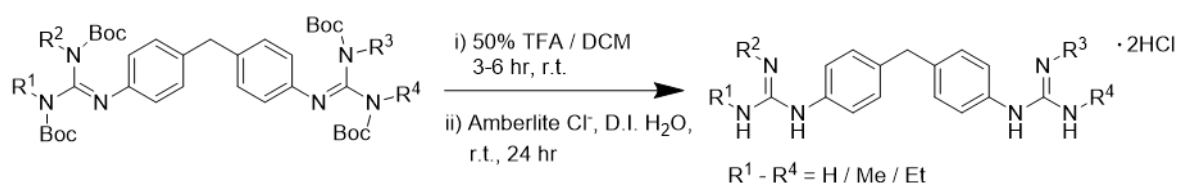
The relevant Boc-protected sample (400 mg) was dissolved in an excess of 50% TFAA dissolved in DCM (20 cm³) and stirred at room temperature for 3-6 hours. The solvent was then reduced by rotary evaporation. The remaining TFA salt was re-dissolved in deionised water (20 cm³) and treated with Amberlite IRA 400 chloride form and allowed to stir gently for 48 hours at room temperature. When the reaction was judged complete using the TLC method, the product was extracted using DCM (3 x 20cm³). The combined organic layers

were dried over MgSO$_4$, filtered and concentrated in vacuum to obtain the hydrochloride salt.
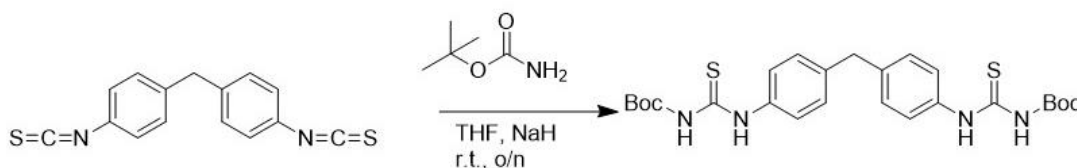
Synthesis of 1,1'-Methylenebis(4-isothiocyanatobenzene)[102]
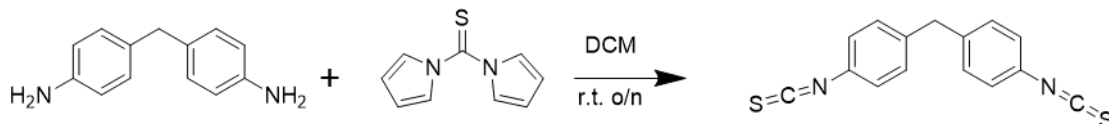
4,4'-Methylenedianiline (1.0 eq.) was dissolved in dry DCM and allowed to stir at 0 °C for 10 minutes before the addition of 1,1'-thiocarbonyl bis-imidazole (2.2 eq.). The reaction was gradually brought to room temperature and stirred for 5 hours. The reaction was judged complete using the TLC method. The solvent was reduced by rotary evaporation to obtain a red-brown solid.

The product was purified using a 6:4 ratio of hexane and ethyl acetate, respectively, in a gravity column chromatography.

Synthesis of 1,1'-(Methylene-di-4,1-phenylene)bis(thiourea)[102]

To a cooled solution of *tert*-butyl carbamate (2.5 eq.) in dry THF (8 cm^3) at 0 °C, NaH 60 % immersion in oil (9 eq.) was added. The reaction mixture was stirred at 0 °C for 20 minutes before adding the previously synthesised 1,1'-Methylenebis(4-isothiocyanatobenzene). The solution was brought to room temperature and allowed to stir for 5 hours. The reaction was monitored by TLC until complete.

Once complete, the reaction was quenched with deionised water (5 cm^3) and stirred for a further 15 minutes. The solvents were reduced by rotary evaporation and the solid obtained was re-dissolved in DCM and washed with deionised water (6 x 20 cm^3). The crude product was purified using gravity column chromatography with an 8:2 ratio of hexane and ethyl acetate respectively.

Synthesis of 1,1'-(Methylenedi-4,1-phenylene)-N-ethoxycarbonyl-bis(thiourea)[101]
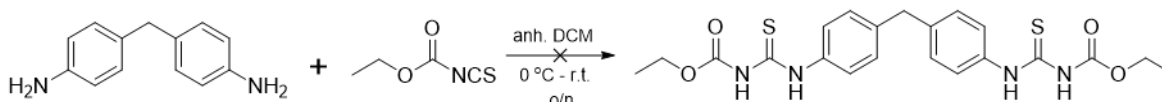
To a solution of 4,4'-methylenedianiline (1.0 eq.) dissolved in anhydrous DCM under argon, ethoxycarbonyl isothiocyanate (2.2 eq.) was added below 0 ºC was added. After 15-20 minutes of stirring below 0 ºC, the reaction was gradually brought back to room temperature and stirred overnight. The reaction was monitored by TLC and once deemed complete the solvent was removed. The product was purified by column chromatography using the appropriate hexane/ ethyl acetate gradient.

5.3   Synthesis and Characterisation

N,N'- (Di-*tert*-butoxycarbonyl)-thiourea (35a)
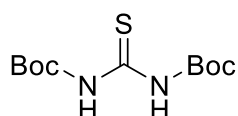
Following Method A, at approximately 0 ºC NaH 60 % immersion in oil (2,166 mg, 4.5 eq., 54.05 mmol) was added to a solution of thiourea (916 mg, 1eq., 12.03 mmol) dissolved in dry THF (205 cm^3). The reaction mixture was brought to room temperature and stirred for 45 minutes. The reaction was cooled back to 0 ºC and di-*tert*-butyl-dicarbonate (7,867 mg, 3 eq., 36.09 mmol) was added. The reaction was brought back to room temperature and stirred overnight.

Upon completion, the reaction was quenched slowly using NaHCO$_3$ saturated solution (10 cm^3) and the solvent was reduced. The solid obtained was re-dissolved in DCM and washed with water (3x 20 cm^3). The combined organic layers were dried over MgSO$_4$, filtered and concentrated in vacuum.

The product was then recrystallised from hot combination solvents, hexane and ethyl acetate, to obtain **35a** (1.4156 g, 42.6%) a white crystalline solid.

Yield: 1.4156 g, 42.6%

Molar Mass: 276.35 gmol^{-1}

MP: 130 – 134 ºC. (Lit. 131 – 135 ºC)[137]

δ$_H$ (400 MHz, CDCl$_3$): 1.54 (s, 18H, CH$_3$-Boc)

δ$_C$ (100 MHz, CDCl$_3$): 27.98 (CH$_3$, Boc), 84.11 (q-C, Boc), 150.30 (C=O, Boc), 177.79 (C=S)

ν_{max} (ATR)/cm^{-1}: 3167.15 (NH), 2989.27, 2936.48, 1768.51 (C=O, ester), 1718.95, 1553.41 (N-H), 1504.28 (N-H), 1451.71, 1393.31 (CH$_3$), 1366.75, 1282.02, 1225.4 (C-N), 1126.50 (C-O), 1073.80(C=S), 883.88, 867.64, 767.42, 746.10, 725.25, 628.64, 562.71

HRMS (m/z APCI$^-$): Calculated for C$_{11}$H$_{20}$N$_2$O$_4$S, [M] 276.11, Found: [M-H]$^-$ 275.1073

4-Amino-4'-[2,3-di(*tert*-butoxycarbonyl)guanidino]diphenylmethane (40a)
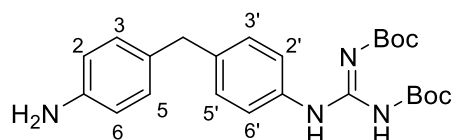
Using Method E, 4,4'-Methylenedianiline (3.0 eq*., 1,024 mg, 5.166 mmol) was dissolved in DCM at 0 °C and reacted with *N,N'*-di(*tert*-butoxycarbonyl)-thiourea (1.0 eq, 476 mg, 1.722 mmol). The mixture was treated with HgCl$_2$ (1.5 eq., 701.28 mg 2.583 mmol) and NEt$_3$ (6 eq., 1.44 cm^3, 10.332 mmol, 0.726 gcm^{-3}) and stirred for 15 minutes at 0 °C. The reaction was gradually brought back to room temperature while stirring and monitored by TLC analysis until complete.

The reaction was filtered through Celite and rinsed with DCM to remove any of the mercury by-product. The filtrate was washed with brine (2 x 20 cm^3) and extracted using DCM and deionised water (3 x 20 cm^3). The combined organic layers were dried over magnesium sulphate (MgSO$_4$), filtered and concentrated using the rotary evaporator to obtain the crude product.

Gravity column chromatography was used to yield the purified product **40a** (500.3 mg, 63.62%) using the appropriate ratio of hexane and ethyl acetate (8:2, respectively).

Yield: 500.3 mg, 63.62%

Molar Mass: 440.54 gmol^{-1}

δ_H (400MHz, CDCl$_3$): 1.54 (d, 18H, CH$_3$-Boc), 3.86 (s, 2H, CH$_2$), 6.67 (d, 2H, J 8Hz, H-2, H-6), 6.97 (d, 2H, J 8Hz, H-2', H6',), 7.15 (d, 2H, J 8Hz, H-3, H-5), 7.52 (d, 2H, J 8Hz, H-3', H-5').

δ_C (100MHz, CDCl$_3$): 28.09 (CH$_3$), 40.50 (CH$_2$), 83.60 (q, Boc), 115.97 (Ar, H-2, H-6), 122.30 (Ar, H-2', H-6'), 129.23 (Ar, H-3, H-5), 129.84 (Ar, H-3', H-5'), 132.14 (q, Ar), 138.27 (q, C-N), 152.89 (C=N), 163.45 (C=O)

N,N'-(Di-*tert*-butoxycarbonyl)dimethylthiourea (19a)
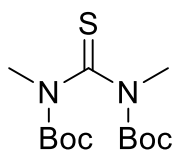
Using Method B, sodium hydride 60 % immersion in oil (933 mg, 4.5 eq, 38.88 mmol) was added to a solution of *N,N'*-dimethylthiourea (1.0 eq, 900 mg, 8.64 mmol) in dry THF (200 cm^3) at 0 °C with stirring. The reaction was slowly brought to room temperature and allowed to stir for 45 minutes. The reaction was then cooled back down to 0 °C and di-*tert*-butyl-dicarbonate (4,148 mg, 2.2 eq, 19.01 mmol) was added carefully. The reaction was brought back to room temperature and allowed to stir overnight.

Upon completion, the reaction was quenched slowly using NaHCO3 saturated solution (25 cm^3) and added to deionised water (150 cm^3) and extracted with ethyl acetate. The combined organic phases were then washed with brine. The extracted organic phase was dried over MgSO$_4$, filtered and concentrated in vacuum.

The product was purified by gravity column chromatography using the appropriate ratio of hexane and ethyl acetate (9:1, respectively) to yield **19a** (1,436.7 mg, 54.69%) a yellow oil.

Yield: 1,436.7 mg, 54.69%

Molar Mass: 304.41 gmol^{-1}

δ$_H$ (400MHz, CDCl$_3$): 1.45 (s, 18H, CH$_3$-Boc), 3.46 (s, 6H, CH$_3$)

δ$_C$ (100MHz, CDCl$_3$): 28.02 (CH$_3$, Boc), 39.51 (C-N), 83.36(q-C, Boc), 151.13 (C=O, Boc), 191.21 (C=S)

ν$_{max}$ (ATR)/cm^{-1}: 2978.59 (N-H), 2939.40, 1718.14 (C=O), 1428.16 (CH$_3$), 1394.08, 1368.72, 1317.15, 1275.81, 1250.26 (C-N), 1159.95 (C-O), 1095.15 (C=S), 1055.89, 980.87, 906.44, 850.78, 756.55, 661.57, 613.50

HRMS (m/z ESI$^+$): Calculated for C$_{13}$H$_{24}$N$_2$O$_4$S, [M] 304.15, Found: [M+Na]$^+$ 327.1355

R$_f$: 7:3 Hexane/Ethyl Acetate, 0.76

4-Amino-4'-[(2,3-di(*tert*-butoxycarbonyl)-*N,N'*-dimethyl)guanidino]diphenylmethane (39a)
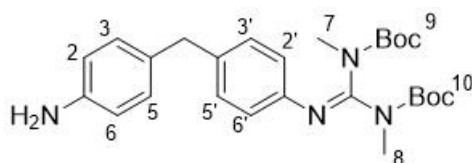
Using Method F, 4,4'-methylenedianiline (977.42 mg, 3.0 eq., 4.93 mmol) was dissolved in DMF at 0 ºC and reacted with **19a** (500 mg, 1 eq., 1.64 mmol). The mixture was treated with $HgCl_2$ (667.89 mg, 1.5 eq., 2.46 mmol) and sodium bicarbonate (826.63 mg, 6 eq., 9.84 mmol) and stirred for 15 minutes at 0 ºC. The reaction was gradually brought back to room temperature while stirring and monitored by TLC analysis until complete.

The reaction was filtered through Celite and rinsed with DCM to remove any of the mercury by-product. The filtrate was washed with brine (2 x 20 cm^3) and extracted using DCM and deionised water (3 x 20 cm^3). The combined organic layers were dried over magnesium sulphate ($MgSO_4$), filtered and concentrated using the rotary evaporator to obtain the crude product.

Gravity column chromatography, using the appropriate ratio of hexane and ethyl acetate, was used to afford **39a** (457.3 mg, 49.7%).

Yield: 457.3 mg, 46.7%

Molar Mass: 468.60 gmol^{-1}

δ_H (400MHz, CDCl$_3$): 1.50 (s, 9H, CH$_3$, Boc-9), 1.43 (s, 9H, CH$_3$, Boc-10), 2.64 (s, 3H, CH$_3$, H-7), 3.33 (s, 3H, CH$_3$, H-8), 3.86 (s, 2H, CH$_2$), 6.68 (d, 2H, J 8Hz, H-2, H-6), 6.81 (d, 2H, J 8Hz, H-2', H-6'), 6.99 (d, 2H, J 8Hz, H-3, H-5), 7.13 (d, 2H, J 8Hz, H-3', H-5').

δ_C (100MHz, CDCl$_3$): 28.22 (CH$_3$, Boc), 28.25 (CH$_3$), 36.16 (C-N), 40.48 (CH$_2$), 81.58 (q, Boc), 82.19 (q, Boc), 115.58 (Ar, H-2, H-6), 122.81 (Ar, H-2', H-6'), 129.61 (Ar, H-3, H-5), 129.74 (Ar, H-3', H-5'), 137.52 (q, Ar), 144.67 (q, C-N), 153.01 (C=N), 153.32 (C=O)

ν_{max} (ATR)/cm^{-1}: 3470.96 (NH), 3376.06 (NH), 2980.82 (CH$_2$), 1715.85 (C=O), 1693.68 (C=N), 1629.59, 1604.04, 1517.92, 1432.52 (CH$_3$), 1346.47, 1257.19 (C-N), 1135.83 (C-O), 1079.36, 948.57, 852.99, 832.53, 766.70, 725.66, 594.64

HRMS (m/z ESI$^+$): Calculated for C$_{26}$H$_{36}$N$_4$O$_4$, [M] 468.27 Found: [M+Na]$^+$ 491.2650

R$_f$: 7:3 Hexane/Ethyl Acetate, 0.25

4-Bis-[(2,3-di(*tert*-butoxycarbonyl)-*N,N'*-dimethyl)guanidino]-diphenylmethane (19b)
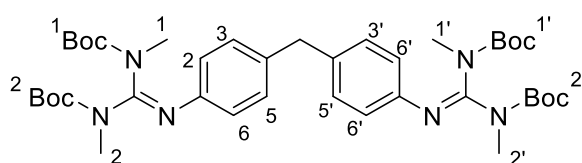
Using Method G, 4,4'-methylenedianiline (374.2 mg, 1.0 eq., 1.89 mmol) was dissolved in DMF at 0 °C and reacted with **19a** (2.5 eq., 1,435 mg, 4.72 mmol). The mixture was treated with $HgCl_2$ (1.5 eq., 1,537.8 mg, 5.664 mmol) and sodium bicarbonate (6 eq., 952.64 mg, 11.34 mmol) and stirred for 15 minutes at 0 °C. The reaction was gradually brought back to room temperature while stirring and monitored by TLC analysis until complete.

The reaction was filtered through Celite and rinsed with DCM to remove any of the mercury by-product. The filtrate was washed with brine (2 x 20 cm^3) and extracted using DCM and deionised water (3 x 20 cm^3). The combined organic layers were dried over magnesium sulphate ($MgSO_4$), filtered and concentrated using the rotary evaporator to obtain the crude product.

Gravity column chromatography was used to obtain the purified product **19b** (788 mg, 56.65%) using the appropriate ratio of hexane and ethyl acetate (8:2, respectively).

Yield: 788 mg, 56.65%

Molar Mass: 738.93 $gmol^{-1}$

δ_H (400MHz, $CDCl_3$): 1.43 (s, 18H, CH_3, Boc-2,2'), 1.51 (s, 18H, CH_3, Boc-1,1'), 2.65 (s, 6H, CH_3, H-2, H-2'), 3.33 (s, 6H, CH_3, H-1, H-1'), 3.92 (s, 2H, CH_2), 6.80 (d, 4H, J 8Hz, H-2, H-2', H-6, H-6'), 7.11 (d, 4H, J 8Hz, H-3, H-3', H-5, H-5').

δ_C (100MHz, $CDCl_3$): 28.21 (CH_3, Boc), 28.24 (CH_3), 34.35 (C-N), 36.20 (C-N), 40.79 (CH_2), 81.67 (q, Boc), 82.30 (q, Boc), 81.67 (q, Boc), 120.92 (Ar, CH, H-2, H-2', H-6, H-6'), 129.70 (Ar, CH, H-3, H-3', H-5, H-5'), 136.98 (q, Ar), 144.74 (q, C-N), 148.62 (C=N), 152.99 (C=O)

ν_{max} (ATR)/cm^{-1}: 2979.16 (NH), 2934.94, 1705.80 (C=O), 1627.21 (C=N), 1604.77, 1504.39, 1433.88 (CH_3), 1336.77, 1323.74, 1248.30 (C-N), 1209.11, 1133.30 (C-O), 1078.96, 1014.19, 946.86, 854.48, 766.66, 733.96, 621.50, 591.71

HRMS (m/z ESI[+]): Calculated for $C_{39}H_{58}N_6O_8$, [M] 738.43 Found: [M+Na][+] 761.4212

R_f: 7:3 Hexane/Ethyl Acetate, 0.56

4-Bis[(2,3-dimethyl)guanidino]diphenylmethane dihydrochloride (19c)
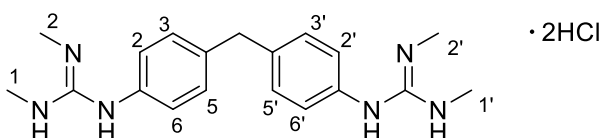
Using Method L, the Boc-protected compound **19b** (340 mg) was dissolved in an excess of 50 % TFAA in DCM (16 cm^3) and stirred at room temperature for 3-6 hours. The solvent

was then reduced by rotary evaporation. The remaining TFA salt was re-dissolved in deionised water (16 cm³) and treated with activated Amberlite IRA 400 chloride form (1 g) and allowed to stir gently for 24 hours at room temperature.

When the reaction was judged complete using the TLC method, the product was extracted using DCM (3 x 20cm³). The combined organic layers were dried over $MgSO_4$, filtered and concentrated in vacuum to obtain the hydrochloride salt, **19c** (168 mg, 98.2%).

Yield: 168 mg, 98.2%

Molar Mass: 338.46 gmol⁻¹

δ_H (400MHz, D_2O): 2.88 (s, 12H, CH_3, H-1, H-2, H-1', H-2'), 4.06 (s, 2H, CH_2), 7.22 (d, 4H, J 8Hz, H-2, H-2', H-6, H-6'), 7.38 (d, 4H, J 8Hz, H-3, H-3', H-5, H-5').

δ_C (100MHz, D_2O): 28.70 (CH_3), 41.67 (CH_2), 127.28 (Ar-CH, H-2, H-6, H-2', H-6'), 131.54 (Ar-CH, H-3, H-5, H-3', H-5'), 134.43 (q, Ar), 141.93 (q, Ar, C-N), 157.17 (C=N)

ν_{max} (ATR)/cm⁻¹: 3446.47 (NH), 3220.32 (NH), 2969.47 (CH_2), 2342.93, 1806.43, 1617.70 (Ar, CH), 1597.63, 1511.95, 1455.77 (CH_3), 1414.97, 1369.83, 1251.56 (C-N), 1186.52, 1102.66, 1018.86, 868.68, 802.08, 720.79, 655.69, 575.28, 568.66

HRMS (m/z ESI⁺): Calculated for $C_{19}H_{26}N_6$ [M] 338.22 Found: [M+H]⁺ 339.2292

HPLC Purity (> 95%): 99.05%

4-[2,3-(*tert*-Butoxycarbonyl)guanidino]-4'-[2,3-(*tert*-Butoxycarbonyl)-*N,N'*-dimethylguanidino]diphenylmethane (25a)
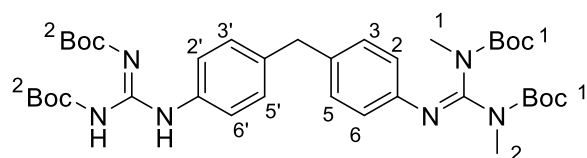
Using Method G, compound **39a** (1.0 eq.*,* 583 mg, 1.325 mmol) was dissolved in DMF at 0 ⁰C and reacted with *N,N'*-di(*tert*-butoxycarbonyl)-thiourea (1.2 eq, 461.7 mg, 1.59 mmol). The mixture was treated with $HgCl_2$ (1.3 eq., 467.7 mg 1.723 mmol) and NEt_3 (6 eq., 1.11 cm³, 7.95 mmol, 0.726 gcm⁻³) and stirred for 15 minutes at 0 ⁰C. The reaction was gradually brought back to room temperature while stirring and monitored by TLC analysis until complete.

The usual work-up was performed, followed by gravity column chromatography to yield the purified product **25a** (674.1 mg, 71.56%) using the appropriate ratio of hexane and ethyl acetate (8:2, respectively).

Yield: 674.1 mg, 71.56%

Molar Mass: 710.87 gmol^{-1}

δ_H (400MHz, CDCl$_3$): 1.51 (s, 18H, CH$_3$, Boc-1), 1.44 (s, 18H, CH$_3$, Boc-2), 2.64 (s, 3H, CH$_3$, H-1), 3.33 (s, 3H, CH$_3$, H-2), 3.92 (s, 2H, CH$_2$), 6.82 (d, 2H, J 8Hz, H-2, H-6), 7.13 (d, 2H, J 8Hz, H-2', H-6',), 7.15 (d, 2H, J 8Hz, H-3, H-5), 7.53 (d, 2H, J 8Hz, H-3', H-5'), 10.29 (br s, 1H, NH-1), 11.65 (br s, 1H, NH-2)

δ_C (100MHz, CDCl$_3$): 28.09 (CH$_3$), 28.23 (CH$_3$, Boc), 34.36 (q, C-N), 36.19 (q, C-N), 40.78 (CH$_2$), 79.57 (q, Boc), 83.66 (q, Boc), 120.89 (Ar, C-H, H-2, H-6), 122.30 (Ar, C-H, H-2', H-6'), 129.32 (Ar, C-H, H-3, H-5), 129.75 (Ar, C-H, H-3', H-5'), 134.84 (q, Ar), 137.72 (q, C-N), 153.01 (C=N), 153.50 (C=O)

ν_{max} (ATR)/cm^{-1}: 3262.16 (N-H), 3151.32 (N-H), 2978.78 (CH$_2$), 2933.76, 1711.33 (C=O), 1628.27 (C=N), 1604.51, 1561.13 (C-O), 1412.42 (CH$_3$), 1337.33, 1235.23, 1147.47, 1056.55, 947.03, 854.25, 807.38, 766.18

HRMS (m/z ESI$^+$): Calculated for C$_{37}$H$_{54}$N$_6$O$_8$ [M] 710.40 Found: [M+Na]$^+$ 733.3913

R$_f$: 7:3 Hexane/Ethyl Acetate, 0.44

4-Guanidino-4'-[*N,N'*-dimethylguanidino]diphenylmethane dihydrochloride (25b)
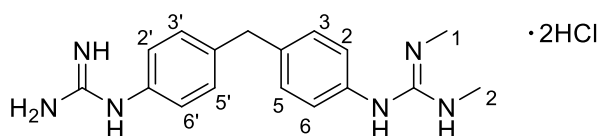
Using Method L, the Boc-protected compound **25a** (340 mg) was dissolved in an excess of 50 % TFAA in DCM (16 cm^3) and stirred at room temperature for 3-6 hours. The solvent was then reduced by rotary evaporation. The remaining TFA salt was re-dissolved in deionised water (16 cm^3) and treated with activated Amberlite IRA 400 chloride form (1 g) and allowed to stir gently for 24 hours at room temperature.

Following the usual work-up the hydrochloride salt, **25b** (311 mg, 86.15%), was afforded.

Yield: 311 mg, 86.15%

Molar Mass: 310.41 gmol^{-1}

δ_H (400MHz, D$_2$O): 2.87 (s, 6H, CH$_3$, H-1, H-2), 4.05 (s, 2H, CH$_2$), 7.20 (d, 2H, J 8Hz, H-2, H-6), 7.25 (d, 2H, J 8Hz, H-2', H-6'), 7.38 (d, 2H, J 8Hz, H-3, H-5), 7.40 (d, 2H, J 8Hz, H-3', H-5')

δ_C (100MHz, D$_2$O): 27.40 (CH$_3$), 40.12 (CH$_2$), 117.73 (Ar, q C), 120.89 (Ar, C-H, H-2, H-6), 126.34 (Ar, C-H, H-2', H-6'), 126.73 (Ar, C-H, J-3, H-5), 130.22 (Ar, C-H, H-3', H-5'), 132.40 (q, Ar), 141.22 (q, C-N), 141.46 (q, C-N), 155.69 (C=N)

ν_{max} (ATR)/cm^{-1}: 3124.05 (N-H), 2341.15 (CH$_2$), 1636.88 (C=N), 1618.26, 1598.55(Ar, CH), 1509.52, 1450.35 (Ar, CH), 1414.90 (CH$_3$), 1366.77, 1297.93 1249.76 (C-N), 1184.41 (C-O), 1159.41, 1111.28, 1051.78, 920.57, 868.36, 80.61, 771.85

HRMS (m/z APCI$^+$): Calculated C$_{17}$H$_{22}$N$_6$ [M] 310.19 Found: [M+H]$^+$ 311.1980

HPLC Purity (> 95%): 98.17%

N,N'-(Di-*tert*-butoxycarbonyl)diethylthiourea (20a)
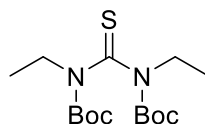
Using Method B, sodium hydride 60 % immersion in oil (4.5 eq, 933 mg, 38.88 mmol) was added to a solution of *N,N'*-diethylthiourea (1.0 eq, 900 mg, 8.64 mmol) in dry THF (200 cm^3) at 0 ºC with stirring. The reaction was slowly brought to room temperature and allowed to stir for 45 minutes. The reaction was then cooled back down to 0 ºC and di-tert-butyl-dicarbonate (2.2 eq, 4,148 mg, 19.01 mmol) was added carefully. The reaction was brought back to room temperature and allowed to stir overnight.

The usual work-up and purification yielded compound **20a** (942.9 mg, 74.63%) a yellow oil.

Yield: 942.9 mg, 74.63%

Molar Mass: 332.46 gmol^{-1}

δ_H (400MHz, CDCl$_3$): 1.34 (t, 6H, CH$_3$), 1.51 (s, 18H, CH$_3$-Boc), 4.13 (bd, 4H, CH$_2$)

δ_C (100MHz, CDCl$_3$): 13.75 (CH$_3$), 27.42 (CH$_2$), 28.07 (CH$_3$, Boc), 48.13 (C-N), 83.17 (q-C, Boc), 85.22 (q-C, Boc*), 146.67 (C=O, Boc*) 150.89 (C=O, Boc), 189.56 (C=S)

*Boc anhydride impurity signal

ν_{max} (ATR)/cm^{-1}: 2978.08 (C-H), 2935.24, 1720.19 (C=O), 1458.49 (CH$_3$), 1363.11, 1313.66, 1251.30 (C-N), 1159.13 (C-O), 1101.26 (C=S), 1085.13, 1070.97, 993.61, 880.68, 846.14, 815.02, 774.94, 759.27, 738.99, 701.82, 658.09

HRMS (m/z ESI$^+$): Calculated for C$_{15}$H$_{28}$N$_2$O$_4$S [M] 332.18 Found: [M+Na]$^+$ 355.1666

R$_f$: 7:3 Hexane/Ethyl Acetate, 0.77

4-Bis-[(2,3-di(*tert*-butoxycarbonyl)-*N,N'*-diethyl)guanidino]-diphenylmethane (20b)
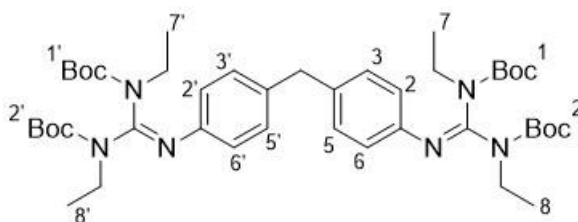
Using Method G, 4,4'-methylenedianiline (1.0 eq., 301.36 mg, 1.52 mmol) was dissolved in DCM at 0 ºC and reacted with **20a** (2.5 eq., 1,274 mg, 3.81 mmol). The mixture was treated with HgCl$_2$ (3 eq., 1,240 mg, 4.57 mmol) and triethylamine (6 eq., 1.28 cm^3, 9.15 mmol) and stirred for 15 minutes at 0 ºC. The reaction was gradually brought back to room temperature while stirring and monitored by TLC analysis until complete.

The reaction was filtered through Celite and rinsed with DCM to remove any of the mercury by-product. The filtrate was washed with brine (2 x 20 cm^3) and extracted using DCM and deionised water (3 x 20 cm^3). The combined organic layers were dried over magnesium sulphate (MgSO$_4$), filtered and concentrated using the rotary evaporator to obtain the crude product. Gravity column chromatography and the preparative TLC method were used in an attempt to isolate the purified compound

Yield: 105.7, 8.76%

Molar Mass: 795.04 gmol^{-1}

δ_H (400MHz, CDCl$_3$): 1.26 (t, 6H, CH$_3$**), 1.36 (s, 2H, Boc, thiourea*), 1.51 (s, 2H, CH$_3$, Boc-bis*), 1.52 (s, 18H, CH$_3$, Boc-mono), 3.88 (s, 2H, CH$_2$**), 3.89 (s, 2H, CH$_2$*), 4.13 (q, 3H, CH$_2$**), 6.51 (s, 2H, H-2, H-6), 7.10 (d, overlapping signal, 5H, J 8Hz, Ar-CH, mono and bis product), 7.26 (d, overlapping signal, 4H, J 8Hz, Ar-CH, mono and bis product).

δ_C (100MHz, CDCl$_3$): 13.83 (CH$_3$), 28.15 (CH$_3$, Boc, thiourea), 28.23 (CH$_3$, Boc, bis*), 28.35 (CH$_3$, Boc, mono**), 40.51 (CH$_2$, mono**), 40.63 (CH$_2$, bis*), 53.46 (CH$_2$), 80.39 (C-O), 118.75 (Ar, CH, H-2, H-6), 129.36 (Ar, CH, H-2', H-6', H-3, H-3', H-5, H-5'), 135.97 (q, C-Ar), 136.36 (q, C-Ar), 152.88 (C=N), 171.23 (C=S, thiourea)

*bis = bis-guanidinium product

**mono = mono-guanidinium side-product

ν_{max} (ATR)/cm^{-1}: 3344.45 (CH), 2977.33 (CH), 2932.58, 1744.87, 1719.75 (C=O), 1642.41 (C=N), 1604.26 (Ar, CH), 1456.89 (CH$_2$), 1390.96 (CH$_3$), 1366.20, 1271.93, 1229.62 (C-N), 1136.91 (C-O), 1065.44, 1045.34, 1020.12, 917.29, 879.47, 852.1, 81168, 764.02, 662.95

HRMS (m/z APCI$^+$): Calculated for C$_{43}$H$_{66}$N$_6$O$_8$ [M] 794.49 Found: [M+H]$^+$ 795.5019

Calculated for C$_{28}$H$_{40}$N$_4$O$_4$ [M] 496.30 Found: [M+H]$^+$ 497.3132

This synthesis resulted in a mixture of the thiourea starting material, bis-guanidinium symmetric compound and the mono-guanidinium compound to be separated via reverse phase column chromatography after the deprotection step (See compound **20c** and **20d** below).

4-Bis[(2,3-diethyl)guanidino]diphenylmethane dihydrochloride (20c)
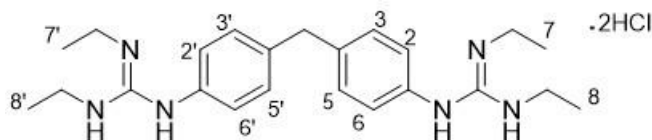
Using Method J, the Boc-protected compound **20b** (105.7 mg) was dissolved in an excess of 50 % TFAA in DCM (12 cm^3) and stirred at room temperature for 3-6 hours. The solvent was then reduced by rotary evaporation. The remaining TFA salt was re-dissolved in deionised water (20 cm^3) and treated with activated Amberlite IRA 400 chloride form (1 g) and allowed to stir gently for 24 hours at room temperature.

Following the usual work-up, with the addition of reverse phase column chromatography, the hydrochloride salt, **20c** (5.7 mg, 9.66%), was afforded.

Yield: 5.7 mg, 9.66%

Molar Mass: 394.57 gmol^{-1}

δ_H (400MHz, D$_2$O): 1.11 (t, 12H, CH$_3$, H-1, H-2, H-1', H-2'), 3.22 (q, 8H, CH$_2$, H-1, H-2, H-1', H-2'), 3.97 (s, 2H, CH$_2$), 7.16 (d, 4H, J 8Hz, H-2, H-6, H-2', H-6'), 7.32 (d, 4H, J 8 Hz, H-3, H-5, H-3', H-5')

δ_C (100MHz, D$_2$O): 13.36 (CH$_3$), 36.53 (CH$_2$), 40.16 (CH$_2$), 126.43 (Ar, C-H, H-2, H-6, H-2', H-6'), 130.20 (Ar, C-H, H-3, H-5, H-3', H-5'), 132.74 (q, Ar), 140.99 (q, C-N), 153.99 (C=N)

HRMS (m/z APCI$^+$): Calculated for $C_{23}H_{34}N_6$ [M] 394.28 Found: [M+H]$^+$ 395.2920

4-Amino-4'-[(*N,N'*-diethyl)guanidino]diphenylmethane hydrochloride (20d)
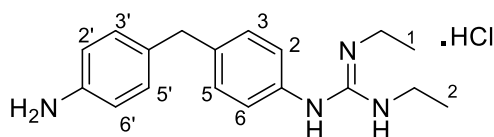
Using Method J, the Boc-protected compound **20b** (105.7 mg) was dissolved in an excess of 50 % TFAA in DCM (12 cm^3) and stirred at room temperature for 3-6 hours. The solvent was then reduced by rotary evaporation. The remaining TFA salt was re-dissolved in deionised water (20 cm^3) and treated with activated Amberlite IRA 400 chloride form (1 g) and allowed to stir gently for 24 hours at room temperature.

Following the usual work-up and a reverse phase gravity column chromatography, the hydrochloride salt **20d** (11.4 mg, 29.6%), was afforded.

**Yield:** 11.4 mg, 29.6%

Molar Mass: 296.42 gmol^{-1}

δ$_H$ (400MHz, D$_2$O): 1.10 (t, 6H, CH$_3$, H-1, H-2), 3.31 (br q, 4H, CH$_2$, H-1, H-2), 3.83 (s, 2H, CH$_2$), 6.75 (d, 2H, J 8Hz, H-2, H-6), 7.08 (d, 2H, J 8Hz, H-2', H-6'), 7.12 (d, 2H, J 8Hz, H-3, H-5), 7.28 (d, 2H, J 8Hz, H-3', H-5')

δ$_C$ (100MHz, D$_2$O): 13.32 (CH$_3$), 36.48 (CH$_2$), 39.85 (CH$_2$), 117.12 (q, C-N), 126.42 (Ar, C-H, H-2, H-6), 129.57 (Ar, C-H, H-2', H-6'), 130.03 (Ar, C-H, H-3, H-5), 132.40 (Ar, C-H, H-3', H-5'), 133.06 (q, Ar), 141.99 (q, C-N), 154.00 (C=N)

HRMS (m/z ESI$^+$): Calculated for $C_{18}H_{24}N_6$ [M] 296.20, Found: [M+H$^+$]$^+$ 297.2080

HPLC Purity (> 95%): 91.35%

1,1'-Methylenebis(4-isothiocyanatobenzene) (37a)
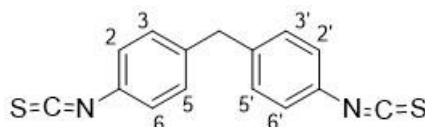
First, 4,4'-methylenedianiline (1.0 eq., 600 mg, 3.026 mmol) was dissolved in dry DCM and allowed to stir at 0 ºC for 10 minutes before the addition of 1,1'-thiocarbonyl bis-imidazole

(2.2 eq., 1,186 mg, 6.66 mmol). The reaction was gradually brought to room temperature and stirred for 5 hours. The reaction was judged complete using the TLC method. The solvent was reduced by rotary evaporation to obtain a red-brown solid and purified using a 6:4 ratio of hexane and ethyl acetate, respectively, by gravity column chromatography yielding compound **37a**, (700 mg, 97%).

Yield: 700 mg, 97%

Molar Mass: 282.38 gmol^{-1}

δ_H (400MHz, CDCl$_3$): 7.17 (dd, 8H, J 8Hz, H-2, H-3, H-5, H-6, H-2', H-3' H-5', H-6'), 3.98 (s, 2H, CH$_2$)

δ_C (100MHz, CDCl$_3$): 40.99 (CH$_2$), 115.94 (C=N), 125.96 (Ar, C-H, J 8Hz H-2, H-6, H-2', H-6'), 129.99 (Ar, C-H, J 8Hz H-3, H-5, H-3', H-5'), 139.57 (q, C-N)

ν_{max} (ATR)/cm^{-1}: 2925.84 (CH$_2$), 2853.72, 2069.65 (N=C=S), 1899.10, 1573.83, 1497.97, 1440.72, 1411.63, 1260.01, 1199.69 (C-N), 1171.67, 1105.83, 1016.32, 927.13, 864.50, 807.46, 783.16, 734.53

HRMS (m/z APCI$^{+/-}$): Calculated for C$_{15}$H$_{10}$N$_2$S$_2$ [M] 282.03 Found: [M+H]$^-$ 281.0213

1,1'-(Methylene-di-4,1-phenylene)bis(thiourea) (37b)
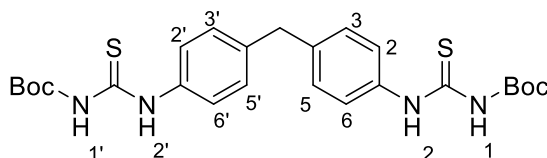
NaH 60 % immersion in oil (9 eq., 544 mg, 22.68 mmol) was added to a cooled solution of tert-butyl carbamate (2.5 eq., 737 mg, 6.29 mmol) in dry THF (8 cm^3) at 0 ºC. The reaction mixture was stirred at 0 ºC for 20 minutes before adding the previously synthesised 1,1'-methylenebis(4-isothiocyanatobenzene) (**37a,** 1 eq. 600 mg, 2.52 mmol). The solution was brought to room temperature and allowed to stir for 5 hours. The reaction was monitored by TLC until complete.

Once complete, the reaction was quenched with deionised water (5 cm^3) and stirred for a further 15 minutes. The solvents were reduced by rotary evaporation and the solid obtained was re-dissolved in DCM and washed with deionised water (6 x 20 cm^3). Purification by gravity column chromatography with an 8:2 ratio of hexane and ethyl acetate, respectively, afforded the pure product, **37b** (211.0 mg, 16.2%)

Yield: 211.0 mg, 16.2%

Molar Mass: 516.68 gmol^{-1}

$δ_H$ (400MHz, CDCl$_3$): 1.55 (s, 18H, CH$_3$, Boc), 4.01 (s, 2H, CH$_2$), 7.23 (d, J 8Hz, 4H, Ar-CH, H-2, H-2', H-6, H-6'), 7.59 (d, J 8Hz, Ar-CH, H-3, H-3', H-5, H-5'), 7.97 (s, 2H, NH-1, NH-1'), 11.47 (s, 2H, NH-2, NH-2')

$δ_C$ (100MHz, CDCl$_3$): 28.03 (CH$_3$, Boc), 40.99 (CH$_2$), 84.27 (C-O), 124.39 (Ar, C-2, C-2', C-6, C-6'), 129.33 (Ar, C-3, C-3', C-5, C-5'), 135.91 (Ar-qC), 139.23 (C-N), 151.86 (C=O), 178.21 (C=S)

$ν_{max}$ (ATR)/cm^{-1}: 3170.00 (NH), 2977.5, 2928.3, 1710.97 (C=O), 1701.58, 1526.82 (C-O), 1508.81, 1365.89, 1352.64, 1251.12 (C-N), 1135.07 (C=S), 1015.82, 851.23, 764.01, 729.71, 695.72, 668.5, 595.1

HRMS (m/z ESI$^{+/-}$): Calculated for C$_{25}$H$_{32}$N$_4$O$_4$S$_2$ [M] 516.19, Found: [M+H]$^-$ 515.1791

1,1'-(Methylenedi-4,1-phenylene)-N-ethoxycarbonyl-bis(thiourea) (36a)
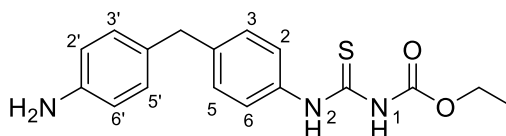
First, 4,4'-Methylenedianiline (1.0 eq., 550 mg, 2.75 mmol) was dissolved in anhydrous DCM under argon below 0 ℃ was added. Ethoxycarbonyl isothiocyanate (2.2 eq., 0.72 cm^3, 6.10 mmol) was added and after approximately 15-20 minutes of stirring below 0 ℃, the reaction was gradually brought back to room temperature and stirred overnight. The reaction was monitored by TLC and once deemed complete the solvent was removed. The product was purified by column chromatography using the appropriate hexane/ ethyl acetate gradient, yielding compound **36a** (136 mg, 10.7%).

Yield: 136 mg, 10.7%

Molar Mass: 329.42 gmol^{-1}

$δ_H$ (400MHz, CDCl$_3$): 1.37 (t, 3H, CH$_3$), 3.99 (s, 2H, CH$_2$), 4.31 (q, 2H, CH$_2$), 7.18 (s, 4H, Ar-CH, H-3, H-3', H-5, H-5'), 7.20 (d, J 8Hz, 2H, Ar-CH, H-2, H-6), 7.59 (d, J 8Hz, H-2', H-6'), 8.05 (s, 1H, NH-1), 11.43 (s, 1H, NH-2)

$δ_C$ (100MHz, CDCl$_3$): 14.20 (CH$_3$), 41.03 (CH$_2$), 63.10 (O-CH$_2$), 124.54 (Ar, C-2, C-6), 125.88 (Ar, C-2', C-6'), 129.29 (Ar, C-3, C-5), 130.08 (Ar, C-3', C-5'), 135.99 (Ar, q-C), 138.91 (Ar, q-C), 140.18 (C-N), 152.76 (C=O), 177.82 (C=S)

ν_{max} (ATR)/cm^{-1}: 3167.18 (NH), 2974.86, 2930.14, 1708.67 (C=O), 1700.97, 1515.89 (C-O), 1506.83, 1300.65, 1350.94, 1250.49 (C-N), 1126.03 (C=S), 1015.87, 871.46, 773.12, 758.31, 702.15, 684.20, 599.14

HRMS (m/z APCI$^+$): Calculated for $C_{17}H_{19}N_3O_2S$, Not Found: 329.12

N-(*tert*-butoxycarbonyl)-N'-methyl thiourea (38a)
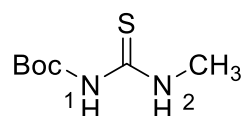
Using Method C, sodium hydride 60 % immersion in oil (1,183 mg, 49.26 mmol, 4.5 eq.) was added carefully to a solution of commercially available unsubstituted thiourea (500 mg, 6.57 mmol, 1.0 eq.) in dry THF (110 ml), at 0 °C with stirring. The reaction was slowly brought to room temperature and allowed to stir for 45 minutes. The reaction was then cooled back down to 0 °C and di-*tert*-butyl-dicarbonate (3,585 mg, 16.43 mmol, 2.5 eq.) was added. After 30 minutes stirring at 0 °C, the reaction was brought back to room temperature and allowed to stir overnight.

After monitoring the formation of the *N,N'*-bis-Boc-thiourea by TLC, the reaction was cooled back to 0 °C and NaH 60% immersion in oil (446.89 mg, 18.62 µmol, 1.7 eq.) was added carefully. After 1 hour, TFA anhydride (1.43 ml, 10.12 µmol, 1.54 eq.) was added. After a further 1 hour stirring at 0 °C, methylamine hydrochloride (683 mg, 10.12 µmol, 1.54 eq.) was added and allowed to fully dissolve in solution before the removal of the ice-bath. The reaction was gradually brought back to room temperature and allowed to stir overnight.

After approximately 16 hours the reaction was deemed complete and cooled to 0 °C. the reaction was quenched via the addition of adding deionised water (40 ml) dropwise to the mixture. Extraction of the product was carried out by using ethyl acetate (4 x 50 ml) and washed with brine (4 x 50 ml). The combined organic phases were dried over MgSO$_4$, filter and concentrate under vacuum. Purification of the product was carried out by column chromatography using a hexane and ethyl acetate gradient mixture, yielding compound **38a** (469 mg, 37.6%).

Yield: 469 mg, 37.6%

Molar Mass: 190.26 gmol^{-1}

MP: 101-104 °C

δ_H (400MHz, CDCl$_3$): 1.50 (s, 9H, Boc-CH$_3$), 3.19 (d, 3H, CH$_3$), 8.02 (bs, 1H, NH-2), 9.71 (bs, 1H, NH-1)

δ_C (100MHz, CDCl$_3$): 27.99 (CH$_3$, Boc), 32.07 (CH$_3$), 83.70 (q-C, Boc), 151.92 (C=O), 180.49 (C=S)

ν_{max} (ATR)/cm^{-1}: 3230.32, 3157.57, 2979.86, 2938.09, 1723.66 (C=O), 1512.33 (N-H), 1456.87 (CH$_3$), 1368.29, 1335.68, 1253.99 (C-N), 1143.59 (C-O), 1039.84, 1000.06 (C=S), 885.72, 765.54, 724.47

HRMS (m/z ESI$^{+/-}$): Calculated for C$_7$H$_{14}$N$_2$O$_2$S [M] 190.09, Found: [M+Na]$^+$ 213.0795

Methyl (Z)-*N,N'*-di(*tert*-butoxycarbonyl)-N-methylcarbamimidothioate (21a)
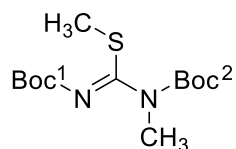
Using Method D, a solution of 1,3-bis-(*tert*-butoxycarbonyl)-2-methyl-2-thiopseudourea (1 g, 1 eq., 3.44 mmol), anhydrous methanol (0.21 cm^3, 1.5 eq., 5.17 mmol), and triphenylphosphine (1.356 g, 1.5 eq., 5.17 mmol) in dry THF, under argon gas, was cooled to -5 °C. Diethyl azodicarboxylate (1.62 cm^3, 3 eq., 10.34 mmol) was added dropwise at a rate such that the reaction mixture was completely colourless before the addition of the next drop. The reaction was then stirred at room temperature overnight. The reaction was monitored by TLC. Once complete, methanol (10 cm^3) was added to the solution and then the solvent was reduced. The product was purified by flash chromatography a hexane and ethyl acetate gradient mixture, yielding compound **21a**, 80.8%.

Yield: 846 mg, 80.8%

Molar Mass: 304.41 gmol^{-1}

Melting Point: oil

δ_H (400MHz, CDCl$_3$): 1.40 (d, 18 H, Boc-CH$_3$), 2.28 (s, 3 H, S-CH$_3$), 3.01 (s, 3H, N-CH$_3$)

δ_C (100MHz, CDCl$_3$): 15.26 (S-CH$_3$), 27.84 (CH$_3$, Boc^1), 27.90 (CH$_3$, Boc^2), 35.47 (N-CH$_3$), 81.56 (q-C, Boc^2), 82.14 (q-C, Boc^1), 151.78 (C=O, Boc^1), 157.76 (C=O, Boc^2), 180.49 (C=S)

ν_{max} (ATR)/cm^{-1}: 2978.43 (C-CH$_3$), 2933.27 (N-CH$_3$), 1922.31, 1838.67, 1714.01 (C=O), 1618.14 (N=C), 1550.34, 1459.11 (CH$_3$), 1425.24, 1393.67, 1365.94, 1332.26, 1241.2 (C-N), 1137.15 (C-O), 1059.7 (S-CH$_3$), 963.07, 854.7, 758.03, 711.09 (C-S), 664.03

HRMS (m/z ESI$^+$): Calculated for C$_{13}$H$_{24}$N$_2$O$_4$S [M] 304.15, Found: [M+Na]$^+$ 304.1352

R$_f$: 1.1 Hexane/Ethyl Acetate, 0.80

Methyl (Z)-*N,N'*-di(*tert*-butoxycarbonyl)-*N*-ethylcarbamimidothioate (22a)
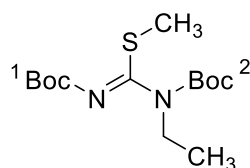
A solution of 1,3-bis-(*tert*-butoxycarbonyl)-2-methyl-2-thiopseudourea (1 g, 1 eq., 3.44 mmol), anhydrous ethanol (0.30 cm^3, 1.5 eq., 5.17 mmol), and triphenylphosphine (1.356

g, 1.5 eq., 5.17 mmol) in dry THF under argon gas was cooled to -5 °C. Diethyl azodicarboxylate (1.62 cm^3, 3 eq., 10.34 mmol) was added dropwise at a rate such that the reaction mixture was completely colourless before the addition of the next drop. The reaction was then stirred at room temperature overnight. The reaction was monitored by TLC. Once complete, methanol (10 cm^3) was added to the solution and then the solvent was reduced. The product was purified by flash chromatography a hexane and ethyl acetate gradient mixture, yielding compound **22a**, 94.8%.

Yield: 1038 mg, 94.8%

Molar Mass: 468.60 gmol^{-1}

Melting Point: oil

δ$_H$ (400MHz, CDCl$_3$): 1.25 (t, 3H, CH$_3$), 1.51 (d, 18 H, Boc-CH$_3$), 2.39 (s, 3 H, S-CH$_3$), 3.59 (q, 2H, CH$_2$)

δ$_C$ (100MHz, CDCl$_3$): 14.10 (CH$_3$), 15.54 (S-CH$_3$), 28.00 (CH$_3$, Boc^1), 28.08 (CH$_3$, Boc^2), 43.98 (CH$_2$), 81.76 (q-C, Boc^2), 82.11 (q-C, Boc^1), 151.70 (C=O, Boc^1), 157.94 (C=O, Boc^2), 163.00 (C=S)

ν$_{max}$ (ATR)/cm^{-1}: 2978.43 (C-CH$_3$), 2933.27 (N-CH$_3$), 1922.31, 1838.67, 1714.01 (C=O), 1618.14 (N=C), 1550.34, 1459.11 (CH$_3$), 1425.24, 1393.67, 1365.94, 1332.26, 1241.2 (C-N), 1137.15 (C-O), 1059.7 (S-CH$_3$), 963.07, 854.7, 758.03, 711.09 (C-S), 664.03

HRMS (m/z ESI$^+$): Calculated for C$_{14}$H$_{26}$N$_2$O$_4$S [M] 318.16, Found: [M+Na]$^+$ 341.1507

R$_f$: 1:1 Hexane/Ethyl Acetate, 0.85

4-Guanidino-4'-[(2,3-di(*tert*-butoxycarbonyl)-N-methyl)guanidino]diphenylmethane (43a)
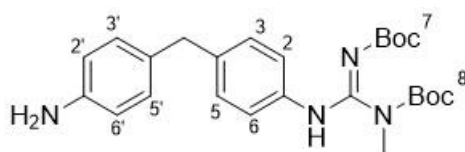
Using Method E, 4,4'-methylenedianiline (3.0 eq., 390 mg, 1.97 mmol) was dissolved in DCM, and the mixture was cooled below 0 °C, and reacted with **21a** (1.0 eq., 200 mg, 0.66 mmol). The mixture was treated with HgCl$_2$ (3 eq., 535 mg, 1.97 mmol) and NEt$_3$ (6 eq., 0.55 cm^3, 3.94 mmol) and stirred for 15 minutes below 0 °C. The reaction was gradually brought back to room temperature while stirring and monitored by TLC analysis until complete.

The reaction was filtered through Celite and rinsed with DCM to remove any of the mercury by-product. The filtrate was washed with brine (2 x 20 cm^3) and extracted using DCM (3 x 20 cm^3) and deionised water (3 x 20 cm^3). The combined organic layers were dried over magnesium sulphate (MgSO$_4$), filtered and concentrated using the rotary evaporator to obtain the crude product. The product was then purified by gravity column chromatography using the appropriate ratio of hexane and ethyl acetate.

Yield: 166 mg, 55.5%

Molar Mass: 454.57 gmol^{-1}

δ$_H$ (400MHz, CDCl$_3$): 1.50 (s, 9H, CH$_3$, Boc), 1.43 (s, 9H, CH$_3$, Boc-10), 3.19 (s, 3H, CH$_3$), 3.82 (s, 2H, CH$_2$), 6.62 (d, 2H, J 8Hz, H-2, H-6), 6.94 (t, 4H, J 8Hz, H-2', H-6', H-3, H-5), 7.14 (d, 2H, J 8Hz, H-3', H-5').

δ$_C$ (100MHz, CDCl$_3$): 27.64 (CH$_3$), 28.14 (CH$_3$, Boc), 40.47 (CH$_2$), 115.28 (Ar, H-3, H-5, H-3', H-5'), 122.62 (Ar, H-2', H-6'), 122.70 (Ar, H-2, H-6), 144.56 (q, C-N)

ν$_{max}$ (ATR)/cm^{-1}: 3450.37, 3367.81 (NH), 3225.07 (NH), 2978.22 (CH$_2$), 2932.32, 1722.70 (C=O), 1641.91 (C=N), 1512.47, 1473.80, 1437.74 (CH$_3$), 1362.76, 1234.59 (C-N), 1139.85 (C-O), 1047.41, 924.06, 854.09, 813.8, 766.25, 699.71, 661.71, 630.05, 603.47, 571.83

HRMS (m/z APCI$^+$): Calculated for C$_{26}$H$_{34}$N$_4$O$_4$ [M] 454.26, Found: [M+H]$^+$ 455.2657

R$_f$: 1:1 Hexane/Ethyl Acetate, 0.37

4-4'-[(2,3-Di(*tert*-butoxycarbonyl)-N-methyl)guanidino]diphenylmethane (21b)
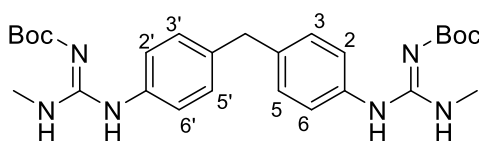
Using Method E, 4,4'-methylenedianiline (1.0 eq., 208 mg, 1.05 mmol) was dissolved in DMF below 0 ºC and reacted with compound **21a** (2.5 eq., 800 mg, 2.63 mmol). The mixture was treated with HgCl$_2$ (3 eq., 855 mg, 3.15 mmol) and triethylamine (6 eq., 0.88 cm^3, 6.30 mmol) and stirred in an ice-bath. The reaction was gradually brought back to room temperature while stirring and monitored by TLC analysis until complete.

The reaction was filtered through Celite and rinsed with DCM to remove any of the mercury by-product. The filtrate was washed with brine (4 x 50 cm^3) and extracted using DCM and deionised water (5 x 50 cm^3). The combined organic layers were dried over magnesium

sulphate ($MgSO_4$), filtered and concentrated using the rotary evaporator to obtain the crude product.

Gravity column chromatography was used to obtain the purified product **21b** (445 mg, 47.9%) using the appropriate ratio of hexane and ethyl acetate (7:3, respectively).

Yield: 445 mg, 47.9%

Molar Mass: 510.64 gmol^{-1}

δ_H (400MHz, $CDCl_3$): 1.41 (s, 18H, CH_3, Boc-1), 3.16 (bs, 6H, CH_3), 3.83 (s, 2H, CH_2), 6.89 (br s, 4H, H-2, H-6, H-2', H-6'), 7.15 (br d, 2H, H-3, H-5, H-3', H-5'), 11.08 (br s, 1H, NH)

**Amorphus intermediate compound resulting in broad signals

δ_C (100MHz, $CDCl_3$): 27.67 (CH_3), 28.04 (CH_3, Boc), 34.76 (q, C-N), 40.62 (CH_2), 82.11 (q, Boc), 121.76 (Ar, C-H, H-2, H-6), 129.68 (Ar, C-H, H-3, H-5), 152.38 (C=N)

ν_{max} (ATR)/cm^{-1}: 2998.34, 2933.14, 2931.28, 1751.44, 1720.91 (C=O), 1655.15 (C=N), 1602.33 (Ar-CH), 1465.55 (-CH_2-) 1453.78 (Ar-CH), 1393.71 (CH_3), 1360.25, 1277.39 1229.96 (C-N), 1169.97 (C-O), 1110.31, 1067.42, 1043.34, 1020.12, 977.60, 907.61, 871.54, 850.31, 801.33, 771.12, 673.94

HRMS (m/z ESI$^+$): Calculated for $C_{37}H_{54}N_6O_8$ [M] 510.40, Found: [M+H]$^+$ 511.4082

R$_f$: 1:1 Hexane/Ethyl Acetate, 0.56

4-4'-[*N*-Methylguanidino]diphenylmethane dihydrochloride (21c)
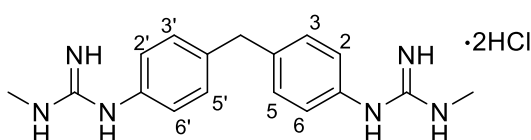
Using Method J, the Boc-protected compound **21b** (444.6 mg) was dissolved in an excess of 50 % TFAA in DCM (20 cm^3) and stirred at room temperature for 3-6 hours. The solvent was then reduced by rotary evaporation. The remaining TFA salt was re-dissolved in deionised water (20 cm^3) and treated with activated Amberlite IRA 400 chloride form (1 g) and allowed to stir gently for 24 hours at room temperature.

Following the usual work-up the hydrochloride salt, **21c** (182.3 mg, 67.5%), was afforded.

Yield: 182.3 mg, 67.5%
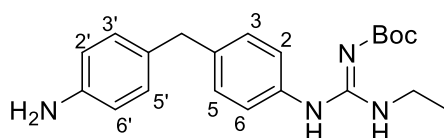
Molar Mass: 310.41 gmol^{-1}

δ_H (400MHz, D$_2$O): 2.80 (s, 6H, CH$_3$), 3.96 (s, 2H, CH$_2$), 7.16 (d, 2H, J 8Hz, H-2, H-6, H-2', H-6'), 7.31 (d, 2H, J 8Hz, H-3, H-5, H-3', H-5')

δ_C (100MHz, D$_2$O): 27.52 (CH$_3$), 40.14 (CH$_2$), 126.38 (Ar, C-H, H-2, H-6, H-2', H-6'), 130.21 (Ar, C-H, H-3, H-5, H-3', H-5'), 132.38 (q, Ar), 141.20 (q, C-N), 156.20 (C=N)

HRMS (m/z ESI$^+$): Calculated for C$_{17}$H$_{22}$N$_6$ [M] 310.19 Found: [M+H]$^+$ 311.1979

HPLC Purity (> 95%): 97.79%

4-Guanidino-4'-[(2,3-di(*tert*-butoxycarbonyl)-N-methyl)guanidino]diphenylmethane (44a)

Using Method E, 4,4'-methylenedianiline (3.0 eq., 250 mg, 1.26 mmol) was dissolved in DCM, and the mixture was cooled below 0 ºC, and reacted with **22a** (1.0 eq., 134 mg, 0.42 mmol). The mixture was treated with HgCl$_2$ (3 eq., 342 mg, 1.26 mmol) and NEt$_3$ (6 eq., 0.35 cm^3, 3.94 mmol) and stirred for 15 minutes below 0 ºC. The reaction was gradually brought back to room temperature while stirring and monitored by TLC analysis until complete.

The reaction was filtered through Celite and rinsed with DCM to remove any of the mercury by-product. The filtrate was washed with brine (2 x 20 cm^3) and extracted using DCM (3 x 20 cm^3) and deionised water (3 x 20 cm^3). The combined organic layers were dried over magnesium sulphate (MgSO$_4$), filtered and concentrated using the rotary evaporator to obtain the crude product. The product was then purified by gravity column chromatography using the appropriate ratio of hexane and ethyl acetate, yielding compound **44a** (227.6 mg, 24.5%)

Yield: 227.6 mg, 24.5%

Molar Mass: 368.48 gmol^{-1}

δ_H (400MHz, CDCl$_3$): 1.22 (br s, 3H, CH$_3$), 1.44 (s, 9H, CH$_3$, Boc), 3.68 (br s, 2H, CH$_2$), 3.79 (s, 2H, CH$_2$), 6.58 (d, 2H, J 8Hz, H-2, H-6), 6.89 (d, 2H, J 8Hz, H-2'), 6.96 (br d, 2H, H-6', H-3, H-5), 7.11 (d, 2H, J 8Hz, H-3', H-5').

δ_C (100MHz, CDCl$_3$): 27.65 (CH$_3$), 28.22 (CH$_3$, Boc), 34.90 (CH$_2$), 40.48 (CH$_2$), 82.23 (q, Boc), 115.58 (Ar, H-3, H-5 H-3', H-5'), 121.80 (Ar, H-2, H-6), 129.70 (Ar, H-2', H-6'), 144.56 (q, C-N), 152.39 (C=N)

ν_{max} (ATR)/cm^{-1}: 3367.69 (NH), 2977.68 (CH$_2$), 2932.87, 1711.74 (C=O), 1606.57 (C=N), 1513.01, 1461.57 (CH$_3$), 1366.34, 1269.50 1231.58 (C-N), 1137.36 (C-O), 1065.51, 1021.03, 967.31, 913.78, 848.44, 812.54, 766.04, 72960, 645.21, 570.51

HRMS (m/z APCI$^+$): Calculated for C$_{26}$H$_{36}$N$_4$O$_4$ [M] 368.27, Found: [M+H]$^+$ 369.2810

R$_f$: 1:1 Hexane/Ethyl Acetate, 0.47

4-4'-[(2,3-Di(*tert*-butoxycarbonyl)-N-ethyl)guanidino]diphenylmethane (22b)
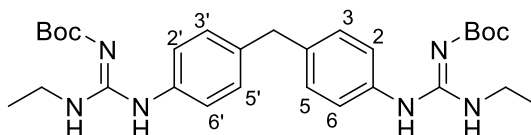
Using Method E, 4,4'-methylenedianiline (1.0 eq., 249 mg, 1.26 mmol) was dissolved in DMF below 0 °C and reacted with compound **22a** (2.5 eq., 1000 mg, 3.14 mmol). The mixture was treated with HgCl$_2$ (3 eq., 1,026 mg, 3.78 mmol) and triethylamine (6 eq., 1.05 cm^3, 7.56 mmol) and stirred in an ice-bath. The reaction was gradually brought back to room temperature while stirring and monitored by TLC analysis until complete.

The reaction was filtered through Celite and rinsed with DCM to remove any of the mercury by-product. The filtrate was washed with brine (4 x 50 cm^3) and extracted using DCM and deionised water (5 x 50 cm^3). The combined organic layers were dried over magnesium sulphate (MgSO$_4$), filtered and concentrated using the rotary evaporator to obtain the crude product.

Gravity column chromatography was used to obtain the purified product **22b** (219 mg, 17.8%) using the appropriate ratio of hexane and ethyl acetate (7:3, respectively).

Yield: 129 mg, 17.8%

Molar Mass: 538.69 gmol^{-1}

δ_H (400MHz, CDCl$_3$): 1.22 (br s, 6H, CH$_3$), 1.44 (s, 18H, CH$_3$, Boc), 3.67 (br s, 4H, CH$_2$), 3.87 (s, 2H, CH$_2$), 6.96 (d, 2H, J 8Hz, H-2, H-6, H-2', H-6'), 7.10 (d, 2H, J 8Hz, H-3, H-5, H-3', H-5')

δ_C (100MHz, CDCl$_3$): 27.72 (CH$_3$), 28.10 (CH$_3$, Boc), 40.67 (CH$_2$), 43.09 (N-CH$_2$), 80.15 (q C, Boc), 82.14 (C-O), 121.92 (Ar, C-H, H-2, H-6, H-2', H-6'), 129.70 (Ar, C-H, H-3, H-5, H-3', H-5'), 152.34 (C=N), 171.30 (C=O)

ν_{max} (ATR)/cm^{-1}: 2977.33 (CH$_2$), 2932.58, 1744.87, 1719.75 (C=O), 1642.41 (C=N), 1604.26 (Ar-CH), 1456.89 (Ar-CH), 1390.96 (CH$_3$), 1366.20, 1271.93 1229.62 (C-N), 1136.91 (C-O), 1065.44, 1045.334, 1020.12, 967.20, 917.29, 879.47, 852.10, 811.68, 764.02, 662.95

HRMS (m/z ESI$^+$): Calculated for C$_{29}$H$_{42}$N$_6$O$_4$ [M] 538.33 Found: [M+Na]$^+$ 561.3197

R$_f$: 1:1 Hexane/Ethyl Acetate, 0.76

4-4'-[*N*-Ethylguanidino]diphenylmethane dihydrochloride (22c)
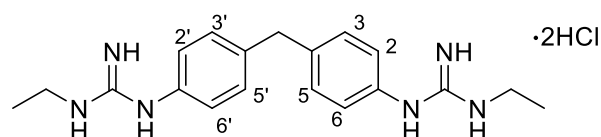
Using Method L, the Boc-protected compound **22b** (219 mg) was dissolved in an excess of 50 % TFAA in DCM (20 cm^3) and stirred at room temperature for 3-6 hours. The solvent was then reduced by rotary evaporation. The remaining TFA salt was re-dissolved in deionised water (20 cm^3) and treated with activated Amberlite IRA 400 chloride form (1 g) and allowed to stir gently for 24 hours at room temperature.

Following the usual work-up the hydrochloride salt, **22c** (115 mg, 83.9%), was afforded.

**Yield:** 115 mg, 83.9%

Molar Mass: 338.46 gmol^{-1}

δ_H (400MHz, D$_2$O): 1.13 (t, 6H, CH$_3$), 3.20 (q, 4H, CH$_2$), 3.97 (s, 2H, CH$_2$), 7.17 (d, 4H, J 8Hz, H-2, H-6, H-2', H-6'), 7.32 (d, 4H, J 8Hz, H-3, H-5, H-3', H-5')

δ_C (100MHz, D$_2$O): 13.13 (CH$_3$), 36.47 (CH$_2$), 40.14 (CH$_2$), 126.37 (Ar, C-H, H-2, H-6, H-2', H-6'), 130.20 (Ar, C-H, H-3, H-5, H-3', H-5'), 132.47 (q, Ar), 141.161 (q, C-N), 155.16 (C=N)

HRMS (m/z APCI$^+$): Calculated for C$_{19}$H$_{26}$N$_6$ [M] 338.22 Found: [M+H]$^+$ 339.2293

HPLC Purity (> 95%): 96.37%

4-[2,3-(*tert*-Butoxycarbonyl)-N-methylguanidino]-4'-[2,3-(*tert*-Butoxycarbonyl)-*N,N'*-dimethylguanidino]diphenylmethane (28a)
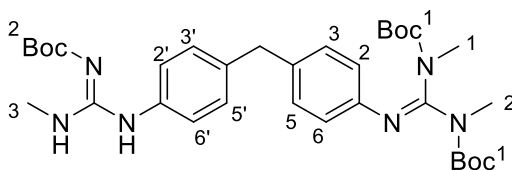
Using Method H, compound **39a** (1.5 eq.*,* 406 mg, 1.34 mmol) was dissolved in DCM below 0 °C and reacted with compound **21a** (1.0 eq, 417 mg, 0.89 mmol). The mixture was treated with HgCl$_2$ (3 eq., 725 mg 2.67 mmol) and NEt$_3$ (8 eq., 0.99 cm^3, 7.12 mmol, 0.726 gcm^{-3}) and stirred for 15 minutes at 0 °C. The reaction was gradually brought back to room temperature while stirring and monitored by TLC analysis until complete.

The usual work-up was performed, followed by gravity column chromatography to yield the purified product **28a** (434.5 mg, 67.4%) using the appropriate ratio of hexane and ethyl acetate (8:2, respectively).

Yield: 434.5 mg, 67.4%

Molar Mass: 624.78 gmol^{-1}

δ_H (400MHz, CDCl$_3$): 1.51 (s, 18H, CH$_3$, Boc-1), 1.44 (s, 9H, CH$_3$, Boc-2), 2.63 (s, 3H, CH$_3$, H-1), 3.25 (br s, 3H, CH$_3$, H-3), 3.32 (s, 3H, CH$_3$, H-2), 3.91 (s, 2H, CH$_2$), 6.79 (d, 2H, J 8Hz, H-2, H-6), 7.00 (br s, 2H, H-2', H-6',), 7.10 (d, 2H, J 8Hz, H-3, H-5), 7.16 (d, 2H, J 8Hz, H-3', H-5')

δ_C (100MHz, CDCl$_3$): 27.64 (CH$_3$), 28.13 (CH$_3$, Boc-2), 28.23 (CH$_3$, Boc-1), 36.09 (q, C-N), 40.74 (CH$_2$), 81.54 (q, Boc-2), 82.19 (q, Boc-1), 120.87 (Ar, C-H, H-2, H-6), 121.84 (Ar, C-H, H-2', H-6'), 129.65 (Ar, C-H, H-3, H-5), 129.76 (Ar, C-H, H-3', H-5'), 136.34 (q, Ar), 145.19 (q, C-N), 153.02 (C=N)

ν_{max} (ATR)/cm^{-1}: 2978.11 (CH$_2$), 1710.15 (C=O), 1632.03 (C=N), 1470.60(C-O), 1430.44 (CH$_3$), 1338.47, 1237.23, 1135.50, 1079.61, 946.01 855.88, 766.21, 592.45

HRMS (m/z ESI$^+$): Calculated for C$_{33}$H$_{48}$N$_6$O$_6$ [M] 624.36, Found: [M+H]$^+$ 625.3711

R$_f$: 7:3 Hexane/Ethyl Acetate, 0.39

4-[*N*-Methylguanidino]-4'-[*N,N'*-dimethylguanidino]diphenylmethane dihydrochloride (28b)
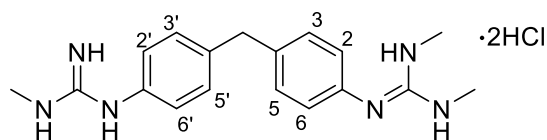
Using Method J, the Boc-protected compound **28a** (434 mg) was dissolved in an excess of 50 % TFAA in DCM (25 cm^3) and stirred at room temperature for 3-6 hours. The solvent was then reduced by rotary evaporation. The remaining TFA salt was re-dissolved in deionised water (25 cm^3) and treated with activated Amberlite IRA 400 chloride form (1 g) and allowed to stir gently for 24 hours at room temperature.

Following the usual work-up the hydrochloride salt, **28b** (183 mg, 94.3%), was afforded.

Yield: 183 mg, 94.3%

Molar Mass: 324.43 gmol^{-1}

δ_H (400MHz, D$_2$O): 2.80 (s, 9H, C-H$_3$), 3.97 (s, 2H, CH$_2$), 7.16 (t, 4H, J 8Hz, H-2, H-6, H-2', H-6'), 7.32 (d, 2H, J 8Hz, H-3, H-5, H-3', H-5')

δ_C (100MHz, D$_2$O): 13.13 (CH$_3$), 36.47 (CH$_2$), 40.14 (CH$_2$), 126.37 (Ar, C-H, H-2, H-6, H-2', H-6'), 130.20 (Ar, C-H, H-3, H-5, H-3', H-5'), 132.47 (q, Ar), 141.161 (q, C-N), 155.16 (C=N)

HRMS (m/z ESI$^+$): Calculated for C$_{18}$H$_{24}$N$_6$ [M] 324.21 Found: [M+H]$^+$ 325.2133

HPLC Purity (> 95%): 99.43%

6. References

(1)   Purves, D.; Augustine, J.; Fitzpatrick, D.; Hall, W. C.; Lamantia, A.-S.; McNamara, J. O.; Williams, S. M. *Neuroscience, 3rd Edition*; Sinauer Associates Inc, 2004.

(2)   Weiten, W. The Biological Bases of Behavior. In *Psychology: Themes and Variations*; Wadsworth Publishing: Toronto: Nelson, 2006.

(3)   Kolb, B.; Whishaw, I. Q. *Fundamentals of Human Neuropsychology*; Worth Publishers, 2009.

(4)   Biga, L. M.; Dawson, S.; Harwell, A.; Hopkins, R.; Kaufmann, J.; LeMaster, M.; Matern, P.; Morrison-Graham, K.; Quick, D.; Runyeon, J. Structure and Function of the Nervous System https://open.oregonstate.education/aandp/chapter/12-1-structure-and-function-of-the-nervous-system/ (accessed May 22, 2020).

(5)   Siegel, G.; Wayne Albers, R.; Brady, S. T.; Price, D. L. *Basic Neurochemistry MOLECULAR, CELLULAR AND MEDICAL ASPECTS*, 7th ed.; Elsevier Academic Press, 2006.

(6)   Nagatsu, T.; Yamakawa, T. The Catecholamine System in Health and Disease-Relation to Tyrosine 3-Monooxygenase and Other Catecholamine-Synthesizing Enzymes. *Proc. Jpn. Acad., Ser. B* **2006**, *82* (10), 388–415.

(7)   Nagatsu, T.; Levitt, M.; Udenfriend, S. Tyrosine Hydroxylase THE INITIAL STEP IN NOREPINEPHRINE BIOSYNTHESIS. *THE JOURNAL OF BIOLOQICAL CHEMISTRY* **1964**, *239* (S).

(8)   Daubner, S. C.; Le, T.; Wang, S. Tyrosine Hydroxylase and Regulation of Dopamine Synthesis. *Archives of Biochemistry and Biophysics* **2011**, *508* (1), 1–12. https://doi.org/10.1016/j.abb.2010.12.017.

(9)   Zhou, J. Norepinephrine Transporter Inhibitors and Their Therapeutic Potential. *Drugs of the Future* **2004**, *29* (12), 1235–1244. https://doi.org/10.1358/dof.2004.029.12.855246.

(10)   Kapalka, G. M. *Nutritional and Herbal Therapies for Children and Adolescents*, 1st ed.; Academic Press, 2009.

(11)   Eillis, L.; Farrington, D.; Hoskin, A. *Handbook of Crime Correlates*, 2nd ed.; Academic Press, 2019.

(12)   Cafasso, J.; Sullivan, D. Adrenaline Rush: Everything You Need to Know https://www.healthline.com/health/adrenaline-rush (accessed May 26, 2020).

(13)   Lotta, T.; Vidgren, J.; Tilgmann, C.; Ulmanen, I.; Melen, K.; Julkunen, I.; Taskinen, J. Kinetics of Human Soluble and Membrane-Bound Catechol O-Methyltransferase: A Revised Mechanism and Description of the Thermolabile Variant of the Enzyme. *Biochemistry* **1995**, *34* (13), 4202–4210. https://doi.org/10.1021/bi00013a008.

(14)   Schott, B. H.; Frischknecht, R.; Debska-Vielhaber, G.; John, N.; Behnisch, G.; Düzel, E.; Gundelfinger, E. D.; Seidenbecher, C. I. Membrane-Bound Catechol-O-Methyl Transferase in Cortical Neurons and Glial Cells Is Intracellularly Oriented. *Frontiers in Psychiatry* **2010**, *1*, 1–9. https://doi.org/10.3389/fpsyt.2010.00142.

(15)   Patrick, G. L. *An Introduction to Medicinal Chemistry*, 5th ed.; Oxford University Press, 2013.

(16)   Flower, D. R. Modelling G-Protein-Coupled Receptors for Drug Design. *Biochimica et Biophysica Acta* **1999**, *1422*, 207–234.

(17)   Efrain   Mudd.   GPCR   Structure,   Adrenergic   Receptors https://www.pharmacologicalsciences.us/adrenergic-receptors/gpcr-structure.html (accessed May 26, 2020).

(18)   Zhang, R.; Xie, X. Tools for GPCR Drug Discovery. *Acta Pharmacologica Sinica*. March 2012, pp 372–384. https://doi.org/10.1038/aps.2011.173.

(19)   OpenStax   College.   Signalling   Molecules   and   Cellular   Receptors https://cnx.org/contents/GFy_h8cu@11.10:H4oMpCSi@10/Signaling-Molecules-and-Cellular-Receptors (accessed May 26, 2020).

(20)   Maehle, A.-H. "Receptive Substances": John Newport Langley (1852–1925) and His Path to a Receptor Theory of Drug Action. *Medical History* **2004**, *48* (2). https://doi.org/10.1017/S0025727300000090.

(21)   Bosch, F.; Rosich, L. The Contributions of Paul Ehrlich to Pharmacology: A Tribute on the Occasion of the Centenary of His Nobel Prize. *Pharmacology* **2008**, *82*, 171–179. https://doi.org/10.1159/000149583.

(22)   Goldstein, D. S. Adrenal Responses to Stress. *Cellular and Molecular Neurobiology* **2010**, *30* (8), 1433–1440. https://doi.org/10.1007/s10571-010-9606-9.

(23)   Wachter, S. B.; Gilbert, E. M. Beta-Adrenergic Receptors, from Their Discovery and Characterization through Their Manipulation to Beneficial Clinical Application. *Cardiology   (Switzerland)*   **2012**,   *122*   (2),   104–112. https://doi.org/10.1159/000339271.

(24)   Rasmussen, S. G. F.; Choi, H.-J.; Rosenbaum, D. M.; Kobilka, T. S.; Thian, F. S.; Edwards, P. C.; Burghammer, M.; Ratnala, V. R. P.; Sanishvili, R.; Fischetti, R. F.; Schertler, G. F. X.; Weis, W. I.; Kobilka, B. K. Crystal Structure of the Human B2 Adrenergic G-Protein-Coupled Receptor. *Nature* **2007**, *450*, 383–387. https://doi.org/10.1038/nature06325.

(25)   Qu, L.; Zhou, Q.; Xu, Y.; Guo, Y.; Chen, X.; Yao, D.; Han, G. W.; Liu, Z. J.; Stevens, R. C.; Zhong, G.; Wu, D.; Zhao, S. Structural Basis of the Diversity of Adrenergic Receptors. *Cell Reports* **2019**, *29* (10), 2929-2935.e4. https://doi.org/10.1016/j.celrep.2019.10.088.

(26)   Chen, X.; Xu, Y.; Qu, L.; Wu, L.; Han, G. W.; Guo, Y.; Wu, Y.; Zhou, Q.; Sun, Q.; Chu, C.; Yang, J.; Yang, L.; Wang, Q.; Yuan, S.; Wang, L.; Hu, T.; Tao, H.; Sun, Y.; Song, Y.; Hu, L.; Liu, Z. J.; Stevens, R. C.; Zhao, S.; Wu, D.; Zhong, G. Molecular Mechanism for Ligand Recognition and Subtype Selectivity of A2C Adrenergic Receptor. *Cell Reports* **2019**, *29* (10), 2936-2943.e4. https://doi.org/10.1016/j.celrep.2019.10.112.

(27)   Langer, S. Z. History and Nomenclature of Alpha1-Adrenoceptors. *European Urology* **1999**, *36*, 2–6. https://doi.org/10.1159/000052310.

(28)   Akinaga, J.; Adolfo García-Sáinz, | J; Pupo, A. S. Updates in the Function and Regulation of α 1-Adrenoceptors. *British Journal of Pharmacy* **2019**, 2339–2342. https://doi.org/10.1111/bph.v176.14/issuetoc.

(29)   O'Donovan, D. H.; Muguruza, C.; Callado, L. F.; Rozas, I. Guanidine-Based A2-Adrenoceptor Ligands: Towards Selective Antagonist Activity. *European Journal of Medicinal Chemistry* **2014**, *82*, 242–254. https://doi.org/10.1016/j.ejmech.2014.05.057.

(30)   Scheinin, M.; Lomasney, J. W.; Hayden-Hixson, D. M.; Schambra, U. B.; Caron, M. G.; Lefkowitz, R. J.; Fremeau, R. T. Distribution of A2-Adrenergic Receptor Subtype Gene Expression in Rat Brain. *Molecular Brain Research* **1994**, *21*, 133–149. https://doi.org/10.1016/0169-328X(94)90386-7.

(31)   Kelly, B. The Design, Synthesis and Evaluation of Aryl Guanidinium Derivatives as A2 Adrenoceptor Antagonists for the Treatment of Depression, 2012.

(32)   Lambert, D. G. Drugs and Receptors. *Continuing Education in Anaesthesia, Critical Care and Pain* **2004**, *4*, 181–184. https://doi.org/10.1093/bjaceaccp/mkh049.

(33)   Rodriguez, F.; Rozas, I.; Ortega, J. E.; Meana, J. J.; Callado, L. F. Guanidine and 2-Aminoimidazoline Aromatic Derivatives as A2-Adrenoceptor Antagonists, 1:

Toward New Antidepressants with Heteroatomic Linkers. *Journal of Medicinal Chemistry* **2007**, *50*, 4516–4527. https://doi.org/10.1021/jm070229q.

(34)   Dardonville, C.; Goya, P.; Rozas, I.; Alsasua, A.; Martin, I.; Borrego, J. New Aromatic Iminoimidazolidine Derivatives as 1-Adrenoceptor Antagonists: A Novel Synthetic Approach and Pharmacological Activity. *Bioorganic & Medicinal Chemistry* **2000**, 1567–1577.

(35)   Wishart, D. S.; Feunang, Y. D.; Guo, A. C.; Lo, E. J.; Marcu, A.; Grant, J. R.; Sajed, T.; Johnson, D.; Li, C.; Sayeeda, Z.; Assempour, N.; Iynkkaran, I.; Liu, Y.; Maciejewski, A.; Gale, N.; Wilson, A.; Chin, L.; Cummings, R.; Le, D.; Pon, A.; Knox, C.; Wilson, M. DrugBank 5.0: A Major Update to the DrugBank Database for 2018. *Nucleic Acids Research* **2018**, *46* (D1). https://doi.org/10.1093/nar/gkx1037.

(36)   Rodriguez, F.; Rozas, I.; Ortega, J. E.; Erdozain, A. M.; Meana, J. J.; Callado, L. F. Guanidine and 2-Aminoimidazoline Aromatic Derivatives as A2-Adrenoceptor Antagonists. 2. Exploring Alkyl Linkers for New Antidepressants. *Journal of Medicinal Chemistry* **2008**, *51* (11), 3304–3312. https://doi.org/10.1021/jm800026x.

(37)   Flood, A.; Trujillo, C.; Sanchez-Sanz, G.; Kelly, B.; Muguruza, C.; Callado, L. F.; Rozas, I. Thiophene/Thiazole-Benzene Replacement on Guanidine Derivatives Targeting A2-Adrenoceptors. *European Journal of Medicinal Chemistry* **2017**, *138*, 38–50. https://doi.org/10.1016/j.ejmech.2017.06.008.

(38)   Kelly, B.; McMullan, M.; Muguruza, C.; Ortega, J. E.; Meana, J. J.; Callado, L. F.; Rozas, I. A2-Adrenoceptor Antagonists: Synthesis, Pharmacological Evaluation, and Molecular Modeling Investigation of Pyridinoguanidine, Pyridino-2-Aminoimidazoline and Their Derivatives. *Journal of Medicinal Chemistry* **2015**, *58* (2), 963–977. https://doi.org/10.1021/jm501635e.

(39)   McMullan, M.; Rozas, I. Conformationally Restricted and Bis-Aryl Gaunidinium, Derivatives: Towards Improved A2-Adrenergic Affinity and Antagonism for Treatment of Depression, 2015.

(40)   Rodriguez, F.; Rozas, I.; Ortega, J. E.; Erdozain, A. M.; Meana, J. J.; Callado, L. F. Guanidine and 2-Aminoimidazoline Aromatic Derivatives as A2-Adrenoceptor Ligands: Searching for Structure-Activity Relationships. *Journal of Medicinal Chemistry* **2009**, *52* (3), 601–609. https://doi.org/10.1021/jm800838r.

(41)   Giovannitti, J. A.; Thoms, S. M.; Crawford, J. J. Alpha-2 Adrenergic Receptor Agonists: A Review of Current Clinical Applications. *Anesthesia Progress* **2015**, *62* (1). https://doi.org/10.2344/0003-3006-62.1.31.

(42)   Cottingham, C.; Wang, Q. A2 Adrenergic Receptor Dysregulation in Depressive Disorders: Implications for the Neurobiology of Depression and Antidepressant Therapy. *Neuroscience and Biobehavioral Reviews*. Elsevier Ltd 2012, pp 2214–2225. https://doi.org/10.1016/j.neubiorev.2012.07.011.

(43)   O'Donovan, D. H.; Rozas, I. A Concise Synthesis of Asymmetrical N,N′-Disubstituted Guanidines. *Tetrahedron Letters* **2011**, *52* (32), 4117–4119. https://doi.org/10.1016/j.tetlet.2011.05.132.

(44)   Committee on the Design and Evaluation of Safer Chemical Substitutions: A Framework to Inform Government and Industry Decision; Board on Environmental Studies and Toxicology; Division on Earth and Life Studies; National Research Council. A Framework to Guide Selection of Chemical Alternatives. *A Framework to Guide Selection of Chemical Alternatives*; Washington (DC): National Academies Press (US), 2014.

(45)   Lipinski, C. A.; Lombardo, F.; Dominy, B. W.; Feeney, P. J. Experimental and Computational Approaches to Estimate Solubility and Permeability in Drug Discovery and Development Settings. *Advanced Drug Delivery Reviews* **1997**, *23* (1–3). https://doi.org/10.1016/S0169-409X(96)00423-1.

(46)   Daina, A.; Michielin, O.; Zoete, V. SwissADME: A Free Web Tool to Evaluate Pharmacokinetics, Drug-Likeness and Medicinal Chemistry Friendliness of Small Molecules. *Scientific Reports* **2017**, *7* (1). https://doi.org/10.1038/srep42717.

(47)   ChemAxon - Software Solutions and Services for Chemistry & Biology https://chemaxon.com/products/marvin (accessed Apr 6, 2020).

(48)   Veber, D. F.; Johnson, S. R.; Cheng, H. Y.; Smith, B. R.; Ward, K. W.; Kopple, K. D. Molecular Properties That Influence the Oral Bioavailability of Drug Candidates. *Journal of Medicinal Chemistry* **2002**, *45* (12), 2615–2623. https://doi.org/10.1021/jm020017n.

(49)   MORIGUCHI, I.; HIRONO, S.; NAKAGOME, I.; HIRANO, H. Comparison of Reliability of Log P Values for Drugs Calculated by Several Methods. *CHEMICAL & PHARMACEUTICAL BULLETIN* **1994**, *42* (4). https://doi.org/10.1248/cpb.42.976.

(50)   MORIGUCHI, I.; HIRONO, S.; LIU, Q.; NAKAGOME, I.; MATSUSHITA, Y. Simple Method of Calculating Octanol/Water Partition Coefficient. *CHEMICAL & PHARMACEUTICAL BULLETIN* **1992**, *40* (1). https://doi.org/10.1248/cpb.40.127.

(51)   Silverstein, K. A. T.; Haymet, A. D. J.; Dill, K. A. *A Simple Model of Water and the Hydrophobic Effect*; 1998.

(52)   Capuzzi, S. J.; Muratov, E. N.; Tropsha, A. Phantom PAINS: Problems with the Utility of Alerts for Pan-Assay Interference Compounds. *Journal of Chemical Information and Modeling* **2017**, *57* (3). https://doi.org/10.1021/acs.jcim.6b00465.

(53)   Pacák, P. Molar refractivity and interactions in solutions I. Molar refractivity of some monovalent ions in aqueous and dimethyl sulfoxide solutions https://www.chemicalpapers.com/file_access.php?file=434a489.pdf (accessed Apr 10, 2020).

(54)   Walters, W. P.; Murcko, M. A. Prediction of 'Drug-Likeness.' *Advanced Drug Delivery Reviews* **2002**, *54* (3). https://doi.org/10.1016/S0169-409X(02)00003-0.

(55)   Hollenberg, P. F. Characteristics and Common Properties of Inhibitors, Inducers, and Activators of CYP Enzymes. *Drug Metabolism Reviews* **2002**, *34* (1–2). https://doi.org/10.1081/DMR-120001387.

(56)   Ertl, P.; Rohde, B.; Selzer, P. Fast Calculation of Molecular Polar Surface Area as a Sum of Fragment-Based Contributions and Its Application to the Prediction of Drug Transport Properties. *Journal of Medicinal Chemistry* **2000**, *43* (20). https://doi.org/10.1021/jm000942e.

(57)   van de Waterbeemd, H. In Silico Models to Predict Oral Absorption. In *Comprehensive Medicinal Chemistry II*; Elsevier, 2007. https://doi.org/10.1016/B0-08-045044-X/00145-0.

(58)   Pajouhesh, H.; Lenz, G. R. Medicinal Chemical Properties of Successful Central Nervous System Drugs. *NeuroRX* **2005**, *2* (4). https://doi.org/10.1602/neurorx.2.4.541.

(59)   Locher, K. P. Structure and Mechanism of ATP-Binding Cassette Transporters. *Philosophical Transactions of the Royal Society B: Biological Sciences* **2009**, *364* (1514). https://doi.org/10.1098/rstb.2008.0125.

(60)   Löscher, W.; Potschka, H. Blood-Brain Barrier Active Efflux Transporters: ATP-Binding Cassette Gene Family. *NeuroRX* **2005**, *2* (1). https://doi.org/10.1602/neurorx.2.1.86.

(61)   Dobson, P. D.; Kell, D. B. Carrier-Mediated Cellular Uptake of Pharmaceutical Drugs: An Exception or the Rule? *Nature Reviews Drug Discovery* **2008**, *7* (3). https://doi.org/10.1038/nrd2438.

(62)   Savjani, K. T.; Gajjar, A. K.; Savjani, J. K. Drug Solubility: Importance and Enhancement Techniques. *ISRN Pharmaceutics* **2012**, *2012*. https://doi.org/10.5402/2012/195727.

(63)   Delaney, J. S. ESOL: Estimating Aqueous Solubility Directly from Molecular Structure. *Journal of Chemical Information and Computer Sciences* **2004**, *44* (3). https://doi.org/10.1021/ci034243x.

(64)   Ali, J.; Camilleri, P.; Brown, M. B.; Hutt, A. J.; Kirton, S. B. Revisiting the General Solubility Equation: In Silico Prediction of Aqueous Solubility Incorporating the Effect of Topographical Polar Surface Area. *Journal of Chemical Information and Modeling* **2012**, *52* (2). https://doi.org/10.1021/ci200387c.

(65)   Bahekar, R. H.; Jain, M. R.; Goel, A.; Patel, D. N.; Prajapati, V. M.; Gupta, A. A.; Jadav, P. A.; Patel, P. R. Design, Synthesis, and Biological Evaluation of Substituted-N-(Thieno[2,3-b]Pyridin-3-Yl)-Guanidines, N-(1H-Pyrrolo[2,3-b]Pyridin-3-Yl)-Guanidines, and N-(1H-Indol-3-Yl)-Guanidines. *Bioorganic & Medicinal Chemistry* **2007**, *15* (9). https://doi.org/10.1016/j.bmc.2007.02.029.

(66)   Laeckmann, D. Synthesis and Biological Evaluation of Aroylguanidines Related to Amiloride as Inhibitors of the Human Platelet Na+/H+ Exchanger. *Bioorganic & Medicinal Chemistry* **2002**, *10* (6). https://doi.org/10.1016/S0968-0896(02)00022-6.

(67)   Aquino, C. J.; Ramanjulu, J. M.; Heyer, D.; Daniels, A. J.; Palazzo, F.; Dezube, M. Synthesis and Structure Activity Relationship of Guanidines as NPY Y5 Antagonists. *Bioorganic & Medicinal Chemistry* **2004**, *12* (10). https://doi.org/10.1016/j.bmc.2004.03.012.

(68)   Abbasi Gharibkandi, N.; Hosseinimehr, S. J. Radiotracers for Imaging of Parkinson's Disease. *European Journal of Medicinal Chemistry* **2019**, *166*. https://doi.org/10.1016/j.ejmech.2019.01.029.

(69)   Haynes, W. M. *CRC Handbook of Chemistry and Physics*, 95th ed.; CRC Press, Taylor and Francis Group, 2009.

(70)   Tan, C. H.; Coles, M. The Chemistry of Guanidine, Guanidinium, and Guanidinate Compounds. *Australian Journal of Chemistry* **2014**, *67* (7). https://doi.org/10.1071/CH14384.

(71)   Dardonville, C.; Rozas, I.; Callado, L. F.; Meana, J. J. I 2 -Imidazoline Binding Site Affinity of a Structurally Different Type of Ligands. *Bioorganic & Medicinal Chemistry* **2002**, *10* (5). https://doi.org/10.1016/S0968-0896(01)00420-5.

(72)   Diez-Cecilia, E.; Kelly, B.; Perez, C.; Zisterer, D. M.; Nevin, D. K.; Lloyd, D. G.; Rozas, I. Guanidinium-Based Derivatives: Searching for New Kinase Inhibitors. *European Journal of Medicinal Chemistry* **2014**, *81*. https://doi.org/10.1016/j.ejmech.2014.05.025.

(73)   Nagle, P. S.; Rodriguez, F.; Nguyen, B.; Wilson, W. D.; Rozas, I. High DNA Affinity of a Series of Peptide Linked Diaromatic Guanidinium-like Derivatives. *Journal of Medicinal Chemistry* **2012**, *55* (9). https://doi.org/10.1021/jm300296f.

(74)   Yamada, T.; Liu, X.; Englert, U.; Yamane, H.; Dronskowski, R. Solid-State Structure of Free Base Guanidine Achieved at Last. *Chemistry - A European Journal* **2009**, *15* (23). https://doi.org/10.1002/chem.200900508.

(75)   Kelly, B.; O'Donovan, D. H.; O'Brien, J.; McCabe, T.; Blanco, F.; Rozas, I. Pyridin-2-Yl Guanidine Derivatives: Conformational Control Induced by Intramolecular Hydrogen-Bonding Interactions. *The Journal of Organic Chemistry* **2011**, *76* (22). https://doi.org/10.1021/jo200954c.

(76)   Blanco, F.; Kelly, B.; Alkorta, I.; Rozas, I.; Elguero, J. Cation–π Interactions: Complexes of Guanidinium and Simple Aromatic Systems. *Chemical Physics Letters* **2011**, *511* (1–3). https://doi.org/10.1016/j.cplett.2011.06.012.

(77)   Pattarawarapan, M.; Jaita, S.; Wangngae, S.; Phakhodee, W. Ultrasound-Assisted Synthesis of Substituted Guanidines from Thioureas. *Tetrahedron Letters* **2016**, *57* (12). https://doi.org/10.1016/j.tetlet.2016.02.050.

(78)   Kim, K. S.; Qian, L. Improved Method for the Preparation of Guanidines. *Tetrahedron Letters* **1993**, *34* (48). https://doi.org/10.1016/S0040-4039(00)61537-X.

(79)   Kelly, B.; Rozas, I. Copper(II) Chloride Promoted Transformation of Amines into Guanidines and Asymmetrical N,N′-Disubstituted Guanidines. *Tetrahedron Letters* **2013**, *54* (30). https://doi.org/10.1016/j.tetlet.2013.05.070.

(80)   Rong, H.-J.; Yang, C.-F.; Chen, T.; Wang, Y.-Q.; Ning, B.-K. Synthesis of Guanidines via the I2 Mediated Desulfurization of N,N′-Di-Boc-Thiourea. *Tetrahedron Letters* **2019**, *60* (34). https://doi.org/10.1016/j.tetlet.2019.150970.

(81)   Yong, Y. F.; Kowalski, J. A.; Lipton, M. A. Facile and Efficient Guanylation of Amines Using Thioureas and Mukaiyama's Reagent. *The Journal of Organic Chemistry* **1997**, *62* (5). https://doi.org/10.1021/jo962196k.

(82)   Ohara, K.; Vasseur, J.-J.; Smietana, M. NIS-Promoted Guanylation of Amines. *Tetrahedron Letters* **2009**, *50* (13). https://doi.org/10.1016/j.tetlet.2009.01.073.

(83)   Musiol, H.-J.; Moroder, L. N, N'-Di-Tert -Butoxycarbonyl-1H-Benzotriazole-1-Carboxamidine Derivatives Are Highly Reactive Guanidinylating Reagents. *Organic Letters* **2001**, *3* (24). https://doi.org/10.1021/ol010191q.

(84)   Dodd, D. S.; Wallace, O. B. Solid-Phase Synthesis of N,N′ Substituted Guanidines. *Tetrahedron Letters* **1998**, *39* (32). https://doi.org/10.1016/S0040-4039(98)01197-6.

(85)   Zapf, C. W.; Goodman, M. Synthesis of 2-Amino-4-Pyrimidinones from Resin-Bound Guanidines Prepared Using Bis(Allyloxycarbonyl)-Protected Triflylguanidine. *The Journal of Organic Chemistry* **2003**, *68* (26). https://doi.org/10.1021/jo035201a.

(86)   Zapf, C. W.; Creighton, C. J.; Tomioka, M.; Goodman, M. A Novel Traceless Resin-Bound Guanidinylating Reagent for Secondary Amines To Prepare N,N'-Disubstituted Guanidines. *Organic Letters* **2001**, *3* (8). https://doi.org/10.1021/ol015576n.

(87)   Guisado, O.; Martínez, S.; Pastor, J. A Novel, Facile Methodology for the Synthesis of N,N′-Bis(Tert-Butoxycarbonyl)-Protected Guanidines Using Polymer-Supported Carbodiimide. *Tetrahedron Letters* **2002**, *43* (39). https://doi.org/10.1016/S0040-4039(02)01390-4.

(88)   Son, Y.; Lim, M.; Khim, J.; Ashokkumar, M. Acoustic Emission Spectra and Sonochemical Activity in a 36kHz Sonoreactor. *Ultrasonics Sonochemistry* **2012**, *19* (1). https://doi.org/10.1016/j.ultsonch.2011.06.001.

(89)   Yin, B.; Liu, Z.; Yi, M.; Zhang, J. An Efficient Method for the Synthesis of Disubstituted Thioureas via the Reaction of N,N′-Di-Boc-Substituted Thiourea with Alkyl and Aryl Amines under Mild Conditions. *Tetrahedron Letters* **2008**, *49* (22). https://doi.org/10.1016/j.tetlet.2008.03.158.

(90)   Feichtinger, K.; Sings, H. L.; Baker, T. J.; Matthews, K.; Goodman, M. Triurethane-Protected Guanidines and Triflyldiurethane-Protected Guanidines: New Reagents for Guanidinylation Reactions. *Journal of Organic Chemistry* **1998**, *63* (23), 8432–8439. https://doi.org/10.1021/jo9814344.

(91)   Mitsunobu, O.; Yamada, M. *Preparation of Esters of Phosphoric Acid 935*; 1967; Vol. 40.

(92)   Beddoe, R. H.; Sneddon, H. F.; Denton, R. M. The Catalytic Mitsunobu Reaction: A Critical Analysis of the Current State-of-the-Art. *Organic and Biomolecular Chemistry*. Royal Society of Chemistry 2018, pp 7774–7781. https://doi.org/10.1039/c8ob01929k.

(93)   Swamy, K. C. K.; Kumar, N. N. B.; Balaraman, E.; Kumar, K. V. P. P. Mitsunobu and Related Reactions: Advances and Applications. *Chemical Reviews* **2009**, *109* (6), 2551–2651. https://doi.org/10.1021/cr800278z.

(94)   Camp, D.; Harvey, P. J.; Jenkins, I. D. The Effect of Solvent Polarity on the Rate of the Mitsunobu Esterification Reaction. *Tetrahedron* **2015**, *71* (23), 3932–3938. https://doi.org/10.1016/j.tet.2015.04.035.

(95)   But, T.; Lu, J.; Toy, P. Organocatalytic Mitsunobu Reactions with 3,5-Dinitrobenzoic Acid. *Synlett* **2010**, *2010* (07). https://doi.org/10.1055/s-0029-1219795.

(96)   But, T. Y. S.; Toy, P. H. Organocatalytic Mitsunobu Reactions. *Journal of the American Chemical Society* **2006**, *128* (30). https://doi.org/10.1021/ja063141v.

(97)   Hirose, D.; Taniguchi, T.; Ishibashi, H. Recyclable Mitsunobu Reagents: Catalytic Mitsunobu Reactions with an Iron Catalyst and Atmospheric Oxygen. *Angewandte Chemie* **2013**, *125* (17). https://doi.org/10.1002/ange.201300153.

(98)   Hirose, D.; Gazvoda, M.; Košmrlj, J.; Taniguchi, T. Systematic Evaluation of 2-Arylazocarboxylates and 2-Arylazocarboxamides as Mitsunobu Reagents. *The Journal of Organic Chemistry* **2018**, *83* (8). https://doi.org/10.1021/acs.joc.8b00486.

(99)   Buonomo, J. A.; Aldrich, C. C. Mitsunobu Reactions Catalytic in Phosphine and a Fully Catalytic System. *Angewandte Chemie International Edition* **2015**, *54* (44). https://doi.org/10.1002/anie.201506263.

(100)   Davey, S. Mitsunobu Minus Waste. *Nature Chemistry* **2013**, *5* (5). https://doi.org/10.1038/nchem.1639.

(101)   Ríos Martínez, C. H.; Lagartera, L.; Kaiser, M.; Dardonville, C. Antiprotozoal Activity and DNA Binding of NSubstituted N-Phenylbenzamide and 1,3- Diphenylurea Bisguanidines . *European Jorunal of Medicinal Chemistry* **2014**, *81*, 481–491.

(102)   Adeyemi Rahman. Guanidine Derivatives as Potential Anti-Infective Agents: Tackling Protozoal Diseases and Mycobacterium Tuberculosis, 2019.

(103)   Bedoya Zurita, M.; Diaz Martin, J. A.; del Sol Moreno, G.; Martin Escudero, U.; Jimenez Bargueno, M. D.; Romanach Ferrer, M.; Purcell, T. A.; Jegham, S.; Defosse, G. Preparation of Imidazoyldihydroindoles as Alpha2-Adrenoceptor Antagonists. FR2735776, December 27, 1996.

(104)   Uhlén, S.; Dambrova, M.; Näsman, J.; Schiöth, H. B.; Gu, Y.; Wikberg-Matsson, A.; Wikberg, J. E. S. []RS79948-197 Binding to Human, Rat, Guinea Pig and Pig

A2A-, A2B- and A2C-Adrenoceptors. . *European Journal of Pharmacology* **1998**, *343* (1), 93–101. https://doi.org/10.1016/S0014-2999(97)01521-5.

(105)   Ferreira, L. G.; dos Santos, R. N.; Oliva, G.; Andricopulo, A. D. Molecular Docking and Structure-Based Drug Design Strategies. *Molecules*. MDPI AG July 1, 2015, pp 13384–13421. https://doi.org/10.3390/molecules200713384.

(106)   Muhammed, M. T.; Aki-Yalcin, E. Homology Modeling in Drug Discovery: Overview, Current Applications, and Future Perspectives. *Chemical Biology and Drug Design*. Blackwell Publishing Ltd January 1, 2019, pp 12–20. https://doi.org/10.1111/cbdd.13388.

(107)   Sethi, A.; Joshi, K.; Sasikala, K.; Alvala, M. *Molecular Docking in Modern Drug Discovery: Principles and Recent Applications*; 2019. https://doi.org/10.5772/intechopen.85991.

(108)   Berman, H. M.; Westbrook, J.; Feng, Z.; Gilliland, G.; Bhat, T. N.; Weissig, H.; Shindyalov, I. N.; Bourne, P. E. The Protein Data Bank. *Nucleic Acids Research* **2000**, *28* (1), 235–242. https://doi.org/10.1093/nar/28.1.235.

(109)   Pinzi, L.; Rastelli, G. Molecular Docking: Shifting Paradigms in Drug Discovery. *International Journal of Molecular Sciences*. MDPI AG September 1, 2019. https://doi.org/10.3390/ijms20184331.

(110)   Englebienne, P.; Moitessier, N. Docking Ligands into Flexible and Solvated Macromolecules. 5. Force-Field-Based Prediction of Binding Affinities of Ligands to Proteins. *Journal of Chemical Information and Modeling* **2009**, *49* (11), 2564–2571. https://doi.org/10.1021/ci900251k.

(111)   Sousa, S. F.; Fernandes, P. A.; Ramos, M. J. Protein-Ligand Docking: Current Status and Future Challenges. *Proteins: Structure, Function and Genetics*. October 1, 2006, pp 15–26. https://doi.org/10.1002/prot.21082.

(112)   Murray, C. W.; Auton, T. R.; Eldridge, M. D. *Empirical Scoring Functions. II. The Testing of an Empirical Scoring Function for the Prediction of Ligand-Receptor Binding Affinities and the Use of Bayesian Regression to Improve the Quality of the Model*; KLUWER/ESCOM, 1998; Vol. 12.

(113)   Li, J.; Fu, A.; Zhang, L. An Overview of Scoring Functions Used for Protein–Ligand Interactions in Molecular Docking. *Interdisciplinary Sciences: Computational Life Sciences*. Springer Berlin Heidelberg June 1, 2019, pp 320–328. https://doi.org/10.1007/s12539-019-00327-w.

(114)   Jayaraman, A.; Jamil, K.; Kakarala, K. K. Homology Modelling and Docking Studies of Human A2-Adrenergic Receptor Subtypes. *Journal of Computer Science & Systems Biology* **2015**, *06* (03). https://doi.org/10.4172/jcsb.1000111.

(115)   Miao, Y.; Nichols, S. E.; Gasper, P. M.; Metzger, V. T.; McCammon, J. A. Activation and Dynamic Network of the M2 Muscarinic Receptor. *Proceedings of the National Academy of Sciences of the United States of America* **2013**, *110* (27), 10982–10987. https://doi.org/10.1073/pnas.1309755110.

(116)   Schneider, J.; Korshunova, K.; Musiani, F.; Alfonso-Prieto, M.; Giorgetti, A.; Carloni, P. Predicting Ligand Binding Poses for Low-Resolution Membrane Protein Models: Perspectives from Multiscale Simulations. *Biochemical and Biophysical Research Communications* **2018**, *498* (2), 366–374. https://doi.org/10.1016/j.bbrc.2018.01.160.

(117)   Thompson, J. D.; Higgins, D. G.; Gibson, T. J. CLUSTAL W: Improving the Sensitivity of Progressive Multiple Sequence Alignment through Sequence Weighting, Position-Specific Gap Penalties and Weight Matrix Choice. *Nucleic Acids Research* **1994**, *22* (22). https://doi.org/10.1093/nar/22.22.4673.

(118)   Laurila, J. M. M.; Xhaard, H.; Ruuskanen, J. O.; Rantanen, M. J. M.; Karlsson, H. K.; Johnson, M. S.; Scheinin, M. The Second Extracellular Loop of α 2A-Adrenoceptors Contributes to the Binding of Yohimbine Analogues. *British Journal of Pharmacology* **2007**, *151* (8), 1293–1304. https://doi.org/10.1038/sj.bjp.0707330.

(119)   Ostopovici-Halip, L.; Curpân, R.; Mracec, M.; Bologa, C. G. Structural Determinants of the Alpha2 Adrenoceptor Subtype Selectivity. *Journal of Molecular Graphics and Modelling* **2011**, *29* (8), 1030–1038. https://doi.org/10.1016/j.jmgm.2011.04.011.

(120)   *Chapter V: A Comparison of the Antagonist Binding Sites of the Human Dopamine Receptors.*

(121)   Kumar, V.; Bansal, G.; Patel, J.; Gopi Mohan, C. Structure-Function Prediction of A2A-, A2B-, and A2C-Adrenoceptors Using Homology Model Assisted Antagonist Binding Study. *Medicinal Chemistry Research* **2014**, *23* (2), 735–746. https://doi.org/10.1007/s00044-013-0677-2.

(122)   Surgand, J.-S.; Rodrigo, J.; Kellenberger, E.; Rognan, D. A Chemogenomic Analysis of the Transmembrane Binding Cavity of Human G-Protein-Coupled Receptors. *Proteins: Structure, Function, and Bioinformatics* **2005**, *62* (2). https://doi.org/10.1002/prot.20768.

(123)   Rozas, I. On the Nature of Hydrogen Bonds: An Overview on Computational Studies and a Word about Patterns. *Physical Chemistry Chemical Physics*. 2007, pp 2782–2790. https://doi.org/10.1039/b618225a.

(124)   Bader, R. F. W. *Atoms in Molecules. A Quantum Theory*; Oxford University Press: Oxford, 1990.

(125)   Reed, A. E.; Curtiss, L. A.; Weinhold, F. Intermolecular Interactions from a Natural Bond Orbital, Donor-Acceptor Viewpoint. *Chemical Reviews* **1988**, *88* (6). https://doi.org/10.1021/cr00088a005.

(126)   Bader, R. F. W.; Carroll, M. T.; Cheeseman, J. R.; Chang, C. Properties of Atoms in Molecules: Atomic Volumes. *Journal of the American Chemical Society* **1987**, *109* (26). https://doi.org/10.1021/ja00260a006.

(127)   Finlay, D. B.; Duffull, S. B.; Glass, M. 100 Years of Modelling Ligand–Receptor Binding and Response: A Focus on GPCRs. *British Journal of Pharmacology*. John Wiley and Sons Inc. April 1, 2020, pp 1472–1484. https://doi.org/10.1111/bph.14988.

(128)   Lazareno, ' S; Birdsall, N. J. M. *Estimation of Competitive Antagonist Affinity from Functional Inhibition Curves Using the Gaddum, Schild and Cheng-Prusoff Equations*; Press Ltd, 1993; Vol. 109.

(129)   Milligan, G. Principles: Extending the Utility of [35 S]GTPgS Binding Assays. *Elsevier review* **2003**, *24*, 87–90.

(130)   Seifert, R.; Wenzel-Seifert, K. Constitutive Activity of G-Proteins-Coupled Receptors: Cause of Disease and Common Property of Wild-Type Receptors. *Naunyn-Schmiedeberg's Archives of Pharmacology*. 2002, pp 381–416. https://doi.org/10.1007/s00210-002-0588-0.

(131)   Koski, G.; Streaty, R. A.; Klee, W. A. Modulation of Sodium-Sensitive GTPase by Partial Opiate Agonists AN EXPLANATION FOR T H E DUAL REQUIREMENT FOR Na' AND GTP IN INHIBITORY REGULATION OF ADENYLATE CYCLASE*. *The Journal of Biological Chemistry* **1982**, *257* (23), 14035–14040.

(132)   Lefkowitz, R. J.; Cerione, R. A.; Benovic, J. L.; Strulovici, B.; Stiles, G. L.; Codina, J.; Birnbaumer, L.; Caron, M. G. Purification, Characterization and Reconstitution of the Adenylate Cyclase-Coupled β-Adrenergic Receptor. In *IUPHAR 9th International Congress of Pharmacology London 1984*; Palgrave Macmillan UK: London, 1984. https://doi.org/10.1007/978-1-349-17613-7_33.

(133)   Schrodinger LLC. Maestro. Schrodinger Inc.: New York 2021.

(134)   Madhavi Sastry, G.; Adzhigirey, M.; Day, T.; Annabhimoju, R.; Sherman, W. Protein and Ligand Preparation: Parameters, Protocols, and Influence on Virtual Screening Enrichments. *Journal of Computer-Aided Molecular Design* **2013**, *27* (3), 221–234. https://doi.org/10.1007/s10822-013-9644-8.

(135)   Yang, A.-S.; Honig, B. An Integrated Approach to the Analysis and Modeling of Protein Sequences and Structures. I. Protein Structural Alignment and a Quantitative Measure for Protein Structural Distance 1 1Edited by F. E. Cohen. *Journal of Molecular Biology* **2000**, *301* (3). https://doi.org/10.1006/jmbi.2000.3973.

(136)   Michaela McMullan. Conformationally Restricted and Bis-Aryl Gaunidinium, Derivatives: Towards Improved A2-Adrenergic Affinity and Antagonism for Treatment of Depression, 2015.

(137)   Sigma   Aldrich.   N,N′-Di-Boc-thiourea https://www.sigmaaldrich.com/catalog/product/aldrich/531820?lang=en&region=IE (accessed Dec 29, 2020).

7. Appendix
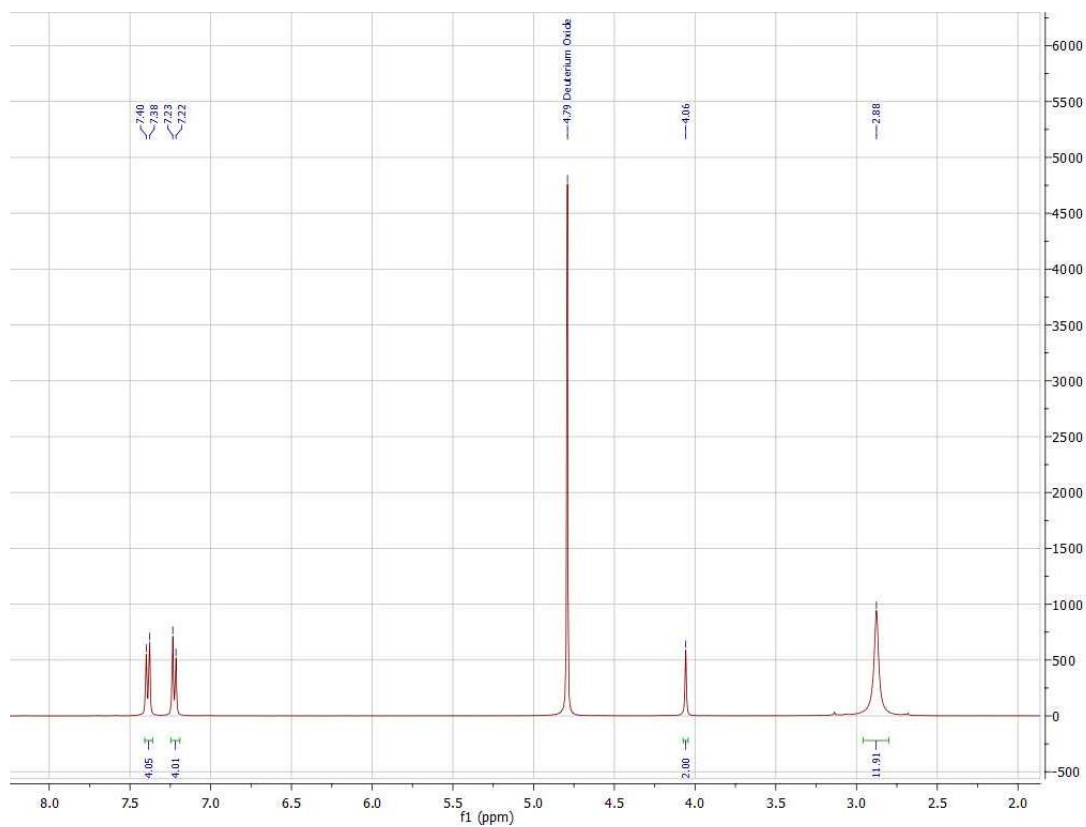
Appendix 1 *^{1}H NMR spectrum of final compound **19c** in D$_2$O*
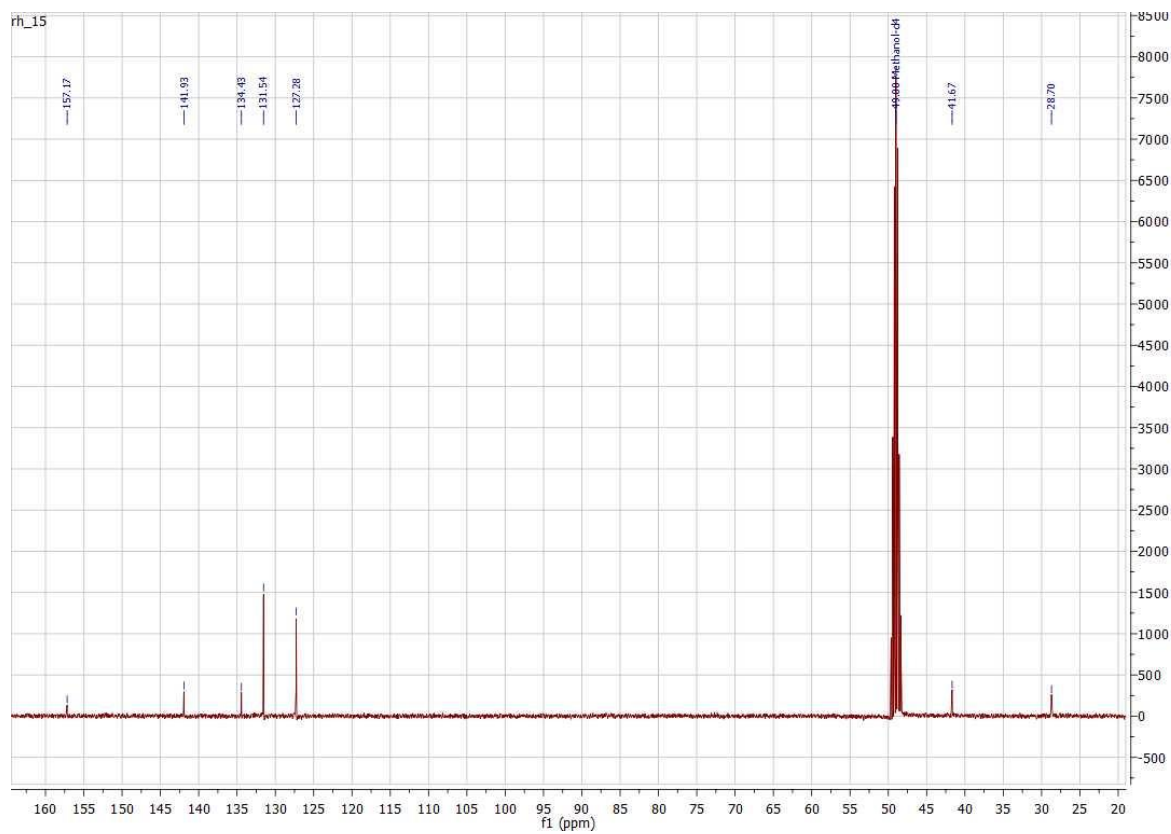
Appendix 2 *^{13}C NMR spectrum of final compound **19c** in MeOD*

Chromatogram : RH16 RUN2_channel1

RH16 RUN2.DATA - Prostar 335 Absorbance Analog Channel 1 LC0908M822
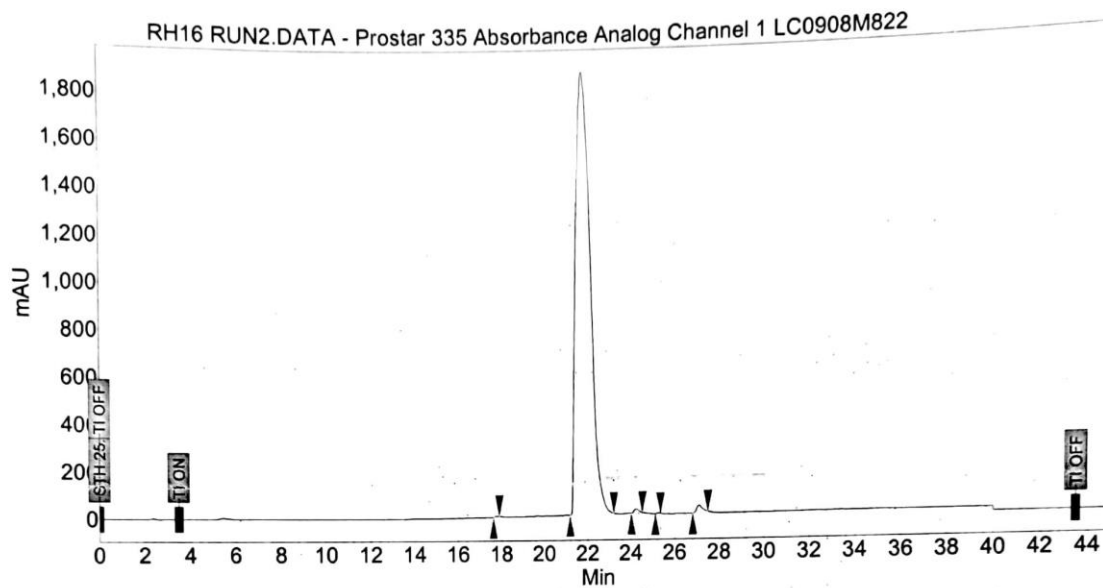
Peak results :

Index	Name	Time [Min]	Quantity [% Area]	Height [mAU]	Area [mAU.Min]	Area % [%]
1	UNKNOWN	17.77	0.02	2.4	0.3	0.022
2	UNKNOWN	21.68	99.05	1878.4	1439.2	99.052
3	UNKNOWN	24.21	0.28	17.1	4.0	0.278
4	UNKNOWN	25.21	0.02	2.8	0.3	0.023
5	UNKNOWN	27.09	0.62	31.8	9.1	0.624
Total			100.00	1932.4	1452.9	100.000

Appendix 3 *HPLC percentage purity check for compound **19c** which displayed 99.05% purity*
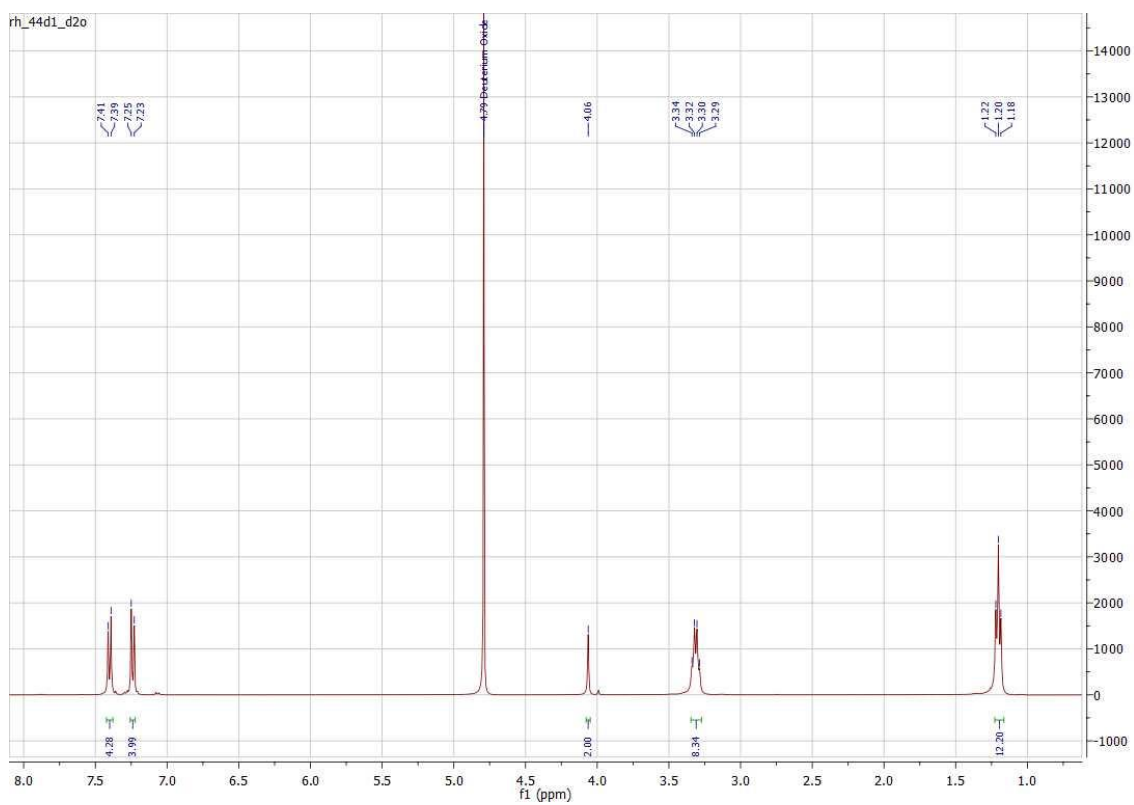
Appendix 4 *¹H NMR spectrum of final compound **20c** in D₂O*
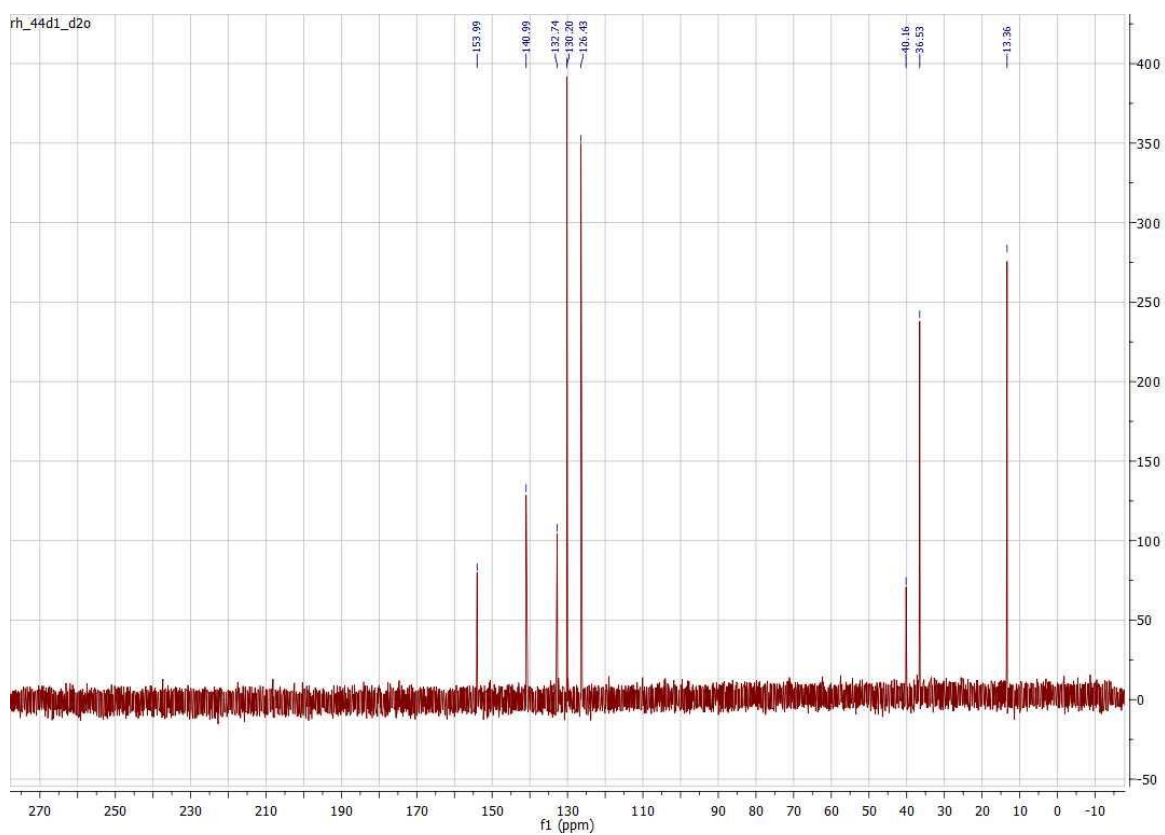
Appendix 5 *¹³C NMR spectrum of final compound **20c** in D₂O*
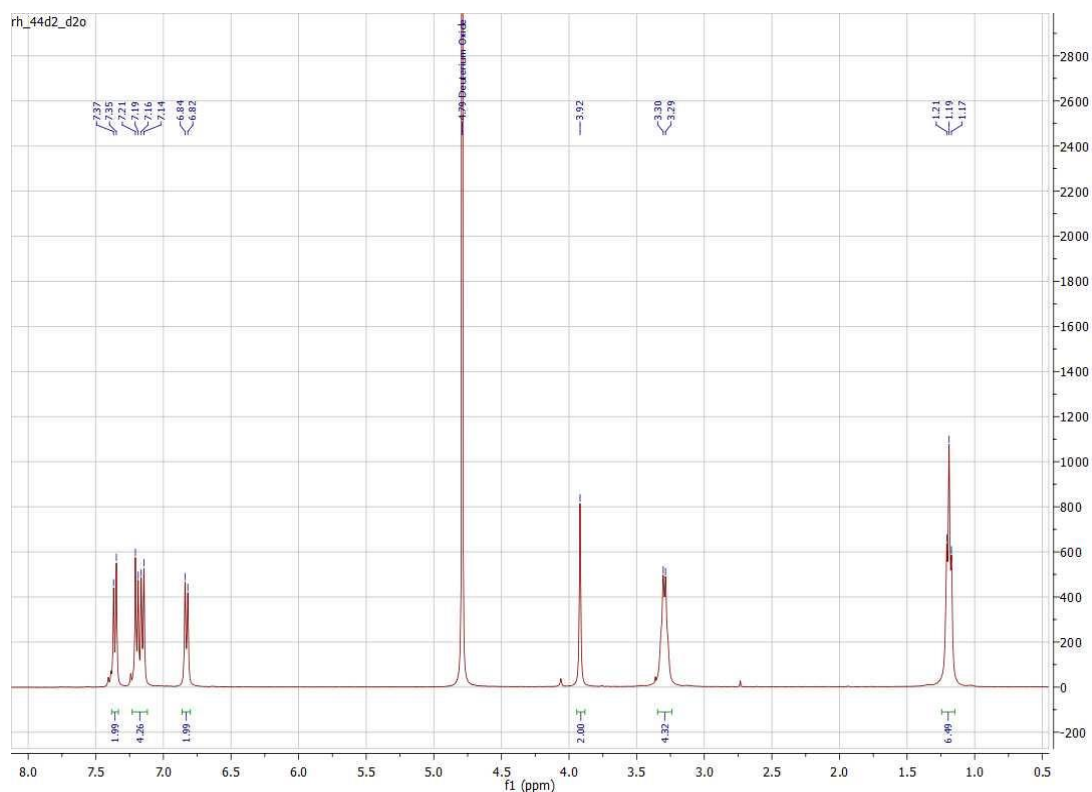
Appendix 6 ^1H NMR spectrum of final compound **20d** in D_2O
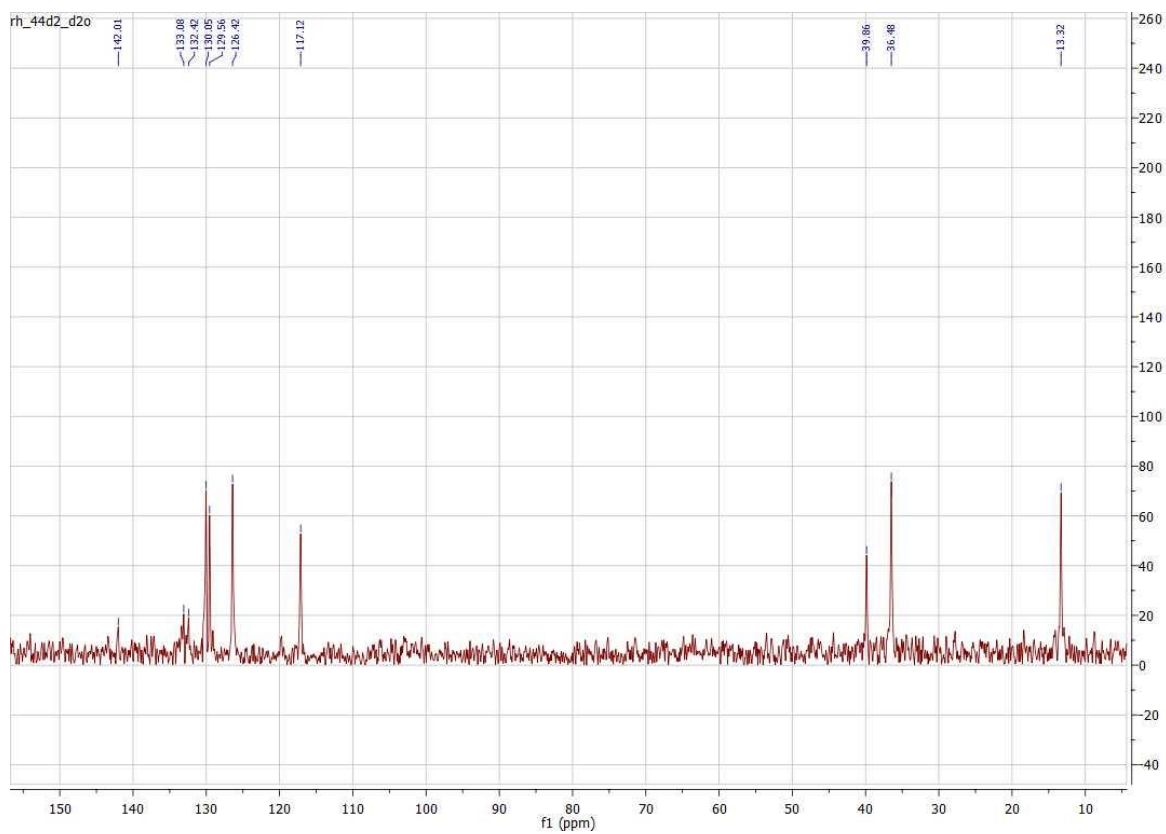
Appendix 7 ^{13}C NMR spectrum of final compound **20d** in D_2O

Chromatogram : RH44D2_channel1
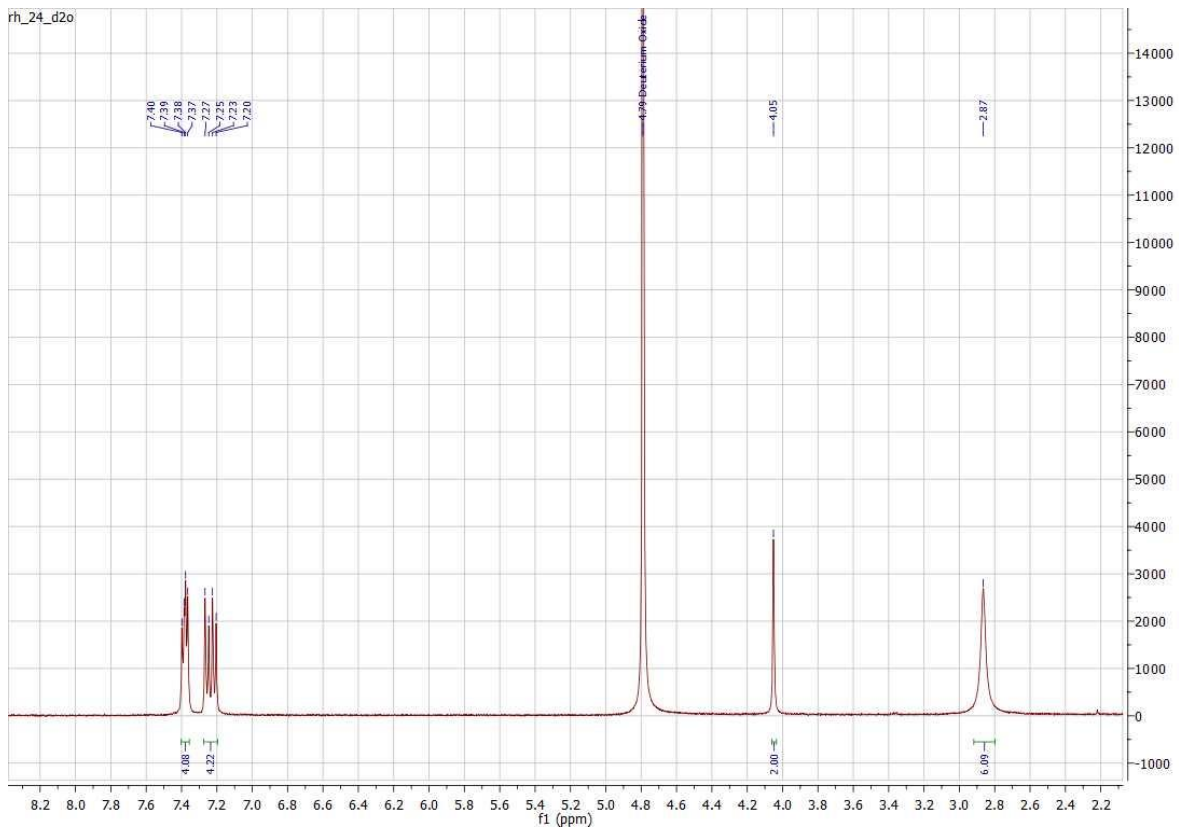
System : HPLC-PDA
Method : Gradient1
User : Daniel

Acquired : 29/10/2020 14:31:31
Processed : 29/10/2020 15:18:59
Printed : 29/10/2020 15:22:14

RH44D2.DATA - Prostar 335 Absorbance Analog Channel 1 LC0908M822
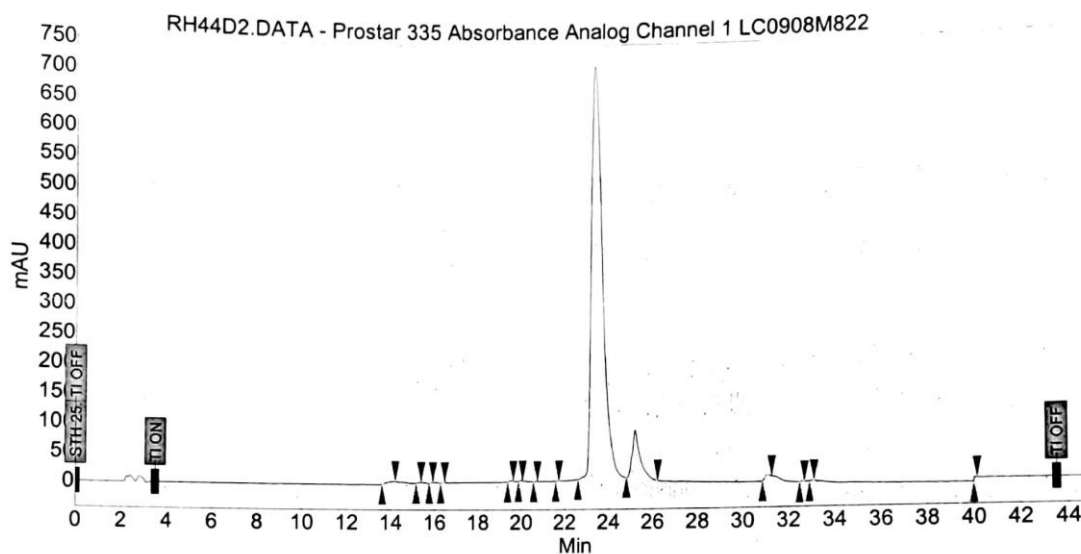
Peak results :

Index	Name	Time [Min]	Quantity [% Area]	Height [mAU]	Area [mAU.Min]	Area % [%]
1	UNKNOWN	13.91	0.14	1.7	0.6	0.135
2	UNKNOWN	15.25	0.01	0.5	0.1	0.015
3	UNKNOWN	15.87	0.01	0.4	0.0	0.009
4	UNKNOWN	16.40	0.01	0.4	0.0	0.010
5	UNKNOWN	19.48	0.05	2.1	0.2	0.053
6	UNKNOWN	19.95	0.02	1.0	0.1	0.020
7	UNKNOWN	20.64	0.01	0.7	0.1	0.012
8	UNKNOWN	21.65	0.01	0.5	0.0	0.009
9	UNKNOWN	23.28	91.35	713.3	411.5	91.348
10	UNKNOWN	25.17	7.95	86.0	35.8	7.945
11	UNKNOWN	31.04	0.29	6.7	1.3	0.294
12	UNKNOWN	32.57	0.03	1.3	0.1	0.028
13	UNKNOWN	32.99	0.02	0.8	0.1	0.019
14	UNKNOWN	40.00	0.10	6.2	0.5	0.103
Total			100.00	821.8	450.5	100.000

Appendix 8 *HPLC percentage purity check for compound **20d** which displayed 91.35% purity, less than the required 95% and therefore was not sent for pharmacological testing*

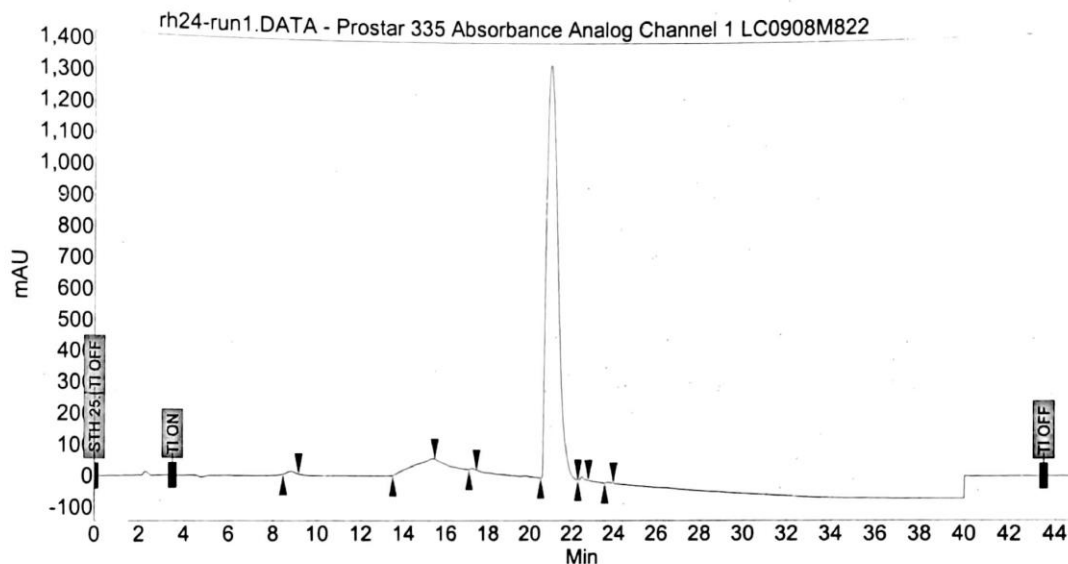**Appendix 9** ^1H NMR spectrum of final compound **25b** in D_2O
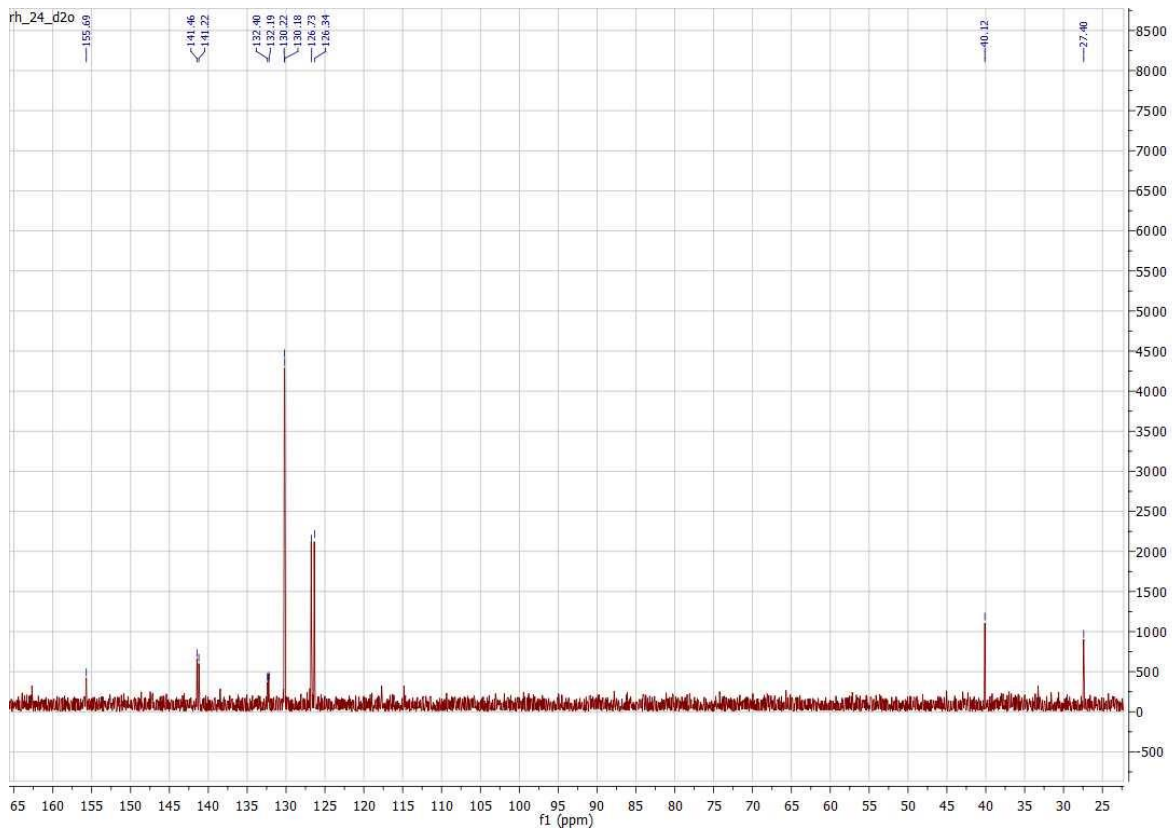
Appendix 10 ^{13}C NMR spectrum of final compound **25b** in $D2O$

Chromatogram : rh24-run1_channel1
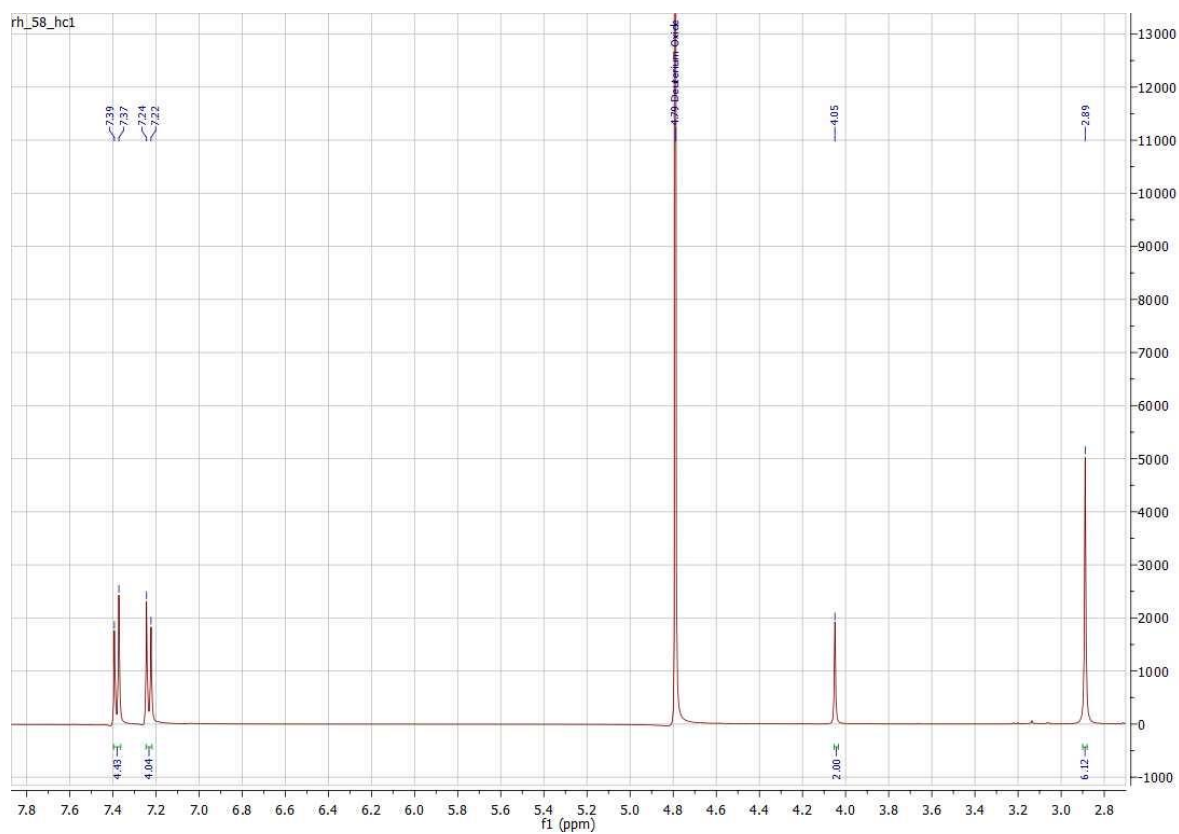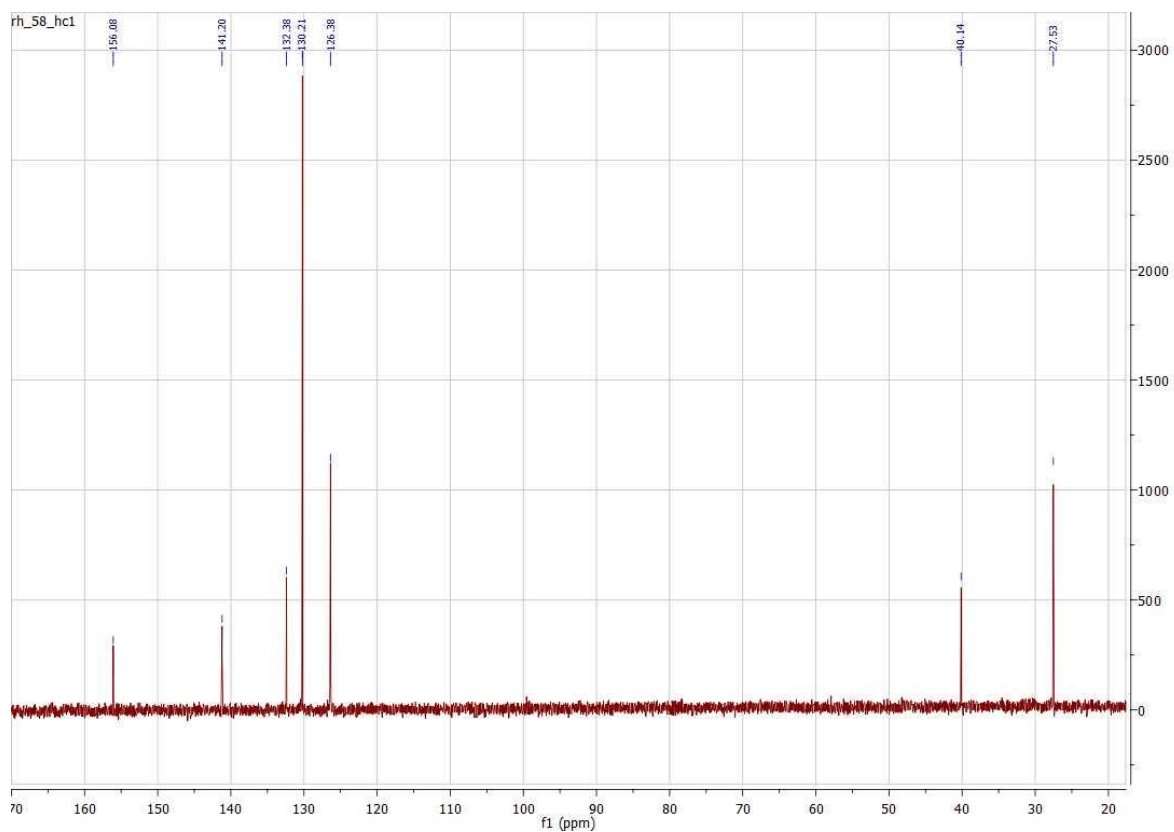
System : HPLC-PDA
Method : Gradient1
User : Daniel

rh24-run1.DATA - Prostar 335 Absorbance Analog Channel 1 LC0908M822

Peak results :

Index	Name	Time [Min]	Quantity [% Area]	Height [mAU]	Area [mAU.Min]	Area % [%]
1	UNKNOWN	8.80	0.41	9.2	3.5	0.411
2	UNKNOWN	14.53	0.98	6.5	8.4	0.979
3	UNKNOWN	17.24	0.09	4.5	0.8	0.091
4	UNKNOWN	20.96	98.17	1354.5	842.2	98.170
5	UNKNOWN	22.47	0.28	13.0	2.4	0.276
6	UNKNOWN	23.73	0.07	3.0	0.6	0.073
Total			100.00	1390.8	857.9	100.000

Appendix 11 *HPLC percentage purity for compound **25b** which displayed 98.17%*

Appendix 12 *¹H NMR spectrum for final compound **21c** in D₂O*
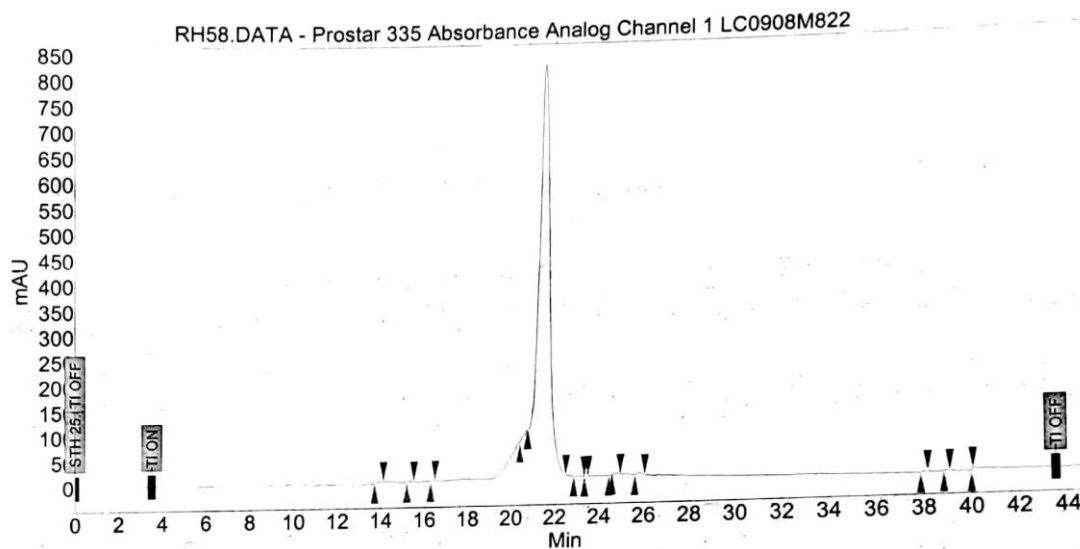

Appendix 13 *¹³C NMR spectrum for final compound **21c** in D₂O*

Chromatogram : RH58_channel1

System : HPLC-PDA
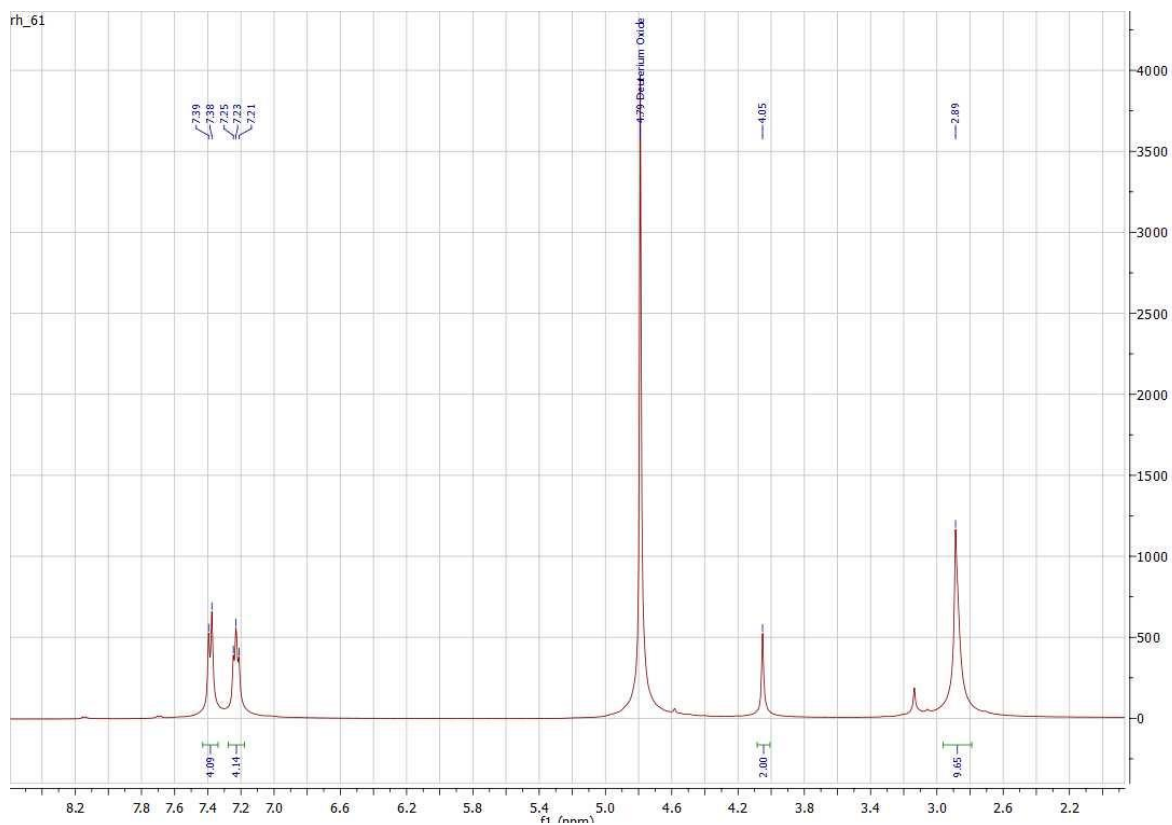Method : Gradient1
User : Daniel

Acquired : 07/10/2020 14:02:55
Processed : 07/10/2020 14:50:24
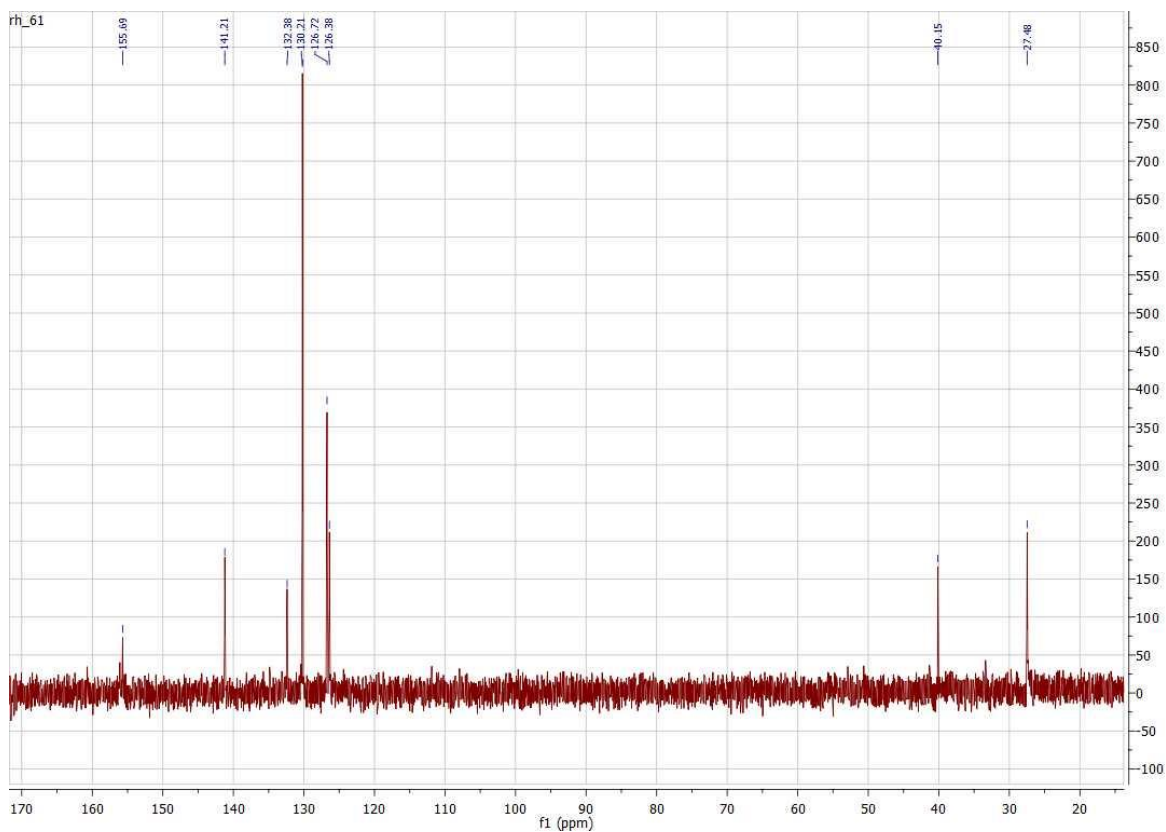Printed : 07/10/2020 14:59:26

RH58.DATA - Prostar 335 Absorbance Analog Channel 1 LC0908M822

Peak results :

Index	Name	Time [Min]	Quantity [% Area]	Height [mAU]	Area [mAU.Min]	Area % [%]
1	UNKNOWN	13.91	0.06	1.1	0.3	0.063
2	UNKNOWN	15.33	0.05	1.3	0.2	0.053
3	UNKNOWN	16.40	0.01	0.4	0.0	0.011
4	UNKNOWN	20.71	1.55	35.7	6.7	1.550
5	UNKNOWN	21.35	97.79	783.0	423.4	97.793
6	UNKNOWN	23.09	0.05	1.3	0.2	0.050
7	UNKNOWN	23.40	0.01	0.6	0.0	0.010
8	UNKNOWN	24.51	0.02	0.9	0.1	0.019
9	UNKNOWN	24.76	0.15	3.6	0.7	0.154
10	UNKNOWN	25.77	0.21	4.5	0.9	0.211
11	UNKNOWN	37.99	0.03	0.8	0.1	0.032
12	UNKNOWN	38.99	0.02	0.6	0.1	0.022
13	UNKNOWN	40.00	0.03	4.2	0.1	0.032
Total			100.00	838.1	433.0	100.000

Appendix 14 *HPLC percentage purity for compound **21c** displaying 97.79%*

Appendix 15 ^{1}H NMR spectrum for the final compound **28b** in D_2O
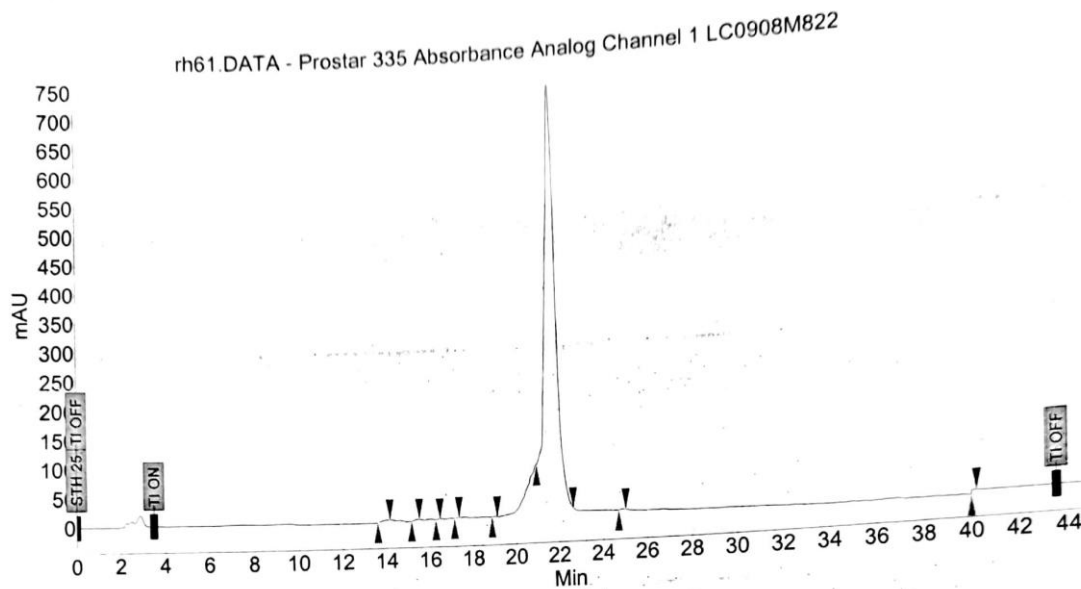

Appendix 16 ^{13}C NMR spectrum for final compound **28b** in D_2O

Chromatogram : rh61_channel1

System : HPLC-PDA
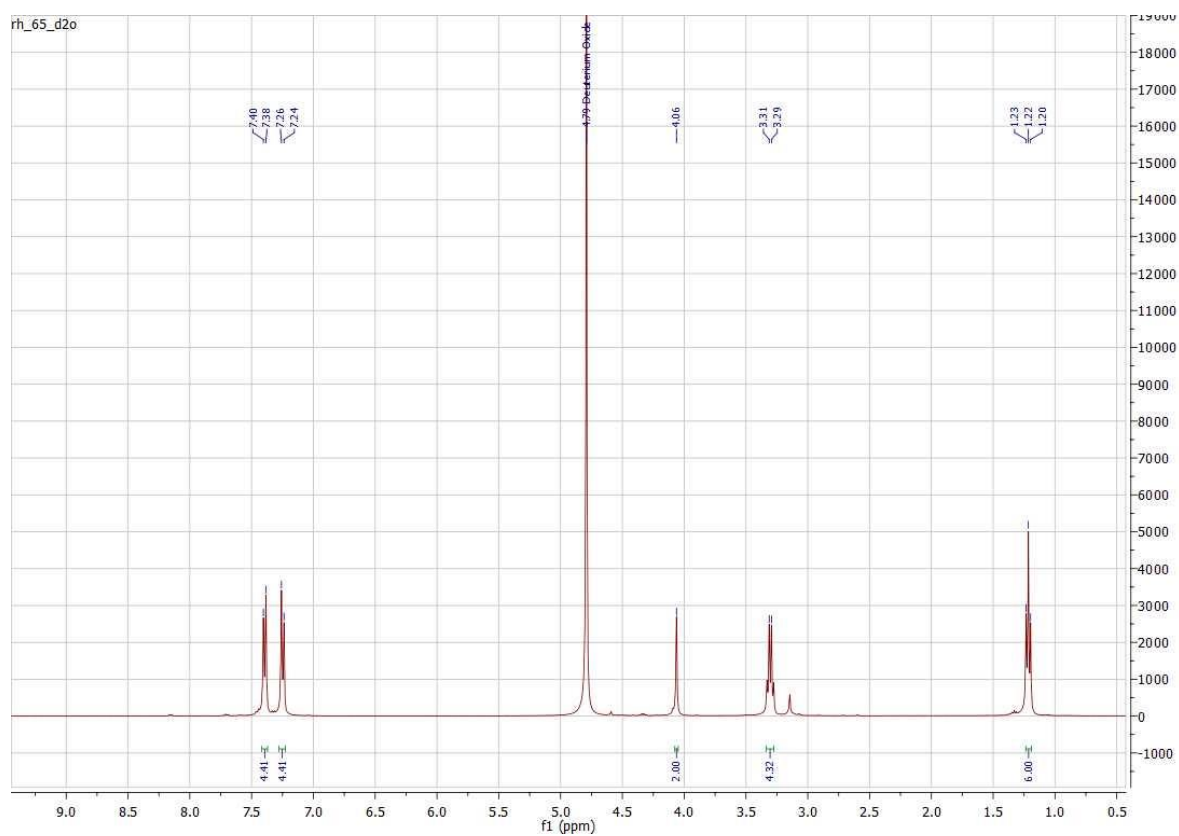Method : Gradient1
User : Daniel

rh61.DATA - Prostar 335 Absorbance Analog Channel 1 LC0908M822

Peak results :

Index	Name	Time [Min]	Quantity [% Area]	Height [mAU]	Area [mAU.Min]	Area % [%]
1	UNKNOWN	13.89	0.16	1.7	0.6	0.159
2	UNKNOWN	15.35	0.06	1.0	0.2	0.061
3	UNKNOWN	16.40	0.01	0.3	0.0	0.010
4	UNKNOWN	17.25	0.01	0.4	0.0	0.013
5	UNKNOWN	18.96	0.04	1.1	0.1	0.040
6	UNKNOWN	21.65	99.43	681.3	352.6	99.431
7	UNKNOWN	24.89	0.07	1.5	0.2	0.070
8	UNKNOWN	40.00	0.22	6.6	0.8	0.215
Total			100.00	694.0	354.6	100.000

Appendix 17 *HPLC percentage purity for compound **28b** with 99.43%*

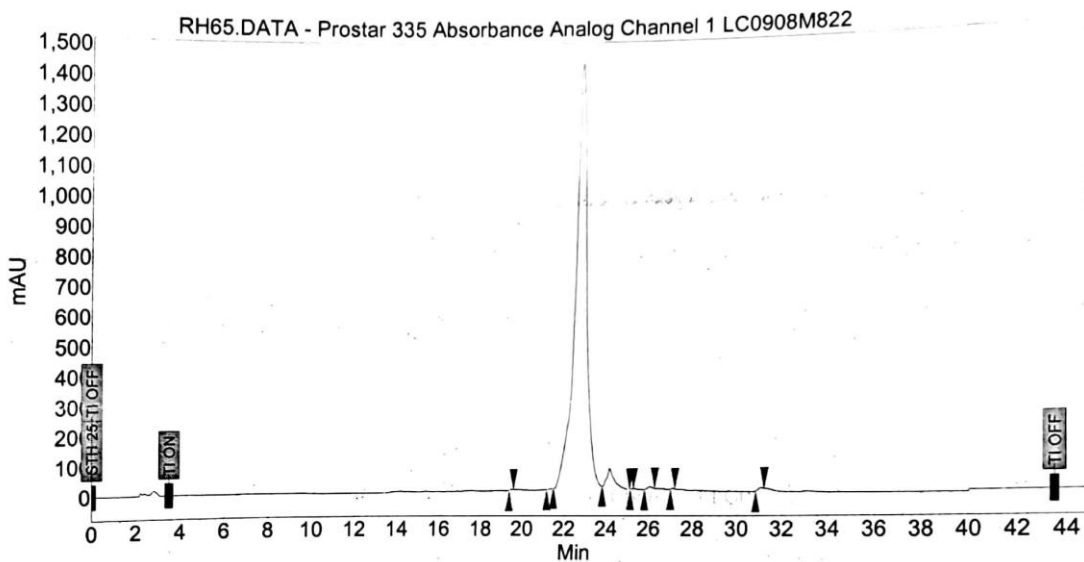**Appendix 18** ^1H NMR spectrum for final compound **22c** in D_2O
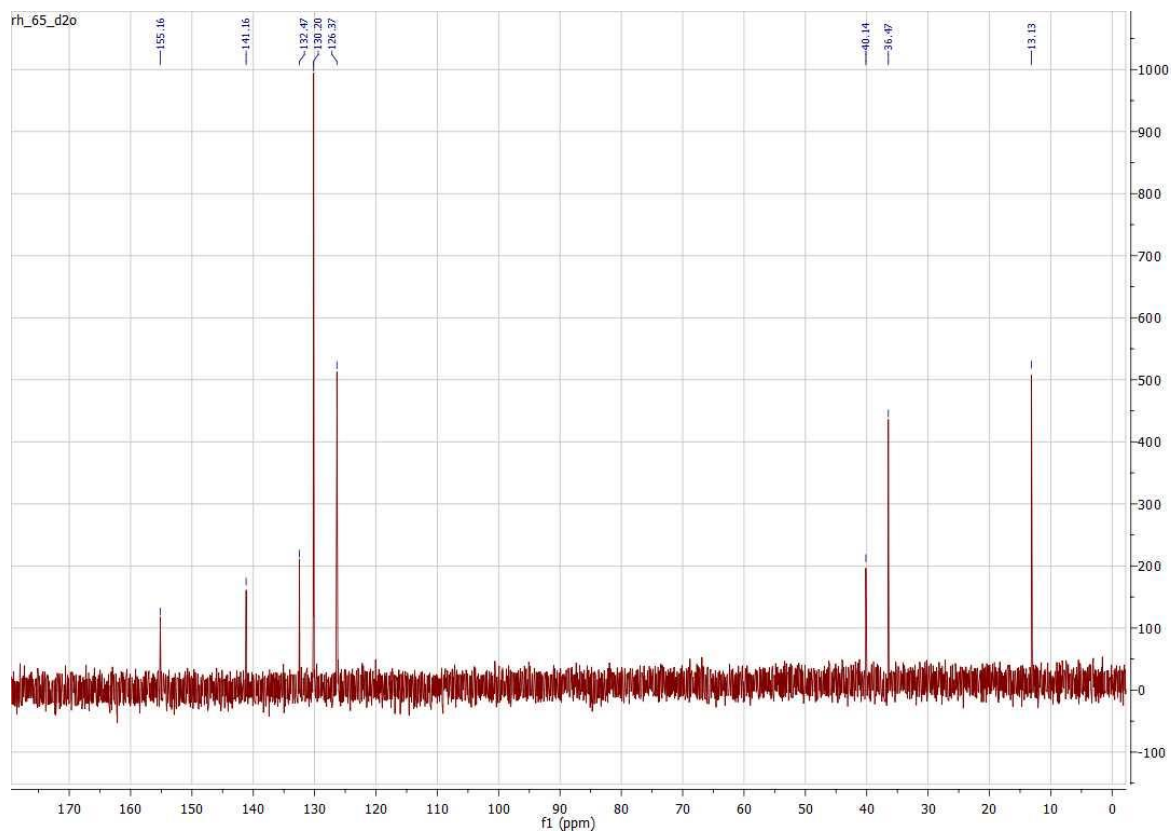
Appendix 19 ^{13}C NMR spectrum for final compound **22c** in D_2O

Chromatogram : RH65_channel1

System : HPLC-PDA
Method : Gradient1
User : Daniel

Acquired : 29/10/2020 13:33:56
Processed : 29/10/2020 14:21:25
Printed : 29/10/2020 14:24:56

RH65.DATA - Prostar 335 Absorbance Analog Channel 1 LC0908M822

Peak results :

| Index	Name	Time [Min]	Quantity [% Area]	Height [mAU]	Area [mAU.Min]	Area % [%]
1	UNKNOWN	19.44	0.03	2.7	0.3	0.028
2	UNKNOWN	21.45	0.07	3.2	0.6	0.068
3	UNKNOWN	22.51	96.37	1437.1	906.1	96.370
4	UNKNOWN	24.11	3.22	71.5	30.2	3.215
5	UNKNOWN	25.17	0.01	0.8	0.1	0.006
6	UNKNOWN	26.00	0.18	7.5	1.7	0.176
7	UNKNOWN	27.05	0.02	1.9	0.2	0.018
8	UNKNOWN	31.01	0.12	6.7	1.1	0.119
Total			100.00	1531.5	940.2	100.000

*Appendix 20* HPLC percentage purity for final compound *22c* with 96.37%
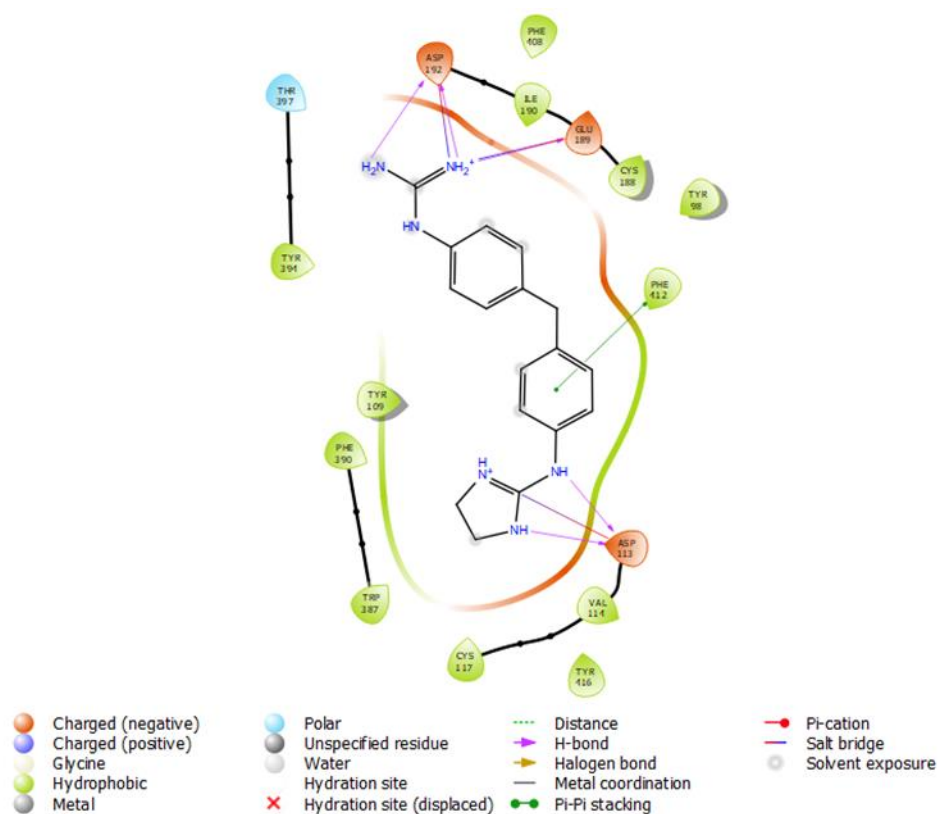
Appendix 21 *Molecular docking of compound **15** with α₂ₐ-AR-X with increased solvent exposure across the ligand (autodock binding affinity: -3.15 kcal/mol)*
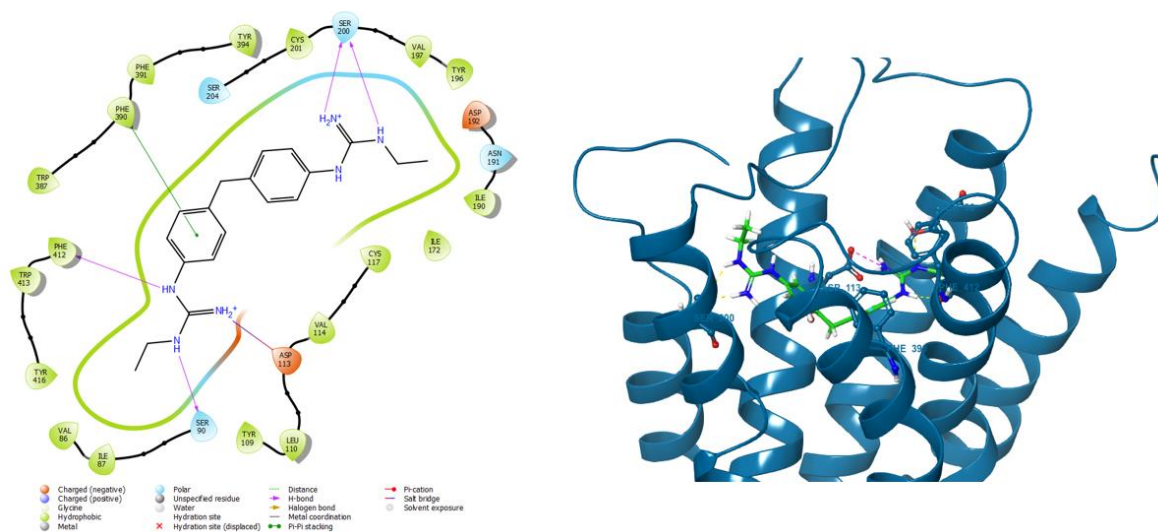
Appendix 22 *Induced-fit docking of compound **22c** with α₂ₐ-AR-Y receptor model in complex with a partial agonist (autodock binding affinity: -9.54 kcal/mol)*
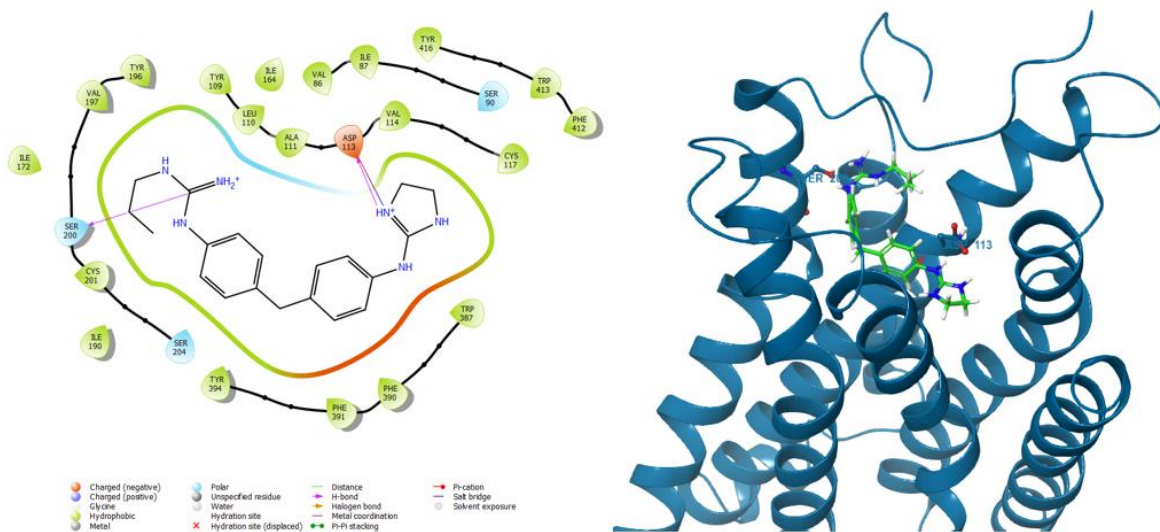
Appendix 23 *Induced-fit docking of compound **16** with α$_{2A}$-AR-Y receptor model in complex with a partial agonist (autodock binding affinity: -8.40 kcal/mol)*
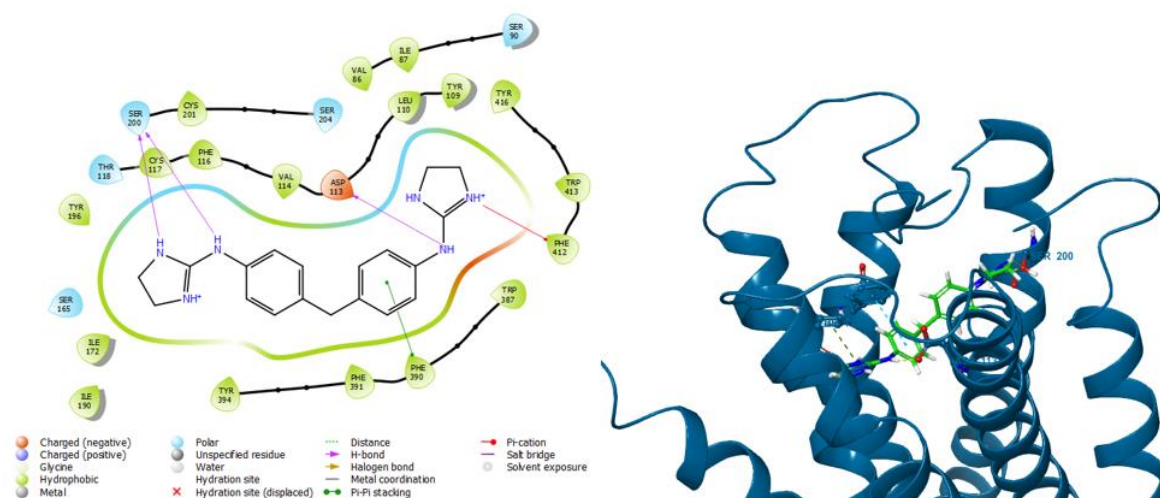
Appendix 24 *Induced-fit docking of lead compound **1** with α$_{2A}$-AR-Y receptor model in complex with a partial agonist (autodock binding affinity: -8.90 kcal/mol)*